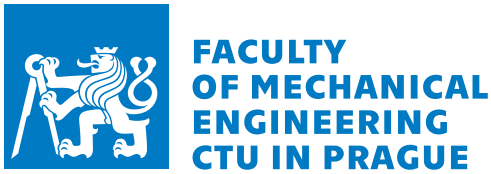

CZECH TECHNICAL UNIVERSITY IN PRAGUE

FACULTY OF MECHANICAL ENGINEERING
DEPARTMENT OF PROCESS ENGINEERING

DOCTORAL THESIS

Pool Boiling of Water–Glycerin Mixtures

DOCTORAL STUDY PROGRAM: MECHANICAL ENGINEERING

BRANCH OF STUDY: DESIGN AND PROCESS ENGINEERING

PRAGUE
April 2022

author: **VIKTOR VAJC**
supervisor: RADEK ŠULC
supervisor-specialist: MARTIN DOSTÁL

"*And when someone builds geometry, he will not derive it from effect to effect all the way to the end, because such work is beyond his strength and time, but an army of ten thousand interpreters will arise around him, who will polish the lessons, take advantage of the fruitful paths, and reap the fruit of the tree. But since they are not slaves and are not driven by the whip, there is no one among them who does not think himself equal to the one true geometrician, because he both understands him and enriches his work.*"

Antoine de Saint-Exupéry, *Citadelle*, Chapter LVIII.

I would like to thank my supervisors, doctor Martin Dostál and doctor Radek Šulc, for their help, guidance, responsiveness, and patience during my studies. I consider myself fortunate to have had you two as my supervisors.

I am very grateful and send my greetings to all my Slovenian colleagues and friends from the Laboratory of Thermal Technology, University of Ljubljana, especially professor Iztok Golobič, doctor Matic Može, doctor Matevž Zupančič, and Mr. Armin Hadžić. The opportunity to cooperate with you has had an essential impact on my knowledge, research, and also on this thesis.

I am obliged to doctor Jiří Moravec, Mr. Pavel Šebrle and doctor Jan Hošek for their help with manufacturing of various parts for my experimental apparatus.

I am also thankful to all my colleagues and friends at the Department of Process Engineering who made my studies, and life in general, bearable and with whom I shared my successes and failures.

And most importantly, I thank my family and my dearests for their support and their confidence in me.

Annotation Sheet

Author's surname:	Vajc
Author's forename:	Viktor
Type of document:	Doctoral thesis
Title:	Pool Boiling of Water–Glycerin Mixtures
Range:	
Number of pages:	138
Number of figures:	47
Number of tables:	14
Number of appendices:	4
Academic year:	2021 / 2022
Language:	English
Institution:	Department of Process Engineering, Faculty of Mechanical Engineering, CTU in Prague
PhD study program:	Mechanical Engineering
Branch of study:	Design and Process Engineering
Supervisor:	doc. Ing. Radek Šulc, Ph.D.
Supervisor-specialist:	Ing. Martin Dostál, Ph.D.
Annotation:	The doctoral thesis focuses on heat transfer during nucleate boiling of water–glycerin mixtures. In the theoretical part, heat transfer during pool boiling of pure fluids and multicomponent mixtures is outlined and discussed together with the mechanisms and parameters of boiling. The thermophysical properties and boiling behavior of water–glycerin mixtures are also addressed. The second part presents the results of heat transfer measurements during saturated and subcooled nucleate pool boiling of water–glycerin mixtures on copper, nickel-plated, and titanium surfaces. The experiments were performed for wide investigated ranges of the heat flux and concentration of glycerin in the boiling mixture. Heat transfer coefficients (HTCs) were observed to deteriorate with an increasing amount of glycerin in the boiling mixture. A significant impact of the mixture effects on HTC was confirmed for all the mixtures and heating surfaces investigated. For the studied experimental conditions, it was found that subcooled boiling on the nickel-plated surfaces occurred in the developed regime. A method was suggested and verified, which can be used to calculate the subcooled boiling HTC in this regime. During boiling on the thin titanium foil, the bubble departure diameter was found to be weakly dependent on the heat flux and independent of the mixture composition. On the contrary, the nucleation frequency increased with the heat flux and concentration of glycerin in the boiling mixture. Correlations were developed, which does not require knowledge of the thermophysical properties of the boiling mixtures, for a straightforward estimation of the measured HTCs and nucleation parameters.
Keywords:	nucleate boiling, pool boiling, saturated boiling, subcooled boiling, heat transfer coefficient, water–glycerin mixtures, mixture effects, infrared thermometry, experimental measurement, correlation

Anotace: Dizertační práce se zabývá přestupem tepla při bublinovém varu binárních směsí voda–glycerin. Teoretická část práce je zaměřena na přestup tepla při objemovém varu čistých kapalin a vícesložkových směsí spolu s mechanismy a nukleačními parametry varu. Jsou zde také diskutovány termofyzikální vlastnosti a chování směsí voda–glycerin při varu. Druhá část prezentuje výsledky experimentálního měření přestupu tepla při nasyceném a podchlazeném bublinovém varu v objemu pro směsi voda–glycerin na měděných, niklovaných a titanových výhřevných površích. Experimenty byly provedeny pro široký rozsah tepelných toků a koncentrací glycerinu ve vroucí směsi. Bylo zjištěno, že s rostoucí koncentrací glycerinu dochází k poklesu součinitele přestupu tepla. Významný vliv tzv. směsných efektů na var byl potvrzen pro všechny zkoumané směsi a výhřevné povrchy. Dále bylo zjištěno, že podchlazený var na poniklovaných površích probíhá za zkoumaných experimentálních podmínek v podchlazeném vyvinutém režimu. Byla navržena a ověřena metoda výpočtu součinitele přestupu tepla v tomto režimu. Při varu na titanové fólii bylo zjištěno, že průměry bublin jsou jen slabě závislé na tepelném toku a nezávislé na složení vroucí směsi. Naopak nukleační frekvence se zvyšovaly jak s tepelným tokem, tak s koncentrací glycerinu ve směsi. Byly navrženy snadno použitelné korelace pro stanovení naměřených součinitelů přestupu tepla a pro hodnoty zkoumaných nukleačních parametrů, které nevyžadují znalost termofyzikálních vlastností vroucích směsí.

Klíčová slova: bublinový var, objemový var, nasycený var, podchlazený var, součinitel přestupu tepla, směs voda–glycerin, efekty směsi, infračervená termometrie, experimentální měření, korelace

Table of Contents

List of Figures

List of Tables

Nomenclature

Latin letters:

a	$(\mathrm{m^2\,s^{-1}})$	thermal diffusivity, $a = \lambda/(\varrho\, c_p)$
Ar	$(-)$	Archimedes number, defined by Equation (1.30)
Bo	$(-)$	Bond number, defined by Equation (1.28)
c_p	$(\mathrm{J\,kg^{-1}\,K^{-1}})$	isobaric specific heat capacity
C		coefficient, parameter
$[C]$	$(-)$	correction matrix, calculated with Equation (A1)
C_0	$(-)$	scaling factor, empirical parameter of the Schlünder correlation (2.27)
C_b	$(-)$	boiling parameter of Yagov correlation (1.76)
C_F	$(-)$	coefficient of Fritz correlation, see Equation (1.26)
C_g	$(-)$	dimensionless growth constant, used in Equation (1.43)
D_{12}	$(\mathrm{m^2\,s^{-1}})$	binary diffusion coefficient
D_b	(m)	bubble departure diameter
D_eq	(m)	equivalent bubble diameter
D_f	(m)	footprint diameter of a zone affected by heat transfer
D_L	(m)	Laplace diameter, defined by Equation (1.27)
f_n	$(\mathrm{s^{-1}})$	nucleation frequency, $f_\mathrm{n} = 1/t_\mathrm{n}$
$f_\mathrm{n}\, D_\mathrm{b}$	$(\mathrm{m\,s^{-1}})$	bubble growth rate
F	$(-)$	correction factor, defined in Equation (2.13)
F_D	$(-)$	suppression factor due to diffusion, see Equation (2.39) or (2.40)
F_p	$(-)$	pressure factor, used in correlations (1.67) and (1.71)
F_α	$(-)$	relative decrease of HTC, defined in Equation (2.15)
Fr	$(-)$	Froude number, $\mathrm{Fr} = u_\mathrm{ch}^2/(L_\mathrm{ch}\, g)$
g	$(\mathrm{m\,s^{-2}})$	gravitational acceleration
Ja′	$(-)$	modified Jakob number, defined in Equation (1.13)
K		coefficient, parameter
L_ch	(m)	characteristic length
m		exponent
M_m	$(\mathrm{kg\,mol^{-1}})$	molar mass
MRE	$(-)$	mean relative error, calculated with Equation (6.3)
n		exponent, index of time layer
n_n	$(\mathrm{m^{-2}})$	active nucleation site density, $n_\mathrm{n} = N_\mathrm{n}/S$
N	$(-)$	number of data points
N_n	$(-)$	number of active nucleation sites
Nu	$(-)$	Nusselt number, $\mathrm{Nu} = \alpha\, L_\mathrm{ch}/\lambda$
p	(Pa)	pressure
p_cr	(Pa)	critical pressure
p_red	$(-)$	reduced pressure, $p_\mathrm{red} = p/p_\mathrm{cr}$
Pr	$(-)$	Prandtl number, $\mathrm{Pr} = \nu/a$
q	$(\mathrm{W\,m^{-2}})$	heat flux
$[q]$	$(\mathrm{W\,m^{-2}})$	matrix of heat flux calculated from matrix $[T_\mathrm{s}]$
q_ac	$(\mathrm{W\,m^{-2}})$	accumulative heat flux, calculated with Equation (8.3)
q_c	$(\mathrm{W\,m^{-2}})$	convective heat flux, calculated with Equation (8.4)
q_cr	$(\mathrm{W\,m^{-2}})$	critical heat flux (CHF), see Figure 1
q_el	$(\mathrm{W\,m^{-2}})$	heat flux generated by electrical heating, see Equation (8.2)
$q^n_{i,j}$	$(\mathrm{W\,m^{-2}})$	value of heat flux over node i,j in the time layer n
q_ONB	$(\mathrm{W\,m^{-2}})$	heat flux required for the onset of nucleate boiling

$q_{\mathrm{pd}\to\mathrm{fd}}$	$(\mathrm{W\,m^{-2}})$	heat flux required for transition to fully developed boiling
Q_{b}	(J)	thermal energy consumed by nucleating bubbles
r	(m)	radial coordinate
R	(m)	radius
$\mathrm{R_a}$	(m)	roughness of the heating surface according to standard ISO 1302
R_{cr}	(m)	critical radius
R_{m}	$(\mathrm{J\,mol^{-1}\,K^{-1}})$	universal gas constant, $R_{\mathrm{m}} = 8314.46\ \mathrm{J\,kmol^{-1}\,K^{-1}}$
$\mathrm{R_p}$	(m)	roughness of the heating surface according to standard DIN 4762
R_{shunt}	(Ω)	nominal resistance of the shunt
Ra	$(-)$	Rayleigh number, $\mathrm{Ra} = \beta_{\mathrm{vol}}\, g\, (T_{\mathrm{s}} - T_{\mathrm{L}})\, L_{\mathrm{ch}}^3/(\nu\, a)$
Re	$(-)$	Reynolds number, $\mathrm{Re} = u_{\mathrm{ch}}\, L_{\mathrm{ch}}\, \varrho/\mu$
S	$(\mathrm{m^2})$	surface area
SEE		standard error of the estimate, calculated with Equation (6.2)
Sn	$(-)$	Scriven number, defined in Equation (2.18)
t	(s)	time
t_{g}	(s)	bubble growth period
t_{n}	(s)	period of nucleation, $t_{\mathrm{n}} = t_{\mathrm{g}} + t_{\mathrm{w}}$
t_{w}	(s)	waiting period
T	$(^\circ\mathrm{C})$	temperature
T_{b}	$(^\circ\mathrm{C})$	bubble-point temperature
$T_{\mathrm{b,s}}$	$(^\circ\mathrm{C})$	bubble-point temperature affected by *mixture effects*
$[T_{\mathrm{cor}}]$	$(^\circ\mathrm{C})$	matrix of corrected temperatures, calculated with Equation (A2)
T_{cr}	$(^\circ\mathrm{C})$	critical temperature
T_{d}	$(^\circ\mathrm{C})$	dew-point temperature
$T_{i,j}^{n}$	$(^\circ\mathrm{C})$	value of temperature over node i,j in the time layer n
T_{L}	$(^\circ\mathrm{C})$	temperature of the liquid bulk
$\bar{T}_{\mathrm{raw}}$	$(^\circ\mathrm{C})$	value of the average raw temperature
$[T_{\mathrm{raw}}]$	$(^\circ\mathrm{C})$	matrix of raw temperatures
T_{red}	$(-)$	reduced temperature, $T_{\mathrm{red}} = T/T_{\mathrm{cr}}$
T_{s}	$(^\circ\mathrm{C})$	temperature of the heating surface
$[T_{\mathrm{s}}]$	$(^\circ\mathrm{C})$	matrix of surface temperatures
T_{sat}	$(^\circ\mathrm{C})$	saturation temperature
$u(\gamma)$		uncertainty of a property γ
u_{ch}	$(\mathrm{m\,s^{-1}})$	characteristic velocity
$u_{\mathrm{r}}(\gamma)$	$(-)$	relative uncertainty of a property γ, $u_{\mathrm{r}}(\gamma) = u(\gamma)/\gamma$
$U(\gamma)$		maximum deviation of a property γ
U_{foil}	(V)	measured voltage across the foil
U_{shunt}	(V)	measured voltage across the shunt
V	$(\mathrm{m^3})$	volume
VP	$(-)$	volatility parameter, defined in Equation (2.38)
w	$(\mathrm{kg\,m^{-2}\,s^{-1}})$	mass flux
x	(m)	Cartesian coordinate
x_i	$(-)$	molar fraction of component i in the liquid phase
$\lvert x_i - y_{\mathrm{i}}\rvert$	$(-)$	equilibrium molar fraction difference
X_i	$(-)$	dimensionless complex of the Stephan and Abdelsalam correlation (1.60)
y	(m)	Cartesian coordinate
y_i	$(-)$	molar fraction of component i in the vapor phase

Greek letters:

α	$(\mathrm{W\,m^{-2}\,K^{-1}})$	heat transfer coefficient (HTC), defined by Equations (1.1), (1.4), and (2.5)
$\hat{\alpha}$	$(\mathrm{W\,m^{-2}\,K^{-1}})$	correlated heat transfer coefficient, used in Equations (6.2) and (6.3)
α_1, α_2	$(\mathrm{W\,m^{-2}\,K^{-1}})$	heat transfer coefficients of pure components
α_b	$(\mathrm{W\,m^{-2}\,K^{-1}})$	*boiling* heat transfer coefficient, defined by Equation (1.10)
α_id	$(\mathrm{W\,m^{-2}\,K^{-1}})$	*ideal* heat transfer coefficient, defined by Equation (2.1) or (2.2)
α_tot	$(\mathrm{W\,m^{-2}\,K^{-1}})$	*total* heat transfer coefficient, defined by Equation (1.9)
β	$(\mathrm{m\,s^{-1}})$	mass transfer coefficient
β_cm	$(^\circ)$	angle of cavity mouth
β_vol	$(-)$	coefficient of volumetric expansion
γ		an unspecified property
δ_foil	(m)	thickness of the investigated foil
δ_ml	(m)	thickness of the microlayer
δ_p	(m)	penetration depth, $\delta_\mathrm{p} = \sqrt{\pi\, a\, t}$
δ_t	(m)	thickness of the thermal boundary layer
Δh_LG	$(\mathrm{J\,kg^{-1}})$	latent heat of vaporization
ΔL_px	(m)	spatial resolution of the recorded IR videos
ΔT	(K)	temperature difference
ΔT_add	(K)	*additional* superheat, used in Equation (2.11)
ΔT_db	(K)	boiling range, defined in Equation (2.16), $\Delta T_\mathrm{db} = T_\mathrm{d} - T_\mathrm{b}$
ΔT_id	(K)	ideal superheat, defined in Equation (2.6)
ΔT_ONB	(K)	temperature difference required for the onset of nucleate boiling
ΔT_sat	(K)	superheat, defined by Equation (1.3)
ΔT_sub	(K)	subcooling, defined by Equation (1.5)
ε	$(-)$	ratio of HTC differences, defined by Equation (7.5)
ϑ_c	$(^\circ)$	contact angle, see Figure 1.3
λ	$(\mathrm{W\,m^{-1}\,K^{-1}})$	thermal conductivity
λ'	$(\mathrm{W\,m^{-1}\,K^{-1}})$	thermal conductivity of the sample, used in Equation (7.3)
μ	(Pa s)	dynamic viscosity
ν	$(\mathrm{m^2\,s^{-1}})$	kinematic viscosity
ξ	$(-)$	relative subcooling, used in Equations (1.39) and (1.40)
ϱ	$(\mathrm{kg\,m^{-3}})$	density
σ	$(\mathrm{N\,m^{-1}})$	surface tension
τ_film	(s)	period of recording of IR videos, $\tau_\mathrm{film} = 1/\mathrm{fps}$
φ	$(^\circ)$	interface angle, $\varphi = \vartheta_\mathrm{c} + \beta_\mathrm{cm}$, used in Equations (1.39) and (1.40)
ω_w	$(-)$	water mass fraction of the liquid phase

Subscripts:

b	boiling, bubble, bubble-point
c	cavity
cr	critical
Cu	copper
d	dew-point
D	diffusion
eq	equivalent
ev	evaporation
f	footprint
G	vapor phase
i	ordinal index
in	initiation
id	ideal
inf	influence
int	interface
j	ordinal index
L	liquid phase
lh	latent heat
max	maximum
min	minimum
ml	microlayer
nc	natural convection
psc	pseudo-single-component
r	relative
red	reduced
ref	reference
s	heating surface
sat	saturation
sub	subcooling
tc	transient conduction
Ti	titanium
tot	total
w	water

Abbreviations:

CHF	critical heat flux
DAQ	data acquisition
fps	frames per second
HTC	heat transfer coefficient
IR	infrared
ONB	onset of nucleate boiling
px	pixel
PEEK	polyether ether ketone
TC	thermocouple

Introduction and Scope of This Thesis

Boiling is a process characterized by the local formation of bubbles over the parts of a heating surface [1]. Boiling (especially the nucleate regime of boiling) offers intense heat transfer at a relatively small driving temperature difference [2,3]. The dependence of the heat flux q on the driving temperature difference (most typically the superheat ΔT_{sat}) is often visualized using the so-called *boiling curve* [4]. A typical boiling curve is shown in Figure 1. Although the proportions of the boiling curve might be different for different geometries of the heating surface (planar, tubular, etc.) and for different boiling conditions (pressure, saturation temperature, etc.), its basic shape should be universal and independent of the surface parameters and boiling conditions.

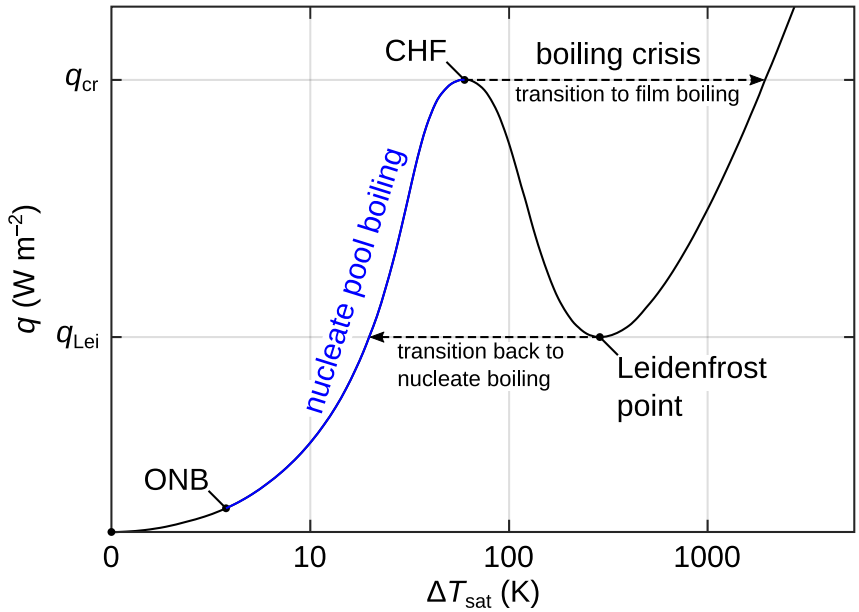

Figure 1: A typical boiling curve. The nucleate boiling regime lies between the point of the onset of nucleate boiling (ONB) and the point of the critical heat flux (CHF).

The boiling curve might be divided into several parts (or *regimes* of boiling):

- The regime of *natural convection* which is represented by the part of the boiling curve from the origin to the onset of nucleate boiling (ONB).
- *Nucleate boiling* lies beyond the ONB and is limited by the point of the critical heat flux (CHF) which is a local maximum of the boiling curve. When nucleate boiling is established, bubbles periodically emerge from the active nucleation sites of the heating surface. Nucleate boiling is often subdivided into more sub-regimes such as the regime of partially developed boiling, the regime of fully developed boiling, and others.
- *Transition boiling* between the point of CHF and the so-called Leidenfrost point which is the a local minimum of the boiling curve beyond CHF. This regime is characterized by the formation of an unstable insulative vapor film which covers the heating surface and causes significant deterioration of heat transfer. The nucleation of bubbles no longer occurs from the nucleation sites of the heating surface, but from the outer layers of the vapor film. The thickness of the film increases with the driving temperature difference and causes a further reduction of heat transfer.
- *Stable film boiling* which occurs beyond the Leidenfrost point. The vapor film is fully stable in this regime. More bubbles are produced from the outer layers of the film when the driving temperature difference is increased.

Nucleate boiling is the most important regime of pool boiling characterized by the highest boiling performance. It is commonly utilized in various industrial applications such as, for example, cooling of electronic devices [5], heat exchangers [6], thickening evaporators [7], distillation [8], refrigeration [9], nuclear engineering [10] and others. In general, the boiling performance is typically evaluated with respect to one or multiple following parameters [11]:

- The *heat transfer coefficient* (HTC), denoted α, which is the ratio between the transferred heat flux q and the driving temperature difference. Generally speaking, HTC quantifies the intensity of heat transfer during boiling. Nucleate boiling is characterized by the highest HTCs relative to all the other regimes of pool boiling.
- The *critical heat flux* (CHF), i.e., the maximum heat flux q_{cr} which might be reached in the regime of nucleate pool boiling before the transition to film boiling and a strong deterioration of HTC occur. The fast transition to film boiling is sometimes called the boiling crisis, see Figure 1, and might lead to a rapid and substantial increase of the temperature of the heating surface and eventually to a severe thermal damage to apparatuses and devices (melting, deformation, etc.). In most applications, the heat flux is carefully monitored and kept well below q_{cr}.
- The temperature difference ΔT_{ONB} and the heat flux q_{ONB} which are required for the *onset of nucleate boiling* (ONB), i.e., for the transition from natural convection to nucleate boiling.
- The *boiling hysteresis* which is the difference between the boiling curves obtained during increasing and decreasing heat flux. A significant hysteresis is typical for boiling of fluids with a high wettability and for surfaces with a narrow distribution of the characteristic dimensions of cavities.

This thesis focuses on heat transfer during saturated nucleate pool boiling of binary mixtures of water and glycerin. Knowledge of HTC during boiling is crucial for cost-saving design and efficient operation of industrial apparatuses. The thesis is divided into three main parts. The first part is theoretical and introduces the reader to the problematic of boiling of pure components and mixtures. It also contains the section which discusses motivation and the current state-of-the-art with respect to boiling of water–glycerin mixtures. The second part presents the experimental measurements of HTC during boiling of water–glycerin mixtures on copper, nickel-plated, and titanium surfaces. In the third part, the findings of the thesis are summarized and the conclusions based on results of experiments are drawn.

PART I

Theoretical Background

1. Saturated and Subcooled Pool Boiling Heat Transfer

The heat transfer coefficient (HTC) is defined with Newton's cooling law

$$\alpha = \frac{q}{\Delta T} \,, \tag{1.1}$$

where q denotes the heat flux and ΔT is a characteristic temperature difference. During boiling, heat is transferred from the heating surface which has a temperature T_s into the boiling liquid at a temperature T_L. The temperature difference between the heating surface and the boiling liquid

$$\Delta T = T_\mathrm{s} - T_\mathrm{L} \,, \tag{1.2}$$

therefore, might be substituted into the denominator of Equation (1.1).

When boiling is saturated, the temperature of the boiling liquid T_L equals to its saturation temperature T_sat. The temperature difference between the heating surface and the saturation temperature of the liquid is called *superheat*

$$\Delta T_\mathrm{sat} = T_\mathrm{s} - T_\mathrm{sat} \,. \tag{1.3}$$

For saturated boiling, $T_\mathrm{L} = T_\mathrm{sat}$ and the superheat is the driving temperature difference. HTC, therefore, might be calculated as

$$\alpha = \frac{q}{T_\mathrm{s} - T_\mathrm{sat}} \,. \tag{1.4}$$

It is worth mentioning that the representation of the heat transfer performance solely by the value of HTC calculated with Equation (1.4) might not be sufficient. Since the superheat ΔT_sat is based on the average temperature of the heating surface T_s, information about the temporal and spatial distribution of the superheat is not taken into account which might lead to misconceptions in the research of boiling [12,13].

Subcooled boiling occurs when the surface is superheated but the temperature of the boiling liquid T_L is lower than its saturation temperature T_sat. *Subcooling* of the liquid is defined as

$$\Delta T_\mathrm{sub} = T_\mathrm{sat} - T_\mathrm{L} \,. \tag{1.5}$$

The superheat (1.3) and the subcooling (1.5) might be substituted into Equation (1.2) to obtain

$$\Delta T = \Delta T_\mathrm{sat} + \Delta T_\mathrm{sub} \,. \tag{1.6}$$

Forster and Greif [14] noticed, by comparing experimental data of others, that when the heat flux during subcooled boiling is higher than a certain limiting heat flux, developed subcooled boiling occurs, and HTC becomes independent of the subcooling. Although Forster and Greif themselves did not use the term *developed subcooled boiling*, I adopted it because reaching the boiling performance independent of various parameters is typical and well-known for the developed regime of saturated boiling. Various researchers observed that the influential parameters, which clearly affect boiling performance in the so-called *partially developed* regime[1] of saturated boiling, become insignificant after boiling becomes (*fully*) *developed*. For example, independence of acceleration, external forces, the shape and dimensions of the heating surface, the inclination angle, the position of a tube in a tube bundle, or the velocity of the boiling fluid during flow boiling was observed and reported in the literature [15–20]. Correlations for the heat flux $q_\mathrm{pd\to fd}$ required for the transition from partially- to fully developed boiling were also proposed in the literature, such as the correlation of Zuber [21]

$$q_\mathrm{pd\to fd} = \frac{1.53\pi}{6}\, \varrho_\mathrm{G}\, \Delta h_\mathrm{LG} \left[\frac{\sigma\, g\, (\varrho_\mathrm{L} - \varrho_\mathrm{G})}{\varrho_\mathrm{L}^2}\right]^{1/4} \tag{1.7}$$

[1] Various definitions of boiling regimes can be found in the literature. For the purpose of this work, the *partially developed* regime is defined as the regime outside of the *fully developed* regime of boiling. The regime is characterized by nucleation of isolated bubbles which do not mutually interact.

or the correlation of Moisis and Berenson [22]

$$q_{\mathrm{pd}\to\mathrm{fd}} = 0.11\,\sqrt{\vartheta_\mathrm{c}}\,\varrho_\mathrm{G}\,\Delta h_\mathrm{LG}\left[\frac{\sigma\,g}{(\varrho_\mathrm{L}-\varrho_\mathrm{G})}\right]^{1/4}, \tag{1.8}$$

where the contact angle ϑ_c should be in degrees. Whether boiling occurs in the fully developed regime might also be noticeable by visual observation of the process of boiling. It was reported that the vertical merging of bubbles (characteristic for developed boiling) starts at more or less the same heat flux as the horizontal merging of neighboring bubbles which might be visible by the naked eye or on a high-speed video footage [23].

When boiling becomes fully developed, the boiling curves obtained for different values of the influential parameters merge into a single curve. This is sometimes designated as the *merging trend* [15]. An advantageous consequence of the *merging trend* is that correlations for developed pool boiling might be used for a wide range of conditions and geometries. In fact, pool boiling correlations might even be suitable for fully developed flow boiling [14,20]. Several explanations of the *merging trend* were proposed in the literature. I outline three theories for illustration:

1. Forster and Greif [14] believe that as the subcooling increases (which for a given ΔT_sat should increase q due to a greater temperature difference between the heating surface and liquid), the bubble radius and average period of nucleation cycles decrease (which decreases HTC due to generally smaller volumes of bubbles). These competing effects cancel themselves out and the surface superheat ΔT_sat, which determines the number of active nucleation sites, becomes the governing temperature difference for HTC.
2. Yagov [17] uses theories of Labuntsov and considers the *merging trend* to be a consequence of the molecular pulsation which occurs deep in the thermal boundary layer. Phenomena that occur deep in the layer are characterized by their independence from any external disturbances.
3. Monde [24] considers boiling to be controlled by a very thin layer of the boiling fluid next to the heating surface. This thin layer is, according to him, independent of the motion of the fluid as well as of the surface conditions.

No matter what the exact cause of the *merging trend* is, the heat flux appears to be not affected by ΔT_sub, and is only a function of ΔT_sat after the developed subcooled regime is reached. This led some researchers [25–27] to consider the superheat ΔT_sat, defined in Equation (1.3), to be the driving temperature difference, and to use the definition of HTC in Equation (1.4) even for subcooled boiling. However, in contrast, there is another cohort of authors [28,29] which relate HTC to the temperature difference defined by Equation (1.6). The inconsistency between both groups might confuse the readers and makes the results of both groups incomparable and misleading. For instance, some authors may report enhancement of HTC with increasing subcooling while others may obtain completely different trends and deterioration of HTC for higher subcooling, as a consequence of different definitions of their HTCs. In this work, I adopt the terminology suggested by El-Genk and Parker [30] and distinguish between the *total*- and the *boiling* heat transfer coefficient during subcooled boiling. The *total* HTC α_tot is defined with the general definition, see Equation (1.1), and contains the temperature difference (1.6) in the denominator

$$\alpha_\mathrm{tot} = \frac{q}{T_\mathrm{s} - T_\mathrm{L}}\,. \tag{1.9}$$

The *boiling* HTC α_b is defined with Equation (1.4)

$$\alpha_\mathrm{b} = \frac{q}{T_\mathrm{s} - T_\mathrm{sat}}\,. \tag{1.10}$$

The relation between the *total*- and the *boiling* HTC is then

$$\frac{1}{\alpha_\mathrm{tot}} = \frac{1}{\alpha_\mathrm{b}} + \frac{\Delta T_\mathrm{sub}}{q}\,. \tag{1.11}$$

For saturated boiling, $\alpha = \alpha_b = \alpha_{tot}$. El-Genk and Parker [30] consider the term $q/\Delta T_{sub}$ in Equation (1.11) to represent the heat transfer resistance due to convection in the liquid pool and due to condensation of bubbles in the subcooled liquid. Although a higher subcooling might increase the *boiling* HTC, it might also simultaneously lower the *total* HTC. El-Genk and Parker [30] consider saturated boiling superior to subcooled boiling because the *total* HTC is generally higher for saturated boiling.

1.1 Boiling Mechanisms

Different underlying mechanisms were proposed to explain the enhancement of heat transfer during boiling. Knowledge of boiling mechanisms enables to develop a physical theory of boiling, to estimate the boiling performance or to predict and explain the impact of various factors on the boiling performance. Mechanistic models should be universal for various boiling liquids, heating surfaces, and conditions (or at least more universal than empirical correlations) [31]. Unfortunately, the mechanisms of pool boiling heat transfer are, in general, poorly understood which limits the mechanistic approach to boiling [15]. Moreover, mechanistic models often require knowledge of various boiling parameters which are not easy to calculate or measure, such as the number of active nucleation sites N_n (or its density n_n), the bubble departure diameter D_b, or the nucleation frequency f_n. Currently, there are no comprehensive models and reliable data for these parameters [31,32].

The following complementary boiling mechanisms were proposed in the literature for the *partially developed* regime of boiling [15,33]:

- Mechanisms of *enhanced convection*. In this work, I distinguish between:
  - *Microconvection*, i.e., microscale movement of the liquid induced by the growth and motion of the vapor–liquid interfaces of bubbles.
  - The *pumping effect* of bubbles which pushes hot liquid away from the heating surface and brings colder liquid from the bulk to the vicinity of the surface.
- Mechanisms related to the *transport of latent heat*. The following are the most important:
  - *Microlayer evaporation* (might be accompanied by possible condensation at the top of bubbles). The transport of latent heat gets stronger when microlayer evaporation is promoted which typically occurs at higher heat fluxes or at lower pressures.
  - *Three-phase contact line heat transfer*. The boiling theories based on this mechanism suppose that most of the heat is transferred near the point where the vapor–liquid interface is in contact with the heating surface.
- *Transient heat conduction* to the liquid in the vicinity of the heating surface and to the liquid displaced in the wakes of departing bubbles. The mechanism is dominant during the waiting periods[2] of nucleation cycles.
- *Natural convection* occurs over the parts of the heating surface which are not influenced by emerging bubbles.

For *fully developed* boiling, mechanisms are, unfortunately, much more complex than for *partially developed* boiling, because at higher heat fluxes, emerging bubbles mutually interact and form complicated vapor formations of mushroom-resembling shapes. A liquid layer called *the macrolayer* is trapped between these formations and the heating surface. Vapor stems emerge from nucleation sites and penetrate the macrolayer. The ratio of the area of the rising stems to the total area was experimentally found to be of about 0.17 [15]. The complicated mechanisms occurring in the macrolayer have a crucial impact on heat transfer and seem not to be affected by parameters, which influence boiling in the *partially developed*

[2] The waiting period is the time period between the nucleation of two successive bubbles from the same nucleation spot.

regime, as was already pointed out when discussing the *merging trend*. The thickness of the macrolayer is a function of the heat flux and usually lies in the range from 0.05 to 1 mm [15].

For i mechanisms which affect boiling heat transfer simultaneously, the heat flux q might be calculated as

$$q = \sum_i q_i \frac{S_i}{S} , \tag{1.12}$$

where q_i and S_i are the heat flux and surface area corresponding to a particular mechanism, respectively. It is common practice to relate S_i to the cross-sectional area of emerging bubbles $S_\mathrm{b} = \pi D_\mathrm{b}^2/4$. For instance, it is usually assumed that the transport of latent heat occurs above the area $S_\mathrm{lh} = N_\mathrm{n} S_\mathrm{b}$. The area of transient conduction is usually calculated as $S_\mathrm{tc} = C_\mathrm{tc} N_\mathrm{n} S_\mathrm{b}$, where the empirical coefficient of the bubble-influenced area $C_\mathrm{tc} > 1$. The coefficient C_tc is often fitted, so it provides the best agreement with the experimental data. The values of C_tc as low as 1.8 and as high as 7.5 were proposed by various researchers [15]. Nevertheless, $C_\mathrm{tc} \approx 4$ is often assumed in mechanistic models [20,34]. The *diameter of influence* $D_\mathrm{inf} = C_\mathrm{inf} D_\mathrm{b}$ is sometimes used, where $C_\mathrm{inf} = \sqrt{C_\mathrm{tc}}$ is given instead of C_tc. Natural convection is often assumed to occur above the area outside of S_tc, which would mean that $S_\mathrm{nc} = S - S_\mathrm{tc}$.

It is also important to point out that although different mechanisms and explanations of boiling heat transfer have been proposed by various researchers in the past, some of the most fundamental experimental observations related to boiling might be explained by more than just a single mechanism or model. For instance, it is common knowledge that for higher heat fluxes, HTC increases, and more bubbles are produced during boiling. Models based on latent heat would relate higher HTC to more latent heat being transported by individual bubbles. However, the increase of HTC might also be a consequence of more intense agitation due to growing and rising bubbles [35], which agrees with the models based on enhanced convection. Careful and accurate experimental observations have to be made to choose one model of boiling over others [36]. The modified Jakob number

$$\mathrm{Ja}' = \frac{c_{p\mathrm{L}}\, \varrho_\mathrm{L}\, \Delta T}{\Delta h_\mathrm{LG}\, \varrho_\mathrm{G}} \tag{1.13}$$

might be an indicator of whether the sensible heat transferred into liquid or the latent heat of phase change is more important with respect to the total heat transfer during boiling. Empirical data were used to obtain values of $\mathrm{Ja}' \approx 160$ for subcooled boiling of water [14], which means that during water boiling, the mechanisms related to the transfer of sensible heat to the boiling liquid are expected to be more important.

In the following parts of this section, individual mechanisms of boiling are introduced and discussed.

Mechanisms Related to Enhanced Convection

Models based solely on the idea of enhanced convection do not consider latent heat to be responsible for heat transfer during boiling. In other words, as Hsu and Graham [37] wrote, "*Bubble is a passive agent that keeps the fluid agitated but is never directly involved in the heat transfer process.*" With increasing number of emerging bubbles, the boundary layer in the vicinity of the heating surface gets disrupted by the turbulent motion induced by growing and collapsing bubbles as well as by the motion of liquid behind the wakes of rising bubbles.

During subcooled boiling of water, a film made of highly superheated liquid, which was approximately 125 µm thick and had a significant thermal resistance, was observed [38]. This film was, however, continuously disrupted by the bubbles emerging from the surface. According to Forster and Greif [14], the characteristic velocities of radial motion induced by growing bubbles, see Figure 1.1, are between 3 and 6 $\mathrm{m\,s^{-1}}$. Forster and Zuber [38] give a range

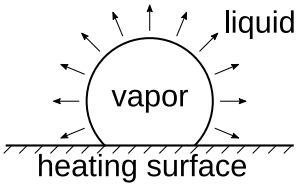

Figure 1.1: Radial motion of liquid induced by growing bubbles.

from 2.5 up to 4.6 m s^{-1}. They also noted that the agitation effect due to radial motion is a decreasing function of pressure and that smaller bubbles tend to grow more rapidly while larger bubbles grow more slowly. The contribution of small and large bubbles to the agitation of the fluid should, therefore, be comparable.

The basic idea that forced convection is responsible for boiling heat transfer was experimentally verified for various (but not all) liquids and boiling conditions. Jakob and Linke [39] were probably the first who proposed that boiling heat transfer is governed with the mechanism of forced convection and that heat is primarily transferred to the liquid and not to the vapor phase. Correlations commonly used for forced convection heat transfer were found to provide a satisfactory agreement with HTCs measured for pool boiling [38,39]. Jakob and Linke made their pioneering experiments with water already in 1933. Their work served as a stepping stone for various different and often used boiling correlations such as those of Rohsenow [20] or Forster and Zuber [38]. For developed flow boiling, the effect of macroscopic forced convection on heat transfer was observed to become negligible. The parameters of emerging bubbles (bubble diameters, bubble velocity, etc.), therefore, seem to be more important than the characteristics of the system and experimental conditions (geometry and dimensions of the heating surface, velocity of the flowing liquid, etc.). This is the reason why parameters related to bubbles are very often employed in the correlations based on enhanced convection [20]. It was already pointed out that such pool boiling correlations might be used even for flow boiling when boiling occurs in the fully developed regime.

Kim [13] reported that transient conduction and microconvection are the dominant mechanisms responsible for heat transfer during boiling of FC-72 and that heat transfer through the microlayer and three-phase contact line contributes less than 25 % to the total heat transfer. They used an array of microheaters and calculated the equivalent bubble diameter D_{eq} based on time integration of the supplied heat flux

$$\frac{\pi D_{\mathrm{eq}}^3}{6} \varrho_{\mathrm{g}} \Delta h_{\mathrm{LG}} = \int_0^t q\, S \,\mathrm{d}t \,. \tag{1.14}$$

According to their observations, heat transferred by the mechanism of microlayer evaporation and the contact line heat transfer are not sufficient for the observed bubble growth rates (they contribute at most 12.5 % to the total heat transfer) which means that transient conduction and microconvection in the boiling liquid are the dominant mechanisms of boiling heat transfer. The superheated liquid layer close to the heating surface was found to act as a reservoir and a source of energy for growing bubbles. However, the contribution of microlayer- and contact-line evaporation to the total heat transfer might become higher during subcooled boiling due to condensation occurring at the top of growing bubbles [13].

The term *enhanced convection* used in this work covers two separate mechanisms proposed by different authors, namely *microconvection* and the *pumping effect* of bubbles. The idea of *microconvection* is based on the turbulent convection of the boiling liquid in the vicinity of the heating surface. Because of that, researchers usually assume that the Nusselt number is a function of the Reynolds number and the Prandtl number, which are both related to the liquid phase, because it is assumed that the major part of heat is transferred from the surface into the liquid [20]. These three dimensionless criteria are typically used for forced convection heat transfer. The function is almost always assumed to be a power function

$$\mathrm{Nu} = C\, \mathrm{Re}^{m_1}\, \mathrm{Pr}_{\mathrm{L}}^{m_2} \,. \tag{1.15}$$

The coefficient C and the exponents m_1 and m_2 are usually found empirically. For instance, Kurihara and Myers [40] claim that based on experiments, dependency $\alpha \propto n_{\mathrm{n}}^{1/3}$ might be assumed. Due to the fact that the velocity in Re is proportional to n_{n}, the exponent $m_1 = 1/3$. The exponent $m_2 = -0.89$ was quantified from the data obtained with a constant value of the active nucleation site density n_{n}. This was latter commented on by Tien [41], according to whom $\alpha \propto n_{\mathrm{n}}^{m}$, where m lies in the range from 0.3 to 0.5. The value $m = 1/3$ can be used only when the effect of natural convection is significant (for instance when there is a low number of active nucleation sites). Nevertheless, Lienhard [42], who followed up Tien, again uses the value $m = 1/3$.

Although microconvection is considered to be an important boiling mechanism, it is most probably not the single one. Forster and Greif [14] pointed out that neither the *merging trend* observed for developed boiling nor the nullification of the effect of forced convection during developed flow boiling is adequately explained by models based solely on microconvection. For instance, the question arises why the effect of forced convection is suppressed in the regime of developed boiling even when forced convection has a higher velocity than the velocity of the liquid motion induced by growing bubbles. Because of that, Forster and Greif proposed that the so-called *pumping effect* of emerging bubbles is responsible for the enhanced heat transfer and is more important than microconvection. During the nucleation of bubbles, hot liquid is pushed away from the vicinity of the heating surface into the bulk, and colder liquid is brought from the bulk towards the heating surface. This mechanism should be 10 to 100 times more intense than forced convection and independent of the velocity of the liquid above the heating surface. It should also be more effective than diffusion by eddies which occurs during microconvection [14]. However, models based solely on the pumping effect also raise questions and contradict some of the experimental findings [37]. For instance, there are ambiguous opinions about the actual volume of liquid which is being replaced and thus participates in the enhanced heat transfer [35].

Mechanisms Related to the Transport of Latent Heat

For boiling of some liquids, significant temperature drops (around 10 or 20 °C) on the heating surface below the growing bubbles were recorded [35]. However, according to the heat transfer models based on enhanced convection, temperature drops should occur after the bubble departure and not during nucleation. This led some scientists to believe that transport of latent heat is the main mechanism of boiling heat transfer. Two most discussed mechanisms, which differ in the localization of the phase change, are mechanisms of *microlayer evaporation* and *contact-line heat transfer*. The microlayer and the contact-line region are schematically illustrated in Figure 1.2.

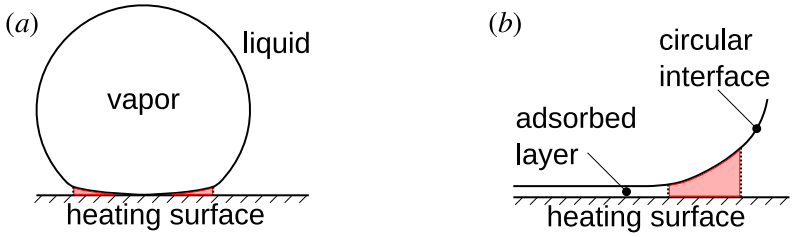

Figure 1.2: The localization of the boiling mechanisms related to the transport of latent heat highlighted in red color (the shapes and thicknesses are intentionally magnified): (*a*) the microlayer between the bubble base and heating surface, (*b*) the three-phase contact region located between the adsorbed liquid layer and the vapor–liquid interface whose curvature corresponds to the current bubble diameter.

Measurements of temperature course in time and optical measurements showed that a significant amount of heat is transferred during evaporation of the so-called *microlayer* which is a thin liquid layer with thickness from approximately 0.5 to about 30 µm trapped between growing bubbles and the heating surface [35,37]. Microlayer heat transfer seems to be especially important for quite large bubbles with diameters from 20 to 30 mm and growth periods higher than 50 ms [13]. Although models were proposed which assume that all heat is transferred from the heating surface to emerging bubbles through the vapor–liquid interface [43], it was experimentally proven that heat transfer during boiling is usually too high to be caused only by the transfer of latent heat stored in the bubbles departing from the heating surface [35,38]. It was also reported that the bubble diameters calculated from the balance between the heat transferred from the heating surface and the latent heat spent for vaporization are much smaller than those which were experimentally measured [13,44]. However, Zuber [21] distinguishes between two regimes of pool boiling: *boiling with*

isolated bubbles and *interference boiling*[3]. According to him, latent heat might be the most important mechanism with respect to total heat transfer when interference boiling is reached [21].

The initial thickness of the microlayer $\delta_{ml,0}$ might be estimated [45] using

$$\delta_{ml,0} \approx C \left(\nu_L \, t_g\right)^{1/2} , \tag{1.16}$$

where the coefficient $C \approx 0.8$, ν_L is the kinematic viscosity of the liquid phase, and t_g is the bubble growth period, which is discussed in Section 1.2 below. The initial thickness of the microlayer was also correlated for water as a function of the radial coordinate $\delta_{ml,0} = 4.66\, r^{0.69}$ and the maximum radius of the microlayer region as a function of the superheat $R_{ml,max} = 1.38 \times 10^{-2}\, \Delta T_{sat}^{1.8}$ [46]. The rate of microlayer evaporation should be almost independent of the heat flux (the transferred heat flux should only affect the duration of individual bubble cycles) [47].

For a steady state of evaporation, the theoretical evaporation mass flux (or the so-called Knudsen rate) w_{ev} might be estimated using the kinetic theory of evaporation

$$w_{ev} = \left(\frac{M_m}{2\,\pi\, R_m\, T_{sat}}\right)^{1/2} \left(p_{sat} - p_g\right) , \tag{1.17}$$

where, p_{sat} is the saturation pressure corresponding to T_{sat} and p_g is the pressure above the free surface of the boiling liquid [35,37,48]. The theoretical maximum heat flux, which is possible due to evaporation, is then

$$q = C_{ev}\, \Delta h_{LG}\, w_{ev,max} , \tag{1.18}$$

where the maximum evaporation mass flux $w_{ev,max}$ might be obtained with Equation (1.17) assuming that $p_g = 0$. The coefficient of evaporation C_{ev} is the correction which lowers the maximum evaporation mass flux $w_{ev,max}$ and depends on the boiling liquid. For instance, coefficients $C_{ev} = 0.040$, 0.02, and 0.045 were experimentally measured for water, ethanol, and methanol, respectively. Some researchers used the evaporation mass flux to combine the convective models of boiling heat transfer with the models of microlayer evaporation. According to these models, heat flows into the bubble from regions near the bubble base and is transported to the top of the bubble where condensation and release of heat into the liquid bulk occurs. Models were also developed which combine microlayer evaporation with forced convection [49].

The *three-phase contact line*, see Figure 1.2, is the zone where the liquid–vapor interface contacts the heating surface. The zone is typically about 1 µm wide [49–51] and contains a very thin liquid meniscus. The thickness of the liquid film in this zone was reported to be from 10 to 100 nm [52]. The three-phase line moves during each nucleation cycle as the liquid trapped between the growing bubble and the heating surface completely evaporates above some portion of the heating surface[4]. According to the model of Stephan and Hammer [49], it is possible to achieve a local heat flux of about 100 times the value of CHF in the contact-line region due to adhesion pressure and due to the strong curvature of liquid meniscus which induces capillary flow and also causes a local change of the liquid volatility. The three-phase region and its neighborhood are characterized by significant and fast local temperature drops and by very intense localized heat transfer. For example, numerical simulations of heat transfer during boiling of a propane–butane mixture predicted values of about 4×10^7 W m^{-2} near the three-phase contact line for the mean value of heat flux over the heating surface 2×10^4 W m^{-2} [53]. It was reported that evaporation at the three-phase contact line is stronger than microlayer evaporation for the liquid–surface combinations characterized by a low wettability [54].

[3] Interference boiling is reached for higher heat fluxes and is characterized by mutual bubble interactions and a decreased spacing between neighboring bubbles. During interference boiling, the distance between two neighboring bubbles is lower than two diameters of bubbles.

[4] To be exact, it does not completely evaporate due to strong adsorption bonds, but forms an adsorption layer with a negligible thickness of a few molecules as illustrated in Figure 1.2 on the previous page [49,52].

Transient Heat Conduction

The transient conduction of heat occurs when a colder liquid from the bulk gets into the vicinity of the heating surface. The movement of liquid is caused by the displacement of the superheated layers of liquid after bubbles depart from the surface. Because of this, heat transfer by transient conduction occurs mainly above active nucleation sites during the waiting periods between two successive nucleation cycles. When there is no bubble nucleation over some portions of the heating surface, the thermal boundary layer grows to a certain limiting thickness which is governed by the disruption of its topmost parts due to turbulence in the liquid [55]. Because of that, the liquid bulk which is far-enough from the heating surface is not affected by transient conduction.

The diameter of the area affected by transient conduction is often assumed to be twice the diameter of each departing bubble [34,56]. Nevertheless, various models based on transient heat conduction differ in the assumed area [35]. Some generalized transient heat conduction models were also developed which are based on the idea that the entire process of bubble growth in a superheated liquid layer might be described with equation for one-dimensional transient heat conduction

$$q = \lambda \, \frac{T_\mathrm{L} - T_\mathrm{int}}{\sqrt{\pi \, a_\mathrm{L} \, t}} \, . \tag{1.19}$$

The equation is valid only when the growing bubbles are completely surrounded by an initially isothermal liquid layer, which was found to be fulfilled for the values of the modified Jakob number $\mathrm{Ja}' \gg 1$, see definition (1.13). In Equation (1.19), the denominator $\sqrt{\pi \, a_\mathrm{L} \, t}$ is the penetration depth δ_p, T_int is the temperature at the vapor–liquid interface and T_L is the temperature of the superheated liquid layer [57]. Although the equation was originally formulated for planar surfaces, it might be used even for bubbles when $\delta_\mathrm{p}/R_\mathrm{b} \ll 1$. The fact that Equation (1.19) was found to be able to quite accurately predict the bubble growth [57] using a substitution

$$\Delta h_\mathrm{LG} \, \varrho_\mathrm{G} \, \frac{\mathrm{d}R_\mathrm{b}}{\mathrm{d}t} = \lambda \, \frac{T_\mathrm{L} - T_\mathrm{int}}{\sqrt{\pi \, a_\mathrm{L} \, t}} \tag{1.20}$$

without considering the effect of inertia and surface tension, seems to indicate that these effects might not be crucial for the bubble growth.

An influential mechanistic model was also developed by Mikic and Rohsenow [34]. The model is based solely on the mechanism of transient conduction, since no additional mechanisms were required for it to produce sufficiently accurate results. In the model, the heat flux due to transient conduction is averaged for a certain nucleation frequency

$$\bar{q} = f_\mathrm{n} \int_0^{t_\mathrm{n}} q \, \mathrm{d}t = f_\mathrm{n} \int_0^{1/f_\mathrm{n}} \frac{\lambda \, \Delta T}{\sqrt{\pi \, a_\mathrm{L} \, t}} \, \mathrm{d}t = 2 \, \frac{\lambda \, \Delta T}{\sqrt{\pi \, a_\mathrm{L}}} \, \sqrt{f_\mathrm{n}} \, . \tag{1.21}$$

The average heat flux $\bar{q}$ is then used for the calculation of the heat flux across the entire heating surface

$$q = \bar{q} \, \pi \, D_\mathrm{b}^2 \, n_\mathrm{n} \, , \tag{1.22}$$

where the area of influence is assumed to be $\pi \, D_\mathrm{b}^2$.

Despite both the models discussed above might provide accurate predictions of heat transfer and bubble growth rates, they lack physical background and were also reported to contradict some experimental findings. Perhaps the most significant objection against these models is that transient conduction was experimentally confirmed only during wall rewetting and not during the entire duration of individual nucleation cycles [13].

Natural Convection

Natural convection occurs over parts of the heating surface which are not influenced by the formation of bubbles [15,56]. Usual correlations verified for natural convection might be used for these regions as

well as for the segment of the boiling curve to the left of the ONB, see Figure 1. For instance, Mikic and Rohsenow [34] used the following correlations in their boiling model:

- For the laminar regime in the range of the Rayleigh number $10^5 < \mathrm{Ra} < 2 \times 10^7$

$$q = 0.54\, \varrho_\mathrm{L}\, c_{p\mathrm{L}} \left(\frac{\beta_\mathrm{vol}\, g\, \Delta T^5\, a_\mathrm{L}^3}{L_\mathrm{ch}\, \nu_\mathrm{L}} \right)^{1/4} , \tag{1.23}$$

  where the characteristic length is assumed to be the square root of the area of the heating surface $L_\mathrm{ch} = \sqrt{S}$.

- For the turbulent regime in the range $2 \times 10^7 < \mathrm{Ra} < 3 \times 10^{10}$

$$q = 0.14\, \varrho_\mathrm{L}\, c_{p\mathrm{L}} \left(\frac{\beta_\mathrm{vol}\, g\, \Delta T^4 a_\mathrm{L}^2}{\nu_\mathrm{L}} \right)^{1/3} . \tag{1.24}$$

  In Equations (1.23) and (1.24), β_vol is the volumetric expansion coefficient, and the definition of the Rayleigh number is

$$\mathrm{Ra} = \frac{\beta_\mathrm{vol}\, g\, (T_\mathrm{s} - T_\mathrm{L})\, L_\mathrm{ch}^3}{\nu_\mathrm{L}\, a_\mathrm{L}} . \tag{1.25}$$

1.2 The Most Important Parameters of Boiling

This section deals with the most important parameters related to pool boiling and its performance. Their influence on boiling heat transfer is discussed and methods suitable for their estimation are suggested. Approaches adopted towards these characteristic parameters are included in various models and theories of boiling. Although the output of correlations presented in this section is usually a single number, a distribution of values is typically recorded during the boiling process [57,58]. For various liquids, it was observed that the distributions of individual boiling parameters are usually close to normal Gaussian distributions [58].

Bubble Departure Diameter

In Section 1.1, I emphasized that the characteristics related to the emerging bubbles are often more important than the parameters of the heating surface such as its geometry or dimensions (especially for the fully developed regime of boiling). Also, the area affected by a certain boiling mechanism might be directly related to the area of bubbles which depends on the bubble diameter D_b. Knowledge of the bubble diameter is, therefore, an important requirement for the modeling and prediction of boiling performance.

The bubble departure diameter is most often calculated using the Fritz [59] correlation

$$D_\mathrm{b} = C_\mathrm{F}\, \vartheta_\mathrm{c}\, D_\mathrm{L} . \tag{1.26}$$

The coefficient $C_\mathrm{F} = 0.0208$ is usually used, because it provides the best agreement with experimental data obtained for various liquids [15,35,60]. The *contact angle* ϑ_c should be placed into (1.26) in degrees. It is the angle between the vapor–liquid interface and the heating surface measured through the liquid phase, as shown in Figure 1.3. During pool boiling of ordinary liquids on common surfaces, the advancing and receding contact angles are typically within only ±5°. Therefore, it is not important to distinguish between static and dynamic contact angles for these cases [31]. The contact angle is strongly dependent on the boiling liquid, on the material of the heating surface, and its micro- and nanostructure [61,62].

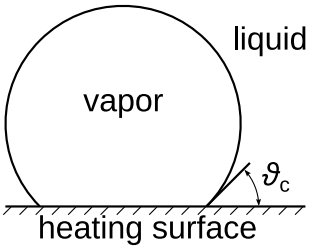

Figure 1.3: The contact angle ϑ_c.

The values of ϑ_c around 45° are typical for ordinary liquids and surfaces and recommended when the exact value of ϑ_c is not known [35]. The contact angle is also typically used to characterize the surface wettability[5] since measurement of the surface energy is much more difficult. According to the classical theories of boiling, the surfaces which have higher contact angles are typically characterized by increased CHF, decreased HTC, and also by increased superheat required for the initiation of boiling [65].

D_L in Fritz correlation (1.26) denotes the *Laplace diameter* of bubbles (or the so-called *capillary constant*)

$$D_L = \sqrt{\frac{\sigma}{g\,(\varrho_L - \varrho_G)}}\,. \tag{1.27}$$

The Laplace diameter is a thermophysical property of the boiling liquid (for example, for water at atmospheric pressure and saturation temperature, $D_L = 2.50$ mm). It might be considered as the diameter of a hemispherical cap for which the balance between the force of surface tension and buoyancy force is established, as a scale of the maximum thickness for which surface tension is able to overcome gravity, or as a scale of the distance to which a perturbation (such as the contact with the heating surface) might protrude [66,67]. The Laplace diameter is related to the Bond number (which is sometimes called the Eötvös number)

$$\mathrm{Bo} = \left(\frac{D_{eq}}{D_L}\right)^2, \tag{1.28}$$

where the equivalent bubble diameter D_{eq} is the diameter of a sphere with the same volume as the bubble. The Bond number is a useful indicator of whether bubbles tend to be spherical or deformed. When $\mathrm{Bo} \ll 1$, surface tension overcomes gravity, and bubbles are much more likely to be spherical. For $\mathrm{Bo} \gg 1$, nonspherical bubbles (ellipsoidal shapes, truncated shapes, caps, puddles, etc.) are expected [67].

Yagov [17] strongly criticizes the fundamental assumption of the Fritz correlation (1.26) that it is possible to calculate the bubble departure diameter from the balance of some chosen forces and labels it as "*delusion enjoyed by almost everyone*". He explains that for a fixed contact angle, there is an infinite number of bubble diameters, which satisfy the balance of some chosen forces and that the diameter D_b obtained with the Fritz correlation (1.26) should be considered as the radius of bubble at which the vapor–liquid interface loses its stability due to small perturbations. There also seems to be a disagreement between different authors on the role of surface tension during nucleation. According to some of them, surface tension holds the growing bubble on the heating surface. Others, on the contrary, suppose that it assists the bubble departure by making the bubble spherical [23]. Nevertheless, the bubble departure diameter D_b and the Laplace diameter D_L are very often used in various boiling correlations [20,21,68,69]. Most often, they are treated as the characteristic lengths of dimensionless numbers (most typically the Reynolds number and the Nusselt number).

According to some researchers, the bubble departure diameter D_b depends on the shapes of cavities and on the superheat [23,33], which is often neglected [44]. During boiling, a distribution of D_b is obtained rather than a constant value [57]. The equilibrium of buoyant- and surface-tension force, which is the basic assumption of the Fritz correlation (1.26), seems to play an important role at a low superheat and a low intensity of the agitation induced by bubbles [38]. The Fritz correlation (1.26) is then applicable and produces satisfactory results. However, for a higher superheat and also for subcooled boiling, dynamic forces (which capture the effects of inertia, flow resistance, and pressure) and the effects of induced

[5] Formerly, the effect of the surface wettability on boiling performance was often considered to be secondary or less important and was included in different parameters of the heating surface (most often its roughness). In the past, a typical common range of contact angles of different surfaces was from about 30° to 110°. Nowadays, it is common to reach contact angles lower than 10° for superhydrophilic and higher than 150° for superhydrophobic surfaces. The effects of contact angle, wettability, and wickability are currently considered to be among the most crucial with respect to the pool boiling performance [63]. Biphilic and superbiphilic surfaces, which consist of a pattern of hydrophobic zones placed on a hydrophilic substrate, are actively developed to simultaneously achieve intense stable nucleation and a strong resupply of the liquid to the heating surface [64].

agitation become more significant. This means that there are some cases for which the balance between the forces assumed by Fritz is not applicable for the prediction of D_b. This might be demonstrated using the experimental evidence obtained during boiling on both sides of a horizontal strip. It was observed that bubbles did not just slide over the bottom side of the strip, but were rather pushed away from it [38]. Clearly, radial forces and radial motion in the vicinity of the heating surface were more important than the effects of buoyancy and surface tension. The correlation of Cole and Shulman

$$D_\mathrm{b} = C_\mathrm{F}\,\vartheta_\mathrm{c}\,D_\mathrm{L}\left[1 + 0.0025\left(\frac{\mathrm{d}D}{\mathrm{d}t}\right)^{3/2}\right] \tag{1.29}$$

approaches the correlation of Fritz as $\mathrm{d}D/\mathrm{d}t \to 0$. It is also consistent with the findings of Forster and Zuber [38], because the growth rate $\mathrm{d}D/\mathrm{d}t$ increases with the superheat and because the intensity of agitation might be related to $\mathrm{d}D/\mathrm{d}t$. Simply said, dynamic forces hold emerging bubbles attached to the heating surface. The bubble departure diameter should, therefore, become larger relative to the result of the Fritz correlation. On the other hand, for subcooled boiling or for larger bubbles, intense condensation might occur at the top of the bubbles. For these cases, bubbles are generally smaller compared with the results of the Fritz correlation (1.26). Nevertheless, heat transfer might be intensified, since simultaneous evaporation at the base of a bubble and condensation at its top might be viewed as a short circuit for heat transfer [70].

Due to the discrepancy between the observed bubble diameters and the Fritz correlation (1.26), a plethora of alternative correlations were proposed. However, it seems that neither a generalized correlation nor a comprehensive model were found for the bubble departure diameter [31]. Different correlations for D_b produce a wide scatter of predicted values, see, for instance, significant spread of the correlated values in Figure 10 in the work of Mohanty and Das [71]. To close this section, I put forward three alternative and often used correlations which can be used to estimate D_b:

1. Kutateladze and Gogonin proposed that the bubble departure diameter D_b depends on the Laplace diameter D_L as well as on the modified Jakob number Ja', see definition (1.13), the Prandtl number of the liquid phase $\mathrm{Pr_L} = \nu_\mathrm{L}/a_\mathrm{L}$, and the Archimedes number

$$\mathrm{Ar} = \frac{(\varrho_\mathrm{L} - \varrho_\mathrm{G})\,\varrho_\mathrm{L}\,g\,D_\mathrm{L}^3}{\mu_\mathrm{L}^2} = \frac{\mathrm{Re}^2}{\mathrm{Fr}}\,\frac{\varrho_\mathrm{L} - \varrho_\mathrm{G}}{\varrho_\mathrm{L}}\,, \tag{1.30}$$

   which is the scale of the effects of gravitational and viscous forces on the motion of bubbles. The rightmost fraction $(\varrho_\mathrm{L} - \varrho_\mathrm{G})/\varrho_\mathrm{L}$ in Equation (1.30) is sometimes called the *buoyancy modulus*. The correlation of Kutateladze and Gogonin, given in [33], has the form

$$D_\mathrm{b} = 0.25\,D_\mathrm{L}\left[1 + 10^5 \times \left(\frac{\mathrm{Ja}'}{\mathrm{Pr_L}}\right)^2 \frac{1}{\mathrm{Ar}}\right]^{1/2} \tag{1.31}$$

   and should be valid in the range $5 \times 10^{-7} \le \mathrm{Ja}'^2\,\mathrm{Pr_L^{-2}}\,\mathrm{Ar}^{-1} \le 0.1$ [33].

2. In their mechanistic model, Mikic and Rohsenow [34] used the correlation developed by Cole and Rohsenow [72]

$$D_\mathrm{b} = C\,D_\mathrm{L}\,\mathrm{Ja}'^{5/4}\,. \tag{1.32}$$

   For water, the coefficient $C = 1.5 \times 10^{-4}$. For other liquids, $C = 4.65 \times 10^{-4}$ [34,72]. The definition of the modified Jakob number Ja' is slightly different from Equation (1.13) and uses the saturation temperature T_sat instead of the temperature difference ΔT in the numerator. The correlation should be valid for $\mathrm{Pr_L} < 0.2$ and should be used for commercial smooth heating surfaces with standard distributions of cavity sizes and for reduced pressures $p_\mathrm{red} < 0.2$ [35]. Although the modified Jakob number Ja' should be able to reflect the effect of pressure on D_b, the correlation was reported to fail for pressures higher than 5 MPa for which Ja' are low.

3. Dhir [31] discusses the correlation of Kocamustafaogullari for high pressures

$$D_\mathrm{b} = 2.64 \times 10^{-5}\, D_\mathrm{L} \left(\frac{\varrho_\mathrm{L} - \varrho_\mathrm{G}}{\varrho_\mathrm{G}} \right)^{0.9} \tag{1.33}$$

and the correlation of Gorenflo for high heat fluxes and elevated pressures

$$D_\mathrm{b} = C \left(\frac{\mathrm{Ja}'^4\, a_\mathrm{L}^2}{g} \right)^{1/3} \left(1 + \sqrt{1 + \frac{2\,\pi}{3\,\mathrm{Ja}'}} \right)^{4/3} , \tag{1.34}$$

where the value of coefficient C has to be selected according to the boiling liquid. For R12, R22 and Propane, the coefficient C = 14.7, 16.0 and 2.78, respectively [32]. The bubble departure diameter generally decreases with pressure [73].

Critical Bubble Radius, Radius of Cavities, and Initiation of Boiling

For a small superheat ΔT_sat, it is possible to calculate the critical radius of vapor nuclei using the equation

$$R_\mathrm{cr} = \frac{2\,\sigma}{p_\mathrm{b} - p_\mathrm{L}} = \frac{2\,\sigma\,T_\mathrm{sat}}{\Delta h_\mathrm{LG}\,\varrho_\mathrm{G}\,\Delta T_\mathrm{sat}} , \tag{1.35}$$

where p_b is the pressure of the vapor phase inside bubbles and p_L is the pressure of the liquid phase far-enough from the vapor–liquid interface. The difference $(p_\mathrm{b} - p_\mathrm{L})$ is called the *Laplace pressure*. Equation (1.35) might be derived after the integration of the Clausius–Clapeyron equation

$$\left(\frac{\mathrm{d}p}{\mathrm{d}T} \right)_\mathrm{sat} = \frac{\Delta h_\mathrm{LG}}{T \left(\varrho_\mathrm{G}^{-1} - \varrho_\mathrm{L}^{-1} \right)} \approx \frac{\Delta h_\mathrm{LG}\, p\, M_\mathrm{m}}{R_\mathrm{m}\, T^2} \tag{1.36}$$

over the interval of pressures from p_L to p_b and the corresponding interval of temperatures from T_sat (the saturated temperature of the liquid) to T_b (the temperature of the superheated liquid layer in the vicinity of the vapor–liquid interface).

Bubbles with radii $R < R_\mathrm{cr}$ are not able to grow in the liquid superheated by ΔT_sat and might eventually condense. Only bubbles with radii $R > R_\mathrm{cr}$ are able to grow at the superheat ΔT_sat. Also, a very important consequence of Equation (1.35) is that smaller bubbles require a larger superheat for them to grow because the critical radius R_cr is indirectly proportional to the superheat ΔT_sat.

Using Equation (1.35), one can calculate the superheat $\Delta T_\mathrm{sat,in}$ required for the initiation of bubble nucleation from a cavity which has a mouth radius R_c

$$\Delta T_\mathrm{sat,in} = \frac{T_\mathrm{sat}}{\Delta h_\mathrm{LG}\,\varrho_\mathrm{G}} \frac{2\,\sigma}{R_\mathrm{c}}\, K . \tag{1.37}$$

The coefficient K is the dimensionless maximum curvature [23]. For contact angles $\vartheta_\mathrm{c} \leq 90°$, the coefficient $K = 1$ due to the fact that the minimum bubble radius during nucleation $R_\mathrm{min} = R_\mathrm{c}/K$ is equal to the cavity mouth radius R_c. However, for $\vartheta_\mathrm{c} > 90°$, the coefficient $K = \sin(\vartheta_\mathrm{c})$, because the growing bubble spreads out of its cavity before its diameter reaches the cavity mouth diameter. Therefore, the radius of the vapor–liquid interface is higher and its curvature and the Laplace pressure lower compared with the previous case. For both cases, the nucleation process is illustrated in Figure 1.4. The minimum radius R_min is crucial for nucleation to occur, because it corresponds to the maximum curvature of the vapor–liquid interface and to the maximum Laplace pressure during nucleation events. It, therefore, determines whether a certain nucleation site is active during boiling.

Correlations based on Equation (1.37) were proposed which enable calculation of the superheat required for the initiation of boiling over the entire heating surface, i.e., the superheat required for ONB. A representative might be

$$\Delta T_\mathrm{sat,ONB} = \frac{1.6\,\sigma\,T_\mathrm{sat}}{R_\mathrm{c}\,\varrho_\mathrm{G}\,\Delta h_\mathrm{LG}} , \tag{1.38}$$

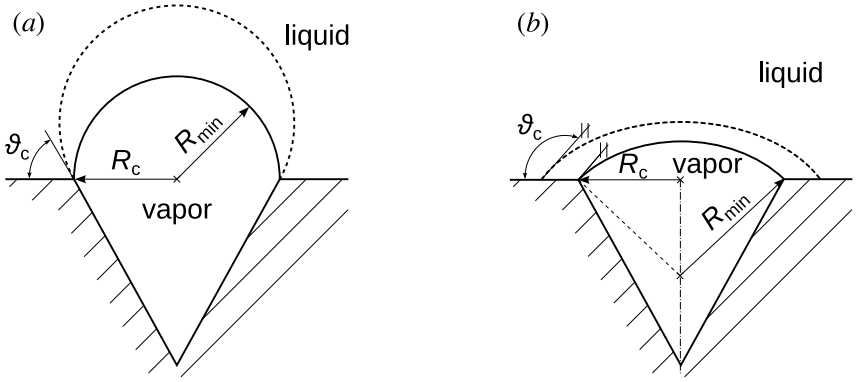

Figure 1.4: The process of bubble nucleation from a single cavity in the range of contact angle: (*a*) $\vartheta_c \leq 90°$, (*b*) $\vartheta_c > 90°$. The vapor–liquid interface depicted with the solid line represents the moment when the minimum diameter of bubble is reached during the nucleation cycle. The dashed line illustrates the following increase of the bubble diameter and the decrease of the interface curvature. Notice that for case (*a*), the minimum bubble radius $R_{min} = R_c$. On the other hand, for case (*b*), $R_{min} = R_c/\sin(\vartheta_c)$.

where R_c represents the average mouth radius of the cavities of the heating surface. It is possible to estimate $R_c \approx 0.8\, R_b$ using the bubble departure radius [74].

Hsu [75] published the criterion for the minimum and the maximum radius of active nucleation sites $R_{c,min}$ and $R_{c,max}$, respectively, above which nucleation occurs during boiling

$$R_{c,min} = \frac{\delta_t \sin\varphi}{2\,(1+\cos\varphi)} \left[1 - \xi - \sqrt{(1-\xi)^2 - \frac{8\,\sigma\, T_{sat}\,(1+\cos\varphi)}{\varrho_G\, \Delta h_{LG}\, \delta_t\, (\Delta T_{sub} + \Delta T_{sat})}} \right], \tag{1.39}$$

$$R_{c,max} = \frac{\delta_t \sin\varphi}{2\,(1+\cos\varphi)} \left[1 - \xi + \sqrt{(1-\xi)^2 - \frac{8\,\sigma\, T_{sat}\,(1+\cos\varphi)}{\varrho_G\, \Delta h_{LG}\, \delta_t\, (\Delta T_{sub} + \Delta T_{sat})}} \right]. \tag{1.40}$$

The relative subcooling $\xi = \Delta T_{sub}/(\Delta T_{sub} + \Delta T_{sat})$. For saturated boiling, $\xi = 0$. The angle of the vapor–liquid interface with respect to horizontal $\varphi = \vartheta_c + \beta_{cm}$, where ϑ_c is the contact angle, see Figure 1.3, and β_{cm} is the angle of the cavity mouth with respect to the horizontal direction (for a conical cavity, $\beta_{cm} = 0°$). The thickness of the thermal boundary layer δ_t for water during boiling is usually in the range from 0.1 mm to 1.0 mm [76–78]. The thickness δ_t around 0.3 mm is usually recommended for water in the literature [37,49]. For subcooled boiling of water, it was reported to increase to about 0.7 mm [79]. The thickness δ_t can also be estimated using either

$$\delta_t \approx \frac{\lambda_L}{\alpha_{nc}}, \tag{1.41}$$

where α_{nc} is the HTC due to natural convection [78,80], or using a suitable correlation valid for turbulent natural convection [23] such as

$$\delta_t = 7.14 \left[\frac{\nu_L\, a_L}{g\, \beta_{vol}\, (T_s - T_L)} \right]^{1/3}. \tag{1.42}$$

According to the standard theories of nucleation, the cavity mouth diameter determines the superheat required for the initiation of boiling above a certain cavity and the shape of the cavity determines its stability after the initiation [81]. Using Equations (1.39) and (1.40), the optimal radii of cavities which are able to provide stable nucleation spots might be calculated. For various contact angles during boiling of water at atmospheric pressure, optimal radii are in the range from 0.1 to 100 µm [55].

Radius of Bubbles and Bubble Growth in Time

A typical relation for the radius of a growing bubble as a function of time is $R(t) = C\,t^{1/2}$ [49,53]. However, based on the sensitive measurements performed with microelectromechanical systems (MEMS), it seems that the period of rapid growth occurs from $t = 0$ to 3 or 5 ms for which $R \propto t^{0.6}$. After this period, the growth continues at a slower rate and $R \propto t^{0.1}$. Nevertheless, the most often used correlations for $R(t)$ are based on the theoretical work of Scriven [82] who derived an equation which describes the growth of a spherically symmetric bubble surrounded with infinite liquid continuum made of a Newtonian binary mixture

$$R(t) = 2\,C_{\mathrm{g}}\,(a_{\mathrm{L}}\,t)^{1/2}\,, \tag{1.43}$$

where C_{g} is a dimensionless growth constant. Equation (1.43) might be applied for pool boiling of pure liquids and binary mixtures and should be valid for all stages of bubble growth with the exception of its earliest stages (Scriven's solutions are asymptotic) [83]. It was proposed and confirmed by measurements that functions $R(t)$ developed for spherical bubbles are also valid for hemispherical bubbles [84].

The following representatives of $R(t)$ correlations might be used:

1. The Labuntsov correlation [17]

$$R(t) = \sqrt{\frac{12\,\lambda_{\mathrm{L}}\,\Delta T\,t}{\Delta h_{\mathrm{LG}}\,\varrho_{\mathrm{G}}}}\,. \tag{1.44}$$

2. The correlation of Benjamin and Balakrishnan [85]

$$D(t) = C\,\mathrm{Ar}^{0.135}\,(\mathrm{Ja}'\,a_{\mathrm{L}}\,t)^{1/2}\,, \tag{1.45}$$

   where the constant $C = 1.55$ for water, CCl_4, and n-hexane. For n-pentane and acetone, $C = 1.55^{-1}$.

3. The correlation of Plesset and Zwick [86–88]

$$R(t) = \left(\frac{12}{\pi}\right)^{1/2} \mathrm{Ja}'\,(a_{\mathrm{L}}\,t)^{1/2}\,. \tag{1.46}$$

Nucleation Frequency and Bubble Growth Rate

The nucleation frequency

$$f_{\mathrm{n}} = \left(t_{\mathrm{w}} + t_{\mathrm{g}}\right)^{-1} \tag{1.47}$$

is related to the bubble-growth period t_{g} and the waiting period t_{w}. Both time periods are illustrated in Figure 1.5. Nucleation frequencies are typically estimated from image analysis either as the time difference between two successive initiations of bubbles or as the time between two departure events from a single nucleation site [89]. It is, unfortunately, quite difficult and subjective to estimate f_{n} [23]. Nucleation frequencies might also be evaulated from bubble departure diameters (measured or estimated) and functions of $R(t)$ presented in previous sections. Higher nucleation frequencies (together with higher nucleation site densities) prevent the formation of large vapor-covered areas, dryout, local overheating

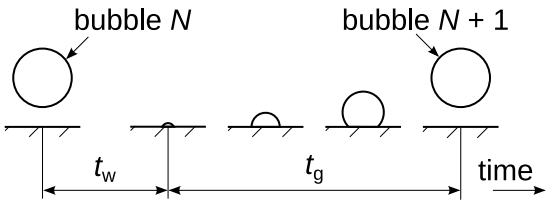

Figure 1.5: The waiting period t_{w} and the growth period t_{g} during the nucleation of two successive bubbles.

of heating surfaces, and transition to film boiling [55]. The nucleation frequency f_n increases with the superheat [23].

The bubble growth rate is given by the product $f_n D_b$ [58]. It is often used as a characteristic velocity u_{ch} in the definition of the Reynolds number. However, the assumption that $u_{ch} = f_n D_b$ is permissible only at lower heat fluxes. For higher heat fluxes, the immediate radius and radial velocity ($u_{ch} = 2 R \dot{R}$) should be used instead [38]. Nevertheless, the bubble growth rate $f_n D_b$ is often discussed and evaluated in the literature dealing with boiling, because it was found that it is more or less independent of various boiling conditions and system parameters[6]. In the study of Tolubinsky and Ostrovsky [58], the bubble growth rate was found to be independent of the parameters of the heating surface, heat flux (even when it increased of about five times), viscosity, and the Prandtl number of the boiling liquid [58]. According to Tolubinsky and Ostrovsky [58], $f_n D_b$ decreases with increasing pressure (almost solely due to decrease of D_b). On the other hand, Nishikawa [90] obtained a constant value of $f_n D_b$ for pressures from 5.5 kPa to 4 MPa. It was also reported that at low heat fluxes (although for some liquids, it might be as much as 80 % of the critical heat flux), both D_b as well as f_n are rather independent of the heat flux and that the enhancement of HTC observed at higher heat fluxes is primarily caused by the increased number of active nucleation sites [57]. The assumption of a constant bubble growth rate $f_n D_b$ means that smaller bubbles should be produced with higher frequencies and vice versa. A value of $f_n D_b = 7.7\ \mathrm{cm\,s^{-1}}$ was proposed for water and CCl_4 [21]. However, according to the results of precise experiments, rather the product $f_n D_b^m$ remains constant, where the exponent m varies in the range from 0.5 to 2 [15,33]. However, correlations based on the value of the exponent $m = 1$ still seem to be the most reliable [32].

The bubble growth rate $f_n D_b$ is very often correlated. The most often used is the correlation

$$f_n D_b = C \left[\frac{\sigma\, g\, (\varrho_L - \varrho_G)}{\varrho_L^2} \right]^{1/4} \tag{1.48}$$

which is based on the empirical equation of Peebles and Garber [91] for the velocity of a bubble rising in a gravitational field[7] [35]. According to the solution presented by Peebles and Garber, the coefficient

$$C = 1.18\, \frac{t_g}{t_g + t_w}\ . \tag{1.49}$$

For $t_g = t_w$, which is often assumed when the exact values of both time periods are not known, the value of the coefficient $C = 0.59$ might be obtained. This result is very close to another recommended value $C = 0.6$ based on experimental measurements [33,92]. However, for heat fluxes $q > 0.2\, q_{cr}$, it was observed that $t_w \ll t_g$ [35].

The Malenkov correlation

$$f_n D_b = \frac{1}{\pi} \left\{ \left[\frac{D_b\, g\, (\varrho_L - \varrho_G)}{2\, (\varrho_L + \varrho_G)} + \frac{2\,\sigma}{D_b\, (\varrho_L + \varrho_G)} \right] + \frac{q}{\varrho_G\, \Delta h_{LG}} \right\}^{1/2} \tag{1.50}$$

should be applicable even for boiling with mutually interacting bubbles. For the situations when bubbles do not mutually interact, the last fraction in Equation (1.50) should be omitted [33]. The correlation should cover situations when $t_w \approx t_g$ as well as when $t_w \ll t_g$ and should provide accurate results even outside the hydrodynamic regime of boiling.

The CFD software ANSYS Fluent [93] implemented the correlation

$$f_n^2 D_b = \frac{4}{3}\, \frac{g\, (\varrho_L - \varrho_G)}{\varrho_L} \tag{1.51}$$

[6] At least for the so-called *hydrodynamic regime* of boiling for which buoyancy and drag are the main force components acting on bubbles [35].

[7] Equation (1.48) is, therefore, valid only for the *hydrodynamic regime* of boiling introduced in the previous footnote.

into its mechanistic model of boiling called *the RPI model*. The correlation was formed for the so-called inertia-controlled bubble growth, which is characterized by a rapid growth of the bubbles of a hemispherical shape, and it is not applicable to subcooled boiling. For the so-called heat-transfer controlled bubble growth which may follow after the inertia-controlled growth and is characterized by rather spherical shapes of growing bubbles and smaller growth rates, the correlation of Mikic and Rohsenow

$$f_{\mathrm{n}}^{1/2}\, D_{\mathrm{b}} = 0.83\, \mathrm{Ja}'\, (\pi\, a_{\mathrm{L}})^{1/2} \tag{1.52}$$

is applicable [15,34].

Density of Active Nucleation Sites

The active nucleation site density

$$n_{\mathrm{n}} = \frac{N_{\mathrm{n}}}{S} \tag{1.53}$$

is defined as the number of active nucleation sites per unit area of the heating surface. The number of active sites N_{n} is often counted from the high-speed recordings of boiling. The active nucleation site density n_{n} is strongly affected by the superheat ΔT_{sat}. Proportionality $n_{\mathrm{n}} \propto \Delta T^m$ is often assumed, where the exponent m depends on the heating surface and usually lies in the range $4 \leq m \leq 6$ [23]. The density of active nucleation sites n_{n} increases with pressure [58].

Benjamin and Balakrishnan [85] formulated the correlation for the active nucleation site density

$$n_{\mathrm{n}} = 218.8\, \mathrm{Pr}_{\mathrm{L}}^{1.63}\, \frac{1}{K_{\mathrm{s}}}\, K_{\mathrm{R_a}}^{-0.4}\, (\Delta T_{\mathrm{sat}})^3\ , \tag{1.54}$$

where the parameter

$$K_{\mathrm{s}} = \sqrt{\frac{\lambda_{\mathrm{s}}\, \varrho_{\mathrm{s}}\, c_{p\mathrm{s}}}{\lambda_{\mathrm{L}}\, \varrho_{\mathrm{L}}\, c_{p\mathrm{L}}}} \tag{1.55}$$

contains the properties of the heating surface in the numerator and the properties of the boiling liquid in the denominator. The roughness parameter

$$K_{\mathrm{R_a}} = 14.5 - 4.5 \left(\frac{\mathrm{R_a}\, p}{\sigma}\right) + 0.4 \left(\frac{\mathrm{R_a}\, p}{\sigma}\right)^2\ . \tag{1.56}$$

Correlation (1.54) can be used for the following ranges of parameters: $1.7 < \mathrm{Pr_L} < 5$, $4.7 < K_{\mathrm{s}} < 93$, $0.02 < \mathrm{R_a} < 1.17$ µm, $5 < \Delta T_{\mathrm{sat}} < 25$ °C, $13 \times 10^{-3} < \sigma < 59 \times 10^{-3}$ N m^{-1}, $2.2 < K_{\mathrm{R_a}} < 14$.

In ANSYS Fluent [93], the empirical correlation

$$n_{\mathrm{n}} = C^n\, (T_{\mathrm{s}} - T_{\mathrm{sat}})^n\ , \tag{1.57}$$

is employed, where the empirical coefficients $n = 1.805$ and $C = 210$ m$^{-2/n}$ K^{-1}.

1.3 Correlations for Heat Transfer during Boiling of Pure Fluids

It is possible to relate the HTC during boiling either with the driving temperature difference ΔT or with the heat flux q using a simple empirical power function

$$\alpha = C\, \Delta T^m \tag{1.58}$$

or, alternatively,

$$\alpha = C'\, q^n\ . \tag{1.59}$$

From the general definition of HTC, see Equation (1.1), one can derive that $n = m/(1+m)$ and that $C' = C^{1-n}$. In his handbook, Stephan [33] lists the following exponents:

- For evaporation during laminar flows, $m = 1/4$ and $n = 1/5$.

- For evaporation during turbulent flows, $m = 1/3$ and $n = 1/4$.
- For nucleate boiling, $0.6 < n < 0.8$ (or $1.5 < m < 4$).

Although the aforementioned range of the exponent n for boiling is generally reported [14], it is only a very rough estimate which might not be applicable for some specific conditions. For example, although $0.6 < n < 0.7$ is a typical range for the developed boiling of common fluids, exponents n close to zero were obtained during boiling of viscous polymer solutions. This suggests that n is a function of either the molar mass or the viscosity of the boiling liquid [87]. Also, the coefficient C' in Equation (1.59) is strongly dependent on the boiling liquid and the heating surface and is often considered to be a function of other parameters characteristic for boiling (thermophysical properties, roughness, pressure, etc.) [94]. Some representatives of correlation (1.59) might be the correlation $\alpha = 1.95\, p^{0.24}\, q^{0.72}$ obtained during boiling of water at pressures 50 kPa $< p <$ 2 MPa [33] or the correlations of Nishikawa et al. [95] $\alpha = 7.14 \cdot 10^{-2}\, p^{0.2}\, q^{0.8}$ for water boiling at $6 < p < 196$ kPa and $\alpha = 1.28 \cdot 10^{-2}\, p^{0.3}\, q^{0.8}$ for ethanol boiling at $19 < p < 98$ kPa, which were both obtained during boiling on smoothed and cleaned copper surfaces. In all three listed correlations, the coefficient C' is assumed to be a function of pressure.

Although some dependence between multiple thermophysical properties or between various dimensionless criteria is typically considered in pool boiling heat transfer correlations, these correlations might be simplified to the basic form of Equation (1.58) or (1.59) [37]. In fact, one is able to create multiple correlations for given experimental data using completely different sets of thermophysical properties because of their mutual interdependence [52]. For example, it was observed that substances consisting of molecules with a higher molar mass M_m tend to have a lower thermal conductivity λ [96]. Therefore, the thermal conductivity λ might be substituted by M_m in pool boiling correlations. According to the handbook of Lienhard and Lienhard [70], the fact that some authors are able to successfully correlate the dependence of heat flux on the driving temperature difference for various materials of the heating surface and for a variety of boiling liquids is just a lucky coincidence, because according to Yamagata, $q \propto \Delta T^a\, n_\mathrm{n}^b$, where n_n is the density of active nucleation sites and empirical exponents are approximately $a \approx 1.2$ and $b \approx 1/3$. The luckiness is in the fact that for the most typical manufacturing processes, the cavities are distributed on the heating surface in such a way that $n_\mathrm{n} \propto \Delta T^c$, where $5 < c < 6$. This makes the heat flux during boiling on these surfaces roughly proportional to $q \propto \Delta T^3$ (more exactly $q \propto \Delta T^d$, where $2.87 \lesssim d \lesssim 3.20$). The Yamagata correlation also implies that for accurate calculation of q or α, accurate determination of n_n is required.

A plethora of heat transfer correlations can be found in the literature dealing with pool boiling. A relatively detailed list can be found in my master's thesis[8] [97] written in 2017. Regarding the main topic of this work, in this section, I discuss only several heat transfer correlations which were found to produce convenient results when they are used for the calculation of HTC during saturated boiling of mixtures. The method for employing these correlations in the calculation of HTC during boiling of mixtures is discussed in Section 2 of this thesis.

Correlation of Stephan and Abdelsalam

The Stephan and Abdelsalam correlation [69] is perhaps the most often used correlation for calculation of the HTC during saturated boiling of pure fluids and of the so-called *ideal* HTC during boiling of mixtures, which is introduced in Section 2.1. It was developed using regression analysis of wide set of experimental data obtained by numerous authors for different fluids (more than 5 000 data points in 72 works). The general form of the correlation is

$$\mathrm{Nu} = C \prod_i X_i^{a_i}\,, \tag{1.60}$$

[8] The thesis is written in Czech language.

where X_i is a suitably chosen and more or less arbitrarily defined dimensionless complex powered by the corresponding exponent a_i. Different dimensionless complexes are employed for different boiling fluids. Some correlations formed for specific boiling liquids are as follows:

- For water boiling at reduced pressures $10^{-4} \leq p_{\mathrm{red}} \leq 0.886$ assuming the value of contact angle $\vartheta_{\mathrm{c}} = 45°$

$$\mathrm{Nu} = 0.246 \times 10^7 \left(\frac{q\, D_{\mathrm{b}}}{\lambda_{\mathrm{L}}\, T_{\mathrm{sat}}}\right)^{0.673} \left(\frac{\Delta h_{\mathrm{LG}}\, D_{\mathrm{b}}^2}{a_{\mathrm{L}}^2}\right)^{-1.58} \left(\frac{c_{p\mathrm{L}}\, T_{\mathrm{sat}}\, D_{\mathrm{b}}^2}{a_{\mathrm{L}}^2}\right)^{1.26} \left(\frac{\varrho_{\mathrm{L}} - \varrho_{\mathrm{G}}}{\varrho_{\mathrm{L}}}\right)^{5.22} \tag{1.61}$$

  with a mean absolute error of 11.3 %.

- For hydrocarbons boiling at reduced pressures $5.7 \times 10^{-3} \leq p_{\mathrm{red}} \leq 0.9$ assuming $\vartheta_{\mathrm{c}} = 35°$

$$\mathrm{Nu} = 0.0546 \left[\left(\frac{q\, D_{\mathrm{b}}}{\lambda_{\mathrm{L}}\, T_{\mathrm{sat}}}\right)\left(\frac{\varrho_{\mathrm{G}}}{\varrho_{\mathrm{L}}}\right)^{0.5}\right]^{0.67} \left(\frac{\varrho_{\mathrm{L}} - \varrho_{\mathrm{G}}}{\varrho_{\mathrm{L}}}\right)^{-4.33} \left(\frac{\Delta h_{\mathrm{LG}}\, D_{\mathrm{b}}^2}{a_{\mathrm{L}}^2}\right)^{0.246} \tag{1.62}$$

  with a mean absolute error of 12.2 %.

- For cryogenic fluids boiling at reduced pressures $4 \times 10^{-3} \leq p_{\mathrm{red}} \leq 0.97$ assuming an extremely low contact angle reported in the literature $\vartheta_{\mathrm{c}} = 1°$

$$\mathrm{Nu} = 4.82 \left(\frac{q\, D_{\mathrm{b}}}{\lambda_{\mathrm{L}}\, T_{\mathrm{sat}}}\right)^{0.624} \left(\frac{\varrho_{\mathrm{s}}\, c_{ps}\, \lambda_{\mathrm{s}}}{\varrho_{\mathrm{L}}\, c_{p\mathrm{L}}\, \lambda_{\mathrm{L}}}\right)^{0.117} \left(\frac{\varrho_{\mathrm{G}}}{\varrho_{\mathrm{L}}}\right)^{0.257} \left(\frac{c_{p\mathrm{L}}\, T_{\mathrm{sat}}\, D_{\mathrm{b}}^2}{a_{\mathrm{L}}^2}\right)^{0.374} \left(\frac{\Delta h_{\mathrm{LG}}\, D_{\mathrm{b}}^2}{a_{\mathrm{L}}^2}\right)^{-0.329} \tag{1.63}$$

  with a mean absolute error of 14.3 %.

- For refrigerants boiling at reduced pressures $3 \times 10^{-3} \leq p_{\mathrm{red}} \leq 0.78$ assuming $\vartheta_{\mathrm{c}} = 35°$

$$\mathrm{Nu} = 207 \left(\frac{q\, D_{\mathrm{b}}}{\lambda_{\mathrm{L}}}\right)^{0.745} \left(\frac{\varrho_{\mathrm{G}}}{\varrho_{\mathrm{L}}}\right)^{0.581} \left(\frac{\nu_{\mathrm{L}}}{a_{\mathrm{L}}}\right)^{0.533} \tag{1.64}$$

  with a mean absolute error of 10.6 %.

The universal correlation was also proposed

$$\frac{\alpha\, D_{\mathrm{b}}}{\lambda_{\mathrm{L}}} = 0.23 \left(\frac{q\, D_{\mathrm{b}}}{\lambda_{\mathrm{L}}\, T_{\mathrm{sat}}}\right)^{0.674} \left(\frac{\varrho_{\mathrm{G}}}{\varrho_{\mathrm{L}}}\right)^{0.297} \left(\frac{\Delta h_{\mathrm{LG}}\, D_{\mathrm{b}}^2}{a_{\mathrm{L}}^2}\right)^{0.371} \left(\frac{\varrho_{\mathrm{L}} - \varrho_{\mathrm{G}}}{\varrho_{\mathrm{L}}}\right)^{-1.73} \left(\frac{a_{\mathrm{L}}^2\, \varrho_{\mathrm{L}}}{\sigma\, D_{\mathrm{b}}}\right)^{0.35} \tag{1.65}$$

for all the substances mentioned above boiling at reduced pressures $10^{-4} \leq p_{\mathrm{red}} \leq 0.97$. A mean absolute error of 22.3 % was reported for correlation (1.65). According to the authors, correlations (1.61) to (1.64) should be preferred over correlation (1.65) due to relatively higher error of the universal correlation [69].

In all the five listed correlations, the Nusselt number is related to the emerging bubbles and is defined as

$$\mathrm{Nu} = \frac{\alpha\, D_{\mathrm{b}}}{\lambda_{\mathrm{L}}}\,, \tag{1.66}$$

where the bubble departure diameter D_{b} should be calculated with the Fritz correlation (1.26). Thome and Shakir [98] recommend that one should still use the values of contact angles assumed by Stephan and Abdelsalam even when the actual contact angle differs (they themselves measured the contact angle for water on their copper surface of about 85°, but still used the value $\vartheta_{\mathrm{c}} = 45°$ for the calculation of bubble departure diameter D_{b}).

Correlation of Gorenflo and Kenning

For boiling of various fluids, especially refrigerants and various hydrocarbons, the correlation of Gorenflo and Kenning [99]

$$\frac{\alpha}{\alpha_{\mathrm{ref}}} = \left(\frac{q}{q_{\mathrm{ref}}}\right)^m F_p \left(\frac{P_{\mathrm{L}}}{P_{\mathrm{L,ref}}}\right)^{0.6} \left(\frac{\mathrm{R_a}}{\mathrm{R_{a,ref}}}\right)^{2/15} \left(\frac{\lambda_{\mathrm{s}}\, \varrho_{\mathrm{s}}\, c_{ps}}{\lambda_{\mathrm{Cu}}\, \varrho_{\mathrm{Cu}}\, c_{p\mathrm{Cu}}}\right)^{1/4}. \tag{1.67}$$

might be applied for reduced pressures $p_{red} < 0.9$. The correlation is based on the theorem of corresponding states[9]. The exponent m and the factor F_p depend only on the reduced pressure p_{red}:

- For water, the exponent $m = 0.9 - 0.3\, p_{red}^{0.15}$ and the factor $F_p = 1.73\, p_{red}^{0.27} + 6.1\, p_{red}^2 + 0.68\, p_{red}^2/(1 - p_{red}^2)$.
- For organic liquids, $m = 0.95 - 0.3\, p_{red}^{0.3}$ and $F_p = 0.7\, p_{red}^{0.2} + 4\, p_{red} + 1.4\, p_{red}/(1 - p_{red})$.

The so-called property ratio $P_L = (dp/dT)_{sat}/\sigma$ is tabulated for various single-component fluids in [99]. The reference value of the property ratio $P_{L,ref} = 1\ \mu m^{-1}\ K^{-1}$. The last fraction in correlation (1.67) is the ratio between the properties of the heating surface and properties of a reference copper heating surface. To calculate α from correlation (1.67), one has to know the reference heat transfer coefficient α_{ref}. This coefficient is either tabulated, estimated from a suitable correlation, or has to be measured during boiling under the following reference conditions: $p_{red,ref} = 0.1$, $q_{ref} = 20\ kW\ m^{-2}$, and $R_{a,ref} = 0.4\ \mu m$.

Correlation of Nishikawa

The Nishikawa [100] correlation

$$\alpha = \frac{31.4\, p_{cr}^{1/5}}{M_m^{1/10}\, T_{cr}^{9/10}} \left(8\, \frac{R_a}{R_{a,ref}}\right)^{0.2\,(1-p_{red})} \frac{p_{red}^{0.23}\, q^{4/5}}{(1 - 0.99\, p_{red})^{0.9}} \tag{1.68}$$

is frequently used mostly, but not only, by Japanese researchers. It is based on the theorem of corresponding states and was originally developed for boiling of R11, R21, R113, and R114 on horizontal copper surfaces in the roughness range $0.022 \le R_p \le 4.31\ \mu m$ at reduced pressures $0.03 \le p_{red} \le 0.98$. The reference roughness $R_{a,ref} = 0.4\ \mu m$. The molar mass M_m needs to be in $(kg\ kmol^{-1})$, the roughness R_a in μm, p_{cr} in pascals, and T_{cr} in kelvins.

Correlation of Cooper

The Cooper [96] correlation

$$\alpha = 55\, p_{red}^{0.12 - 0.2\, \log R_p}\, (-\log p_{red})^{-0.55}\, M_m^{-0.5}\, q^{0.67} \tag{1.69}$$

for various liquids is also based on the theorem of corresponding states. In his previous work, Cooper [101] proposed and verified that boiling correlations might be simplified to the basic form

$$\alpha = C\, q^n\, p_{red}^{m_1}\, T_{red}^{m_2}\, (1 - T_{red})^{m_3}\ , \tag{1.70}$$

where the coefficient C and exponents m_i and n are fitting parameters. This simplification was found to produce errors below ±5 % relative to various verified pool boiling correlations. Correlation (1.69) is a modified version of (1.70) which includes the effect of roughness of the heating surface (the effect of roughness is assumed to decrease with increasing pressure) and also the implicit effect of the thermal conductivity of the boiling liquid, which is lower for liquids composed of larger molecules characterized by a higher value of the molar mass M_m. The unit of M_m in correlation (1.69) is $(kg\ kmol^{-1})$. The roughness $R_p \approx 0.4\, R_a$. It is recommended to use the value $R_p = 1\ \mu m$ when the exact value of R_p (μm) is not known. The correlation was formed for various media in the range of molar masses $2 \le M_m \le 2\,000\ kg\ kmol^{-1}$ boiling at reduced pressures $0.001 \le p_{red} \le 0.9$.

[9] The theorem of corresponding states is based on an assumption that every thermophysical property γ related to a certain reference value γ_{ref} is a function of the reduced pressure, i.e., $\gamma/\gamma_{ref} = f(p_{red})$. Due to the fact that HTC is often assumed to be a certain function of various thermophysical properties, there is no need to measure these properties at elevated pressures, because it might be simply assumed that the ratio of actual HTC α to the reference value of HTC α_{ref} depends on the reduced pressure, i.e., $\alpha/\alpha_{ref} = f'(p_{red})$ [18]. The reference value α_{ref} is, however, needed to apply the theorem of corresponding states. Sometimes, the values of α_{ref} obtained from experiments are tabulated [99]. Otherwise, α_{ref} has to be measured or calculated with a suitable correlation. The empirical function f' depends on the boiling liquid and might often include another boiling parameters (most typically the heat flux or the roughness of the heating surface) [18,33].

Correlation of Mostinski

The Mostinski [102] correlation

$$\alpha = 0.00417\, p_{\mathrm{cr}}^{0.69}\, q^{0.7}\, F_p \tag{1.71}$$

proposed in 1963 is also often used, despite the fact that it is the oldest correlation in this list. It is often presented in the alternative form

$$\alpha = 1.167 \cdot 10^{-8}\, p_{\mathrm{cr}}^{2.3}\, \Delta T_{\mathrm{sat}}^{2.333}\, F_p^{3.333}\ . \tag{1.72}$$

In both correlations, the critical pressure p_{cr} is in kPa. The empirical equation for the pressure-correction factor

$$F_p = 1.8\, p_{\mathrm{red}}^{0.17} + 4\, p_{\mathrm{red}}^{1.2}\, 10\, p_{\mathrm{red}}^{10} \tag{1.73}$$

was also presented by Mostinski. Instead of Equation (1.73), Palen [103] recommends to use the two following alternative functions for design purposes:

- For reduced pressures $p_{\mathrm{red}} \leq 0.2$,

$$F_p = 2.1\, p_{\mathrm{red}}^{0.27} + \left[9 + \left(1 - p_{\mathrm{red}}^2\right)^{-1}\right] p_{\mathrm{red}}^2\ . \tag{1.74}$$

- For reduced pressures $p_{\mathrm{red}} > 0.2$,

$$F_p = 1.8\, p_{\mathrm{red}}\ . \tag{1.75}$$

Correlation of Yagov

The Yagov [52] correlation is based on the approximative model of boiling. Based on the assumption that the total transferred heat flux consists of the convective heat flux and of the heat flux transferred due to strong evaporation near the three-phase contact region, correlation

$$q = 3.43 \times 10^{-4}\, \frac{\lambda_{\mathrm{L}}^2\, \Delta T^3}{\nu_{\mathrm{L}}\, \sigma\, T_{\mathrm{sat}}} \left(1 + \frac{\Delta h_{\mathrm{LG}}\, \Delta T\, M_{\mathrm{m}}}{2\, R_{\mathrm{m}}\, T_{\mathrm{sat}}^2}\right)\left(1 + \sqrt{1 + 800\, C_{\mathrm{b}}} + 400\, C_{\mathrm{b}}\right) \tag{1.76}$$

was formed, where the boiling parameter

$$C_{\mathrm{b}} = \frac{\Delta h_{\mathrm{LG}}\, (\varrho_{\mathrm{G}}\, \nu_{\mathrm{L}})^{3/2}}{\sigma\, (\lambda_{\mathrm{L}}\, T_{\mathrm{sat}})^{1/2}} \tag{1.77}$$

is dimensionless and the saturation temperature T_{sat} is in kelvins. Correlation (1.76) has to be solved iteratively, because the HTC α is contained in the temperature difference $\Delta T = q/\alpha$.

2. Pool Boiling of Multicomponent Mixtures

Separation processes are probably the most obvious application of boiling of multicomponent mixtures. Besides that, mixture boiling can also be employed in various industrial sectors, such as chemical, petrochemical, pharmaceutical, air-separation, refrigeration, or air-conditioning applications [104]. This specific type of boiling might also bring several advantages over boiling of single-component fluids:

- Desired thermophysical properties and improved behavior might be achieved by mixing fluids which are about to be enhanced. For example, mixtures of water and ethylene glycol avoid the risk of freezing, mixtures of highly flammable and nonflammable fluids can reduce flammability to an acceptable level [105] and maintain the desired thermophysical properties, etc.
- The employment of mixtures might be more ecological compared with single-component fluids, as they are able to significantly reduce the global-warming potential [106,107].
- Some mixtures might have a beneficial effect on the boiling process. They were particularly reported to significantly increase the critical heat flux [108], to stabilize the boiling process, or to make the heat removal from heating surfaces more uniform [109,110]. For some mixtures, enhancement of pool boiling HTC was achieved [107,111,112].
- Thermodynamic cycles which involve boiling of mixtures might have higher efficiencies compared with the cycles operating with single-component fluids. For instance, the Kalina cycle, which is based on the circulation of ammonia–water mixture, is considered as a replacement of the classic water-based Rankine cycle for power plants [113]. Improvements in the cooling capacity and cooling efficiency were also reported [106].
- Flow boiling of suitable mixtures is able to reduce the thermodynamic irreversibility (lower the loss of exergy) for apparatuses such as heat exchangers, heat pumps, and thermal engines which operate either with cold- and heat sources of variable temperature [6,88,114] or with a high temperature difference between the heat source and heat sink [115].

On the other hand, boiling of mixtures also brings several disadvantages compared with boiling of pure fluids. The following are the most serious:

- The heat transfer coefficient is reduced compared with boiling of single-component fluids [116].
- For a more accurate estimation of the boiling performance (or some other quantities, such as cooling performance), detailed knowledge is often required of the thermophysical properties of the mixture and of its phase equilibriums. However, there is a higher uncertainty in the properties and general behavior of mixtures which makes their performance and behavior much more unpredictable relative to pure fluids.

In this section, boiling of binary miscible mixtures of liquids is discussed. In other words, the mixtures are assumed to form a homogeneous solution of two liquid components. Researchers usually investigate the following four groups of miscible mixtures: 1) mixtures of organic liquids, 2) aqueous solutions, 3) refrigerants contaminated by oils, and 4) mixtures containing surfactants [107]. In the literature, most of the experiments with boiling of mixtures were conducted on tubular heating surfaces at atmospheric pressure [107].

2.1 Deterioration of Heat Transfer during Boiling of Mixtures

HTC is a strong function of the composition of the boiling liquid [117]. Although there are some exceptions (noted in Section 2.4), the HTC during boiling of multicomponent mixtures is generally reduced compared with boiling of pure liquids. More precisely, the HTC of the boiling mixture α is lower than the so-called *ideal heat transfer coefficient* α_{id}, as illustrated in Figure 2.1. The decrease of HTC during mixture boiling

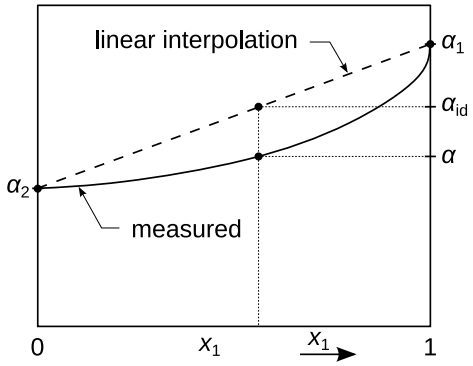

Figure 2.1: The decrease of the HTC α relative to the value of the *ideal* HTC α_{id}.

is a general trend which was confirmed for different types of mixtures (with negative, zero, and positive deviations from Raoult's law), various roughnesses, inclination angles, pressures and other experimental conditions [118]. The following two methods might be used for the calculation of the *ideal* HTC:

1. Interpolation between the HTCs of pure components α_i. It is common practice to number the components with respect to their volatility ($i = 1$ for the most volatile, $i = 2$ for the second most volatile, etc.). Generally, two interpolation formulas are used. The vast majority of researchers assume that the *ideal* HTC is equal to the harmonic mean

$$\frac{1}{\alpha_{id}} = \sum_i \frac{x_i}{\alpha_i} , \tag{2.1}$$

   where the weight factor x_i is the molar fraction of component i and α_i is the HTC during boiling of the pure component i under the same conditions as those of the boiling mixture, see α_1 and α_2 in Figure 2.1. The formula is based on the linear interpolation of the *ideal* superheat and is derived in Section 2.3 below. Besides that, some authors [119] use a simpler linear interpolation of HTC

$$\alpha_{id} = \sum_i x_i \alpha_i , \tag{2.2}$$

   which is illustrated in Figure 2.1 for an unspecified binary mixture. Sporadically, some researchers [120] use mass fractions ω_i as weight coefficients in Equations (2.1) and (2.2) instead of x_i, but the majority prefer the molar fractions x_i. The values of α_{id} obtained with Equations (2.1) and (2.2) do not differ much from each other, except for when there is a large difference between the HTCs of pure components α_i [107,119]. For each heat transfer correlation formulated for such mixtures, one should always follow the way chosen by its authors for the calculation of α_{id}.

2. Calculation of α_{id} using pure-fluid correlations such as those given in Section 1.3. In this case, the thermophysical properties of the boiling mixture are inserted into the selected correlation. The calculated value α_{id} then represents the HTC during boiling of a hypothetical single-component fluid with the same thermophysical properties as those of the boiling mixture. The advantage of this method is that it can be applied even when the HTCs of pure components are not available. The main drawback is that knowledge of various thermophysical properties of the mixture is required which can be very laborious to obtain, especially at elevated pressures [112,119,121] or for mixtures which contain some highly volatile components [122,123]. Because of that, interpolated properties of the boiling mixture are very often used. Although more or less complicated formulas for estimation of individual properties can be found in the literature, linear interpolation

$$\bar{\gamma} = \sum_i x_i \gamma_i \tag{2.3}$$

   is typically used, where $\bar{\gamma}$ is the interpolated value of a certain mixture property and γ_i is the property of the pure component i. However, interpolation (2.3), should be used with caution, because some

mixtures evince strong nonlinear variations of some of their properties with respect to their composition. This is noticeable in Figure 2.2 which was adopted from the paper of Fujita and Tsutsui [124]. Quite often, only one or two properties of the boiling mixture exhibit nonlinear dependency on its composition [125]. However, HTCs estimated with heat transfer correlations are strongly dependent on input values of thermophysical properties [126]. Although significant errors might be produced, linear interpolation (2.3) is still very often used even for the mixtures characterized by a strong nonlinearity of their properties. Various corrections are employed afterward to reduce the error caused by the linear interpolation of nonlinear properties. This approach is often questioned and criticized [125,127]. Furthermore, the mixture correlations and models which include empirical constants and various correction factors cannot be easily extended to include mixtures with higher number of components [119].

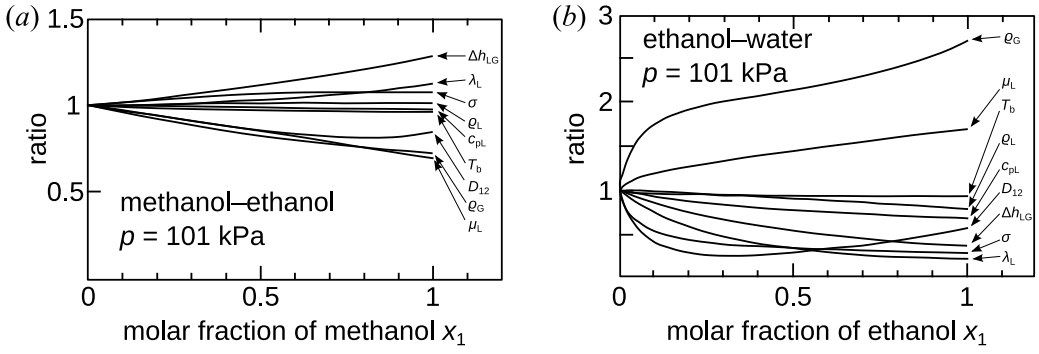

Figure 2.2: The dependence of nine different thermophysical properties on the liquid composition: (*a*) sufficiently linear variations for the mixtures of methanol–ethanol, (*b*) nonlinear and stronger variations for the mixtures of ethanol–water. Adopted from Fujita and Tsutsui [124].

2.2 Mixture Effects

The term *mixture effects* is used for the various factors responsible for the deterioration of HTC observed during boiling of mixtures [124,125,128]. All *mixture effects* might be viewed as manifestations of the local or global shifts of the liquid composition, which is the most characteristic aspect of mixture boiling [6,118]. The shifts are caused by the fact that during boiling, bubbles are enriched with the more volatile component(s) due to the vapor–liquid equilibrium. The concentration of the less volatile component(s), therefore, increases in the liquid layer close to the heating surface. Some researchers consider the growing bubbles to be completely surrounded with the liquid depleted of the more volatile component(s) [98,125]. Others suggest that the depletion occurs more locally, for instance only in the microlayer [129,130]. Nevertheless, the local surplus of the less volatile component(s) in the liquid layer has a crucial impact on the process of boiling. The following *mixture effects* are the most often considered by researchers:

- The saturation temperature of the liquid layer depleted of the more volatile component(s) increases. Because of this, the actual superheat of the liquid layer in the vicinity of the heating surface becomes lower than the superheat ΔT_{sat} which is related to the saturation temperature of the liquid bulk, see definition (1.3). The superheat ΔT_{sat}, which is often called *the apparent superheat,* is therefore greater than the actual driving temperature difference during boiling of mixtures [119,127].
- The diffusive mass flux of the more volatile component(s) from the bulk is induced by the concentration gradient between the liquid bulk and the liquid layer close to the heating surface. The boiling performance thus becomes dependent on mass transfer which is, however, a much slower and less intense process

compared with heat transfer. The impact of mass transfer on HTC might be viewed as an additive heat transfer resistance [98,117].

- The local changes of various thermophysical properties which are caused by the different local compositions of the boiling mixture. For some mixtures, these changes are rather linear. For others, they can be highly nonlinear and difficult to predict [124].
- The mixture composition affects various boiling parameters, such as the energy needed for bubble nucleation, the number of active nucleation sites, the bubble departure diameter, the nucleation period, and others [125,131]. For example, bubble departure diameters are expected to be lower due to the mass transfer resistance which limits the supply of more volatile component(s) to the interface of the growing bubbles.
- The retardation of the fundamental mechanisms of heat transfer, such as microlayer evaporation or microconvection, might occur [131]. For example, the effects of inertia and surface tension on nucleation were reported to be diminished (more precisely, they are important only during the initial expansion of bubble nuclei) as the bubble growth quickly becomes limited by mass transfer [82].

Currently, there are no methods which would enable one to predict the contribution of individual *mixture effects* to the total decrease of heat transfer for individual cases of mixture boiling [132]. Nevertheless, the first and the second item on the list above seem to be the most important, as they are the most often discussed and considered in the literature. This is also the reason why various correlations for mixture boiling typically involve quantities and properties mostly related to mass transfer regardless of their difficult measurement and their strong variation with composition [6,107].

2.3 Heat Transfer Coefficients During Boiling of Multicomponent Mixtures

During pool boiling of mixtures, the heat transfer coefficient α, for a given heat flux q, can be defined with Newton's cooling law, see Equation (1.1). For saturated boiling of mixtures, the superheat

$$\Delta T_{\mathrm{sat}} = T_{\mathrm{s}} - T_{\mathrm{b}} \tag{2.4}$$

is calculated according to the Equation (1.3), where the saturation temperature T_{sat} was substituted by the *bubble-point* temperature T_{b} of the liquid bulk. The *bubble-point* temperature is a function of the composition of the liquid phase, as depicted in Figure 2.3. Therefore, the heat transfer coefficient might be defined as

$$\alpha = \frac{q}{\Delta T_{\mathrm{sat}}} = \frac{q}{T_{\mathrm{s}} - T_{\mathrm{b}}} \,. \tag{2.5}$$

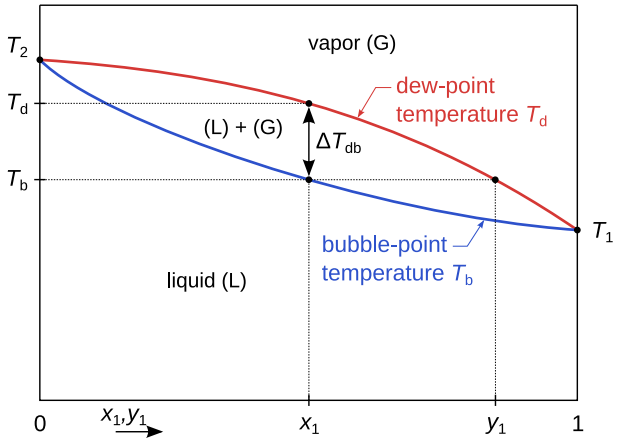

Figure 2.3: A typical phase diagram of an unspecified binary mixture.

Due to the fact that the HTC during saturated boiling of mixtures is lower than the *ideal* HTC, a higher superheat is required for a given heat flux q compared with the so-called *ideal superheat* which is, by definition, calculated using linear interpolation

$$\Delta T_{\mathrm{id}} = \sum_i x_i \, \Delta T_{\mathrm{sat},i} \; . \tag{2.6}$$

The *ideal superheat* ΔT_{id} might be viewed as the temperature difference, which would theoretically have been reached during mixture boiling, if the *mixture effects* had not affected the boiling performance. Alternatively, it might also be regarded as the driving temperature difference $\Delta T_{\mathrm{id}} = T_{\mathrm{s}} - T_{\mathrm{b,s}}$, where $T_{\mathrm{b,s}}$ denotes the local elevated *bubble-point* temperature of the liquid layer in the vicinity of the heating surface, which is affected by the *mixture effects*. The temperature $T_{\mathrm{b,s}}$ is often implicitly included in HTC correlations. For binary mixtures, it might be approximated as

$$T_{\mathrm{b,s}} \approx T_{\mathrm{s}} + \frac{\mathrm{d}T_{\mathrm{b}}}{\mathrm{d}x_1} \left(x_{1\mathrm{s}} - x_1 \right) \, , \tag{2.7}$$

where $x_{1,\mathrm{s}}$ represents the liquid composition in the liquid layer affected by the *mixture effects* and might be calculated employing the film theory of diffusion [98,117]. The temperature difference $\Delta T_{\mathrm{sat},i}$ in Equation (2.6) is the superheat reached during boiling of pure component i at a given heat flux q. It can, therefore, be calculated by rearranging Newton's cooling law, see Equation (1.4),

$$\Delta T_{\mathrm{sat},i} = \frac{q}{\alpha_i} \, , \tag{2.8}$$

where α_i is either measured or calculated with a suitable correlation for boiling of the pure component i at the same heat flux q as the boiling mixture [112] and, perhaps, at the same pressure p (Gorenflo et al. [133], however, suggests the same reduced pressure p_{red} to maintain the corresponding state of the pure fluid and of the mixture).

The *ideal* HTC might then be defined with respect to the *ideal* superheat

$$\alpha_{\mathrm{id}} = \frac{q}{\Delta T_{\mathrm{id}}} \; . \tag{2.9}$$

The combination of Equations (2.6), (2.8) and (2.9) gives

$$\alpha_{\mathrm{id}} = \frac{q}{\sum_i x_i \, \Delta T_{\mathrm{sat},i}} = \frac{q}{\sum_i x_i \, \frac{q}{\alpha_i}} = \left(\sum_i \frac{x_i}{\alpha_i} \right)^{-1} \tag{2.10}$$

which is the interpolation formula given by Equation (2.1). Due to the fact that $\alpha < \alpha_{\mathrm{id}}$ during boiling of mixtures, the superheat $\Delta T_{\mathrm{sat}} = T_{\mathrm{s}} - T_{\mathrm{b}}$ needs to be higher than the *ideal* superheat ΔT_{id} for a given heat flux q, which comes naturally by comparing Equations (2.5) and (2.9). In other words, as the *bubble-point* temperature T_{b} locally rises due to the depletion of the more volatile component(s) in the liquid layer close to the heating surface, the temperature of the heating surface T_{s} has to increase to maintain the driving temperature difference between the heating surface and the liquid layer for the given q. Therefore, the equation

$$\Delta T_{\mathrm{sat}} = \Delta T_{\mathrm{id}} + \Delta T_{\mathrm{add}} = \Delta T_{\mathrm{id}} \, (1 + F) \tag{2.11}$$

might be formed, where $\Delta T_{\mathrm{add}} > 0$ is the *additional* superheat required to overcome the local rise of the *bubble-point* temperature T_{b}. The correction factor

$$F = \frac{\Delta T_{\mathrm{add}}}{\Delta T_{\mathrm{id}}} \tag{2.12}$$

represents the relative increase of superheat due to the *mixture effects* with respect to the *ideal* superheat ΔT_{id}. According to Equation (2.11), the *apparent* superheat ΔT_{sat} is always greater than the *ideal* superheat ΔT_{id}.

However, the *ideal* superheat ΔT_{id} is the actual driving temperature difference of heat transfer during boiling of mixtures[10].

Combining Equations (2.5), (2.9) and (2.11), the relation

$$\alpha = \frac{\alpha_{\mathrm{id}}}{1+F} \tag{2.13}$$

might be obtained. Equation (2.13) is important, because the correction factor F is typically correlated in the heat transfer correlations developed for boiling of mixtures (some of these correlations are discussed in Section 2.5).

The alternative equation

$$\alpha = F_\alpha \, \alpha_{\mathrm{id}} \tag{2.14}$$

can also be found, although less often, in the literature, where the coefficient $F_\alpha < 1$ represents the relative decrease of HTC. The value of F_α typically lies between 0.8 and 1.0, although values lower than 0.4 are also quite common (especially for mixtures with a high difference in the boiling temperatures of pure components). From the last two equations, it follows that

$$F_\alpha = \frac{1}{1+F} \, . \tag{2.15}$$

For a fixed composition of the boiling mixture, HTCs are generally less dependent on the pressure and heat flux with respect to boiling of pure fluids. Simultaneously, for a higher heat flux, HTC was reported to be a stronger function of composition for binary as well as ternary mixtures [124,134–136]. See, for example, Figure 2.4 adopted from Inoue et al. [134] which was obtained during boiling of the mixture of R22 and R11 at the elevated pressure of 0.7 MPa. Although for this specific mixture, the lowest HTCs were obtained for $\omega_1 \approx 0.3$, the composition, for which the lowest HTCs are achieved, is unique to each individual boiling mixture.

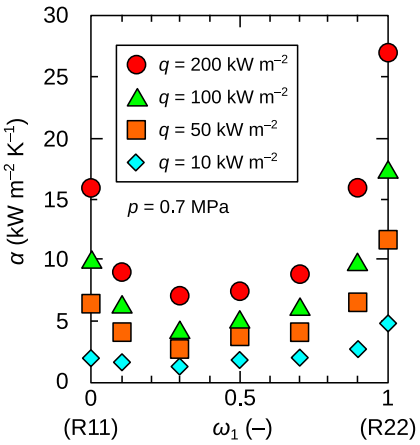

Figure 2.4: HTCs measured for R22–R11 mixtures at four various heat fluxes. Adopted from Inoue et al. [134].

The correction factor F as well as the *additional* superheat ΔT_{add} are usually assumed to be linear functions of the equilibrium molar fraction difference $|y_i - x_i|$ [109,117,137] and of the *boiling range* [98,108,124]

$$\Delta T_{\mathrm{db}} = T_{\mathrm{d}} - T_{\mathrm{b}} \, , \tag{2.16}$$

which is the temperature difference between the *dew-point* and the *bubble-point* temperature, as illustrated in Figure 2.3. Parameter $|y_i - x_i|$[11] is the difference between the molar fraction of the vapor y_i which is in equilibrium with the liquid in the bulk, which has molar fraction x_i, see y_1 which corresponds to x_1 in Figure 2.3. The equilibrium molar fraction difference $|y_i - x_i|$ typically represents the effect of the mass transfer resistance for the more volatile component(s) to reach the layers of liquid close to the heating surface [124]. HTC was reported to decrease more strongly with increasing $|y_i - x_i|$. This trend is further

[10] It is, in fact, needed to use ΔT_{id} instead of ΔT_{sat} to obtain reliable results when using the various universal correlations valid for pure liquids as well as mixtures. For example, it is possible to use the correlation of Plesset and Zwick, see Equation (1.46), for mixtures, but ΔT_{id} has to be employed instead of ΔT_{sat} to calculate the modified Jakob number Ja′, see definition (1.13).

[11] The absolute value allows to express the difference either for the more volatile component i of the investigated mixture for which $y_i - x_i > 0$, or for the less volatile component j for which $y_j - x_j = (1 - y_i) - (1 - x_i) = x_i - y_i < 0$. This might become useful, as, for instance, azeotropic mixtures have a positive difference on one side of the azeotrope, but a negative difference on the other side. Based on his experiments, Afgan [109] explicitly states that HTC does depend on the equilibrium molar fraction difference regardless of whether it is positive or negative.

accented under higher pressures [112]. The dependence of HTC on both ΔT_{db} and $|y_i - x_i|$ might vary for different boiling mixtures [138]. Because of that, additional parameters are often needed to capture the observed trends [73]. For example, Nahra and Næss [127] observed a better correspondence of HTC to the trend of ΔT_{db} relative to the trend of $|y_1 - x_1|$ for the mixtures of methanol and 1-pentanol. However, for specific mixtures (for instance, ammonia–water mixtures), completely different and unpredictable HTC trends were reported with respect to both ΔT_{db} and $|y_1 - x_1|$ which is typically caused by higher values of either ΔT_{db} or $|y_1 - x_1|$ [115]. In contrast, the boiling behavior of the mixtures characterized by lower values of ΔT_{db} and $|y_1 - x_1|$ might be comparable to boiling of single-component liquids [139]. Some representatives of such mixtures might be methylethylketone–benzene, benzene–cyclohexane or methylethylketone–cyclohexane for which ΔT_{db} is lower than 1 °C.

2.4 Specific Cases of Mixture Boiling

In this section, four specific topics related to boiling of mixtures are briefly outlined which are important to better understand the topic of mixture boiling.

Boiling of Binary Mixtures

In the literature, binary mixtures are the main target of research. For the mixtures with three or more components, heat transfer data are inconsistent, limited, and insufficient for generalized conclusions [132]. There is no verified theory which could be used to estimate relative contributions of individual components to the total drop of HTC for the mixtures consisting of more than two components [124]. Also, it is a very difficult task to measure the vapor–liquid equilibriums for these mixtures. This is also the reason why most heat transfer correlations are presented only for binary mixtures [124,127]. Applicability of correlations developed for binary mixtures to the mixtures with more components is uncertain and generally not advised. The conclusions of the works, which studied whether the decrease of HTC is smaller or larger for ternary mixtures relative to binary mixtures, are ambiguous.

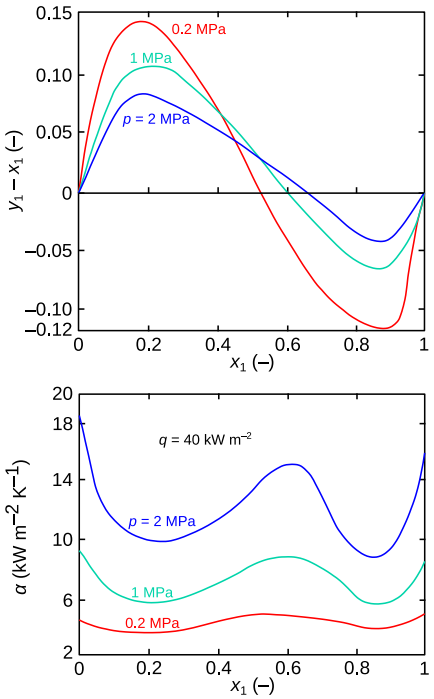

Figure 2.5: HTC deterioration for the binary azeotropic mixture of R23 and R13. Adopted from Jungnickel et al. [116].

Boiling of Azeotropic Mixtures

For an azeotropic mixture precisely at the azeotropic composition, there should be no observable drop of HTC and the measured HTC should be equal to the *ideal* HTC [140]. This is due to the fact that for the azeotrope, the vapor and liquid phases are of the same composition and the *mixture effects* are, therefore, absent. HTC at the azeotropic composition can thus be calculated with pure-fluid correlations, see Section 1.3. Furthermore, for the binary azeotropic mixtures which are not at their azeotropic composition, it is necessary to evaluate all concentrations (typically the molar fractions x_i and y_i) with respect to the azeotrope and not to the both pure components. The decrease of HTC occurs on both sides of the azeotrope, as demonstrated in Figure 2.5 adopted from the work of Jungnickel et al. [116]

for boiling of azeotropic mixtures of R23 and R13 at three different pressures[12]. Heat transfer is influenced by the *mixture effects* on both sides of the azeotrope [116].

Enhancement of Heat Transfer for Specific Mixtures

Occasionally, enhancement of HTC with respect to the *ideal* HTC α_{id} is observed during boiling of specific mixtures [105,141]. The improvement is often explained as a consequence of favorable variation of the different thermophysical properties of the mixture, which promotes boiling. The most often discussed properties responsible for the increase of HTC are: the saturation vapor pressure [109,141], the surface tension [130], the contact angle [142] or the wettability [143]. Some typical representatives of mixtures which, only for certain compositions, were reported to exhibit HTC enhancement are: water with small additions of oil or alcohols [107,111,144], oil in refrigerants [107], the mixtures of water and ethylene glycol [145], the mixtures of water and glycerin [130,143], amine–water solutions [130], liquids with additions of surfactants [144], or the mixtures of various coolants [105].

Subcooled Pool Boiling of Mixtures

In Section 1, it was discussed that although the *boiling* HTC might increase with the subcooling, a drop of the *total* HTC is expected during subcooled boiling. In the literature, subcooled boiling has been investigated mostly for pure single-component fluids. Regarding mixtures, there are couple of studies [147–149] which focused on the enhancement of CHF during subcooled boiling of the mixtures of refrigerants. Other studies [150,151] aimed to reach the so-called *microbubble emission boiling*[13]. However, the effect of subcooling on HTC during boiling of binary mixtures has not yet been systematically studied, and the number of works is very limited. Hu et al. [152] observed that a higher subcooling is capable of enhancing the *total* HTC and CHF for the self-rewetting[14] mixtures of heptanol and water. On the other hand, Hui and Thome [146] measured a decrease of the *total* HTC at higher subcoolings for ethanol–water and ethanol–benzene mixtures, see Figure 2.6. However, the drop of the *total* HTC caused by the increased subcooling was lower compared with pure fluids. Furthermore, the measured HTCs were reported to be rather insensitive to the nucleation site density during subcooled boiling.

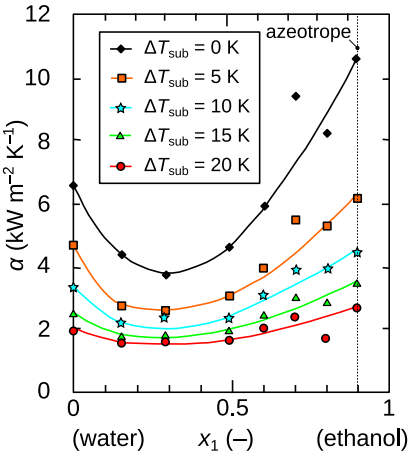

Figure 2.6: HTCs measured for various compositions and subcoolings of ethanol–water mixtures. Adopted from Hui and Thome [146].

[12] Leaving aside azeotropic mixtures, Figure 2.5 on the previous page also shows an interesting trend that lower HTCs and a weaker dependency of HTC on the composition were measured for mixtures of R23 and R13 when pressure was decreased. Although a similar trend was also obtained for different mixtures, for instance the mixtures of methylethylketone–toluene [117], an opposite trend was also observed. For example, Arima et al. [114] measured higher HTCs and slightly stronger dependencies of HTC on the composition during boiling of ammonia–water mixtures at 0.7 MPa relative to the HTCs obtained at 1.5 MPa.

[13] Microbubble emission boiling is the regime of subcooled boiling characterized by the emission of relatively small bubbles. The regime is typically reached at a high subcooling of about 50 K. For some specific single-component liquids and mixtures, this regime was reported to increase the boiling performance [150,151].

[14] During boiling of self-rewetting fluids, the so-called *inverse Marangoni flow* of the liquid is induced during boiling. Because of the inverse Marangoni flow, the liquid is spontaneously flowing from the cold regions of the liquid bulk towards the hot spots on the heating surface due to the gradient of surface tension. The gradient is caused by local changes of concentration (solutal Marangoni flow) and temperature (thermal Marangoni flow). For self-rewetting fluids, the thermal Marangoni flow acts in the same direction as the solutal Marangoni flow [153,154].

2.5 Correlations for Heat Transfer during Boiling of Mixtures

Afgan [109] lists three basic approaches which are typically employed for estimation of HTC during boiling of mixtures:

1. The solution of the Rayleigh–Plesset equation[15] which is then used to calculate the bubble growth rate and the movement of the vapor–liquid interface in a liquid binary mixture. This solution was presented by Scriven [82] for spherical bubbles growing in a binary mixture, see Equation (1.43), and latter picked up by van Stralen [86] who derived a modified version of Equation (1.46) valid for binary mixtures

$$R(t) = \left(\frac{12}{\pi}\right)^{1/2} \mathrm{Ja}' \, \mathrm{Sn} \, (a_\mathrm{L} \, t)^{1/2} \,, \tag{2.17}$$

   where the Scriven number

$$\mathrm{Sn} = \frac{(\mathrm{d}R/\mathrm{d}t)_\text{mixture}}{(\mathrm{d}R/\mathrm{d}t)_\text{pure-fluid}} = \left[1 - (y_1 - x_1)\left(\frac{a_\mathrm{L}}{D_{12}}\right)^{1/2}\left(\frac{c_{p\mathrm{L}}}{\Delta h_\mathrm{LG}}\right)\left(\frac{\mathrm{d}T_\mathrm{b}}{\mathrm{d}x_1}\right)\right]^{-1} \tag{2.18}$$

   is the ratio between the bubble growth rate in the mixture and in a hypothetical pure fluid with the same thermophysical properties [88,121,155]. For single-component fluids and azeotropes, Sn = 1. Otherwise, Sn < 1, because the last fraction in definition (2.18) is negative [121,139]. Besides $R(t)$ and $(\mathrm{d}R/\mathrm{d}t)$, the Scriven number Sn was found to influence other boiling parameters as well. This is due to the fact that the Scriven number might be viewed as a correction for the loss of *available* superheat due to the *mixture effects* which have crucial impact not only on the course of $R(t)$, but also on other boiling parameters (the influence of the *mixture effects* on HTC was already discussed in Section 2.3). For instance, according to the correlation of Calus and Leonidopoulos [120], $F_\alpha = \mathrm{Sn}$, where the coefficient F_α was defined in Equations (2.14) and (2.15). Later, Thome [156] analytically derived that $F_\alpha = \mathrm{Sn}^{7/5}$. A different example might be the simple dependency

$$\frac{D_\mathrm{b}}{D_\mathrm{b,id}} = \mathrm{Sn}^{4/5} \tag{2.19}$$

   often used for the calculation of the bubble departure diameter D_b during boiling of mixtures, where $D_\mathrm{b,id}$ is the bubble departure diameter of a hypothetical single-component liquid with the same thermophysical properties as those of the boiling mixture [88]. Typically, minimum bubble departure diameters (and Scriven numbers) during boiling of mixtures are expected for the compositions which closely correspond to the highest equilibrium molar fraction difference $|y_1 - x_1|$ [88]. Similarly to pure fluids, bubble departure diameters during mixture boiling were also reported to decrease with pressure [73].

2. Relate the drop of HTC to the boiling range ΔT_db [98,121,124]. For instance, Thome [121] assumes that the *additional* superheat equals to the boiling range ($\Delta T_\mathrm{add} = \Delta T_\mathrm{db}$). Based on Equation (2.12), the correction factor F thus equals to

$$F = \frac{\Delta T_\mathrm{db}}{\Delta T_\mathrm{id}} \,. \tag{2.20}$$

   The assumption is based on the idea that for $q \to q_\mathrm{cr}$, all the liquid that approaches the heating surface evaporates. The vapor composition y_1 should, therefore, be equal to the composition of the liquid in the bulk x_1. Or, in other words, the increase of the temperature of the liquid layer affected

[15] The Rayleigh–Plesset equation describes the movement of the bubble interface in a liquid continuum. It is a second-order differential equation written in spherical coordinates, which can be obtained from the r-component of the Navier–Stokes equations using the substitution for the radial velocity $u_r = (R/r)^2 \, u_R$, where u_R is the radial velocity of the vapor–liquid interface of a bubble which has an instantaneous radius R, and using the substitution $p_\mathrm{b} = p_\mathrm{L} + 2\,\sigma/R + 4\,\mu_\mathrm{L}\,\dot{R}/R$ which is based on the fact that the pressure inside a bubble is given by the local pressure of the surrounding liquid, by the Laplace pressure, and by normal viscous stresses which all act against the bubble growth [67].

by the *mixture effects* is limited by the *dew-point* temperature [138]. The liquid layer near the heating surface has concentration $x_1(T_d)$, as depicted in Figure 2.7. One can then estimate that the maximum

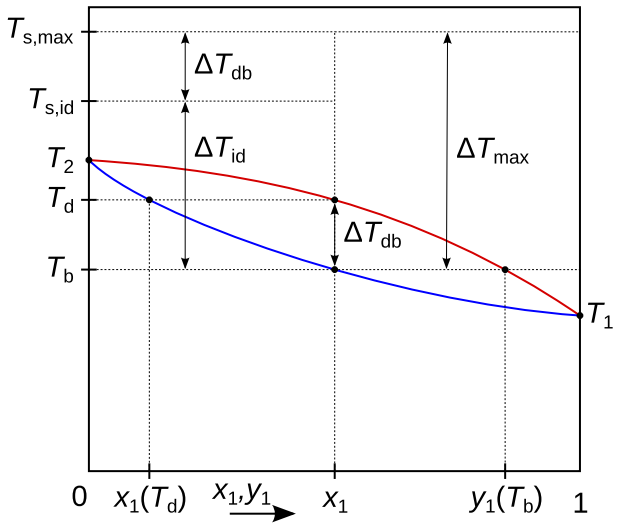

Figure 2.7: The maximum superheat $\Delta T_{max} = \Delta T_{id} + \Delta T_{db}$ reached for a binary mixture at $q \to q_{cr}$.

superheat $\Delta T_{max} = \Delta T_{id} + \Delta T_{db}$. Although this assumption might seem valid only for heat fluxes close to q_{cr} (or, at best, for intermediate and relatively high heat fluxes), correlation (2.20) was found to be still quite accurate for heat fluxes far below q_{cr}. Thome guesses that its accuracy for lower heat fluxes might be due to microlayer evaporation being the dominant heat transfer mechanism [121]. In fact, it is even possible to use correlation (2.20) to predict the upper limit of possible deterioration of heat transfer for any heat flux. The result should then be interpreted as a conservative (and possibly underpredicted) estimation of HTC. To obtain more accurate results, the *additional* superheat ΔT_{add} can be related to the boiling range ΔT_{db} using a simple relation [118,157]

$$\Delta T_{add} = C\, \Delta T_{db} \,. \tag{2.21}$$

The coefficient C is then a function of the heat flux q and should satisfy two limiting conditions: $C \to 0$ for $q \to q_{ONB}$, where q_{ONB} is the heat flux at ONB required for initiation of boiling, and $C \to 1$ for $q \to q_{cr}$ (which is the limiting case assumed by Thome). Combining Equations (2.12) and (2.21), the correction factor F can be calculated using

$$F = C\, \frac{\Delta T_{db}}{\Delta T_{id}} \,. \tag{2.22}$$

3. Relate the change of HTC to the change of the critical cavity radius R_{cr}, see Equation (1.35). According to this approach, minimum heat transfer coefficient obtained for a given heat flux at a certain composition can be predicted considering the variation of $(\partial p/\partial T)_{sat}$ which causes a certain change of the critical cavity radius R_{cr}, see Section 1.2.

Similarly to pure fluids, there is a plethora of mostly empirical or semi-empirical heat transfer correlations which were developed for boiling of mixtures. Only the most important, often-used, and influential correlations for boiling of binary mixtures are presented in this section. The correction factor F, see Equations (2.11) and (2.13), is by far the most often correlated quantity in the literature dealing with boiling of mixtures.

Correlation of Stephan and Preusser

According to the correlation of Stephan and Preusser [137], the correction factor F linearly depends on the equilibrium molar fraction difference $|y_i - x_i|$. For a mixture which consists of N components

$$F = \left| \sum_{i=1}^{N-1} C_{iN} \, (y_i - x_i) \right| , \tag{2.23}$$

where the component N is the one with the lowest volatility (or with the highest boiling point). Each coefficient C_{iN} has to be found empirically. For binary mixtures, the correlation is simply

$$F = C_{12} \, |y_1 - x_1| \tag{2.24}$$

which was proposed already in 1969 by Stephan and Körner [158]. Stephan and Preusser [137] correlated the coefficient C_{12} in correlation (2.24) as a function of pressure

$$C_{12} = C'_{12} \left(0.88 + 0.21 \times 10^{-5} \, p \right) \tag{2.25}$$

in the range 0.1 MPa $\leq p \leq$ 1 MPa. The coefficient C'_{12} is the value of C_{12} at 100 kPa. The value of the coefficient C'_{12} has to be selected for each individual mixture and lies in the range $0.42 \leq C'_{12} \leq 3.56$. When the exact value is not known, an average value has to be used. Hewitt [15] gives $C'_{12} = 1.53$ which is the average value for approximately 150 different mixtures. According to Stephan [33], $C'_{12} = 1.4$. Ünal [159] agrees with $C'_{12} = 1.53$, but only if the condition $|y_1 - x_1| < 0.635$ is satisfied.

In correlation (2.24), the coefficient C_{12} is not a function of q, as was suggested by later studies [116,121]. Correlations (2.23) and (2.24) were not verified in the range of molar fractions $x_1 < 0.021$ [159].

Later, Happel and Stephan [160] proposed that

$$F = C_{12} \, |y_1 - x_1|^n \, , \tag{2.26}$$

where the coefficient C_{12} and the exponent n have to be found experimentally for a given mixture, heat flux, and pressure.

Correlation of Schlünder

In 1982, Schlünder [117,161] presented his semi-theoretical correlation for multicomponent mixtures

$$F = \frac{\alpha_{\mathrm{id}}}{q} \left\{ \sum_{i=1}^{N-1} \left(T_{\mathrm{sat},N} - T_{\mathrm{sat},i} \right) (y_i - x_i) \left[1 - \exp\left(\frac{-C_0 \, q}{\varrho_{\mathrm{L}} \, \Delta h_{\mathrm{LG}} \, \beta_{\mathrm{L}}} \right) \right] \right\} \tag{2.27}$$

which can be simplified for binary mixtures

$$F = \frac{\alpha_{\mathrm{id}}}{q} \left(T_{\mathrm{sat},2} - T_{\mathrm{sat},1} \right) (y_1 - x_1) \left[1 - \exp\left(\frac{-C_0 \, q}{\varrho_{\mathrm{L}} \, \Delta h_{\mathrm{LG}} \, \beta_{\mathrm{L}}} \right) \right] . \tag{2.28}$$

The correlation had a strong influence on other researchers. It is based on the film model of diffusion and on mixing laws. Schlünder neglected the mass transfer resistance in the vapor phase and assumed that the equilibrium molar fraction difference $|y_i - x_i|$ at the vapor–liquid interface is the same as in the bulk. This assumption was reported to be "*very inexact*", especially when the molar fraction x_i is located near the ends of the bubble-point curve [98,125]. The so-called scaling factor C_0 is the ratio of the area of the heating surface to the surface of the vapor–liquid interfaces of all emerging bubbles, which is multiplied by the proportion of the heat flux used to form the bubbles [117]. If it is assumed that all of the heat is transferred to the vapor bubbles, then $C_0 \approx 1$, which is the value recommended by Schlünder. The mass transfer coefficient for the liquid phase $\beta_{\mathrm{L}} \approx 2 \times 10^{-4}$ m s^{-1} was also recommended by Schlünder [117]. This value was measured for the mixtures of SF_6 and R12, but is also typical for falling-film vaporization

of organic mixtures and for physical and chemical absorption either in aerated agitated vessels, in bubble columns or in jet reactors [117]. Gorenflo [162] suggests to use $C_0/\beta_l = 1 \times 10^4\ \mathrm{s\,m^{-1}}$. To apply the Schlünder correlation, the *ideal* HTC should be calculated with the pure-fluid correlation of Stephan and Abdelsalam, see Equation (1.60).

Thome and Shakir [98] slightly modified correlation (2.28). They employed Equation (2.7) in their calculations and used the approximation

$$\frac{\mathrm{d}T_\mathrm{b}}{\mathrm{d}x_1} \approx \frac{\Delta T_\mathrm{db}}{x_{1\mathrm{s}} - y_{1\mathrm{s}}}\,, \tag{2.29}$$

where $y_{1\mathrm{s}}$ is the vapor molar fraction which corresponds to the molar fraction $x_{1\mathrm{s}}$ of the liquid layer affected by the *mixture effects*. This approximation should be more accurate compared with the one used by Schlünder who assumed that $\mathrm{d}T_\mathrm{b}/\mathrm{d}x_1 \approx T_{\mathrm{sat},2} - T_{\mathrm{sat},1}$. Using approximation (2.29), Thome and Shakir formed the correlation

$$F = \frac{\alpha_\mathrm{id}}{q}\,\Delta T_\mathrm{db}\left[1 - \exp\left(\frac{-C_0\,q}{\varrho_\mathrm{L}\,\Delta h_\mathrm{LG}\,\beta_\mathrm{L}}\right)\right] \tag{2.30}$$

and recommended to choose $C_0 = 1$ and to find an optimal mass transfer coefficient in the range $1 \times 10^{-4} \le \beta_\mathrm{L} \le 5 \times 10^{-4}\ \mathrm{m\,s^{-1}}$. Correlation (2.30) was compared with the boiling data measured for ethanol–water, methanol–water, 1-propanol–water and acetone–water mixtures.

Correlation of Fujita and Tsutsui

Fujita and Tsutsui [6,132] presented their correlation

$$F = \frac{\alpha_\mathrm{id}}{q}\,\Delta T_\mathrm{db}\left[1 - 0.8\,\exp\left(-\frac{q}{10^5}\right)\right] \tag{2.31}$$

for aqueous, nonaqueous, zeotropic and azeotropic mixtures with a linear- or a nonlinear variation of their thermophysical properties and higher as well as lower values of their boiling range ΔT_db and equilibrium molar fraction difference $|y_i - x_i|$. The correlation is based on Equation (2.21) and should respect the fact that the *bubble-point* temperature $T_{\mathrm{b,s}}$ of the liquid layer near the surface, see Equation (2.7), varies with the heat flux. Correlation (2.31) was transformed into a dimensionless form and extended for ternary mixtures

$$F = \frac{\alpha_\mathrm{id}}{q}\,\Delta T_\mathrm{db}\left\{1 - \exp\left[\frac{-60\,q}{\varrho_\mathrm{G}\,\Delta h_\mathrm{LG}}\left(\frac{\varrho_\mathrm{G}^2}{\sigma\,g\,(\varrho_\mathrm{L} - \varrho_\mathrm{G})}\right)^{1/4}\right]\right\}. \tag{2.32}$$

The *ideal* HTC should be calculated either with the correlation of Stephan and Abdelsalam (1.60) or with the correlation of Nishikawa (1.68).

Correlation of Inoue and Monde

Inoue et al. [108] presented the correlation for the coefficient C from Equations (2.21) and (2.22)

$$C = 1 - 0.75\,\exp\left(-0.75 \times 10^{-5}\,q\right), \tag{2.33}$$

which was obtained from their experiments with mixtures of various Freons characterized by a wide boiling range ΔT_db from 75.0 to 102.8 °C. Freon mixtures were boiled at pressures from 250 to 700 kPa and at a wide range of heat fluxes up to q_cr. The correlation was further tested on mixtures of alcohols and fluorocarbons. Based on their experiments with mixtures of ammonia and water, Inoue and Monde [138] correlated their data with the linear combination of correlation (2.22) and the Schlünder correlation (2.28) to respect the effect of both ΔT_db and $|y_i - x_i|$ on the measured deterioration of HTC. They published the correlation

$$F = \frac{\alpha_\mathrm{id}}{q}\left\{a\,C\,\Delta T_\mathrm{db} + b\,\left(T_{\mathrm{sat},2} - T_{\mathrm{sat},1}\right)\,(y_1 - x_1)\left[1 - \exp\left(\frac{-C_0\,q}{\varrho_\mathrm{L}\,\Delta h_\mathrm{LG}\,\beta_\mathrm{L}}\right)\right]\right\}, \tag{2.34}$$

where the empirical adjustable coefficients $a = 0.15$ and $b = 0.25$ were proposed by Inoue and Monde [138]. These coefficients might be changed for different mixtures. The coefficient C is calculated with correlation (2.33). The coefficients of the Schlünder correlation $C_0 = 1$ and $\beta_L = 2 \times 10^{-4}\ \mathrm{m\,s^{-1}}$ were recommended when using correlation (2.34).

Model of Kandlikar

Kandlikar [125] developed a theoretical boiling model for binary mixtures which is based on the analysis of the bubble growth and diffusion of components in the liquid bulk. The model considers the actual composition $x_{1,s}$ and the corresponding saturation temperature $T_{sat,s}$ at the vapor–liquid interface of growing bubbles. The model should be applicable even for highly nonideal binary mixtures with nonlinear dependencies of their thermophysical properties on composition. The main drawback of the model is that it requires the values of thermophysical properties of the boiling mixture and both pure components, knowledge of vapor–liquid equilibrium, and values of single-component HTCs. Also, the model is quite complex and requires to iteratively solve the system of equations discussed below.

Based on the universal correlation of Stephan and Abdelsalam (1.65), the equation for calculation of the so-called *pseudo-single-component* HTC

$$\alpha_{psc} = \bar{\alpha}_{mix} \left(\frac{T_{sat}}{\bar{T}_{sat}}\right)^{-0.674} \left(\frac{\Delta h_{LG}}{\Delta \bar{h}_{LG}}\right)^{0.371} \left(\frac{\varrho_G}{\bar{\varrho}_G}\right)^{0.297} \left(\frac{\sigma}{\bar{\sigma}}\right)^{-0.317} \left(\frac{\lambda_L}{\bar{\lambda}_L}\right)^{0.284} \tag{2.35}$$

is proposed [125]. In Equation (2.35), the thermophysical properties with bars are the interpolated properties of the boiling mixture calculated with Equation (2.3). The properties in the numerators of the individual fractions of Equation (2.35) are the actual properties of the boiling mixture. The average heat transfer coefficient of the mixture $\bar{\alpha}_{mix}$ is calculated with the equation

$$\bar{\alpha}_{mix} = 0.5 \left[(x_1\,\alpha_1 + x_2\,\alpha_2) + \left(\frac{x_1}{\alpha_1} + \frac{x_2}{\alpha_2}\right)^{-1} \right], \tag{2.36}$$

where the HTCs of both pure components α_1 and α_2 should be obtained at the same pressure, or at the same reduced pressure, or at the same system temperature as of the mixture [125]. The actual HTC during mixture boiling is assumed to be

$$\alpha = F_D\,\alpha_{psc}\,, \tag{2.37}$$

where F_D is the suppression factor due to diffusion. According to the value of the so-called volatility parameter

$$VP = \frac{c_{pL}}{\Delta h_{LG}} \left(\frac{a_L}{D_{12}}\right)^{1/2} \left| \frac{dT_b}{dx_1} (y_1 - x_1) \right|, \tag{2.38}$$

the suppression factor F_D is calculated using the following equations:

- For $VP > 0.005$,

$$F_D = \frac{2.13}{\pi} \left[1 + \frac{c_{pL}}{\Delta h_{LG}} \left(\frac{a_L}{D_{12}}\right)^{1/2} \frac{T_{sat,s} - T_{sat}}{\gamma} \right]^{-1}. \tag{2.39}$$

- For $0 < VP \leq 0.005$,

$$F_D = 1 - 64.0\,VP\,. \tag{2.40}$$

The liquid molar fraction at the vapor–liquid interface, which is required to calculate the corresponding saturation temperature $T_{sat,s}$, is obtained using the relation

$$x_{1,s} = x_1 - \frac{2.13}{\pi}\,Ja'_D \left(\frac{a_L}{D_{12}}\right)^{1/2} \frac{\varrho_G}{\varrho_L} (y_{1,s} - x_1)\,. \tag{2.41}$$

The modified Jakob number Ja'_D in Equation (2.41) accounts for the effect of the mass transfer due to diffusion

$$\mathrm{Ja}'_\mathrm{D} = (T_\mathrm{s} - T_\mathrm{sat}) \left\{ \frac{\varrho_\mathrm{G}}{\varrho_\mathrm{L}} \left[\frac{\Delta h_\mathrm{LG}}{c_{p\mathrm{L}}} + \left(\frac{a_\mathrm{L}}{D_{12}} \right)^{1/2} \frac{T_\mathrm{sat,s} - T_\mathrm{sat}}{\gamma} \right] \right\} . \tag{2.42}$$

In Equations (2.39) and (2.42), the parameter

$$\gamma = \frac{x_1 - x_{1,\mathrm{s}}}{y_{1,\mathrm{s}} - x_{1,\mathrm{s}}} . \tag{2.43}$$

The system of equations listed above has to be solved iteratively. The following algorithm might be applied: 1) calculate α_psc, 2) make an initial estimate of $x_{1,\mathrm{s}} < x_1$ (for example, $x_{1,\mathrm{s}} = x_1 - 0.05$) and an initial estimate of the HTC α (it might be roughly estimated with a pure-fluid correlation), 3) calculate $T_{\mathrm{sat,s}}$ and $y_{1,\mathrm{s}}$ corresponding to $x_{1,\mathrm{s}}$ according to the vapor–liquid equilibrium, 4) calculate the temperature of the heating surface $T_\mathrm{s} = T_\mathrm{sat} + q/\alpha$, 5) calculate γ, Ja'_D and a new value of $x_{1,\mathrm{s}}$, 6) calculate VP and F_D, 7) calculate a new value of the HTC α, 8) repeat the algorithm from step 3) until the difference between the latest and the previously calculated α becomes negligible.

3. Boiling of Water–Glycerin Mixtures

3.1 Production and Utilization of Glycerin

Glycerin (glycerine, glycerol, 1,2,3-propanetriol)[16] is environmentally friendly stable trivalent alcohol which is a colorless, odorless, sweet-tasting, nontoxic, hygroscopic and viscous liquid with a high boiling point [163,164]. Nowadays, there is a surplus of excessive glycerin on the global market which is mainly caused by the production of biodiesel. Approximately 90 % of the total produced glycerin stems from the biodiesel production [165]. Biodiesel (typically fatty acid methyl ester) is usually produced by the transesterification of triglycerides (either from vegetable oils, animal fats, or microalgae) [166]. Triglycerides are made of unsaturated fats connected to a glycerin base, as illustrated in Figure 3.1. Transesterification is a chemical reaction which follows a basic reaction scheme

$$\text{tryglyceride (fat or oil)} + \text{alcohol} \xrightarrow[\text{catalyst}]{\text{base}} \text{glycerin} + \text{ester}\,,$$

where methanol is the most-often used alcohol for its reactivity, high conversion rates, relatively easy production, and nonpolar molecules [167].

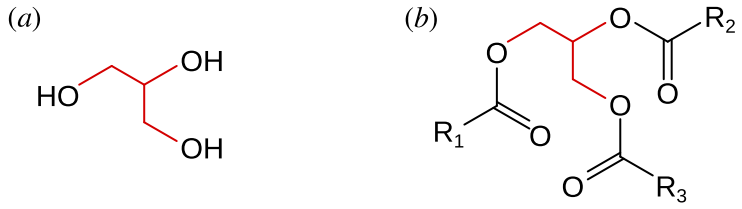

Figure 3.1: The structural formulas of: (*a*) glycerin $C_3H_5(OH)_3$, (*b*) an unspecified triglyceride with the highlighted glycerin base. R_1, R_2 and R_3 stand for alkyl groups, which might be identical or different from each other.

Glycerin is the main byproduct of transesterification. Approximately 1 kg of low-cost crude glycerin of rather low quality (purity of about 50 %) is produced per each 10 kg of biodiesel [166,168,169]. The worldwide production of glycerin, estimated from the total biodiesel production reported and predicted by OECD [170], is shown in Figure 3.2. High-grade glycerin is commonly used in the food, pharmaceutical, and cosmetics industries. In the future, other ways of glycerin utilization are expected to be developed, which will decrease the production cost of biodiesel [166]. Currently, there is growing interest and ongoing research towards suitable utilization of glycerin. The following options seem to be the most promising:

- Utilization as an ecological and bio-based solvent whose characteristics are comparable to water or simple aliphatic alcohols [163,171,172].
- Utilization as an entrainer for vacuum distillation or as an absorbent [168,173,174].
- Employment as an additive for its antifreezing, moisture-retaining, and thickening capabilities [163].
- Nitration to produce nitroglycerin which might be used for manufacturing of explosives or drugs [163].
- Catalytic conversion or pyrolysis to other valuable chemicals such as syngas [175,176].
- Fermentation (microbial conversion) to valuable products such as 1,3-propanediol [177].

To find reasonable and well-suited applications, the thermophysical, chemical and transport properties of glycerin and its mixtures have to be thoroughly studied and described together with their behavior in various apparatuses at different operating conditions.

[16] Although all of these names are most often used interchangeably, *glycerol* is sometimes reserved for the chemical compound 1,2,3-propanetriol and *glycerin(e)* for the purified commercial products which contains more than 95 % of glycerol [163]. In this work, I do not distinguish between glycerin(e) and glycerol and use only the term glycerin.

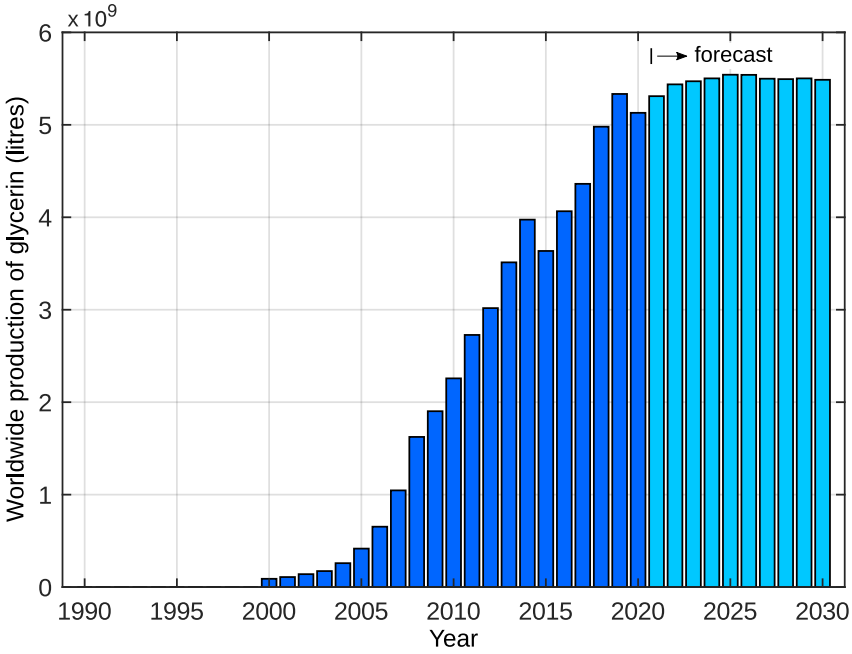

Figure 3.2: The annual production of glycerin estimated from the worldwide biodiesel production [170].

Boiling of mixtures of glycerin usually takes place inside of distillation columns. Flash distillation at subatmospheric pressures in the order of 10 kPa is usually employed to lower the boiling temperature and prevent thermal decomposition and degradation of glycerin [168,175,178]. Distillation is often performed in the following processes:

- Regeneration of the entrainer during extractive distillation. Glycerin might be employed as an entrainer for the extractive distillation of mixtures of ethanol and water. Extractive distillation is the most widely used method for the production of anhydrous ethanol [179]. Glycerin is one of the most effective substances which are able to suppress the azeotropic behavior of ethanol–water mixtures [168,174]. A mass fraction of about 10 % of glycerin is needed for complete suppression [171]. It has been also reported that the presence of glycerin increases the relative volatility of ethanol to water and raises the purity of the produced ethanol [171,173]. Glycerin is more effective and also cheaper than commonly used entrainers, such as ionic liquids or ethylene glycol (which is also toxic and harmful) [168,173]. Similar entraining capabilities of glycerin were also reported for 1-propanol–water and 2-propanol–water mixtures [180,181].
- Separation of ethanol from mixtures of water and glycerin. The mixtures of water and glycerin are used to absorb the ethanol vapor carried by CO_2. Glycerin mixtures have been reported to improve the rate of absorption compared with pure water (at least for lower concentrations of glycerin in the mixture). Since these mixtures have a higher boiling point than water, they enable more efficient regeneration of the solvent [174].
- Purification processes. Pure glycerin is usually manufactured by purification of low-grade glycerin. It can be also synthesized from propene [165,182]. Distillation is often used either to increase the glycerin concentration or as a step which follows after various purifying processes (neutralization, crystallization, filtration, centrifugation, and others) [175]. To produce glycerin of a high purity, distillation has to be done under medium vacuum from about 0.5 to 1.5 kPa and unwanted chemical reactions have to be suppressed [165,175]. Vacuum distillation is capable of producing pharmaceutical-grade glycerin with purity greater than 99.9 % [169]. Distillation might also be used as a single step of purification for the

manufacturing of technical-grade glycerin. Purification processes are quite expensive and demanding. Therefore, it should be a priority to utilize crude and low-grade glycerin whenever possible [172].

3.2 Properties and Phase Diagram of Water–Glycerin Mixtures

Despite that glycerin is a common and thoroughly described substance, the thermophysical properties and phase equilibriums of water–glycerin mixtures are rarely addressed. The thermophysical properties of water–glycerin mixtures adopted from scarce literature sources are given in Table 3.1 for different water mass fractions of the liquid phase ω_w, which correspond to the water molar fractions x_w.

Table 3.1: The thermophysical properties of water–glycerin mixtures at different concentrations adopted from the literature.

ω_w (−)	x_w (−)	M_m (kg kmol^{-1})	T_b (°C)	T_d (°C)	dT_b/dx_w (°C)	ϱ_L (kg m^{-3})	μ_L (mPa s)	σ (mN m^{-1})	λ_L (W m^{-1} K^{-1})	c_{pL} (J kg^{-1} K^{-1})	Δh_{LG} (kJ kg^{-1})	D_{12} (m^2 s^{-1})
1.00	1.00	18.02	100.0	100.0	−28.3	958	0.28	58.91	0.678	4 217	2 257	–
0.98	1.00	18.31	100.2	150.8	−28.5	963	0.29	57.84	0.681	4 183	2 262	2.44×10^{-9}
0.95	0.99	18.77	100.4	166.5	−28.9	970	0.31	58.06	0.687	4 131	2 270	2.42×10^{-9}
0.90	0.98	19.59	100.7	180.5	−29.5	982	0.34	58.43	0.664	4 046	2 283	2.40×10^{-9}
0.85	0.97	20.49	101.0	189.9	−30.1	993	0.37	58.80	0.636	3 969	2 294	2.36×10^{-9}
0.80	0.95	21.47	101.4	197.4	−30.9	1 004	0.40	59.11	0.613	3 891	2 304	2.33×10^{-9}
0.70	0.92	23.75	102.4	209.5	−32.7	1 027	0.50	59.55	0.558	3 640	2 304	2.25×10^{-9}
0.60	0.88	26.56	103.7	219.8	−35.1	1 052	0.62	59.93	0.508	3 389	2 304	2.15×10^{-9}
0.50	0.84	30.14	105.4	229.4	−38.4	1 077	0.80	60.03	0.457	3 222	2 304	2.03×10^{-9}
0.40	0.77	34.82	108.0	238.8	−43.3	1 104	1.05	60.12	0.410	2 992	2 304	1.86×10^{-9}
0.30	0.69	41.23	112.0	248.2	−51.3	1 120	1.50	60.30	0.368	2 782	2 313	1.64×10^{-9}
0.20	0.56	50.53	119.3	259.1	−67.0	1 140	2.08	60.48	0.335	2 552	2 322	1.31×10^{-9}
0.10	0.36	65.26	136.4	271.6	−112.9	1 155	2.77	60.50	0.301	2 423	2 322	0.80×10^{-9}
0.00	0.00	92.09	290.2	290.2	−3 573	1 170	2.34	60.51	0.285	2 322	806	–

Notes: The water molar fraction x_w corresponds to the mass fraction ω_w. The *bubble-point* temperate T_b, the *dew-point* temperature T_d, and the gradient dT_b/dx_w were evaluated from the *non-random two-liquid* model presented in Mokbel et al. [183]. The density of the liquid phase ϱ_L was published in the report of *Glycerine Producers' Association* [184] for 100 °C. The properties of pure water (the first line in the table) were also evaluated with *X Steam*. The dynamic viscosity μ_L at the saturation temperature was read from the chart presented in [184]. The surface tension σ is given in [184] for 90 °C. The thermal conductivity of liquid λ_L was extrapolated using the linear functions $\lambda_L = C_1 + C_2\,T$ given in [184] for the temperature range from 10 to 80 °C. The specific isobaric heat capacity of the liquid c_{pL} (the corresponding temperature is not mentioned) and the latent heat Δh_{LG} were taken from Watkins [185]. The diffusion coefficient D_{12} was extrapolated based on linear fitting of the experimental data from Rausch et al. [186]. The properties are listed for the standard atmospheric pressure. Interpolation was applied when necessary.

Glycerin is fully miscible with water [165,184]. The mixtures of water and glycerin exhibit Newtonian behavior [187] and are characterized by a great difference between the viscosities of both components (at 20 °C, glycerin and water have dynamic viscosities of 1 410 mPa s and 1 mPa s, respectively) [83,163]. Water–glycerin mixtures evince a weak dependence of surface tension on their composition [188] with a small negative deviation from values interpolated between both pure components [83]. This is beneficial for boiling research, since the effects of surface tension often coincide with other *mixture effects* [60,118] and might strongly affect boiling mechanisms [108] and parameters, see, for example, the influence of σ on the bubble departure diameter D_b in Equations (1.26) and (1.27).

Two recent works of Mokbel et al. [183] from 2012 and Soujanya et al. [189] from 2010 contain experimental datasets and models of vapor–liquid equilibriums which include water glycerin mixtures. Both models consider the real behavior of the liquid phase caused by its activity.

- Mokbel et al. [183] investigated the vapor–liquid equilibrium and saturated vapor pressure of water–glycerin mixtures at pressures from 32 to 163 kPa. They fitted the saturated vapor pressure with the Antoine equation

$$\ln p = A - \frac{B}{T + C} \tag{3.1}$$

and employed the *non-random two-liquid* (NRTL) model for calculation of the phase equilibriums. They published the following empirical parameters of the NRTL model for water–glycerin mixtures: $C^0_{12} = 113\,883$, $C^0_{21} = -1\,053.78$, $\alpha^0_{12} = 0.3$, $C^T_{12} = -46$, $C^T_{21} = -1.3$. Usually, only the first three parameters are required for three-parametric NRTL models. The two additional parameters C^T_{12} and C^T_{21} are used to include the effect of temperature on the two so-called *interaction parameters* of the model. For NRTL models, it is commonly assumed that the so-called *non-randomness parameters* are equal for both components ($\alpha^0_{12} = \alpha^0_{21}$). The Parameters of NRTL models should be independent of the composition and temperature [190].

- Soujanya et al. [189] performed ebulliometry to measure the boiling temperature of water–glycerin mixtures and also to find the parameters of *Wilson* model for a given and maintained concentration of the mixture which was boiled at various fixed pressures in the range from 15.19 to 95.3 kPa. For instance, for pressure of 95.3 kPa (which is the closest to the standard atmospheric pressure), they present the parameters of the Wilson model: $\Lambda_{12} = 1.2875$, $\Lambda_{21} = 1.9025$. The published values of Λ_{12} and Λ_{21} vary with pressure without any evident trend. Both parameters might also weakly depend on temperature, which is usually neglected [190]. The authors also report the coefficients of the Antoine equation (3.1), which are listed in Table 3.2. Mokbel et al. [183] consider ebulliometry to be inappropriate for mixtures which evince a high difference between boiling temperatures of their pure components (such as water–glycerin mixtures).

Table 3.2: The coefficients of the Antoine equation (3.1) used by Soujanya et al. [189].

Substance	A (Pa)	B (Pa °C^{-1})	C (°C)
water	23.1939	3816.44	227.02
glycerin	22.1295	4487.04	132.95

Figure 3.3 shows the diagram of the vapor–liquid equilibrium near atmospheric pressure obtained with the NRTL model of Mokbel et al. [183] and the Wilson model of Soujanya et al. [189]. In the diagram, the experimental data points of Carr et al. [191] and Watkins [185], which were measured at atmospheric pressure, are shown for comparison. Both models were evaluated using the coefficients of the Antoine equation given in Table 3.2. Although both models predict almost the same composition of the vapor phase for $\omega_w > 0.2$, they differ for the liquid phase. For the water mass fractions of the liquid phase $\omega_w > 0.3$, the model of Mokbel et al. predicts slightly higher *bubble-point* temperatures T_b (on average by 1.6 °C). For mass fractions $\omega_w < 0.2$, higher T_b was obtained with the model of Soujanya et al. (on average by 10.8 °C).

Based on Figure 3.3, the following conclusions can be put forward:

- For wide range of liquid water mass fraction ω_w, the vapor phase is composed almost solely of water. For $\omega_w > 0.10$, the corresponding vapor mass- and molar fractions are higher than 0.999 and the vapor phase might be considered to be composed only of water.
- The *bubble-point* temperature T_b only slightly increases with decreasing ω_w for mixtures with a higher water content. However, for mixtures with $\omega_w < 0.2$, there is a very strong increase of T_b when the water concentration is decreased.
- There is a high temperature difference of about 190 °C between the saturation temperatures of pure glycerin $T_{sat,2}$ and pure water $T_{sat,1}$ at atmospheric pressure.

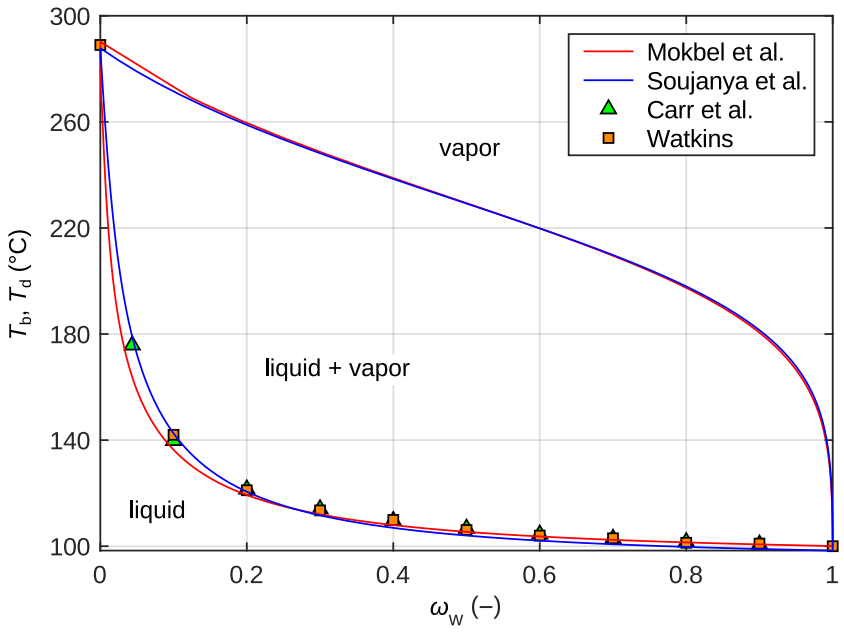

Figure 3.3: The phase diagram of water–glycerin mixtures near atmospheric pressure calculated with the models of Mokbel et al. [183] and Soujanya et al. [189], which are compared with the experimental results published by Carr et al. [191] and Watkins [185].

- The mixtures of water and glycerin have a wide boiling range ΔT_{db}, see definition (2.16). The values of boiling range evaluated for various water mass fractions are shown in Figure 3.4. The maximum value $\Delta T_{db} = 140.7$ °C corresponds to $\omega_w = 0.18$.

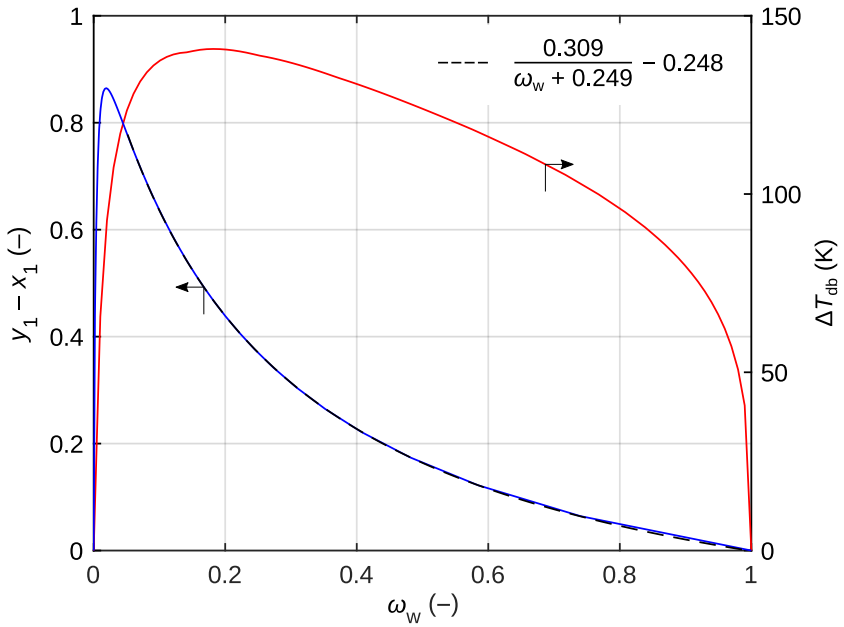

Figure 3.4: The dependency of the boiling range ΔT_{db} and of the equilibrium molar fraction difference $|y_1 - x_1|$ on the water mass fraction ω_w of water–glycerin mixtures.

- The equilibrium molar fraction difference $|y_i - x_i|$ increases with the decrease of ω_w for the range of ω_w from 1.00 down to approximately 0.05. In this range, the hyperbolic function

$$|y_i - x_i| = \frac{0.309}{\omega_w + 0.249} - 0.248 \tag{3.2}$$

represents the course quite well, see Figure 3.4. All 95 % confidence intervals remain below 1 % for the values of the three empirical coefficients of Equation (3.2). The maximum value $|y_i - x_i| = 0.86$ corresponds to $\omega_w = 0.02$.

3.3 Boiling Behavior of Water–Glycerin Mixtures

Water–glycerin mixtures are generally stable. Boiling of these mixtures at standard atmospheric pressures should not lead to the thermal decomposition of glycerin when the water mass fraction ω_w is higher than 0.06. However, for lower ω_w, glycerin is prone to thermal decomposition. Tolubinsky et al. [188] were somehow able to perform HTC measurements during boiling of the mixture with ω_w of 0.04, but the decomposition made it impossible to measure the HTCs for pure glycerin. This also means that the interpolation between HTCs of pure components, discussed in Section 2.1 and illustrated in Figure 2.1, as well as the interpolation of thermophysical properties, see Equation (2.3), are both not applicable for mixtures of water and glycerin, because the thermal decomposition complicates the experimental measurements of the HTCs and thermophysical properties for pure glycerin at the saturation temperature. Due to that, a pure-fluid correlation based on known thermophysical properties has to be used to calculate the *ideal* HTCs of water–glycerin mixtures.

Boiling of stable water–glycerin mixtures is significantly affected by the following three main factors which were already pointed out in Section 3.2:

1. Both pure components have a high difference between their saturation temperatures of about 190 °C at atmospheric pressure. Also, water–glycerin mixtures exhibit a very high boiling range ΔT_{db} in the order of 100 °C, as was shown in Figure 3.4.
2. The vapor phase is composed almost solely of water for water mass fractions $\omega_w > 0.10$.
3. Even a significant change of the composition does not lead to a significant change of the *bubble-point* temperature T_b for mixtures with a higher ω_w.

Although these three factors do not hold true for water–glycerin mixtures with a higher glycerin content, they are securely valid in the range $\omega_w > 0.3$ and significantly influence the boiling performance, parameters, and general boiling behavior. For example, bubble departure diameters were reported to be approximately constant for $\omega_w > 0.3$ mixtures which was ascribed to the factors listed above [188].

Table 3.3 gives the overview of pool boiling experiments with water–glycerin mixtures which were reported in the literature. Although the widest investigated ranges of heat flux and concentration were covered in the work of Sternling and Tichacek [192], the authors did not perform experiments for mixtures with water mass fractions ω_w higher than 0.75. The works listed in Table 3.3 report a general reduction of HTC with the increasing concentration of glycerin in the boiling mixture. The following *mixture effects* were considered by the authors of the works given in Table 3.3:

- Changes in thermodynamic properties due to the addition of glycerin [128,194].
- The decrease of the effective temperature difference [143].
- The mass transfer resistance due to preferential evaporation of the more volatile component [126,128].

A minor enhancement of HTC was reported for very low concentrations of glycerin in the boiling mixture, which was attributed to changes in the surface tension and wettability due to the addition

Table 3.3: The experimental measurements of HTC during pool boiling of water–glycerin mixtures reported in the literature.

Authors	Surface	Material	Pressure	ω_w (−)	q (kW m^{-2})
Sternling and Tichacek (1961) [192]	tube	stainless steel	atmospheric	0.00 to 0.75	25 to 495
Sarafraz et al. (2012) [126,193]	tube	stainless steel	atmospheric[1]	0.95 to 0.99	5 to 92
Alavi Fazel et al. (2013) [143]	tube	stainless steel	atmospheric	0.65 to 1.00	up to 92
Kuo (2014) [194][2]	tube	*Inconel 600*	atmospheric	0.03 to 0.20	up to 1 350
McNeil et al. (2017) [128]	bundle	brass	20 kPa[3]	0.38[4]	10 to 65

[1] The boiling pressure is not explicitly stated. The authors report just the degassing pressure from 10 to 15 kPa.
[2] Although Kuo [194] focuses on the film boiling of water–glycerin mixtures to decompose glycerin into syngas, he also published results from four runs performed in the nucleate regime of boiling.
[3] The reported pressure of 5 kPa above the liquid level and the investigated tube bundle submerged approximately 1.6 m deep in water together give a local pressure of about 20 kPa.
[4] The concentration of the boiling mixture was estimated from viscosity measurements.

of glycerin [130,143,195]. The possible enhancement of HTC during boiling of specific mixtures was discussed in Section 2.4. For water–glycerin mixtures, Alavi Fazel et al. [143] report that HTCs obtained during pool boiling on a stainless steel rod were enhanced by approximately 15 or 20 % for concentrations $\omega_w > 96$ % at heat fluxes lower than 84 kW m^{-2}. Yang et al. [195] also observed an improvement during flow boiling inside microchannels. They achieved maximum enhancement of 16 % at concentrations ω_w of about 94 % at heat fluxes below 35 kW m^{-2}. Alavi Fazel et al. [143] suggested that at low concentrations of the less volatile component in a binary mixture which has a wide boiling range, mass transfer resistance does not play a significant role and the actual HTC corresponds to the *ideal* HTC for low and medium heat fluxes. They measured HTCs comparable to *ideal* HTCs during their experiments with water–glycerin mixtures boiling at atmospheric pressure, when water mass fraction ω_w was higher than 0.65 and heat fluxes lower than 70 kW m^{-2}. They also propose that for water–glycerin mixtures, only water gets vaporized and glycerin moves away from the heating surface into the liquid bulk due to the dynamic effects induced by the formation of bubbles [143].

McNeil et al. [128] performed experiments with subcooled boiling of water–glycerin mixtures on tube bundles at a local pressure of about 20 kPa. They observed a lower heat flux of about 10 to 25 kW m^{-2} required for ONB with respect to heat fluxes from 25 to 40 kW m^{-2} which were needed for the ONB of pure water. The superheat required for the ONB was 4 K for water–glycerin mixtures and 5 K for water. Kuo [194] observed a rise of the critical heat flux with increasing concentration of glycerin in highly concentrated mixtures. He reports the critical heat flux of 0.96 and 1.35 MW m^{-2} for $\omega_w = 0.20$ and 0.03, respectively.

Alavi Fazel et al. [143] successfully employed the Stephan and Abdelsalam pure-fluid correlation together with the Schlünder mixture correlation to correlate their pool boiling data with a mean relative error of 11 % for water–glycerin mixtures with concentrations ω_w from 1.00 to 0.65 which were boiled at heat fluxes up to 95 kW m^{-2}. Sarafraz and Peyghambarzadeh [126] discuss the impact of thermophysical properties on the HTCs calculated for water–glycerin, water – monoethylene glycol and water – diethylene glycol mixtures. They state that the authors of heat transfer correlations often do not specify which properties or methods for their estimation should be used together with their correlations. Sarafraz and Peyghambarzadeh calculated HTCs with the combination of the Stephan and Abdelsalam [69] correlation and the Schlünder [161] correlation. For mixtures of water and glycerin, they used properties evaluated with the Peng–Robinson equation of state and obtained an average deviation of about 9 % between their experimentally measured HTCs and the correlated values. However, for the same data set and the same combination of correlations, they obtained a much higher average deviation of about 36 % when the Redlich–Kwong equation of state was employed to obtain the properties of the mixture.

4. Research Gaps in the Literature

Based on the literature survey presented in the previous sections, the following research gaps and issues related to the experimental investigation of nucleate pool boiling of water–glycerin mixtures at atmospheric pressure were identified:

- The review of the literature showed that heat transfer experiments have not yet been performed to investigate boiling of water–glycerin mixtures on planar surfaces.

  > **Issue 1:** Is the heat transfer performance of water–glycerin mixtures, reported in the literature mostly for stainless steel tubes, comparable with other surface materials or geometries?

- Heat transfer data for pool boiling of water–glycerin mixtures on heating surfaces made of different materials are missing in the literature. Copper surfaces were not investigated even though copper is the most often studied material of the heating surface in the pool boiling literature.

  > **Issue 2:** Do experiments performed on different surfaces reveal some trends specific to the investigated mixtures rather than trends commonly described in the literature, which are valid only for a certain liquid–surface combination?

- HTC trends during boiling of water–glycerin mixtures with lower and medium amount of glycerin have not been reported for medium and high heat fluxes. Table 3.3 shows that mixtures with water mass fraction $0.75 \leq \omega_w \leq 1.00$ were investigated only at relatively low heat fluxes below 92 kW m^{-2}.

  > **Issue 3:** Does HTC during boiling of mixtures with lower glycerin content follow the same trends as those measured for mixtures with higher glycerin concentration? Is boiling of these mixtures significantly affected by the *mixture effects*?

- The enhancement of HTC, reported in the literature during boiling of water–glycerin mixtures on stainless steel tubes and in microchannels at relatively low heat flux levels, has not been verified for planar surfaces or different materials of the heating surface.

  > **Issue 4:** Are water–glycerin mixtures able to provide higher HTCs, relative to pure water, during boiling on planar heating surfaces made of different materials?

- Values of important boiling parameters related to bubble nucleation and governing boiling mechanisms are unknown for water–glycerin mixtures and have not yet been addressed by researchers. Analyses of boiling parameters, based on contactless measurement methods, have not been performed for mixtures of water and glycerin.

  > **Issue 5:** Do the heat flux and concentration of glycerin in the boiling mixture impact the most important parameters and mechanisms related to heat transfer and bubble nucleation?

- Researchers have not yet investigated subcooled boiling of water–glycerin mixtures. Heat transfer performance during subcooled boiling of mixtures is mostly unexplored.

  > **Issue 6:** Is the impact of subcooling on the HTC during subcooled boiling of water–glycerin mixtures more important than the effect of mixture composition?

- The commonly employed pure-fluid correlations and mixture correlations discussed in Sections 1.3 and 2.5, respectively, are often difficult to apply and require knowledge of various thermophysical properties and the vapor–liquid equilibriums. Suitable correlations are needed to quickly estimate HTCs, which might then be used for modeling of boiling heat transfer.

  > **Issue 7:** Is it possible to find some correlations in the literature or propose suitable empirical correlations which would enable fast and straightforward calculation of the measured HTCs?

- The stability and repeatability of the measured HTCs have not been reported or investigated in the literature for water–glycerin mixtures, and is rarely addressed in studies related to boiling.

  > **Issue 8:** Are heating surfaces made of different materials prone to degradation or interaction with water–glycerin mixtures? Are the HTCs measured for all investigated materials comparable and stable?

5. Aims of This Thesis

With respect to Section 4, the following goals related to pool boiling of water–glycerin mixtures were set to be explored in the next part of this thesis:

- Measure the HTCs during pool boiling of water–glycerin mixtures on flat heating surfaces.
- Investigate the boiling performance of water–glycerin mixtures on heating surfaces made of different materials, i.e., copper, nickel-plated, and titanium surfaces. Compare the HTCs measured for these surfaces.
- Evaluate whether some of the trends observed during boiling of water–glycerin mixtures on heating surfaces made of different materials might be considered universal for the investigated mixtures and not constrained to a specific liquid–surface combination.
- Study boiling of water–glycerin mixtures with higher water mass fraction ω_w at medium and higher heat fluxes q, i.e., in the range of water mass fraction $0.60 \leq \omega_w \leq 1.00$ at heat flux $q > 100\ \mathrm{kW\,m^{-2}}$.
- Assess the possible enhancement of heat transfer during boiling of water–glycerin mixtures with lower glycerin concentration.
- Decide whether the impact of the *mixture effects* on HTC is substantial for the investigated water–glycerin mixtures.
- Using contactless infrared thermometry, evaluate the bubble departure diameters, nucleation frequencies, and bubble growth rates during boiling of water–glycerin mixtures.
- Based on the trends of measured nucleation parameters, identify the governing heat transfer mechanisms during boiling of water–glycerin mixtures.
- Measure the HTCs during subcooled boiling of water–glycerin mixtures, observe the effect of subcooling on HTC, and suggest a method for HTC calculation during subcooled boiling of the investigated mixtures.
- Develop suitable correlations which would enable quick estimation of the measured HTCs for convenient modeling of heat transfer.
- Examine the stability of the heat transfer performance over time for the investigated heating surfaces. Observe whether the tested heating surfaces are prone to degradation or whether they interact with water–glycerin mixtures.

5.1 Structure of Part II

In the following Part II of this thesis, the results of the experimental measurements of the nucleate pool boiling HTCs of water–glycerin mixtures are presented. Part II is subdivided into the following sections:

- Section 6 presents the details and results of the experiments performed on a smooth copper heating surface for the water–glycerin mixtures with water mass fractions from 1.00 (pure water) down to 0.40. Measurements were conducted at heat fluxes from about 25 to 270 $\mathrm{kW\,m^{-2}}$.
- Section 7 discusses the saturated and subcooled pool boiling experiments which were performed on five smooth nickel-plated samples for the water–glycerin mixtures with water mass fractions from 1.00 down to 0.60. For saturated boiling, the heat flux was altered from 50 to 650 $\mathrm{kW\,m^{-2}}$. Subcooled boiling was studied at three discrete heat flux levels of about 250, 450, and 650 $\mathrm{kW\,m^{-2}}$ and subcoolings from 30 down to 0 K.
- Section 8 deals with the measurements performed with a smooth thin titanium foil which was monitored with infrared camera. The captured footage was analyzed to obtain the HTC trends and values of

nucleation parameters during boiling of the water–glycerin mixtures with water mass fractions from 1.00 down to 0.60. For mixtures with a higher water mass fractions ($\omega_w \geq 0.85$), heat fluxes from about 25 up to 200 kW m^{-2} were investigated. For mixtures with a higher amount of glycerin, the maximum investigated heat flux was limited to 150 kW m^{-2}.

- Section 9 points out general trends which were found to be valid for all the investigated heating surfaces. Since boiling experiments were performed for three different surface materials, the boiling behavior observed for all tested surfaces is considered universal for the investigated water–glycerin mixtures.
- Section 10 briefly recapitulates the parameters, outputs, and important findings of the performed experiments.

PART II

Pool Boiling Experiments

6. Experiments with Thick Copper Sample

6.1 Motivation, Novelty, and Parameters of Experiments

The heating surfaces made of copper are the most often studied in the literature dealing with pool boiling due to the high thermal conductivity of copper, which results in small temperature gradients inside of the tested samples. This enables reaching of high heat fluxes at relatively small temperatures inside a sample. However, boiling of water–glycerin mixtures on copper surfaces has not yet been investigated in the literature. Experiments were thus performed which aimed to:

- Design and build an apparatus and develop a methodology which would enable the measurement of pool boiling HTCs for pure liquids and binary mixtures.
- Perform pool boiling experiments on copper samples for wide ranges of the heat flux and concentration.
- Find or develop suitable correlations which could be used to quickly calculate the measured HTCs.
- Assess whether mixtures with a lower amount of glycerin are able to enhance pool boiling HTC.
- Observe whether the HTCs measured at low heat fluxes correspond to the *ideal* HTCs.

Experimental measurements were performed for saturated nucleate pool boiling of the binary mixtures of water and glycerin at atmospheric pressure on a smooth copper surface. The mixtures were studied with the water mass fractions of the liquid phase from 100 % (pure water) down to 40 % which corresponds to molar fractions from 1.00 down to 0.77. In this range, the *bubble-point* temperature does not shift significantly and the vapor phase is composed almost solely of water. Heat fluxes from 25 up to 270 kW m^{-2} were investigated. CHF was not reached during the experiments, since the transition to film boiling might lead to the thermal decomposition of glycerin and affect the surface structure, boiling performance, and repeatability of measurements, as was reported in the literature [196–198] and observed in one of our studies [199].

The novelty of the presented experimental results might be briefly outlined by the following points:

- There are no experimental data for the boiling performance of water–glycerin mixtures on copper surfaces.
- There are no data for mixtures with a high concentration of glycerin at higher heat fluxes. Although Sternling and Tichacek [192] investigated a wide range of heat fluxes, see Table 3.3, their data do not contain the mixtures with low content of glycerin. Conversely, Alavi Fazel et al. [143] experimented with the mixtures of high ω_w, but only in a relatively narrow heat flux range.
- The boiling performance and stability of surfaces when they are in contact with water–glycerin mixtures have not been addressed in the literature.

The obtained results presented and discussed in this section were previously published in our article [200].

6.2 Experimental Apparatus

The experimental apparatus was designed at the Department of Process Engineering, CTU in Prague, to measure HTCs for various single-component liquids and mixtures. The apparatus is shown in Figure 6.1. It consists of a cylinder made of borosilicate glass (*Boro 3.3* according to ISO 3385 standard) with an inner diameter of 200 mm and a height of 500 mm. The cylinder stays on a flat PTFE gasket placed on the stainless steel[17] bottom with a square 50 × 50 mm cut. A cubic copper block is inserted through the

[17] The material of all stainless steel parts is 1.4301 according to ČSN EN 10 0027-2 (which corresponds to AISI 304 or to 17 240 according to ČSN 42 0002).

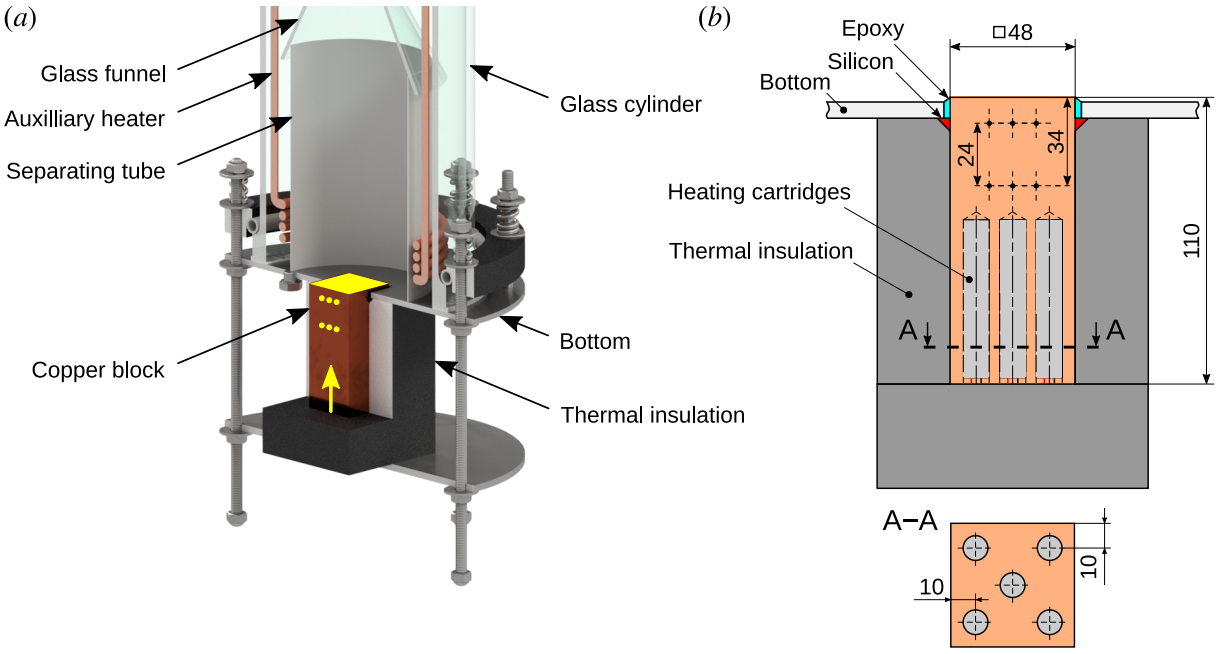

Figure 6.1: The experimental apparatus designed at CTU in Prague: (*a*) The assembled apparatus. Yellow color marks the heating surface, six thermocouple holes, and the orientation of the heating cartridges inside the copper block. Adopted from Vajc et al. [200]. (*b*) Cross-section view and the dimensions of the copper block.

cut with its top face slightly above the bottom, see Figure 6.1. The square top face of the block with the roughness R_a of about 0.4 µm and dimensions of 48 × 48 mm serves as the heating surface on which boiling takes place. The block is glued together with the bottom using the combination of thermoresistant silicone *Ceresit CS 28* and epoxy resin *EPO-TEK 302-3M-R*. The block is surrounded with the thermal insulation made of cellular glass *Foamglas Perinsul S* which has a nominal thermal conductivity of about 0.05 $W\,m^{-1}\,K^{-1}$ and an operational temperature up to 430 °C.

Five heating cartridges with a nominal power of 5 × 300 W, a diameter of 10 mm, and a length of 60 mm are placed in five vertical holes which were drilled into the bottom face of the copper block. The diameters of the holes were carefully adjusted to reduce the thermal resistance of the air gaps between the heaters and the block as much as possible. The power to the heating cartridges is supplied and regulated via *TWINTEX PPW-1560* laboratory power supply. From the top of the glass cylinder, a coil-shaped auxiliary heater with a nominal power of 3 kW is installed to maintain the saturation temperature of the boiling liquid. It is made of an *Inconel-800* tube which has an outer diameter of 8.5 mm. The heater is powered with a variable autotransformer. A stainless steel tube with an outer diameter of 142 mm, a wall thickness of 1 mm and a height of 200 mm is standing on the bottom inside the glass cylinder to separate the liquid pool above the heating surface from the auxiliary heater. A glass funnel is placed on the tube which helps to maintain the saturation temperature of the liquid above the heating surface.

The temperature field inside the copper block was measured with thermocouples (TCs). Six horizontal holes with a diameter of 1 mm and a length of 24 mm were drilled into the copper block. Inside these holes, six ungrounded K-type (chromel–alumel) sheathed TCs *Omega GKMQSS-M100U-150* are embedded. These TCs were glued into the block with alumina-based *Aremco Ceramabond 670* glue. The three rows of TCs inside the block enable one to take the local distribution of HTC above the heating surface into account. The temperature of the boiling liquid was measured with two ungrounded K-type TC probes *Omega TJ2-CASS-IM15U-600* which were submerged in the liquid above the heating surface through the top of the glass funnel. Eight cold-junction TC probes *Omega TRP-K-36* were connected to the measuring

TCs and inserted into two calibration reference chambers *Omega TRCIII-A*. All TCs were connected to the PC via *JanasCard AD24USB* data-acquisition (DAQ) module.

The apparatus is opened to the surroundings. Ambient pressure was monitored with pressure sensor *Comet T7510*. During boiling of the investigated mixtures, water was continuously pumped into the apparatus with dosing pump *ProMinent BT4a* to maintain a constant composition and a constant level of boiling mixture during measurements (for all the tested water–glycerin mixtures, the vapor phase was composed almost only of water, see Figure 3.3).

6.3 Measurement Procedure and Calculation of HTC

Surface Cleaning and Measurement Protocol

Before the first experimental run, the copper heating surface was cleaned with acetone and left for five days. The surface was then passivized by boiling in water for ten hours. The heating surface was neither cleaned nor treated between consecutive experimental runs to prevent any possible interaction of the cleaned surface with the boiling liquid. The time period of about half an hour, which was required to reach the first steady state of boiling for each run, was found to be sufficient for degassing of the boiling liquid, as no discrepancies were observed between the data points obtained at the beginning of each run and the remaining data points. Before each experimental run, water and glycerin were carefully weighted and mixed together at room temperature. A volume of approximately 5 liters of the mixture was prepared and poured into the apparatus. The cartridge and auxiliary heaters were then turned on and the liquid was heated until it started to boil. Throughout the whole run, the dosing pump was on and the power supplied to the auxiliary heater was kept constant.

Steady-State Method of Measurement

Each of the data points, presented in Section 6.5 below, was obtained in the steady state of boiling. The criterion for judging whether boiling reached the steady state was the maximum temperature difference between all the temperatures measured at a given time and the same temperatures measured one minute earlier. Boiling was considered to reach the steady state when the maximum difference continuously oscillated around zero and its magnitude stayed below approximately 0.3 °C. Steady states were reached after about 15 min from the moment the voltage supplied to the heating cartridges was altered. Each steady state was maintained for approximately 15 minutes. After this period, the electrical power supplied to the cartridge heaters was altered. Usually, the highest power was supplied to the cartridge heaters at the start of each run to obtain the first steady-state point at the highest investigated heat flux. Then, for other steady-state points, the heat flux was decreased in a step-by-step manner. This procedure is recommended to reduce the hysteresis of the boiling phenomenon [6,143]. However, some of the data points were recorded for an increasing heat flux, but they did not exhibit any noticeable discrepancy due to hysteresis. In total, 109 data points were obtained. Each of the nine presented runs was conducted in a single day and took approximately 10 hours to measure. After each run was finished, the apparatus was cooled down and the liquid was pumped out. The apparatus was left in this state overnight and a new run was started in the morning. The apparatus was never disassembled for all presented runs to achieve the highest possible repeatability.

The heat flux is calculated from the temperatures measured with the TCs inside the copper block. Assuming that the conduction in the block is one-dimensional and that the temperature gradient inside the block is linear, Fourier's law

$$q = \lambda \frac{\Delta T}{L} \tag{6.1}$$

might be applied, where $\Delta T = T_{\mathrm{bot}} - T_{\mathrm{up}}$ is the temperature difference between the both lines of TCs, T_{bot} and T_{up} are the average temperatures in the bottom- and the upper line, respectively, and the length $L = 24$ mm is the distance between the both lines of TCs. A constant value of the thermal conductivity of copper $\lambda = 400\ \mathrm{W\,m^{-1}\,K^{-1}}$, which is commonly used in the literature [201], was assumed. The heat transfer coefficient α is defined with Equation (2.5) for boiling of mixtures. The *bubble-point* temperature T_{b} was calculated as the mean temperature measured with both immersed TCs. The temperature of the heating surface T_{s} was linearly extrapolated using the temperature difference ΔT and the length L.

To evaluate the correspondence between the measured HTCs and heat transfer correlations, the standard error of the estimate

$$\mathrm{SEE} = \sqrt{\frac{\sum_i (\alpha_i - \hat{\alpha}_i)^2}{N}} \tag{6.2}$$

and the mean relative error

$$\mathrm{MRE} = \frac{\sum_i (\,|\hat{\alpha}_i/\alpha_i - 1|\,)}{N} \tag{6.3}$$

were calculated. In Equations (6.2) and (6.3), i is the ordinal number of one of the measured data points, α_i is the HTC corresponding to a certain data point measured at a certain heat flux, $\hat{\alpha}_i$ denotes the HTC estimated at the same heat flux by some correlation, and N is the total count of the measured data points.

Dynamic Method of Measurement

Može et al. [196,202] showed that a continuous increase of heat flux during measurements does not impact the measured HTCs when the increase is sufficiently slow. This was also verified by numerical simulations whose results are published in the supplementary information of one of our studies [203]. Such a dynamic method of measurement speeds up individual experimental runs and thus reduces the impact of heating surface degradation on measured values.

At CTU, we have also developed a dynamic method for the measurement of HTC during boiling of mixtures which enables to measure HTC as a function of the concentration of the boiling mixture in a single experimental run, and which provides faster measurements compared with the ordinary steady-state method [200]. When the method is applied, water vapors are allowed to escape the opened apparatus throughout each experimental run. This leads to a change of the actual concentration of the boiling mixture and to a variation of the measured HTC. The mixture is boiled until the liquid level drops close to the heating section of the auxiliary heater. The experiment is then stopped to prevent air from coming into contact with the heater.

Although it is possible to determine the actual composition of the boiling mixture by sampling, we estimated the composition from the measured boiling temperatures using the vapor–liquid equilibrium diagram, see Figure 3.3. The advantage of this approach is that it is not necessary to measure the liquid composition or the amount and composition of the released vapor. On the other hand, precise measurement of liquid temperature is required, especially for mixtures with a flat dependence of the *bubble-point* temperature on the composition (which is the case of the investigated water–glycerin mixtures). The HTC and heat flux were calculated from the measured values using exactly the same procedure as for the steady-state measurements.

6.4 Measurement Uncertainties

Uncertainty of heat transfer coefficient $u(\alpha)$ was analyzed for the performed measurements based on the propagation of uncertainty. The following maximum deviations were assumed: for temperature $U(T) = 0.5\ ^{\circ}\mathrm{C}$, for length or distance $U(L) = 1$ mm, and for thermal conductivity $U(\lambda) = 50\ \mathrm{W\,m^{-1}\,K^{-1}}$. For all

of these deviations, a uniform rectangular distribution was assumed. The corresponding standard deviation for an unspecified quantity $u(\gamma)$ was, therefore, calculated as $u(\gamma) = U(\gamma)/\sqrt{3}$.

Experiments were done in the range of heat flux from around 20 up to 270 kW m^{-2}. Since the resulting uncertainty $u(\alpha)$ depends on the directly and indirectly measured parameters, it is necessary to employ the measured values of the HTC α, the heat flux q and the temperatures T_s and T_b to calculate the HTC uncertainty $u(\alpha)$. The calculation was done for three different heat flux levels (low, medium, and high) measured during pool boiling of pure water. The four parameters used for the uncertainty analysis are given in Table 6.1 together with the resulting uncertainty $u(\alpha)$ and the measured pressure at which experiments took place. For the measurement performed at a high heat flux, represented by the first line of Table 6.1, the resulting uncertainty $u(\alpha) = 1.5$ kW m^{-2} K^{-1}, which gives the relative uncertainty of 9 %. For a medium heat flux, represented by the second point in Table 6.1, the uncertainty $u(\alpha) = 0.57$ kW m^{-2} K, and the relative uncertainty is of about 13 %. For the lowest heat flux in Table 6.1, the uncertainty $u(\alpha) = 0.57$ kW m^{-2} K was obtained, which means a relative error of about 23 %. The resulting values indicates that to lower the uncertainty of HTC $u(\alpha)$ below 20 %, measurements should be performed at heat fluxes higher than approximately 25 kW m^{-2}.

Table 6.1: The HTC uncertainty $u(\alpha)$ and the data used for its estimation which were measured during boiling of pure water under pressure p.

Point	$\alpha \pm u(\alpha)$ (kW m^{-2} K^{-1})	q (kW m^{-2})	T_s (°C)	T_b (°C)	p (kPa)
1	17.56 ± 1.48	191.4	109.6	98.7	100.24
2	4.39 ± 0.57	40.0	107.6	98.5	100.24
3	2.45 ± 0.57	18.5	105.8	98.2	99.72

6.5 Results and Discussion of Steady-State Measurements

Repeated Runs and Stability of the Heating Surface

Figure 6.2 shows the HTCs measured for two successive repeated runs performed for the $\omega_w = 1.00$ and $\omega_w = 0.90$ mixtures (this is also the reason why there are more data points in the following figures for these two mass fractions). The measured HTCs are comparable with the Stephan and Abdelsalam correlation (1.65). A fresh boiling liquid was used for each of the repeated runs. Slightly lower HTCs were measured for both second runs. Although the relative differences are less than 9 % between the measured data points and the arithmetic mean of both runs for both investigated concentrations, the decrease of HTC measured during repeated runs is systematic and might have been caused by the inherent randomness of the boiling process. Randomness of various parameters related to the boiling performance (such as the nucleation frequency, bubble coalescence, distribution of active cavities on the heating surface, and others) has been reported in the literature [26,204–208]. The stability of the copper heating surface might also have been affected due to prolonged exposure to glycerin and mutual interaction between the surface and the boiling fluid. It has been reported that copper salts are sometimes able to catalyze glycerin oxidation. Because of this, inhibitors have been suggested to be used when glycerin is treated or stored in copper-containing (or iron-containing) vessels [163]. The reactivity and morphological changes of copper, manifested either by enhancement or deterioration of the boiling performance, were also addressed in other works [197,198,209,210]. Changes of the surface structure and of the chemical composition during boiling of water–1-butanol mixtures on copper surfaces were also confirmed by scanning electron microscopy and Raman spectroscopy, respectively, in one of our studies [199].

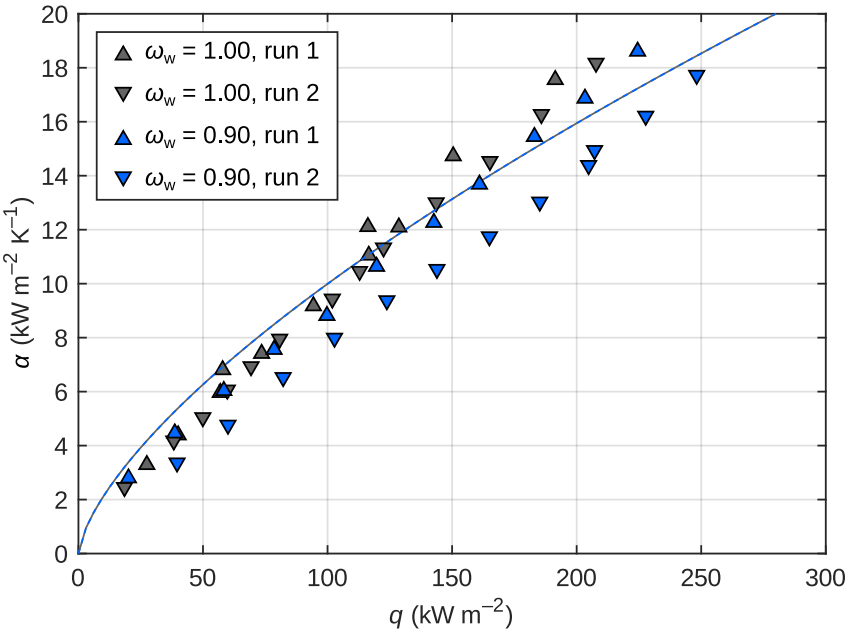

Figure 6.2: Repeatability of measurements for the $\omega_w = 1.00$ and 0.90 mixtures and the comparison with the correlation of Stephan and Abdelsalam [69]. Published in [200].

Impact of Mixture Effects on HTC

Figure 6.3 shows the HTCs measured during saturated pool boiling of water–glycerin mixtures at atmospheric pressure for water mass fractions from 1.00 (pure water) down to 0.40, the values of *ideal* HTCs predicted for individual concentrations by the pure-fluid correlation of Stephan and Abdelsalam [69], see Equation (1.65), and the experimental data measured by Sternling and Tichacek [192] and by Sarafraz

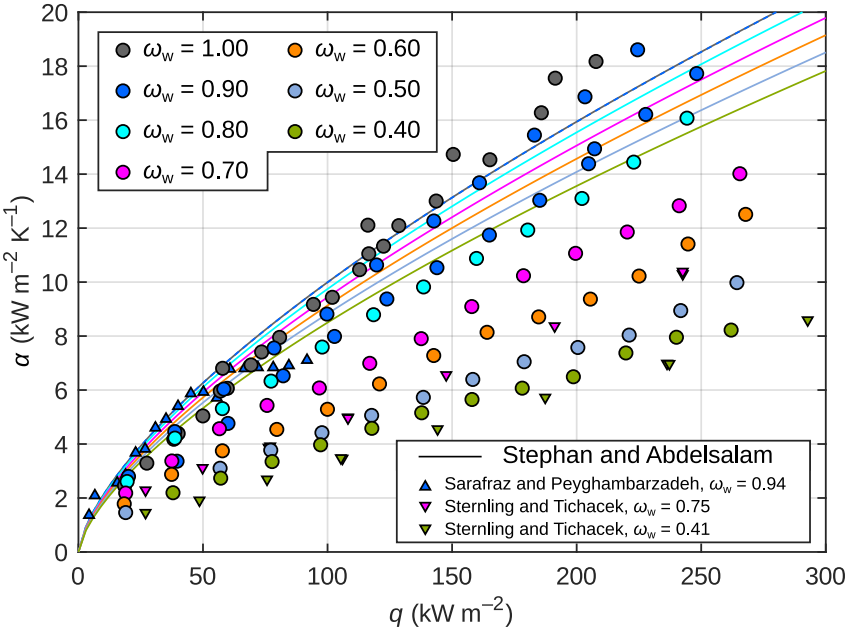

Figure 6.3: The measured HTCs compared with the correlation of Stephan and Abdelsalam [69] and with the experimental data sets of Sarafraz and Peyghambarzadeh [126] and of Sternling and Tichacek [192]. Published in [200].

and Peyghambarzadeh [126]. However, their experiments were performed on a different surface and a different geometry, see Table 3.3. Because of that, some discrepancies between their and present data points are expected. The thermophysical properties of the water–glycerin mixtures were taken from Table 3.1. The errors SEE = 3.4 kW m^{-2} K^{-1} and MRE = 42 % between the correlated *ideal* HTCs and the measured data points were calculated using Equations (6.2) and (6.3), respectively. In Figure 6.3, the gray and blue lines overlap which means that the the correlated *ideal* HTCs are similar for $\omega_w = 1.00$ and $\omega_w = 0.90$ mixtures. However, there is a noticeable drop of the measured HTCs for these two concentrations which indicates that the *mixture effects* significantly influence the boiling performance even for mixtures with a low glycerin content. The difference between the measured and *ideal* HTCs increases with higher concentration of glycerin in the mixture due to the enhanced *mixture effects* which cause a stronger heat transfer deterioration. The measured and *ideal* HTCs are not equal even for lower heat fluxes and higher water mass fractions, which was suggested in the literature [143]. To correlate the measured HTCs, it is, therefore, necessary to employ mixture correlations for all the investigated mixtures and heat fluxes.

Figure 6.4 shows the comparison between the measured HTCs and the mixture correlation of Schlünder [117], see Equation (2.28), which was evaluated using the *ideal* HTCs obtained with the Stephan and Abdelsalam correlation and the empirical coefficients $C_0 = 1$ and $\beta_L = 2 \times 10^{-4}$ m s^{-1}. The correlated

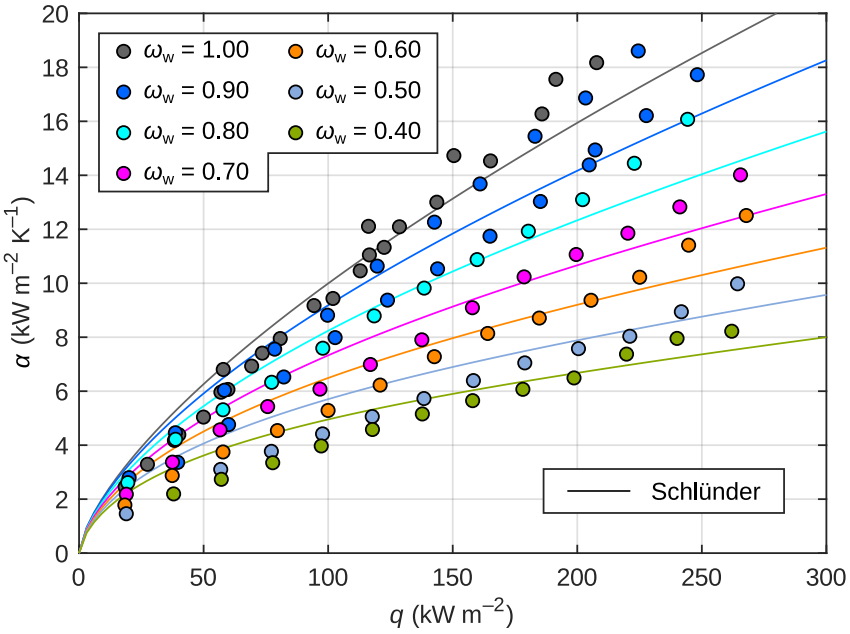

Figure 6.4: The measured data compared with the mixture correlation of Schlünder [117] evaluated with the coefficients $C_0 = 1$ and $\beta_L = 2 \times 10^{-4}$ m s^{-1}. *Ideal* HTCs were calculated with the pure-fluid correlation of Stephan and Abdelsalam [69]. Published in [200].

values correspond quite well to the measured HTCs. The errors SEE = 1.0 kW m^{-2} K^{-1} and MRE = 14 % were calculated between the measured and correlated HTCs. Since the values of C_0 and β_L might change for different mixtures, as discussed in Section 2.5, it was assumed that $C_0 = 1$ and the optimal mass transfer coefficient β_L was found in the range $1 \times 10^{-4} \leq \beta_L \leq 5 \times 10^{-4}$ m s^{-1} recommended by Thome and Shakir [98] by minimizing the SEE (this is analogous to the regression analysis using the least squares method). The optimal coefficient $\beta_L = 1.83 \times 10^{-4}$ m s^{-1} was found which provides SEE of 1.0 kW m^{-2} K^{-1} and MRE of about 13.5 %. Since the value of β_L remains close to the original value and the improvement in both the errors is negligible, the original coefficients proposed by Schlünder are considered to be suitable for the studied mixtures. The deviation between the measured HTCs and the

Schlünder correlation is shown in Figure 6.5. The Schlünder correlation overestimates the lower HTCs obtained at lower heat fluxes. This might be a result of the increased measurement uncertainty at lower heat fluxes. Nevertheless, the deviation remains below ±20 % for HTCs higher than about 7 kW m^{-2} K^{-1}.

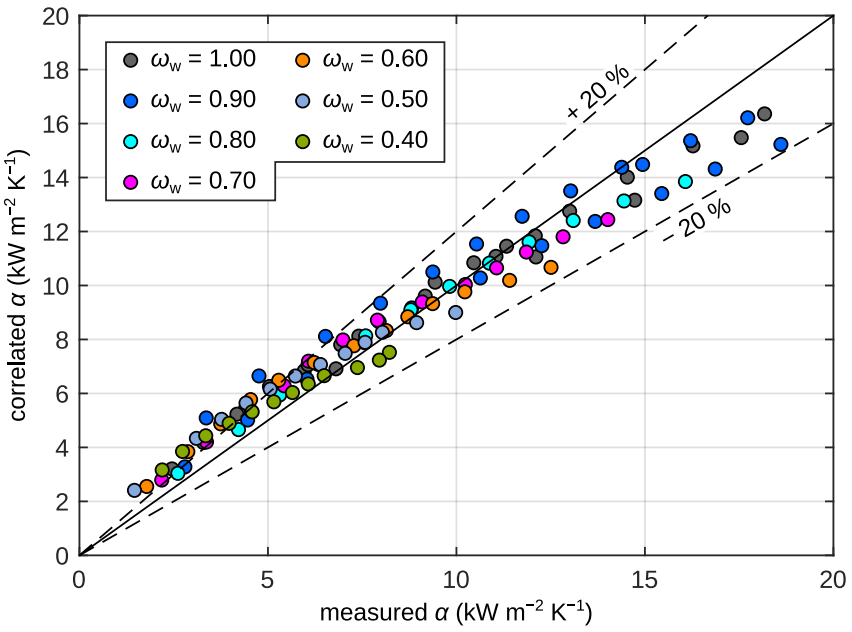

Figure 6.5: The correspondence between the measured HTCs and the correlation of Schlünder [117] evaluated with the coefficients $C_0 = 1$ and $\beta_L = 2 \times 10^{-4}$ m s^{-1}. *Ideal* HTCs were calculated with the pure-fluid correlation of Stephan and Abdelsalam [69].

Own Empirical Correlation for HTC

An empirical correlation was developed for the investigated water–glycerin mixtures boiling on copper surfaces, which does not require thermophysical properties of the boiling mixture and offers a fast and straightforward calculation of HTC. The proposed correlation

$$\alpha = 0.59\, q^{0.714+0.130\omega_w} \tag{6.4}$$

can be used in the ranges of the investigated heat fluxes $25 \le q \le 270$ kW m^{-2} and water mass fractions $0.40 \le \omega_w \le 1.00$. The correspondence between the correlation and the measurements is plotted in Figure 6.6 which shows that almost all data points do not deviate by more than ±20 % from the predictions of the correlation. Correlation (6.4) was obtained by separate fits of power functions $\alpha = C\, q^n$, see also Equation (1.59), to the data points corresponding to each investigated concentration. A series of *F-tests* and employment of *Akaike information criterion* for the set of individual coefficients C and exponents n showed that the parameter C might be considered independent of the water mass fraction ω_w and that the exponent n might be approximated using a linear function of ω_w. The function $\alpha = C_1\, q^{C_2+C_3\omega_w}$ was, therefore, fitted to the experimental data set. The coefficients and their 95 % confidence intervals $C_1 = 0.59 \pm 0.20$ W^{1-m} m^{2m-2} K^{-1}, $C_2 = 0.714 \pm 0.027$, $C_3 = 0.130 \pm 0.005$ provided the best fit. The exponent m in the unit of the coefficient C_1 might be calculated as $m = C_2 + C_3\, \omega_w$. In correlation (6.4), the exponent of the heat flux lies close to the upper limit of the range $0.6 < m < 0.8$ often stated in the literature [33] as a range typical for nucleate pool boiling of various liquids. To use correlation (6.4), the heat flux q needs to be in (W m^{-2}), the water mass fraction ω_w is dimensionless and the resulting α is in (W m^{-2} K^{-1}). The errors SEE of 0.5 kW m^{-2} K^{-1} and MRE below 6 % were calculated between the measured and correlated HTCs.

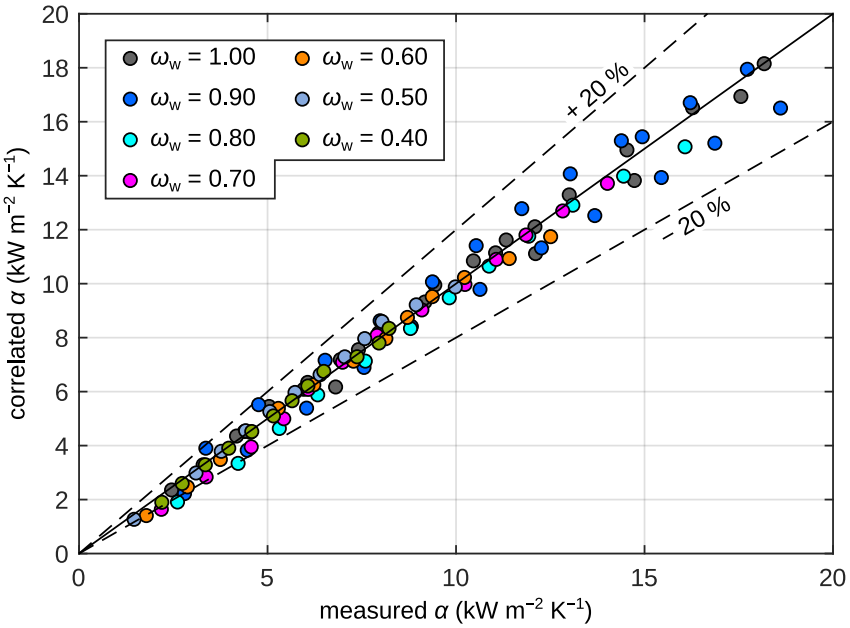

Figure 6.6: The correspondence between the measured HTCs and correlation (6.4).

6.6 Results and Discussion of Dynamic Measurements

The dynamic measurement method, described in Section 6.3, was speculatively tested on the water–glycerin mixture with the initial water mass fraction $\omega_w = 0.70$. The mixture was boiled down to $\omega_w = 0.35$. Figure 6.7 shows the dependence of the measured HTC on the composition of the boiling mixture and the comparison with steady-state measurements which are represented by empirical correlation (6.4). During the measurement, the heat flux slightly varied from approximately 165 down to 150 kW m^{-2},

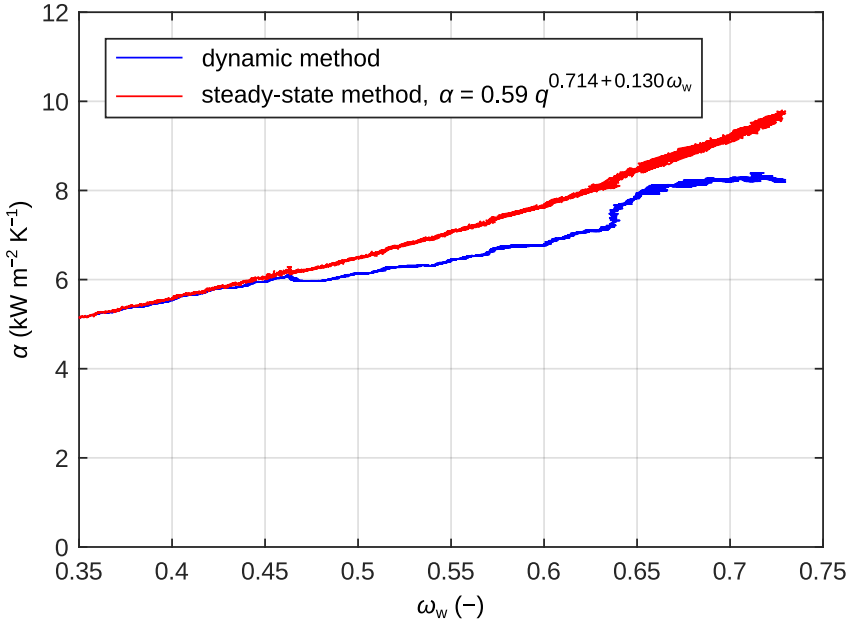

Figure 6.7: The impact of the actual composition of the boiling liquid on HTC obtained with the dynamic method of measurement and the comparison with correlation (6.4) which represents the steady-state measurements. Published in [200].

because the employed power supply could not be set to maintain a constant power throughout the experiment. Nevertheless, the measured data correspond quite well to correlation (6.4) for ω_w from 0.35 to 0.45. For higher ω_w, the results of the dynamic method are slightly lower relative to the steady-state measurements. Nevertheless, the difference remains acceptable for all investigated concentrations. For instance, for $\omega_w = 0.5$, the ratio between HTCs measured by both methods is approximately 94 %. For $\omega_w = 0.75$, the ratio decreases to about 85 %. The difference between both methods is caused by a flat dependence of the *bubble-point* temperature on the mixture composition, see Figure 3.3, which makes estimation of actual boiling composition difficult, especially for mixtures with a higher ω_w. To overcome this, it is either necessary to do periodic sampling of the boiling liquid throughout each run or to use some more accurate models of vapor–liquid equilibriums and perform precise measurements of the temperature of the liquid bulk. Moreover, the dynamic method might be further improved using a power supply with an adaptive power control to maintain a stable constant heat flux level throughout the entire experimental run.

6.7 Summary of Experimental Results

Based on the experimental results presented in this section, the following conclusions can be deduced for boiling of water–glycerin mixtures on copper surfaces:

- HTC decreases with increasing concentration of glycerin in the boiling mixture. The decrease is steeper for mixtures with a higher water content.
- The *mixture effects* significantly affect HTC for all of the investigated water mass fractions from 0.40 to 1.00 and heat flux levels from 25 to 270 kW m^{-2}.
- No enhancement of HTC was observed for any investigated heat flux and composition of the boiling mixture.
- Boiling on the flat copper surface was successfully correlated with the combination of the Schlünder mixture correlation and the pure-fluid correlation of Stephan and Abdelsalam using the empirical parameters $C_0 = 1$ and $\beta_L = 2 \times 10^{-4}$ m s^{-1} recommended by Schlünder.
- The own empirical correlation was developed for the calculation of HTC which does not require the thermophysical properties or vapor liquid equilibrium data of boiling mixtures.
- HTC slightly deteriorated for repeated runs which might be due to randomness of boiling or instability of the investigated copper surfaces.
- The developed dynamic method provided results comparable with the commonly employed steady-state method of measurement. For more accurate results, a more precise indirect estimation of the liquid composition is required.

7. Experiments with Thick Nickel-Plated Samples

7.1 Motivation, Novelty, and Parameters of Experiments

During my internship at the Laboratory for Thermal Technology, University of Ljubljana, experiments with saturated and subcooled boiling of water–glycerin mixtures were done on five smooth nickel-plated copper samples produced by the very same manufacturing procedure. The investigated copper samples were chemically nickel-plated to create a stable heating surface and to eliminate possible instability and reactivity of copper surfaces [199,209–212]. The following objectives were set for the experimental research:

- Observe the dependence of HTC on subtle changes of the mixture concentration in the range of high water mass fractions and molar fractions ($\omega_w \geq 0.90$, $x_w \geq 0.98$). On the basis of the results presented in Section 6.5 and of the literature, a stronger dependence of the boiling performance on the mixture concentration and a possible enhancement of HTC are expected for mixtures with a low content of glycerin.
- Evaluate the stability of the nickel-plated copper surfaces and their boiling performance via multiple repeated runs and long-term experiments.
- Correlate the measured saturated and subcooled HTCs and evaluate whether the correlations suitable for copper surfaces, see Section 6, are also suitable for the nickel-plated surfaces.
- Observe the effect of subcooling on HTC and compare it with the effect of the mixture concentration.

The experiments were performed for saturated and subcooled boiling of water–glycerin mixtures at atmospheric pressure in a wide range of heat flux. Saturated and subcooled HTCs were measured for the mixtures with the water mass fractions ω_w = 1.00, 0.98, 0.95, 0.90, 0.85, 0.80, 0.70, and 0.60 which correspond to molar fractions from 1.00 down to 0.88. The saturated boiling experiments were performed using the dynamic method of measurement, described by Može et al. [213] and validated in our study [203], in the heat flux range from 50 to 650 kW m^{-2}. The subcooled measurements were conducted for all the investigated compositions at discrete heat flux levels of approximately 250, 450, and 650 kW m^{-2}. To assess the effect of subcooling on HTC, the measurements were done at a continuously decreasing subcooling from 30 down to 0 K. CHF was not investigated during both saturated and subcooled experiments to prevent the thermal decomposition of glycerin and changes of the surface structure.

The novelty of the outlined experimental research might be summarized by the following points:

- There are no experimental data related to the boiling performance of water–glycerin mixtures on nickel surfaces.
- The HTC during subcooled boiling of mixtures is largely unexplored. The effect of subcooling on the HTC during mixture boiling has not been described in the literature.
- Four concentrations in the range of ω_w from 0.90 to 1.00 were studied to observe the effect of small glycerin additions on saturated and subcooled HTCs and to assess the possible enhancement of heat transfer reported in the literature for mixtures with a low content of glycerin.

The obtained results presented and discussed in this section were previously published in our article [214].

7.2 Experimental Apparatus

The experiments were performed using the experimental apparatus shown in Figure 7.1. The boiling chamber is made of the glass cylinder clamped between two stainless steel flanges. During measurements, the chamber is filled with 200 g of the investigated liquid. The tested cylindrical sample is insulated

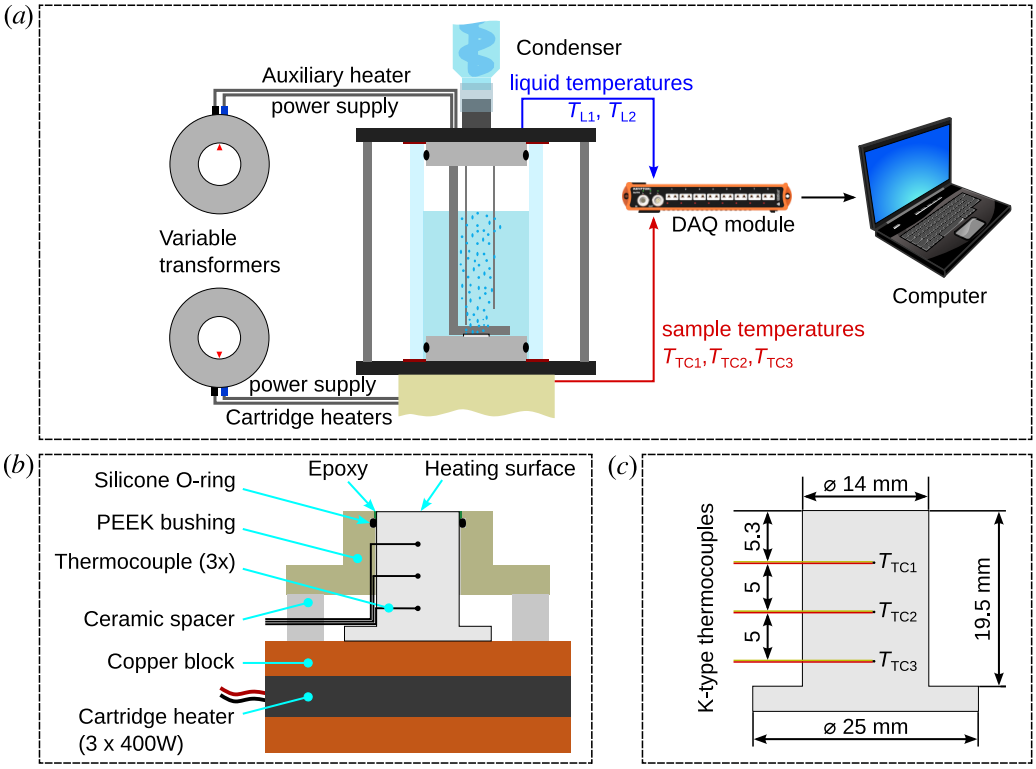

Figure 7.1: The experimental apparatus for thick nickel-plated samples built by the research team at the Laboratory for Thermal Technology: (*a*) the boiling chamber and the equipment, (*b*) the tested sample, bushing, and heating block with cartridge heaters, (*c*) the dimensions of the sample and positions of TCs.

with a polyether ether ketone (PEEK) bushing and mounted onto a copper block. Flexible epoxy glue *Duralco 4538* is used to seal the gap between the PEEK bushing and the sample and to prevent nucleation along the perimeter of the heating surface. The sample is inserted into the apparatus through a hole made in the bottom flange. Three AC-powered cartridge heaters with nominal power of 3×400 W are accommodated in the copper block and controlled with variable transformer *Metrel HSN 260/8*. An auxiliary immersion heater is used to preheat and degas the boiling liquid before the start of each measurement, to maintain liquid temperature during saturated runs, and to gradually decrease the subcooling of the boiling liquid during subcooled runs. A glass water-cooled condenser is attached to the top flange of the boiling chamber.

Five identically manufactured cylindrical nickel-plated copper samples (named Sample 1 to Sample 5) were investigated. The flat top nickel-plated face of each tested samples serves as the heating surface on which boiling takes place. Three unsheathed K-type *Omega* TCs are glued into each sample using *Resbond 989FS* adhesive. The TCs are vertically aligned and 5 mm apart. The highest TC is 5.3 mm below the heating surface. The temperature of the liquid is measured with two sheathed K-type *Omega* TCs submerged at different depths. The signals from the TCs are acquired with *Dewesoft KRYPTONi-8xTh* DAQ module at a frequency of 10 Hz. TC voltages are converted to temperatures using the NIST 9th degree polynomial [215]. Cold-junction temperature is measured with a Pt1000 probe and is used to offset the measured voltages before the conversion.

7.3 Measurement Procedure and Calculation of HTC

Table 7.1 presents the number of subcooled and saturated runs performed for each of the investigated nickel-plated samples. Due to a significant discrepancy between the HTCs measured during water boiling using Samples 1 and 2, comparative water boiling experiments were performed with Samples 3 and 4 to

Table 7.1: The number of saturated and subcooled runs performed for each of the tested samples and concentrations investigated.

Sample	Saturated runs								Subcooled runs							
ω_w =	1.00	0.98	0.95	0.90	0.85	0.80	0.70	0.60	1.00	0.98	0.95	0.90	0.85	0.80	0.70	0.60
1	6	3	3	3	3	3	3	3	6	3	3	3	3	3	3	3
2	3+4	3+3	4+4	3	3	3+3	3	3	3+5	3+5	3+5	3	3	5	3	5
3	10*	0	0	0	0	0	0	0	0	0	0	0	0	0	0	0
4	6	0	0	0	0	0	0	0	3	0	0	0	0	0	0	0
5	7	3	3	3	3	3	3	3	3	3	3	0	0	0	0	0

Notes: $x + y$ means that at first, x runs were done for a certain investigated concentration. Then, after the whole series of saturated and subcooled experiments was finished for all investigated concentrations, y repeated runs were performed.
* Long-term water boiling for approximately 40 hours was maintained on the heating surface of Sample 3. Ten measurements were conducted during the period.

verify the previously measured values. Long-term saturated water boiling was maintained on the heating surface of Sample 3 for about 40 hours to assess its stability and the effect of its aging on HTC. For Sample 4, saturated and subcooled water tests were conducted. Since the measurements with Samples 3 and 4 confirmed the previously observed trends and HTCs, additional experiments were performed with Sample 5. For Sample 5, saturated runs were performed at all investigated concentrations and subcooled runs only at the three highest concentrations (this was due to the fact that the trends of subcooled experiments were found to be very predictable and it was not necessary to do them for all the investigated concentrations). In total, 110 saturated and 82 subcooled runs were performed for all tested samples.

Cleaning and Degassing of the Heating Surface

Before inserting the sealed and mounted sample into the boiling chamber, its top surface was rinsed with 2-propanol and wiped with a lint-free wipe. After the sample was put in place, the chamber was filled with 200 g of twice-distilled water and the auxiliary heater was turned on. The water was degassed through vigorous boiling on the auxiliary heater for 45 min. Next, the cartridge heaters were turned on and boiling was established on the heating surface at approximately 200 kW m^{-2} for 15 min to expel any noncondensable gases from its cavities. Then, the liquid was cooled to below 80 °C to condense the the vapor nuclei in the cavities of the surface. Saturated runs were performed afterward.

Experiments in Saturated States

During each saturated run, the heat flux was continuously increased at a rate below 0.2 kW m^{-2} s^{-1} in the natural convection regime and below 2 kW m^{-2} s^{-1} in the nucleate boiling regime and a continuous up-going boiling curve was recorded. In the supplementary material of our study [203], we performed numerical simulations and experimental data comparison to confirm that such a slow continuous increase of the heat flux has a negligible impact on the measured values. When a heat flux of about 650 kW m^{-2} was achieved, the power supplied to the cartridge heaters was slowly decreased and a down-going curve was recorded. The auxiliary heater was operating throughout the whole run to maintain the saturation temperature of the boiling fluid. At the end of each saturated run, the heating cartridges and auxiliary heater were turned off and the liquid was cooled below 90 °C to condense the vapor nuclei in the cavities. Three consecutive saturated runs were performed for each investigated sample and concentration to analyze the measurement repeatability and the stability of the tested samples.

The methodology suggested by Može et al. [208] was employed to calculate the heat flux, superheat, and HTC for saturated runs. One-dimensional heat conduction inside the copper sample was assumed, since lateral losses were found negligible due to the relatively small thermal conductivity of the PEEK bushing.

The temperature gradient ($\mathrm{d}T/\mathrm{d}x$) in the sample was calculated from the temperature difference between the uppermost and lowermost TCs and the distance between them. The heat flux q was obtained using Fourier's law

$$q = -\lambda \frac{\mathrm{d}T}{\mathrm{d}x} \,. \tag{7.1}$$

The thermal conductivity of copper was calculated with the polynomial function

$$\lambda = 2.83 \times 10^{-4}\, T^2 - 0.165\, T + 378.1 \,, \tag{7.2}$$

where λ ($\mathrm{W\,m^{-1}\,K^{-1}}$) is the thermal conductivity of copper and T (°C) denotes the temperature within the sample. Polynomial (7.2) is based on the results of the laser-flash measurements of thermal diffusivity of the copper rod from which the tested samples were manufactured [208].

The temperature of the heating surface T_s is extrapolated using the temperature T_TC1 measured by the topmost TC. First, the thermal conductivity λ is evaluated at T_TC1 with Equation (7.2) and put into Equation (7.1) to obtain the heat flux q. The temperature T_s is then extrapolated using the values of T_TC1 and q. Secondly, the mean temperature between T_TC1 and T_s is calculated and put into Equation (7.2) to obtain the thermal conductivity λ'. This allows for a more accurate calculation of T_s, because the dependence of thermal conductivity on temperature is taken into account. The temperature T_s is then calculated with the equation

$$T_\mathrm{s} = T_\mathrm{TC1} - \frac{q\,\Delta x_\mathrm{1s}}{\lambda'} \,, \tag{7.3}$$

where $\Delta x_\mathrm{1s} = 5.3$ mm is the vertical distance between the uppermost TC and the heating surface. The (saturated) HTC α was then calculated with Equation (2.5). The *bubble-point* temperature T_b was obtained as the average temperature measured with both submerged TCs. It should be reminded that for saturated boiling, the *saturated*, *total*, and *boiling* HTCs are equal to each other, see relation (1.11).

Experiments in Subcooled States

To perform the experiments with subcooled boiling, we developed the following procedure. After each third saturated run was finished, three subcooled runs were performed at heat flux levels maintained at approximately 250, 450, and 650 $\mathrm{kW\,m^{-2}}$ during the entire run. At the beginning of each run, the liquid was cooled below 65 °C to reach a subcooling higher than 30 K. Then, the variable transformer was manually adjusted in such a way that the heat flux quickly increased and stabilized at the desired level. After the target heat flux was reached, the auxiliary heater was turned on to slowly decrease the subcooling of the liquid. Saturated boiling was eventually reached after about 20 min. Throughout each run, the heat flux was constantly monitored and the output voltage of the variable transformer was manually adjusted to maintain as steady heat flux as possible. The same methodology as for saturated runs was then applied for calculation of q and T_s. The *total* HTC was then calculated with Equation (1.9). The temperature of the liquid T_L (which was increasing in time) was taken as the average of both temperatures measured with submerged TCs.

When three subcooled runs were finished, the concentration of glycerin in the boiling liquid was increased. Glycerin (*Carl Roth*, ≥ 98%) was precisely weighted in a beaker, mixed with a small amount of the boiling liquid pumped out of the boiling chamber to decrease its viscosity, and added into the boiling chamber. After the addition, the mixture was homogenized by vigorous boiling on the auxiliary heater and then cooled below 90 °C to prepare it for the next series of saturated runs.

7.4 Measurement Uncertainties

The method presented by Može et al. [208] was used for calculation of the measurement uncertainties. The following uncertainties were evaluated experimentally: 0.16 mm for the distance between the neighboring

TCs, 0.18 mm for the distance between the uppermost TC and heating surface, 0.19 K at 100 °C and 0.30 K at 250 °C for the temperature measurements. A relative uncertainty of 1.5 % for thermal conductivity was estimated based on the accuracy of the laser-flash measurement of thermal diffusivity. The calculated values of the relative uncertainties of the HTC $u_r(\alpha)$, heat flux $u_r(q)$, and superheat $u_r(\Delta T_{sat})$ are listed in Table 7.2 for the lowest, medium and highest investigated heat fluxes.

Table 7.2: The relative uncertainties of the HTC $u_r(\alpha)$, heat flux $u_r(q)$, and superheat $u_r(\Delta T_{sat})$ calculated for low, medium, and high heat flux levels. Published in [214].

q (kW m^{-2})	$u_r(\alpha)$ (%)	$u_r(q)$ (%)	$u_r(\Delta T_{sat})$ (%)
50	22.3	20.2	2.7
300	5.6	4.1	1.9
650	4.3	2.7	2.0

7.5 Results and Discussion for Saturated Runs

In this section, the experimental data obtained during saturated runs are presented and discussed. Although continuous dependencies were obtained with the dynamic method of measurement, equidistant discrete points are presented in all following figures in this section for the sake of clarity. Due to the fact that the boiling hysteresis and discrepancies between the values measured during repeated runs were rather negligible, average the data for all repeated runs evaluated from up- and down-going boiling curves are presented in this section.

Performance and Stability of Individual Samples during Boiling of Water

Figure 7.2 shows the HTCs measured during boiling of water for the five investigated samples. The measured HTCs are quite comparable for smaller heat fluxes, but differ for heat fluxes higher than

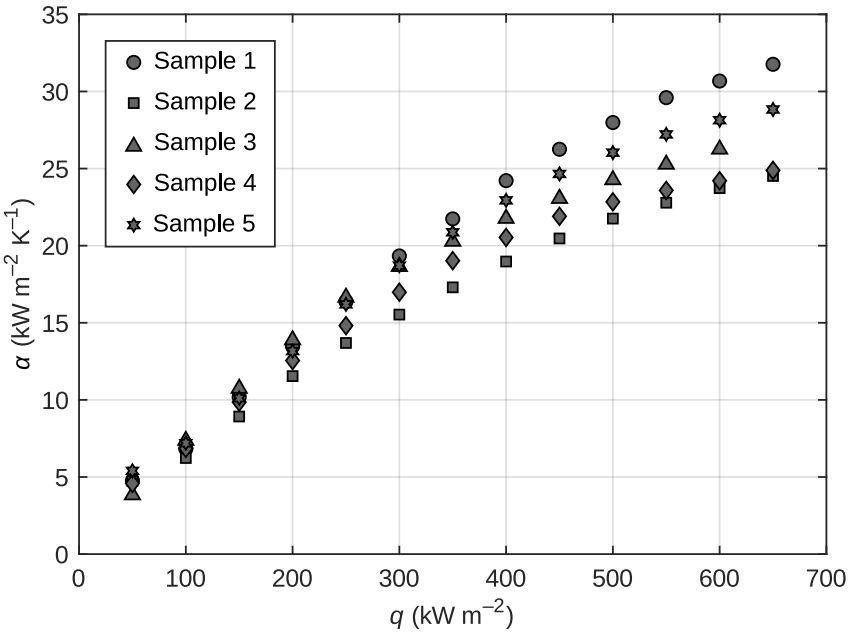

Figure 7.2: The comparison of the HTCs measured during boiling of pure water for all investigated samples. Published in [214].

approximately 100 kW m^{-2}. The highest and lowest HTCs were measured for Samples 1 and 2, respectively. A negligible variation of HTC was measured for the repeated runs done with Sample 2 after finishing the whole series of saturated and subcooled runs, which indicates that the heating surface remained stable and that surface aging and contamination did not affect the measured values. To further verify that the deviation between Sample 1 and Sample 2 was not caused by some surface defects or other distinctive factors, comparative water runs were performed with Samples 3 and 4. Although water was boiled over 40 hours on Sample 3, the continuous measurements of HTC confirmed the general stability of nickel-plated surfaces and the repeatability of measurements. The HTCs measured for Sample 3 were more or less between those measured for Samples 1 and 2. For Sample 4, the HTCs measured during comparative water tests were generally lower (especially for higher heat fluxes) and comparable with Sample 2. The heat transfer performance of Sample 5 was the second highest of all the samples investigated. Although comparable with Sample 1 for lower heat fluxes, its performance was lower for heat fluxes higher than approximately 350 kW m^{-2}. Due to the fact that all water experiments were repeated multiple times and that the long-term stability of the studied surfaces was favorable, the significant spread of HTCs, observed especially during boiling of pure water and mixtures of a higher water mass fraction ω_w, is considered to be characteristic for the studied smooth nickel-plated surfaces. All obtained data were, therefore, used for further analyses. The discrepancy between the heat transfer performance of individual samples is most likely caused by activation of different nucleation sites and variation in nucleation site density, which were observable during the experiments by the naked eye.

Averaged Data Set and HTC Deterioration

Since this work aims at general trends valid for nickel-plated surfaces and not at the heat transfer performance of individual samples, all the following analyses are done for the measured HTCs which were averaged across all investigated samples. This averaged data set is shown in Figure 7.3 for all the investigated heat fluxes and concentrations together with the experimental data published by Sternling and Tichacek [192] and by Vajc et al. [200] presented in Section 6. The data in Figure 7.3 evince a deterioration

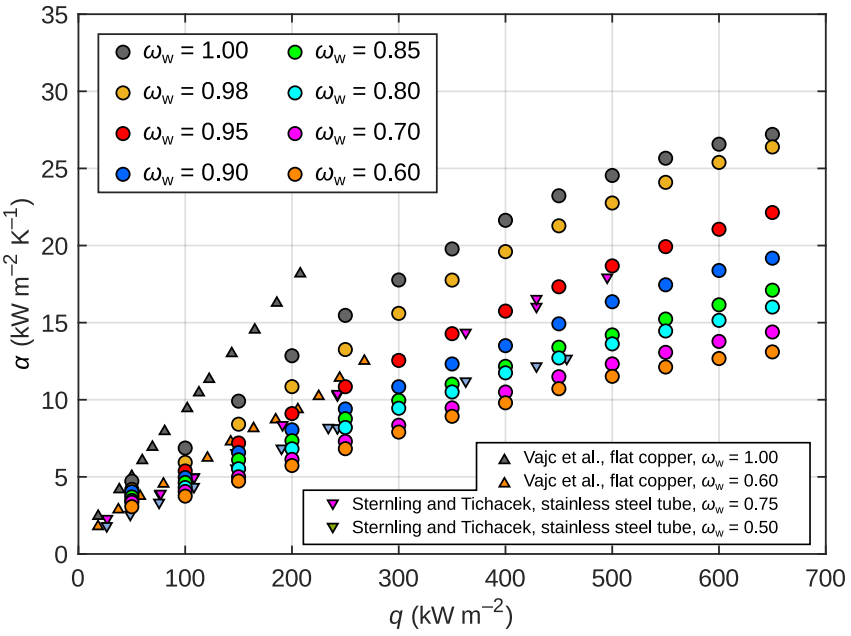

Figure 7.3: The measured HTCs averaged across all the studied samples and the comparison with the experimental data of Vajc et al. [200], see Section 6, and of Sternling and Tichacek [192]. Published in [214].

of HTC with decreasing ω_w. Although this general trend was obtained for each of the tested samples, the exact values of the HTC and its relative decrease due to the lowering of ω_w was unique for each sample. Nevertheless, for all investigated samples, the drop of HTC was more pronounced for higher ω_w and no HTC enhancement was detected for any heat flux and concentration investigated. The observed trends generally agree with the measurements performed on the copper surface presented in Section 6. Although lower HTCs of about 65 % were measured for nickel-plated surfaces relative to the copper surface, as noticeable in Figure 7.3, the relative drop of HTC of about 50 % measured for the copper surface when ω_w was decreased from 1.00 to 0.60 agrees very well with the relative drop in the present data set. The measured values of HTC published by Sternling and Tichacek, see Figure 7.3, which were obtained on stainless steel tubes, also follow a trend comparable with the present data set. According to their data, a deterioration of about 25 % occurred when they decreased ω_w from 0.75 down to 0.50. This is comparable with the drop in the present data set when ω_w was lowered from 0.85 to 0.60.

Pure-Fluid Correlations

Figure 7.4 shows the averaged data set and the trends of the *ideal* HTC correlated with the pure-fluid correlation of Stephan and Abdelsalam [69], see Equation (1.65), and with the pure-fluid correlation of Yagov [52], see Equation (1.76). Both correlations were evaluated employing the thermophysical properties

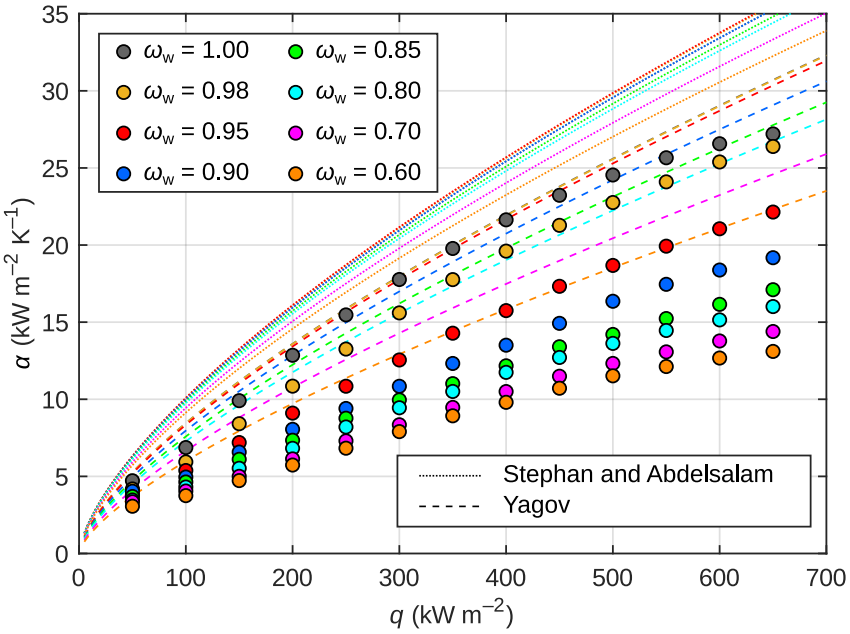

Figure 7.4: The measured data compared with the pure-fluid correlation of Stephan and Abdelsalam [69] and the pure-fluid correlation of Yagov [52]. Published in [214].

given in Table 3.1. The combination of the correlation of Stephan and Abdelsalam and the Schlünder correlation, was found to agree with the experimental results obtained on the copper surface presented in Section 6. The same combination was also used by Alavi Fazel et al. [143] for boiling of water–glycerin mixtures on stainless steel tubes. However, the pure-fluid correlation of Stephan and Abdelsalam was found to be inappropriate for the tested nickel-plated surfaces, because it significantly overpredicts the HTC measured for the investigated mixtures (including pure water). The values of SEE and MRE between the correlation and the averaged data set, are 9.7 kW m^{-2} K^{-1} and 77 %, respectively. The correlation predicts similar HTCs for the ω_w = 1.00 and 0.90 mixtures and slightly higher HTCs for the ω_w = 0.98 and 0.95 mixtures, which does not agree with the measured data. The pure-fluid correlation of Yagov, on the other hand, is more conservative and closer to the data points which is also evident by lower values

of SEE and MRE of about 5.4 kW m^{-2} K^{-1} and 41 %, respectively. The Yagov correlation predicts only a slight decrease of HTCs for the ω_w = 1.00, 0.98, and 0.95 mixtures, which also does not correspond to the present data, since a strong deterioration of HTC was measured for mixtures with a low content of glycerin. The difference between the trends in the present data and both pure-fluid correlations is caused by the impact of the *mixture effects* on HTC which is important even for the lowest investigated values of the glycerin concentration in the boiling mixture.

Mixture Correlations

Correlation of Schlünder

HTCs measured for the copper surface presented in Section 6 were successfully correlated with the combination of the Stephan and Abdelsalam [69] pure-fluid correlation and the Schlünder [117] mixture correlation. However, for the present data, this combination produces significant errors (SEE = 6.3 kW m^{-2} K^{-1} and MRE = 51 %). Since the correlation of Stephan and Abdelsalam was shown to substantially overrate HTC, see Figure 7.4, it was tested whether using the Yagov pure-fluid correlation, which is in better agreement with experiments, gives better correspondence with the present data when combined with the correlation of Schlünder. Figure 7.5 shows the comparison between the measured data and the combination of the Schlünder and the Yagov correlation. Although the correlated values agree quite well with the data for

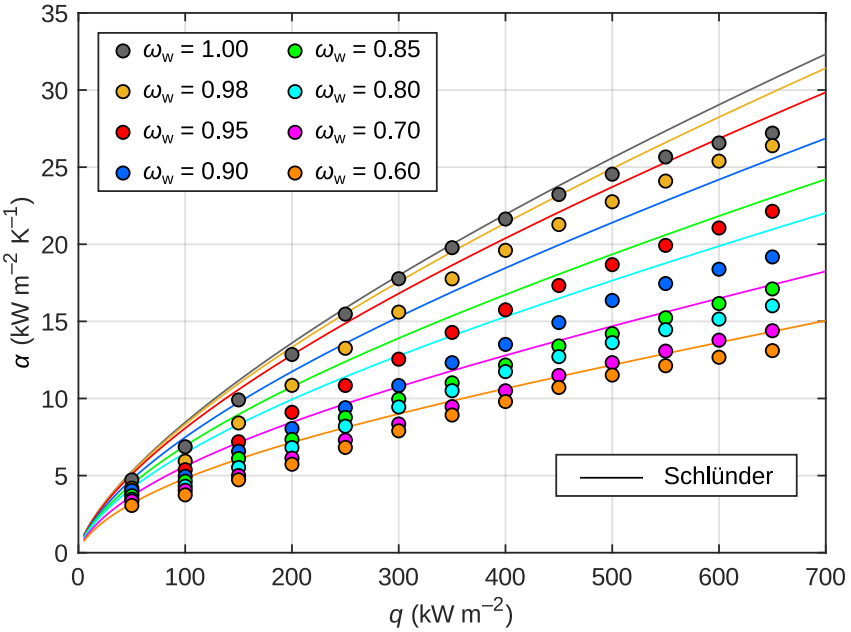

Figure 7.5: The measured data compared with the combination of the mixture correlation of Schlünder [117] and the pure-fluid correlation of Yagov [52]. The empirical coefficients $C_0 = 1$ and $\beta_L = 2 \times 10^{-4}$ m s^{-1} were employed. Published in [214].

the highest and lowest investigated ω_w, the intermediate concentrations are not predicted with a sufficient accuracy. Lower, but still unacceptable errors (SEE of 3.4 kW m^{-2} K^{-1} and MRE of about 26 %) were calculated between the calculated values and data points. Although the replacement of the pure-fluid correlation was able to reduce both errors almost by half, the Schlünder correlation seems not to be applicable for the nickel-plated copper surfaces due to substantial overprediction of HTCs for mixtures with ω_w from 0.95 down to 0.70. Optimizing the empirical coefficients C_0 and β_L of the Schlünder correlation, see Equation (2.28), does not substantially reduce both errors, as SEE of 3.0 kW m^{-2} K^{-1} and MRE of about 22 % were obtained for the optimal coefficients $C_0 = 1$ and $\beta_L = 1 \times 10^{-4}$ m s^{-1}.

Finding a Suitable Combination of Pure-Fluid and Mixture Correlations

The HTCs correlated with the combinations of different mixture correlations presented in Section 2.5 and of the pure-fluid correlation of either Stephan and Abdelsalam or Yagov, were compared with the measured averaged data set. The obtained values of SEE and MRE are listed in Table 7.3 for each individual combination and for the recommended or optimized empirical coefficients. The lowest errors were obtained using the correlation of Inoue and Monde [138] and the model of Kandlikar [125] for which the *pseudo-single-component* HTC was calculated with the pure-fluid correlation of Yagov (it is not possible to employ Equation (2.36), since the value of α_2 for pure glycerin is not known and cannot be measured due to the decomposition of glycerin at higher boiling temperatures). The optimization of the empirical coefficients a and b contained in the Inoue and Monde correlation, see Equation (2.34), results in only a small reduction of both SEE and MRE. Therefore, the original coefficients recommended by Inoue and Monde are considered applicable for boiling of water–glycerin mixtures on nickel-plated copper surfaces.

Table 7.3: The calculated values of SEE and MRE, see Equations (6.2) and (6.3), between the measured data and the listed combinations of correlations. Published in [214].

Mixture correlation	Pure-fluid correlation	SEE ($\mathrm{kW\,m^{-2}\,K^{-1}}$)	MRE (%)
Schlünder (2.28)			
$\beta_L = 2 \times 10^{-4}\ \mathrm{m\,s^{-1}}$	Stephan and Abdelsalam (1.65)	6.3	51
$\beta_L = 2 \times 10^{-4}\ \mathrm{m\,s^{-1}}$	Yagov (1.76)	3.4	26
$\beta_L = 1 \times 10^{-4}\ \mathrm{m\,s^{-1}}$	Yagov (1.76)	3.0	22
Stephan and Preusser (2.24)			
$C_{12} = 1.53$	Stephan and Abdelsalam (1.65)	8.5	67
$C_{12} = 1.53$	Yagov (1.76)	4.6	35
$C_{12} = 3.56$	Yagov (1.76)	3.8	28
Fujita and Tsutsui (2.32)	Stephan and Abdelsalam (1.65)	7.9	53
	Yagov (1.76)	7.7	50
Kandlikar (2.37)	Stephan and Abdelsalam (1.65)	4.5	34
	Yagov (1.76)	1.9	13
Inoue and Monde (2.34)			
$a = 0.15$, $b = 0.25$	Stephan and Abdelsalam (1.65)	3.1	19
$a = 0.15$, $b = 0.25$	Yagov (1.76)	2.2	12
$a = 0.09$, $b = 0.85$	Yagov (1.76)	1.9	12

The comparison of the correlation of Inoue and Monde with the measured averaged data set is depicted in Figure 7.6. Although the correlation predicts a strong deterioration of HTC relative to pure water for the $\omega_w = 0.98$ mixture, which was not confirmed by the measurements, there is a satisfactory agreement between the correlated and measured values for the remaining concentrations. The correspondence between the correlation of Inoue and Monde and measurements is also documented in Figure 7.7 according to which, most of the correlated values do not deviate by more than ±15 % from the data points averaged separately for each tested sample.

In Table 7.3, it might also be noticed that significant SEE and MRE were obtained for the correlation of Fujita and Tsutsui and that both errors seem to be quite independent of the employed pure-fluid correlation. This is due to the fact that the Fujita and Tsutsui correlation substantially undervalues HTCs for all investigated boiling mixtures regardless of the employed pure-fluid correlation. It was, therefore, investigated whether correlations of Thome [121], Thome and Shakir [98], and Inoue et al. [108], see Equations (2.20), (2.30), and (2.33), respectively, which all consider the boiling range ΔT_{db} to have a leading impact on HTC, might be employed instead of the correlation of Fujita and Tsutsui. However, all

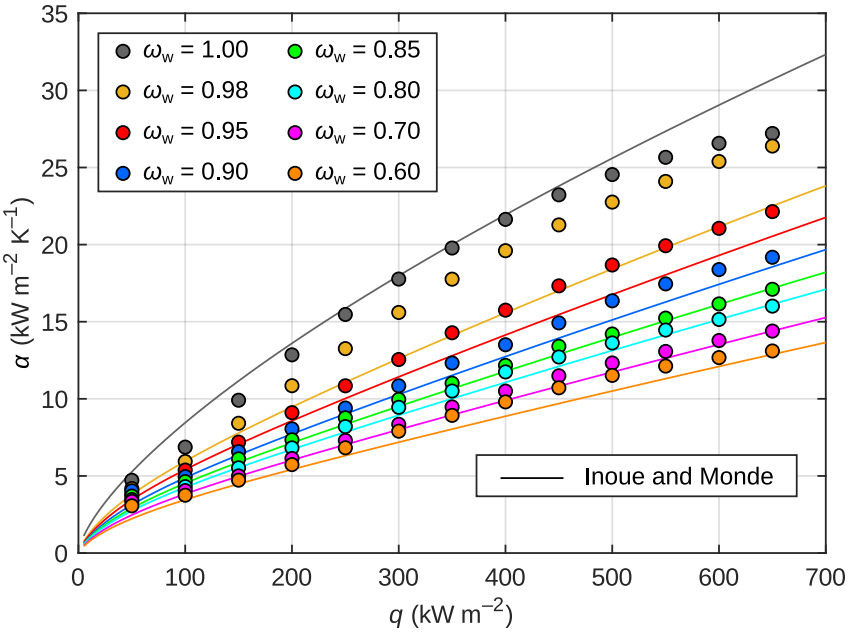

Figure 7.6: The averaged data set and the predictions of the combination of the mixture correlation of Inoue and Monde [138] and the pure-fluid correlation of Yagov [52]. The empirical coefficients $a = 0.15$ and $b = 0.25$ were employed. Published in [214].

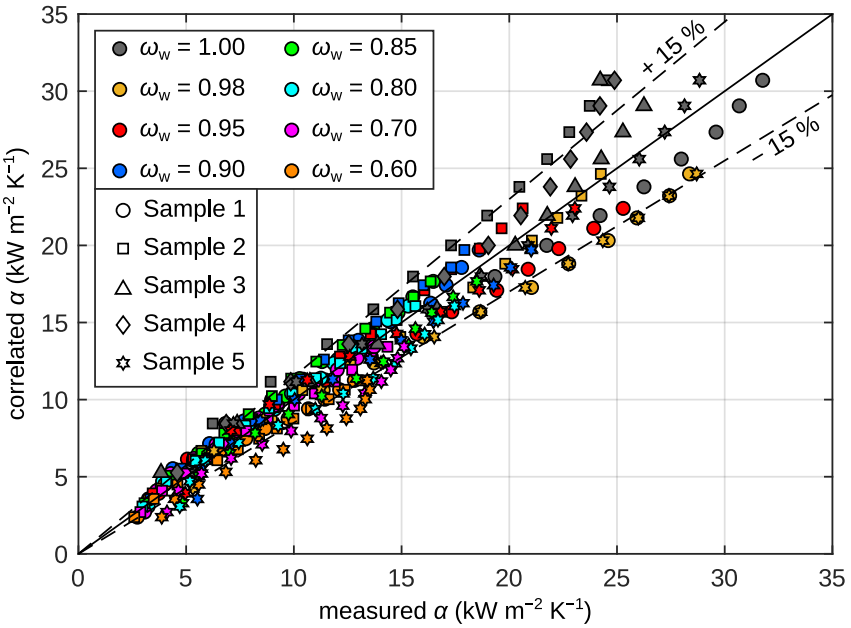

Figure 7.7: The deviation of the combination of the mixture correlation of Inoue and Monde [138] and the pure-fluid correlation of Yagov [52] from the measured HTCs averaged for each individual sample. The empirical coefficients $a = 0.15$ and $b = 0.25$ were employed. Published in [214].

three correlations undervalued HTC even more than the correlation of Fujita and Tsutsui and produced even greater SEE and MRE. With respect to the obtained results, the correlations based primarily on the boiling range ΔT_{db} are considered inappropriate for water–glycerin mixtures due to the very high values of ΔT_{db} characteristic for these mixtures, as was illustrated in Figure 3.4.

Own Empirical Correlation for HTC

The empirical correlation

$$\alpha = q^{0.70}\left[1.30\,\mathrm{e}^{-10.6(1-\omega_{\mathrm{w}})} + 1.18\right] \tag{7.4}$$

was developed to quickly estimate the measured HTCs. The correlation does not require any thermophysical properties of the boiling mixture and is valid for the water–glycerin mixtures with ω_{w} from 1.00 down to 0.60 boiling on smooth nickel surfaces at heat fluxes from 25 up to 650 kW m^{-2}. The correlation is based on the asymptotic deterioration of HTC with decreasing ω_{w}. The drop of HTC is assumed to be asymptotic, because it appears to be very significant for higher ω_{w}, but much more subtle and almost barely measurable for the lowest investigated water mass fractions ($\omega_{\mathrm{w}} = 0.70$ and 0.60). This is also noticeable in Figure 7.8, which shows the asymptotic decrease of the ratio ε defined as

$$\varepsilon = \frac{\alpha - \alpha_{0.6}}{\alpha_{1.0} - \alpha_{0.6}}\,, \tag{7.5}$$

where α is the HTC measured at a certain mass fraction, $\alpha_{1.0}$ is the HTC measured for pure water, and $\alpha_{0.6}$ is the HTC measured for the $\omega_{\mathrm{w}} = 0.60$ mixture.

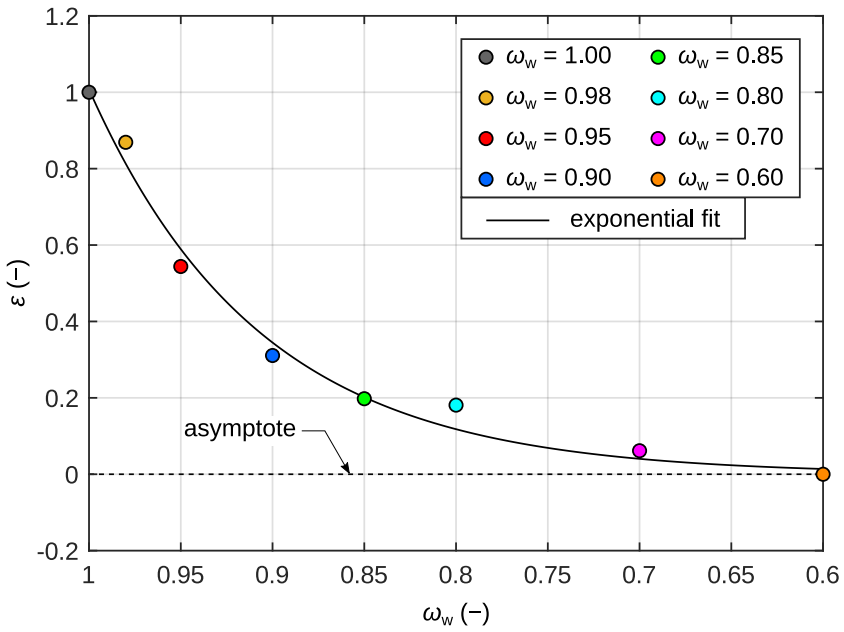

Figure 7.8: The asymptotic decrease of the ratio ε, see definition (7.5), with the decreasing mass fraction ω_{w}. Published in [214].

Empirical correlation (7.4) is valid for α in (W m^{-2} K^{-1}), q in (W m^{-2}), and ω_{w} (−). The coefficients and their 95 % confidence intervals $C_1 = 1.30 \pm 0.03$, $C_2 = -10.6 \pm 0.6$, and $C_3 = 1.18 \pm 0.02$ were obtained by fitting the three-parametric exponential function $\alpha = q^{0.70}\left[C_1\,\mathrm{e}^{C_2(1-\omega_{\mathrm{w}})} + C_3\right]$ to the experimental data. The exponent of the heat flux q was fixed at 0.70, because it best agreed with the data (although the

errors produced by the correlation are not strongly dependent on the value of the exponent). The values SEE = 1.7 kW m^{-2} and MRE = 11 % were evaluated between the measured data and correlation (7.4). The predictions of correlation (7.4) and averaged data set are plotted in Figure 7.9. The maximum deviations between correlation (7.4) and the measured HTCs are mostly comparable with, or lower than ±15 % for the measured HTCs greater than about 6 kW m^{-2} K^{-1}, as demonstrated in Figure 7.10.

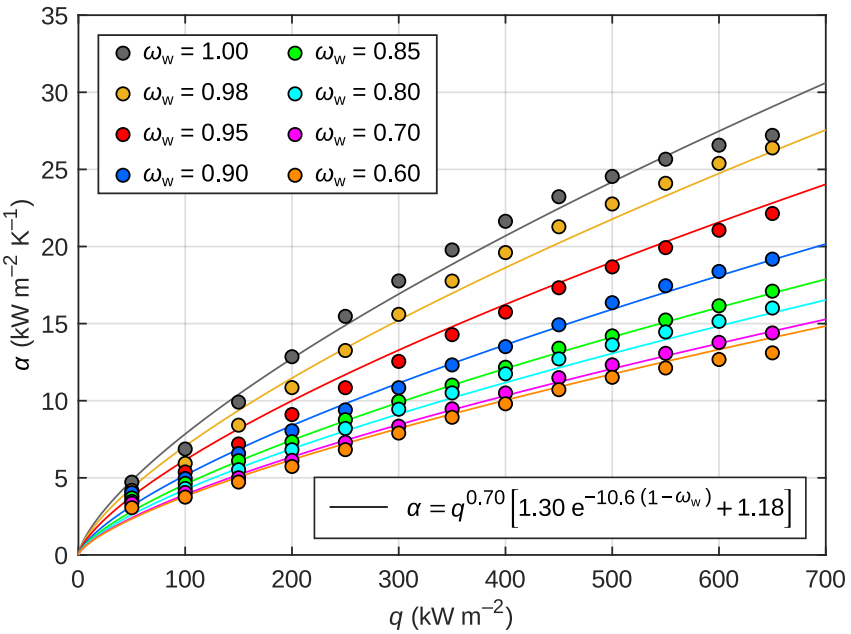

Figure 7.9: The averaged data set compared with empirical correlation (7.4). Published in [214].

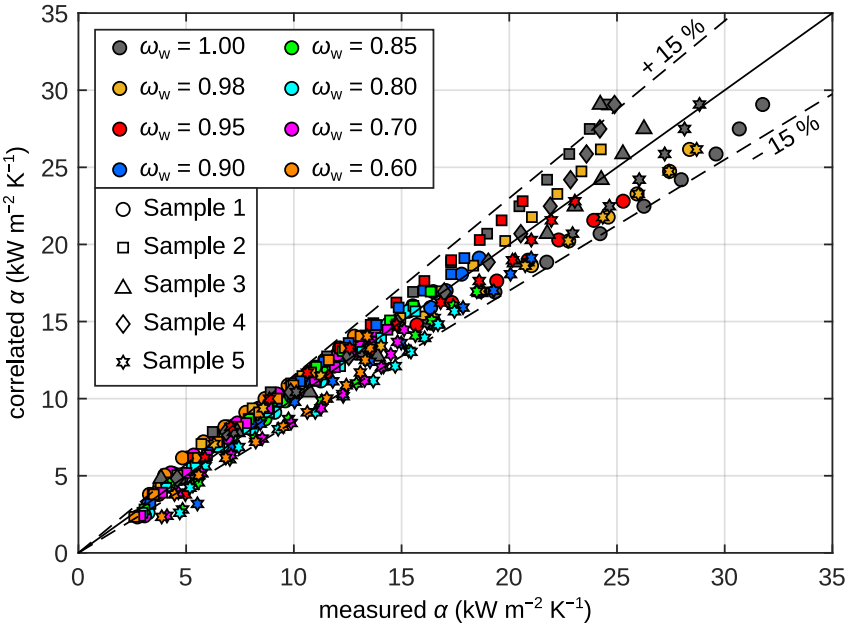

Figure 7.10: The deviation of empirical correlation (7.4) from the measured data averaged for each individual sample. Published in [214].

Figure 7.11 shows the contour map of HTC as a function of ω_w and q. The contours were plotted using empirical correlation (7.4).It is clearly visible that the contour lines become strongly curved for higher heat fluxes and that smaller HTCs are reached for mixtures with a higher amount of glycerin, relative to the HTCs obtained for pure water. For instance, the HTC obtained at the maximum investigated heat flux of 650 kW m^{-2} for the mixture with $\omega_w = 0.60$, corresponds to that obtained for pure water at a heat flux of only about 300 kW m^{-2}. The more straight and almost horizontal contour lines in the right part of Figure 7.11 indicate that HTC becomes less dependent on composition when ω_w is decreased, which is consistent with the asymptotic deterioration of HTC, which was discussed above and shown in Figure 7.8.

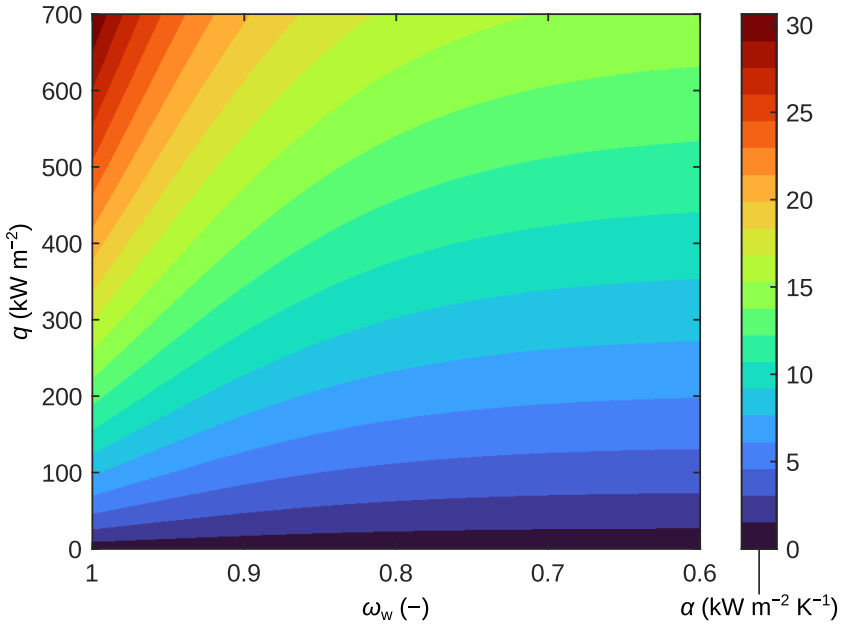

Figure 7.11: The contour map of HTC calculated with empirical correlation (7.4). Published in [214].

7.6 Results and Discussion for Subcooled Runs

This section presents the results of measurements obtained during subcooled runs and their comparison with suitable predictive models. Although subcooling was continuously decreased during each experimental run, discrete data points are plotted at the selected levels of subcooling in all following figures in this section, to make them more readable and uncluttered.

Developed Regime of Subcooled Boiling

Figure 7.12 shows the temperatures of the heating surface of Sample 1, extrapolated from the temperatures measured inside the sample. For the sake of clarity, only the data points obtained at heat fluxes around the lowest investigated heat flux level of 250 kW m^{-2} are shown in Figure 7.12 which demonstrates that at these heat fluxes, the measured surface temperatures T_s are more or less constant and independent of subcooling (the relatively minor unsteady changes of T_s are caused by the manual adjustments of the power supplied to the heating cartridges to maintain the desired heat flux level throughout each run). For higher heat flux levels as well as for different samples, the constant surface temperatures independent of subcooling were also measured. The independence of the surface temperature T_s on the subcooling ΔT_{sub} indicates that *developed subcooled boiling*, which was discussed in Section 1, was reached for all the samples, concentrations, and heat fluxes investigated. Although *developed subcooled boiling* was observed

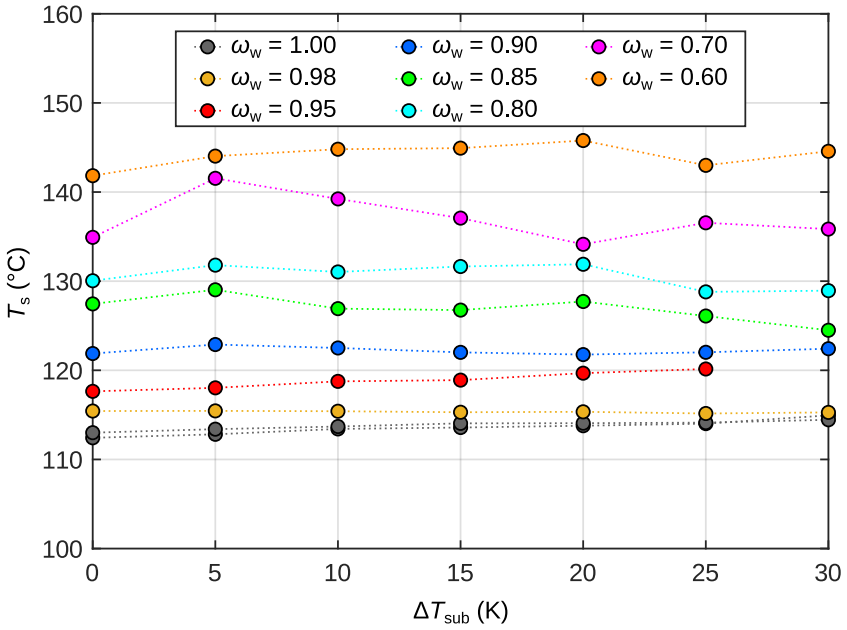

Figure 7.12: The temperature of the heating surface T_s measured at various levels of subcooling ΔT_{sub}. For clarity, only the data obtained for Sample 1 in the range $200 < q < 300$ kW m^{-2} are shown. Published in [214].

by researchers for various single-component boiling liquids [216–219], it was not studied for mixtures. The limiting heat flux $\hat{q}$, beyond which subcooled boiling becomes independent of subcooling, depends on the combination of the boiling liquid and heating surface. For instance, HTCs independent of subcooling were achieved at heat fluxes higher than 70 kW m^{-2} during pool boiling of water on a stainless steel tube [219]. The heat flux needed for the transition from the *partially developed* to the *fully developed* regime of boiling predicted with Zuber correlation, see Equation (1.7), and with the correlation of Moisis and Berenson, see Equation (1.8), is the highest for the $\omega_w = 0.80$ mixture for which the values $q_{pd \to fd}$ of 171 kW m^{-2} and 158 kW m^{-2} were calculated, respectively. However, these values are only informative, because both correlations were developed for boiling of pure fluids.

Calculation of HTC for the Regime of Developed Subcooled Boiling

Combining the Inoue and Monde Correlation and the Yagov Correlation

Due to the fact that the temperature of the heating surface T_s and the superheat ΔT_{sat} were both measured to be independent of the subcooling ΔT_{sub}, it is possible to predict the *boiling* HTC α_b, see definition (1.10), using a suitable mixture correlation. The *total* HTC α_{tot} might then be calculated using Equation (1.11). In Figure 7.13, the measured *total* HTCs are compared with the results of Equation (1.11), where α_b was calculated with the combination of the correlation of Inoue and Monde and the correlation of Yagov. This combination was found to be suitable for saturated HTCs, see Section 7.5. The trends predicted by Equation (1.11) capture the measured course of the *total* HTC α_{tot} which decreases for a higher subcooling. Once again, only the runs obtained for Sample 1 at heat flux levels $200 < q < 300$ kW m^{-2} are shown in Figure 7.13 for clarity, but all the figures are quite similar for all the samples and heat fluxes investigated. SEE and MRE between the calculated and measured α_{tot} is 1.6 kW m^{-2} K^{-1} and 9 %, respectively, for all the samples and heat fluxes investigated. A direct comparison between the *total* HTCs α_{tot} calculated by Equation (1.9) and the measured values is presented in Figure 7.14. Although the vast majority of data

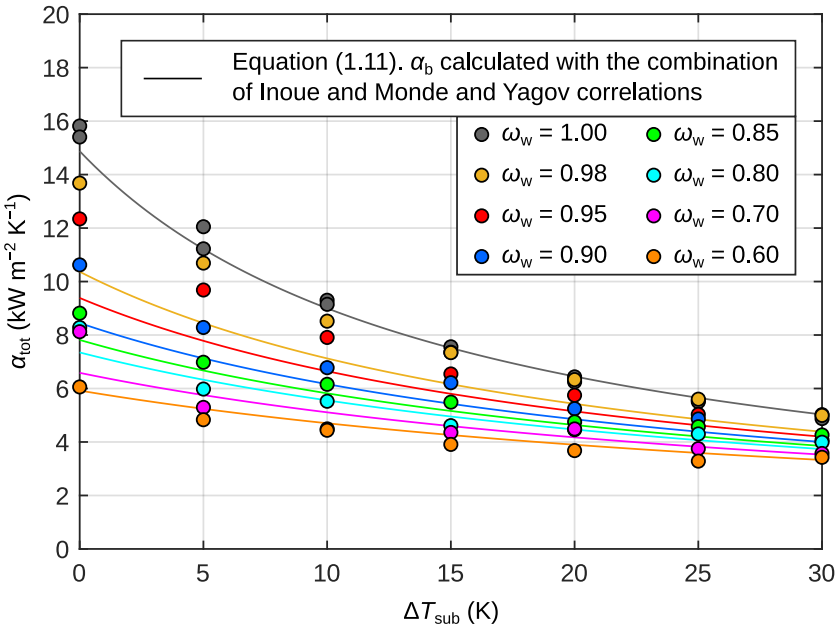

Figure 7.13: The measured *total* HTCs and the predictions of Equation (1.11), where α_b was calculated with the combination of the Inoue and Monde [138] mixture correlation and the Yagov pure-fluid correlation [52]. The empirical coefficients $a = 0.15$ and $b = 0.25$ were employed. Only the data obtained for Sample 1 at $200 < q < 300$ kW m^{-2} are shown for clarity. Published in [214].

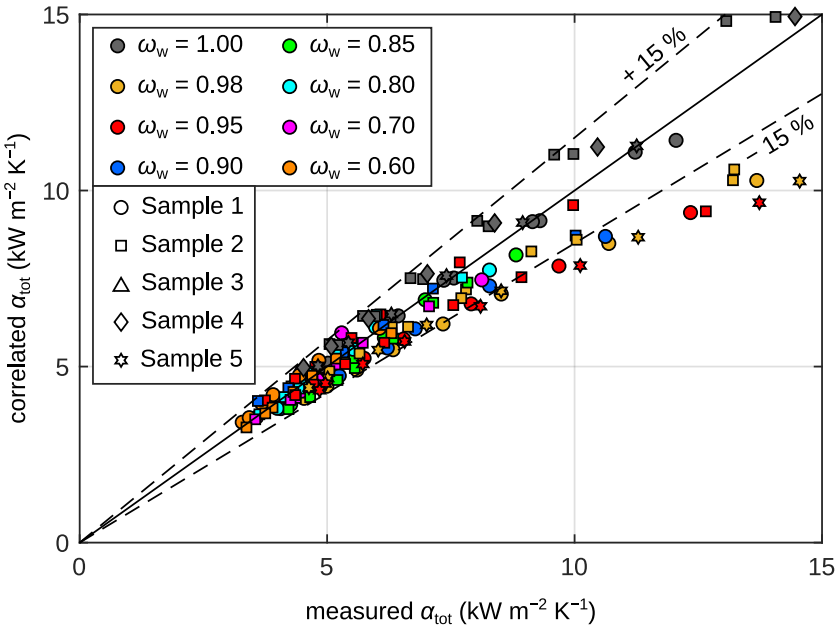

Figure 7.14: The comparison of the measured *total* HTCs, which were averaged for each of the investigated samples, with the predictions of Equation (1.9) where α_b was calculated with the combination of the Inoue and Monde [138] mixture correlation and the pure-fluid correlation of Yagov [52]. The empirical coefficients $a = 0.15$ and $b = 0.25$ were employed. Published in [214].

points do not deviate by more than ±15 %, there are some data obtained at higher heat fluxes and HTCs which are underpredicted by more than ±15 %.

Using Own Empirical Correlation

When empirical correlation (7.4), developed for saturated boiling, is employed for the calculation of α_b instead of the combination of the Inoue and Monde correlation and the correlation of Yagov, the empirical correlation

$$\frac{1}{\alpha_{tot}} = \frac{1}{q^{0.70}\left[1.30\,e^{-10.6(1-\omega_w)} + 1.18\right]} + \frac{\Delta T_{sub}}{q} \tag{7.6}$$

is obtained. Correlation (7.6) produces a slightly lower SEE of about 1.1 kW m^{-2} K^{-1} and MRE below 7 % when compared with the experimental data. For correlation (7.6), deviations lower than or comparable with ±15 % were obtained for all the measured *total* HTCs, as shown in Figure 7.15.

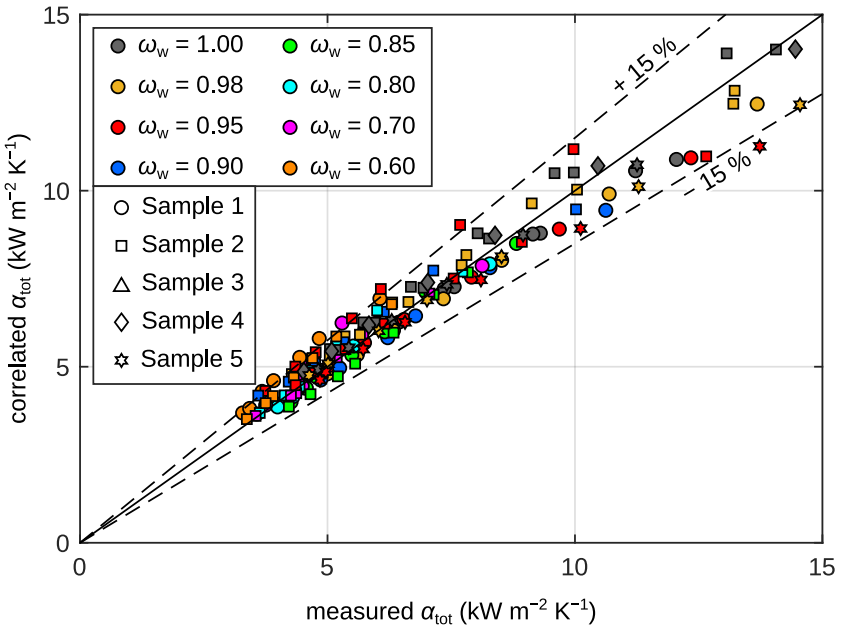

Figure 7.15: The comparison of the measured *total* HTCs, which were averaged for each of the investigated samples, with the predictions of empirical correlation (7.6). Published in [214].

Figure 7.16 shows the contour map of the *total* HTC as a function of the mass fraction ω_w and of the subcooling ΔT_{sub} during the subcooled boiling at the heat flux level of 300 kW m^{-2}. The contours were obtained using empirical correlation (7.6). The contour lines are more or less straight and diagonal for higher mass fractions ω_w at all investigated subcoolings ΔT_{sub}. This indicates that for these ranges of ω_w and ΔT_{sub}, neither the subcooling nor the water mass fraction have a dominant effect on the *total* HTC. However, for lower ω_w, the contour lines bend and become more horizontal which means that the impact of subcooling on the *total* HTC becomes more important relative to the variations of ω_w. Furthermore, the stripes of a constant *total* HTC are closer to each other and more dense in the bottom left corner of the map. This implies that the effect of the subcooling and composition on the *total* HTC is more important for the less subcooled mixtures with a lower content of glycerin.

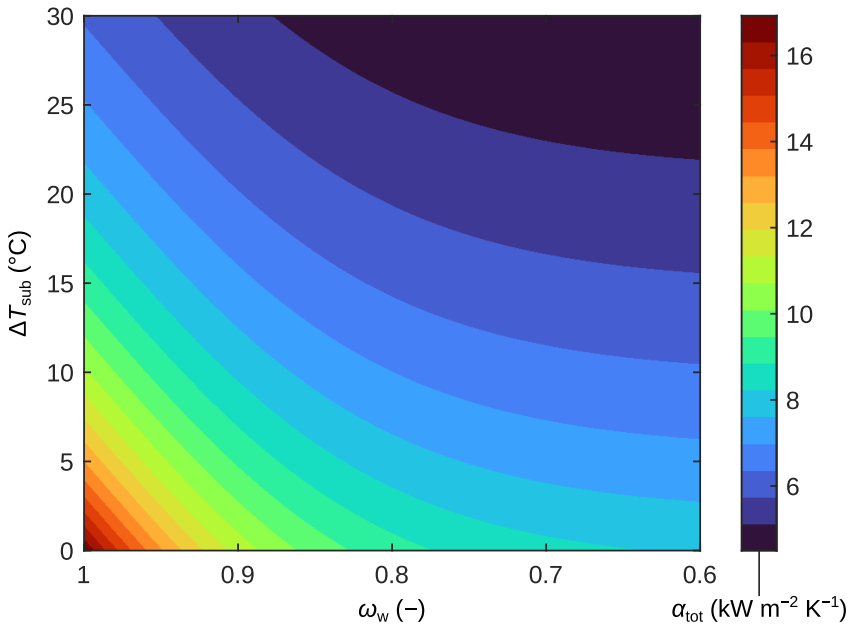

Figure 7.16: The contour map of the *total* HTC calculated for $q = 300$ kW m^{-2} using empirical correlation (7.6). Published in [214].

Reminder

In the end of this section, I would like to emphasize and remind the readers that the results of the correlations for saturated boiling might be employed into Equation (1.11) only when the temperature of the heating surface does not depend on the liquid subcooling or, in other words, after the *developed subcooled regime* is established. Outside of the regime of developed subcooled boiling, the dependency of HTC on subcooling is more complex, see, for instance, the studies of Judd et al. [220], Rainey et al. [218], Ulucakli and Merte [221], or Forster and Greif [14].

7.7 Summary of Experimental Results

The following conclusions can be drawn from the results of the experiments with saturated boiling of water–glycerin mixtures on nickel-plated surfaces:

- HTC decreases with the increasing concentration of glycerin in the boiling mixture. The decrease is more significant for mixtures with a higher water content.
- The *mixture effects* significantly affect HTC for all concentrations and heat flux levels investigated.
- No enhancement of HTC was observed for any heat flux or composition of the boiling mixture investigated.

The three conclusions above agree with those presented for the copper surface in Section 6.7. The following conclusions are unique to the saturated boiling experiments performed on nickel-plated surfaces:

- The measured HTCs were significantly different during boiling of water for the five investigated samples, especially at higher heat fluxes. A relative HTC differences of about ±14 % were measured between individual samples.
- The HTCs measured for nickel-plated surfaces are generally lower relative to those measured for copper surfaces for a given heat flux. For the ranges of the heat flux and mass fraction investigated for both

surface materials, the HTCs measured for the nickel-plated surfaces reached of about 65 % relative to those measured for the copper surface presented in Section 6.

- The investigated nickel-plated surfaces are characterized by a very stable boiling performance, as was confirmed during the multiple repeated runs and long-term boiling experiments.
- Combinations of the mixture correlation of Inoue and Monde and of the modified model of Kandlikar with the pure-fluid correlation of Yagov are suitable for boiling of glycerin on nickel-plated surfaces. On the contrary, the combination of the Stephan and Abdelsalam pure-fluid correlation and of the Schlünder mixture correlation, which was considered suitable for copper surfaces, was found to be not applicable for the studied nickel-plated surfaces.
- The own empirical correlation was formed for estimation of HTC, which does require neither the thermophysical properties nor the vapor liquid equilibrium data of boiling mixtures.

For the subcooled boiling measurements performed on nickel-plated surfaces, it was observed that:

- The developed subcooled boiling regime was reached for all heat fluxes, subcoolings, and concentrations investigated.
- The correlations suitable for saturated boiling of mixtures are able to predict the subcooled boiling HTC in the regime of developed subcooled boiling.
- The effects of subcooling and composition on the *total* HTC are stronger for less subcooled mixtures with a lower content of glycerin.

8. Experiments with Thin Titanium Foil

8.1 Motivation, Novelty, and Parameters of Experiments

In Sections 6 and 7, the measurements of HTCs were performed on thick copper and nickel-plated samples, respectively. In this section, the measurement of the boiling parameters of water–glycerin mixtures is performed with an IR camera, which allows much more detailed analysis of the boiling performance and of important boiling parameters. The apparatus built by the research team at the Laboratory for Thermal Technology, University of Ljubljana, was used to monitor the temperature field of a thin titanium foil which was electrically heated. Titanium was selected as the investigated material, because it provides more sharper temperature footprint of bubbles, limited lateral conduction, more homogeneous heat flux, and better repeatability and stability of consecutive experiments, relative to stainless steel foils. Foils made of copper are not usable for this measurement because of the high electrical conductivity of copper which would result in low generated heat fluxes. A single piece of titanium foil was used for all performed experiments, to maintain the same distribution of cavities of the heating surface and to achieve the highest possible repeatability.

Experiments were conducted to accomplish the following targets:

- Calculate HTC from the average temperatures of the heating surface and observe the resulting trends of HTC during boiling of water–glycerin mixtures on the titanium foil.
- Analyze the distributions of the measured superheats for all investigated mixtures.
- Observe whether the same cavities are active during repeated runs for different concentrations of the mixture.
- Observe how nucleation parameters change with the heat flux and concentration of the boiling mixture.

The measurements were carried out for the water–glycerin mixtures with water mass fractions ω_w of 1.00, 0.98, 0.95, 0.90, 0.85, 0.80, 0.70, and 0.60, which correspond to molar fractions x_w from 1.00 down to 0.88. The investigated heat flux was from about 1 kW m^{-2} to 200 kW m^{-2} for pure water and from about 1 kW m^{-2} to 175 or 150 kW m^{-2} for the mixtures. All investigated heat fluxes are safely below the CHF. We decided to decrease the maximum investigated heat flux for mixtures with a lower ω_w due to the HTC deterioration which could result in thermal damage to the foil. Steady states of boiling were reached for all the captured data points. Stable continuous nucleation was observed for heat fluxes higher than approximately 50 kW m^{-2}.

The novelty of the performed experiments might be briefly characterized by the following statements:

- Boiling of water–glycerin mixtures on titanium surfaces has not yet been investigated.
- The analysis of boiling of water–glycerin mixtures (or of some other mixture with a similar boiling behavior) based on IR footage (or some other contactless methods of measurement) has not yet been performed.
- The values of nucleation parameters and their trends with the changing composition of the boiling mixture are unknown and missing in the literature. They are often estimated using the correlations valid for pure fluids, which were discussed in Section 1.2.

The obtained results presented and discussed in this section were previously published in our article [222].

8.2 Experimental Apparatus

The experiments were performed using the apparatus shown in Figure 8.1 designed by the researchers at the Laboratory for Thermal Technology, University of Ljubljana. The boiling chamber with the dimensions

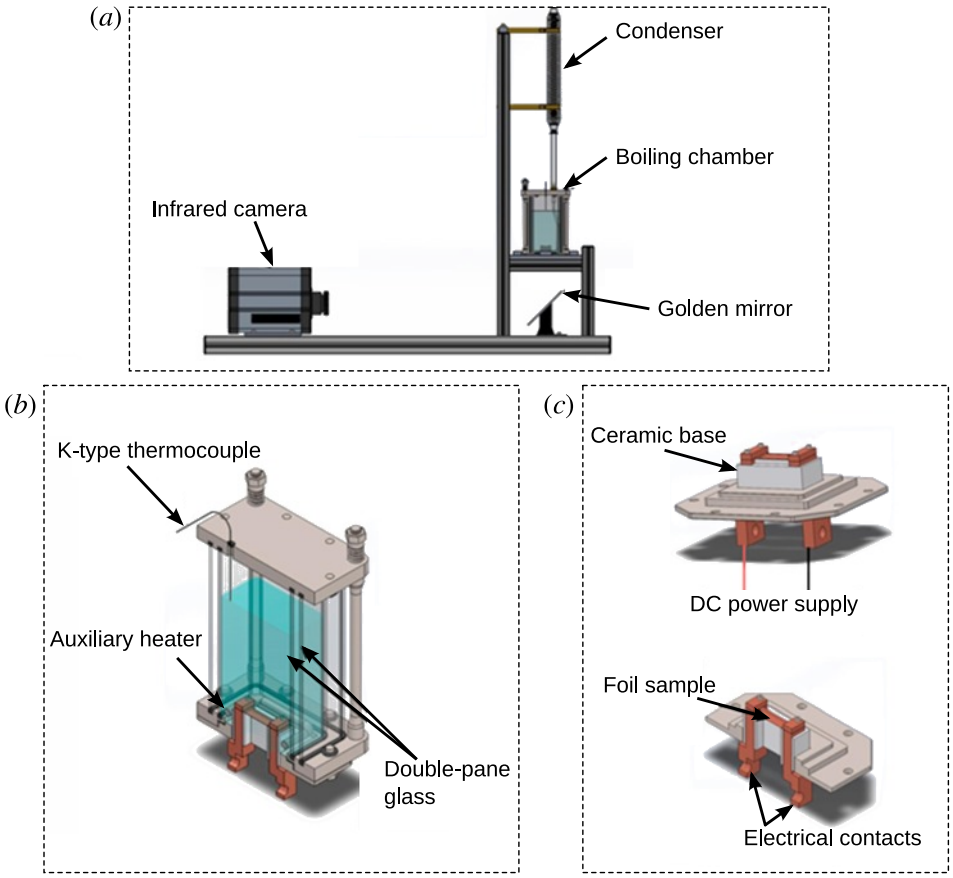

Figure 8.1: The experimental apparatus for thin foil samples built by the research team at the Laboratory for Thermal Technology: (*a*) side view of the experimental stand, (*b*) cross-sectional view of the boiling chamber, (c) the assembly which holds the foil. Adopted from Voglar et al. [223].

of 100 × 100 mm and height of 170 mm made of double-pane glass is clamped between two steel flanges. A glass water-cooled condenser is attached to the top flange. The assembly which holds the tested thin foil is screwed with the bottom flange. A single rectangular titanium foil with purity of 99.99 %, thickness $\delta_{\text{foil}} = 25$ µm, effective area of 27.6 × 17.7 mm and roughness R_a of about 0.07 µm was used for all the experiments performed. The foil was glued together with a ceramic base made of *Macor* using *Duralco 4538* epoxy resin, and clamped between two electrical contacts made of nickel-plated copper. At the center of the ceramic base is a rectangular borehole with dimensions of 23 × 13 mm so that it is possible to film the bottom side of the foil with an infrared (IR) camera. The bottom side of the foil is painted with a high-emissivity paint of the average spectral emissivity $\varepsilon = 0.90$ in the infrared band from 3 to 5 µm [12,224].

Science-grade IR camera *FLIR SC6000* is used to film the temperature distribution on the bottom side of the thin foil. A golden mirror is placed below the boiling chamber at an angle of 45° to prevent a potential damage to the camera due to possible leakage of the liquid. The electrical contacts of the foil assembly are connected to DC power supply *TDK Lambda GEN 10-1000* which has output voltage from 0 to 10 V and output current from 0 to 1 000 A. The current from the power supply is measured indirectly using shunt *EMPRO LAB-1000-100* which has a nominal electrical resistance $R_{\text{shunt}} = 1 \times 10^{-4}$ Ω. The temperature of the liquid is measured with two K-type TCs immersed in the boiling liquid about 5 and 15 mm above the tested foil. All the measured electrical signals are processed with DAQ multiplexer unit *AGILENT 34972A*. An auxiliary heater of a hook-resembling shape is immersed in the liquid to maintain

the saturation temperature. The heater has a nominal power of about 0.5 kW and is powered with variable autotransformer *Metrel HSN 206/8*.

8.3 Calculation of Heat Flux and HTC

The heat flux generated by electrical heating in the foil can be calculated with the equation

$$q_{\mathrm{el}} = \frac{U_{\mathrm{foil}}\, U_{\mathrm{shunt}}}{S_{\mathrm{foil}}\, R_{\mathrm{shunt}}}\,, \tag{8.1}$$

where U_{foil} is the measured voltage across the foil, S_{foil} is the surface of the foil, and $U_{\mathrm{shunt}}/R_{\mathrm{shunt}}$ is the current flowing through the foil calculated from the measured voltage across the shunt U_{shunt} and the nominal electrical resistance of the shunt R_{shunt}. However, due to lateral conduction and heat accumulation, only a part of q_{el} is eventually transferred to the boiling fluid, as depicted in Figure 8.2, where q is the heat flux transferred to the fluid, q_{ac} is the heat flux accumulated in the foil, which is related to the temporal gradients of surface temperature, and q_{c} is the heat flux laterally conducted within the foil, associated with the spatial gradients of surface temperature in both Cartesian directions of the foil surface (denoted x and y).

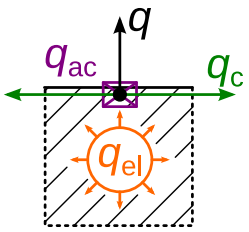

Figure 8.2: Heat flux partitioning.

The heat balance

$$q = q_{\mathrm{el}} - q_{\mathrm{ac}} - q_{\mathrm{c}} \tag{8.2}$$

might be assumed for the heat flux components illustrated in Figure 8.2. For a control volume around a given node $[i,j]$ in the 2D space and time layer n, the accumulative and convective heat fluxes might be calculated from the temperature fields recorded with the IR camera. Using finite-difference schemes, the approximations

$$q_{\mathrm{ac}} = \delta_{\mathrm{foil}}\, \varrho_{\mathrm{Ti}}\, c_{p\mathrm{Ti}}\, \frac{\partial T}{\partial t} \approx \delta_{\mathrm{foil}}\, \varrho_{\mathrm{Ti}}\, c_{p\mathrm{Ti}}\, \frac{T^{n}_{i,j} - T^{n-1}_{i,j}}{\tau_{\mathrm{film}}}\,, \tag{8.3}$$

$$q_{\mathrm{c}} = \delta_{\mathrm{foil}}\, \lambda_{\mathrm{Ti}} \left(\frac{\partial^2 T}{\partial x^2} + \frac{\partial^2 T}{\partial y^2} \right) \approx \delta_{\mathrm{foil}}\, \lambda_{\mathrm{Ti}}\, \frac{4\,T^{n}_{i,j} - T^{n}_{i+1,j} - T^{n}_{i-1,j} - T^{n}_{i,j+1} - T^{n}_{i,j-1}}{\Delta L^2_{\mathrm{px}}} \tag{8.4}$$

might be obtained from the Fourier–Kirchhoff equation assuming the infinitesimal element of the control volume $\mathrm{d}V = \mathrm{d}x\,\mathrm{d}y\,\delta_{\mathrm{foil}}$, the element of the control surface $\mathrm{d}S = \mathrm{d}x\,\mathrm{d}y$, and that the length elements $\mathrm{d}x$ and $\mathrm{d}y$ are equal to the spatial resolution of the IR camera $\Delta L_{\mathrm{px}} = 0.11$ mm (ΔL_{px} is the distance between two neighboring pixels) which was measured before the boiling experiments took place. The time period between two consecutive frames $\tau_{\mathrm{film}} = 1/\mathrm{fps} = 625$ µs. A positive value of q_{ac} means that heat was accumulated in the control volume during the time period or recording τ_{film}. A positive value of q_{c} means that heat was conducted out of the control volume. The following thermophysical properties of titanium at temperatures around 100 °C were adopted from Milošević and Maglić [225]: $\lambda_{\mathrm{Ti}} = 18.6\ \mathrm{W\,m^{-1}\,K^{-1}}$, $c_{p\mathrm{Ti}} = 547\ \mathrm{J\,kg^{-1}\,K^{-1}}$, $a_{\mathrm{Ti}} = 7.56\times10^{-6}\ \mathrm{m^2\,s^{-1}}$. The density of titanium $\varrho_{\mathrm{Ti}} = 4\,498\ \mathrm{kg\,m^{-3}}$ was obtained from the definition of the thermal diffusivity a_{Ti}.

8.4 Measurement Procedure

Before the foil assembly was screwed to the bottom flange of the apparatus, the foil was rinsed with 2-propanol and dried with a lint-free wipe. After the apparatus was assembled, 400 g of twice-distilled water was carefully weighted and poured into the boiling chamber. The water was degassed for 45 minutes by vigorous boiling on the auxiliary heater. Then, boiling on the surface was initiated at a heat flux of around 100 $\mathrm{kW\,m^{-2}}$ for about 1 minute to expel any gas entrapped inside the cavities of the foil. After

that, the foil power supply was turned off and the degassing continued for 15 more minutes. When the procedure was completed, the liquid was left to cool down to condense the remaining vapor nuclei until it reached a temperature below 80 °C. The same degassing procedure was performed for the investigated mixtures when the experiments were suspended for more than couple of hours.

At the start of each experimental run, the liquid was heated by the auxiliary heater to the saturation temperature and left to boil for several minutes. Then, a series of measurements were performed at the discrete heat flux values q_{el} of 0, 1, 10, 25, 50, 75, 100, 125, 150, 175, and 200 kW m^{-2}. The heat flux q_{el} generated by the electrical heating was continuously monitored using the custom-made LabVIEW interface and was always increased during all experimental runs. This was a precaution to obtain at least some measured data in the case that the foil was unable to withstand higher heat fluxes and melted. The heat flux q_{el} was increased from 0 to 200 kW m^{-2} for water and highly concentrated water–glycerin mixtures. For mixtures with a higher glycerin content, it was limited to 175 or 150 kW m^{-2} to prevent foil melting due to the HTC deterioration and higher temperatures of the foil. The stable states of boiling are established more or less instantaneously on thin foils due to their low heat capacity and fast responsiveness. After the desired heat flux was set, the auxiliary heater was switched off to not influence the process of bubble nucleation from the foil and IR footage was acquired. A rectangular area which consisted of 126 horizontal and 94 vertical pixels was filmed with the IR camera for a duration of 3 seconds at a frame rate of 1 600 fps. The treatment of the IR videos recorded with the camera is described in Appendix A. After the IR video was captured, the auxiliary heater was turned back on and the heat flux q_{el} was altered by changing the current of the DC power supply. The IR camera was switched on at least 3 hours before the measurements to cool down its detector.

After each experimental run was finished, the boiling liquid was cooled below 90 °C to condense all vapor nuclei trapped in the cavities of the foil. When a series of two consecutive runs was finished, the required amount of glycerin was weighted and poured into the boiling chamber to increase the glycerin concentration of the boiling liquid to a desired level. After the addition, vigorous boiling of the liquid was maintained on the auxiliary heater for a couple of minutes to homogenize the boiling mixture.

8.5 Measurement Uncertainties

The relative propagated uncertainty of the heat flux $u_{\mathrm{r}}(q)$ of about 0.25 % of the measured value was obtained from the analysis of Equation (8.1) [223]. For the conversion of IR images to temperatures, a calibration curve was used which was experimentally measured in the range from 80 to 180 °C at steps of 5 °C. During the calibration, the uncertainty of temperature measurements $u(T) = 1$ K was determined. Both $u_{\mathrm{r}}(q)$ and $u(T)$ were found to be quite independent of temperature. The *noise equivalent differential temperature* (which can also be viewed as the thermal sensitivity of the IR camera) is less than 20 mK. For such a low value, the uncertainty of the temperature differences between neighboring pixels is significantly lower than the temperature uncertainty $u(T)$. The maximum uncertainty of HTC determined from the values of $u_{\mathrm{r}}(q)$ and $u(T)$ was found to be of about $u(\alpha) = 1.7$ kW m^{-2} K^{-1}. The relative uncertainty of HTC decreases for higher heat fluxes and superheats. Heat losses due to natural convection into the stagnant air beneath the foil and the temperature drop across the thickness of the foil might both be considered negligible [226].

8.6 Results and Discussion

Distributions of Superheat

The distributions of the superheat of the heating surface were investigated. The superheat ΔT_{sat}, see definition (2.4), was calculated from the *bubble-point* temperatures T_b measured with the immersed TCs and from the temperatures of the heating surface recorded with the IR camera, which were stored in matrices $[T_s]$ (the method used for calculation of matrices $[T_s]$ from the measured data is described in Appendix A). The superheat ΔT_{sat} seems to follow a normal Gaussian distribution, as illustrated in Figure 8.3 which shows two examples of histograms obtained during boiling of water and the $\omega_w = 0.60$ mixture at $q = 175\ \mathrm{kW\,m^{-2}}$. It is evident that higher values and wider distribution of superheat were measured for the $\omega_w = 0.60$ mixture. Superheat distributions were analyzed for all 119 measurements performed. The arithmetic mean and standard deviation of the measured surface superheat are listed in Appendix B for all investigated heat fluxes and concentrations. The mean value of ΔT_{sat} and its standard deviation were found to rise slightly and steadily with the increasing concentration of glycerin in the mixture and with increasing heat flux. Tolubinsky and Ostrovsky [58] observed that during boiling of pure water and pure ethanol, various boiling parameters follow a normal Gaussian distribution.

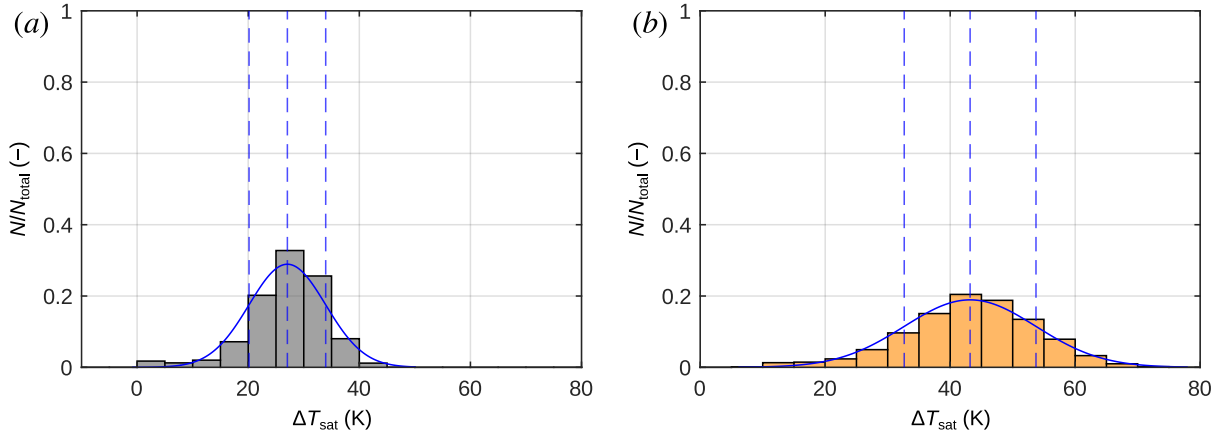

Figure 8.3: The histograms of the relative probability of superheats obtained at $q = 175\ \mathrm{kW\,m^{-2}}$ for: (*a*) pure water, (*b*) the $\omega_w = 0.60$ mixture. The dashed lines mark the positions of the mean value and standard deviation. The full line is the corresponding normal Gaussian distribution.

Boiling Curves and HTCs

To visualize boiling curves and HTCs with respect to the heat flux and composition of the boiling mixture, averaging was performed over the whole $[x,y,t]$ domains of individual surface temperature matrices $[T_s]$. The temperature matrix $[T_s]$ and heat flux matrix $[q]$, calculated with Equations (8.2), (8.3), and (8.4), were thus both averaged in space and time. Then, HTC was calculated using definition (2.5), where the *bubble-point* temperature T_b was taken as the arithmetic mean of the temperatures measured with the immersed TCs. Figure 8.4 shows the dependence of the HTC α on the heat flux q and mass fraction ω_w. The values measured during both experimental runs were averaged and a single data row is shown for each individual concentration for the sake of clarity. The boiling curves corresponding to Figure 8.4 measured during both experimental runs are shown in Appendix C. In Figure 8.4, the measured HTCs are also compared with the data from Sections 6 and 7 obtained for the $\omega_w = 0.60$ mixture. In general, lower HTCs which reached of about 45 % and 70 % relative to the previously investigated copper and nickel-plated surfaces, respectively, were measured with the titanium foil. The smaller HTCs might be

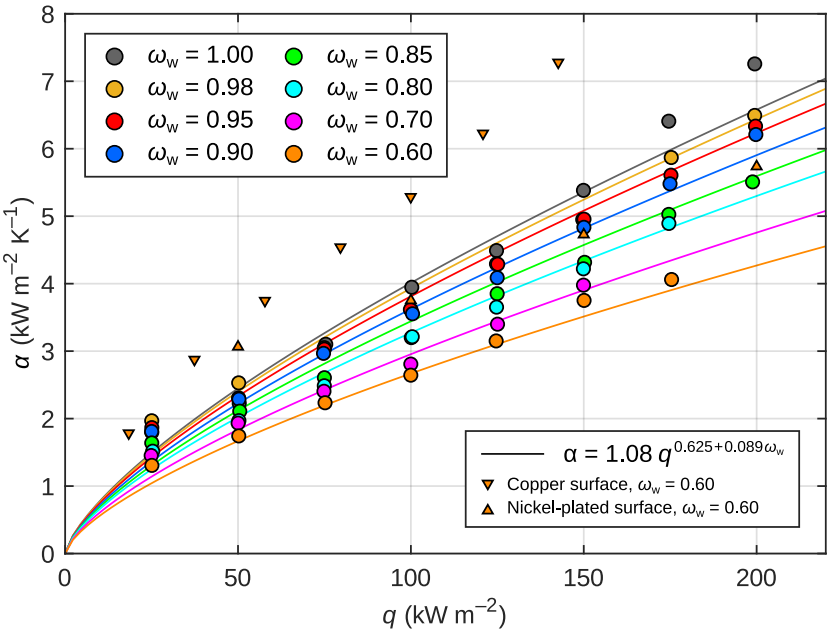

Figure 8.4: The HTCs obtained from the IR footage after the integration in space and time compared with the HTCs measured for the copper and nickel-plated surfaces presented in Sections 6 and 7, respectively. Data are also compared with empirical correlation (8.5) which is derived in the following subsection. Published in [222].

attributed to a limited number of active nucleation sites observed during boiling on the tested foil. A small value of the thermal capacity of the foil might be also responsible for the lower measured HTCs [227]. Nevertheless, in Figure 8.4, the deterioration of HTC for mixtures with a lower ω_w is clearly visible for higher heat fluxes. Also, the decrease of HTC is more noticeable for higher ω_w, which is consistent with the conclusions presented in Sections 6 and 7. Although it seems that HTC might have been enhanced for lower heat fluxes, the trend is not convincing, because for lower heat fluxes, only a very limited number of nucleating bubbles was observed, as listed in Appendix D, which significantly affects the measured values. Also, the fact that in Figure 8.4, HTC appears to be a convex function of q is questionable and is most probably caused by limited number of nucleation sites, by the narrow range of investigated heat fluxes, or by the relatively small monitored area of the foil.

Own Empirical Correlation for HTC

The measured HTCs might be correlated using the function

$$\alpha = 1.08\, q^{0.625+0.089\omega_w} \tag{8.5}$$

for the investigated heat flux range from 0 to 200 kW m^{-2} and the water mass fractions ω_w from 1.00 down to 0.60. Correlation (8.5) is similar to Equation (6.4) proposed for the copper surface in Section 6. The coefficients and their 95 % confidence intervals $C_1 = 1.08 \pm 0.35$ W^{1-m} m^{2m-2} K^{-1}, $C_2 = 0.625 \pm 0.030$ and $C_3 = 0.089 \pm 0.009$ were obtained by fitting the function $\alpha = C_1\, q^{C_2+C_3\omega_w}$ to the experimental data. The exponent of the heat flux q in correlation (8.5) lies between 0.63 and 0.71 for the investigated mixtures which is consistent with the range $0.6 < m < 0.8$ typically given in the literature [33]. Figure 8.4 shows an acceptable agreement between correlation (8.5) and the experimental points. The errors SEE = 0.2 kW m^{-2} K^{-1} and MRE = 6.4 % between the measured and correlated values were calculated. When using correlation (8.5), the heat flux q has to be in (W m^{-2}), the water mass fraction ω_w is dimensionless, and the calculated α is in (W m^{-2} K^{-1}).

Values and Trends of Boiling Parameters

The three-dimensional matrices $[T_s]$ of the surface temperature were analyzed with custom-made scripts which were developed to identify the sudden drops of temperature caused by bubble nucleation. For each nucleation event, the position of bubble center in time, the footprint diameter D_f in time[18] the bubble growth period t_g and the nucleation period $t_n = t_w + t_g$[19] were evaluated and stored. These values were then used to calculate nucleation frequencies $f_n = 1/t_n$, maximum footprint diameters D_f and growth rates $f_n D_f$ of the temperature footprints. Since the characteristics of cavities (such as cavity mouth diameters, their shapes, etc.) might significantly affect the values of the investigated parameters, it is necessary to find some stable active nucleation sites which are active for the various investigated compositions and heat fluxes and provide a representative number of bubbles. Then, it is possible to evaluate the studied parameters only for these sites of the foil and compare the values corresponding to each individual nucleation site.

Finding Stable Active Nucleation Sites

From the list of recorded nucleation events, the total number of bubbles nucleating from the filmed area of the heating foil was calculated and is listed in Appendix D for all experimental runs. For the purpose of further analysis, the area filmed with the IR camera was divided into 10 horizontal and 14 vertical rectangles which produced 140 rectangular zones with dimensions of about 0.99×1.03 mm. These zones were numbered from the left bottom corner of the monitored area, as shown in Figure 8.5. For the zones adjacent to the boundary of the area, which are painted gray, the boiling parameters were not evaluated, since only fractions of emerging bubbles were visible above these zones and it was not possible to reconstruct the shapes and radii of these bubbles. Zone 44 is highlighted in Figure 8.5, because it was, by far, the most active nucleation spot and the only one which was observed to be active for all investigated concentrations.

127	128	129	130	131	132	133	134	135	136	137	138	139	140
113	114	115	116	117	118	119	120	121	122	123	124	125	126
99	100	101	102	103	104	105	106	107	108	109	110	111	112
85	86	87	88	89	90	91	92	93	94	95	96	97	98
71	72	73	74	75	76	77	78	79	80	81	82	83	84
57	58	59	60	61	62	63	64	65	66	67	68	69	70
43	44	45	46	47	48	49	50	51	52	53	54	55	56
29	30	31	32	33	34	35	36	37	38	39	40	41	42
15	16	17	18	19	20	21	22	23	24	25	26	27	28
1	2	3	4	5	6	7	8	9	10	11	12	13	14

Figure 8.5: Numbering of the zones into which the filmed area of the titanium foil was divided for further analyzes.

The inherent randomness of the boiling process is documented in Figure 8.6 which shows the positions of active nucleation sites (or zones) on the titanium foil during boiling of pure water at heat flux of 200 kW m^{-2}. The active sites are colored according to the number of bubbles produced from each of them. For the

[18] Using the IR videos, it is possible to evaluate only the footprint diameter D_f of the zone on the foil whose temperature is affected by heat transfer during bubble nucleation. Although the diameter D_f of the zone might be slightly different from the bubble diameter D_b, it might be assumed that both are directly proportional to each other and that the trends observed for D_f are also valid for D_b. This was verified in our study [222]. Nevertheless, I use the term *footprint diameter* and the label D_f instead of D_b in this section for clarity.

[19] It is generally difficult to determine t_w and t_g from the image analysis of a high-speed video footage [23]. Even though the beginnings of individual nucleation cycles are clearly visible using infrared thermometry, it is still quite subjective to decide what is the exact moment when a bubble detaches from the heating surface.

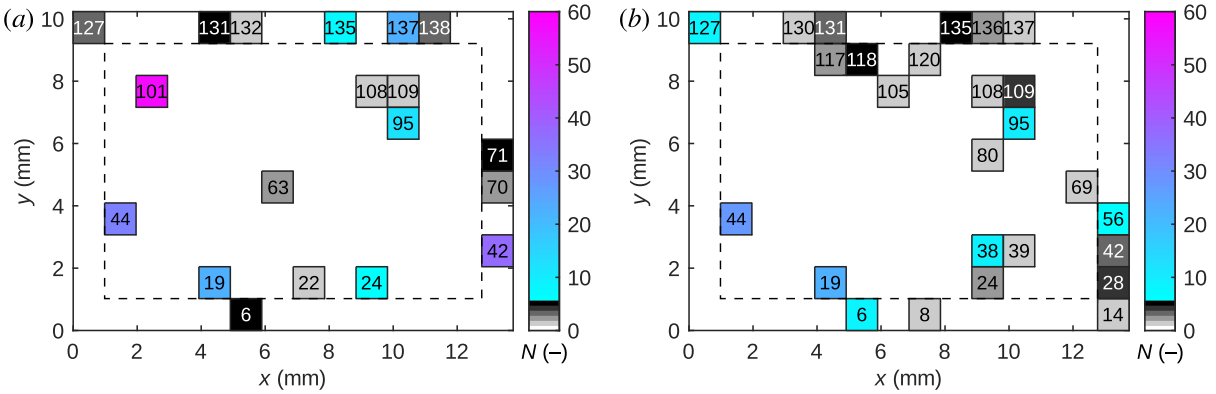

Figure 8.6: The distribution of active nucleation sites during boiling of water at $q = 200\ \mathrm{kW\,m^{-2}}$: (*a*) for the first performed run, (*b*) for the second run.

zones painted black or gray, less than five bubbles were detected. These zones were not evaluated, because they were not considered to provide stable nucleation. Although for the first run, the most active were Zone 101 and Zone 44 which produced 56 and 32 bubbles, respectively, during the second run, Zone 101 was inactive, and most bubbles emerged from Zone 44 for which 28 bubbles were detected. In other words, the most active nucleation spot during the first run was not even activated during the second run even despite the fact that the second run was performed immediately after the first run, the very same measurement methodology was applied and the target heat flux was set using a sensitive precise laboratory power source. Such a random and unpredictable activation of different nucleation sites was the cause of discrepancies in the total number of bubbles observed during individual runs for the same heat flux and composition, which might be noticed in Table A2 in Appendix D.

It was noted that the nucleation site corresponding to Zone 44 provided very stable and periodic nucleation for all investigated compositions of the boiling fluid. This is documented in Table A3 in Appendix D which gives the total number of bubbles emerging from Zone 44 for each heat flux q and mass fraction ω_w investigated. For heat fluxes lower than $100\ \mathrm{kW\,m^{-2}}$, no bubbles were detected above Zone 44 during boiling of pure water. Therefore, bubbles emerging from Zone 44 were analyzed only for $q \geq 100\ \mathrm{kW\,m^{-2}}$ to assess the impact of q and ω_w on nucleation parameters during boiling.

Bubble Diameters, Nucleation Frequencies, and Bubble Growth Rates

Tables 8.1, 8.2, and 8.3 show the values of the maximum footprint diameter D_f, the nucleation frequency f_n, and the bubble growth rate $f_\mathrm{n}\,D_\mathrm{f}$, respectively, which are compared with the results of some of the

Table 8.1: The maximum footprint diameters D_f (mm) measured for the bubbles emerging from Zone 44 and the bubble departure diameters D_b calculated with the correlations presented in Section 1.2.

		ω_w (–)							
		1.00	0.98	0.95	0.90	0.85	0.80	0.70	0.60
Measured at	$q = 100\ \mathrm{kW\,m^{-2}}$	–	5.1	5.3	5.0	5.1	5.2	4.7	5.2
	$q = 125\ \mathrm{kW\,m^{-2}}$	5.1	4.8	4.5	4.7	4.9	5.3	4.8	4.5
	$q = 150\ \mathrm{kW\,m^{-2}}$	4.9	4.5	4.4	4.7	5.1	5.0	4.8	4.0
	$q = 175\ \mathrm{kW\,m^{-2}}$	4.5	4.5	4.5	4.7	4.6	5.2	–	3.7
	$q = 200\ \mathrm{kW\,m^{-2}}$	4.6	4.4	4.4	4.5	4.5	–	–	–
Correlation of	Fritz (1.26)	4.5	4.4	4.4	4.4	4.4	4.4	4.4	4.3
	Kutateladze and Gogonin (1.31)	6.9	7.7	7.7	7.7	8.1	8.0	7.7	7.6
	Cole and Rohsenow (1.32)	0.5	0.5	0.5	0.5	0.4	0.4	0.4	0.4

Table 8.2: The nucleation frequencies f_n (s^{-1}) measured for the bubbles emerging from Zone 44 compared with the frequencies calculated with the correlations for $f_n D_b$ presented in Section 1.2 under the assumption that D_b equals to the result of the Fritz correlation, see Equation (1.26).

		ω_w (−)							
		1.00	0.98	0.95	0.90	0.85	0.80	0.70	0.60
Measured at	q = 100 kW m^{-2}	–	4.3	3.4	4.3	4.5	5.4	5.9	7.3
	q = 125 kW m^{-2}	3.7	5.6	7.1	6.6	7.1	8.3	9.0	11.9
	q = 150 kW m^{-2}	8.0	7.8	9.8	10.2	10.5	10.8	12.0	13.8
	q = 175 kW m^{-2}	9.5	11.7	13.0	12.8	13.7	12.9	–	16.5
	q = 200 kW m^{-2}	12.9	14.2	15.5	16.7	15.7	–	–	–
Correlation of	Malenkov (1.50)	15.8	15.9	15.9	15.9	15.9	16.0	16.0	16.1
	Peebles and Garber (1.48)	20.6	20.8	20.8	20.8	20.8	20.9	20.9	21.0

Table 8.3: The footprint growth rates $f_n D_f$ (mm s^{-1}) calculated using the measured values listed in Tables 8.1 and 8.2 and compared with the bubble growth rates $f_n D_b$ estimated with the correlations presented in Section 1.2.

		ω_w (−)							
		1.00	0.98	0.95	0.90	0.85	0.80	0.70	0.60
Measured at	q = 100 kW m^{-2}	–	22	18	21	23	28	28	38
	q = 125 kW m^{-2}	19	27	32	31	35	44	44	53
	q = 150 kW m^{-2}	39	35	43	48	53	54	57	55
	q = 175 kW m^{-2}	43	53	58	60	63	66	–	60
	q = 200 kW m^{-2}	59	63	67	74	71	–	–	–
Correlation of	Malenkov (1.50)	71	70	70	70	70	70	70	69
	Peebles and Garber (1.48)	92	92	92	92	92	92	91	91

correlations listed in Section 1.2. All the measured parameters in Tables 8.1 to 8.3 are the averages of the values acquired from the analysis of the bubbles originating from Zone 44. The results of the correlations in Tables 8.1 to 8.3 were obtained employing the thermophysical properties given in Table 3.1 together with the value of contact angle $\vartheta_c = 86°$ reported in the literature for water on thin titanium foils [226]. The correlated values of f_n were calculated from the correlated bubble growth rates $f_n D_b$ assuming that D_b is equal to the Fritz diameter, see correlation (1.26). According to all employed correlations, the boiling parameters are independent of the heat flux q[20].

Based on Tables 8.1 to 8.3, the maximum footprint diameter D_f, which oscillates between 3.7 and 5.3 mm, appears to be independent of ω_w. On the contrary, the nucleation frequency f_n significantly increases with the heat flux and also mildly rises with the concentration of glycerin in the boiling mixture. The increase of growth rate $f_n D_f$ obtained at a higher q for a lower ω_w is thus caused solely by the higher measured nucleation frequencies. A series of *F-tests* and *Akaike information criterion* were evaluated for the measured boiling parameters presented in Tables 8.1 to 8.3 and for various model functions. These statistical tests showed that the footprint diameter D_f might be considered independent of the mass fraction ω_w and weakly dependent on the heat flux q according to the function

$$D_f = 4.54 \times 10^{-2}\, q^{-0.19} \tag{8.6}$$

[20] The Malenkov correlation, which is the only one which contains the heat flux q, see Equation (1.50), was evaluated outside of the *interference regime* of boiling. It was, therefore, assumed that bubbles do not mutually interact and the last fraction of Equation (1.50) was omitted.

and that the nucleation frequency f_n depends on both q and ω_w and might be approximated with the function

$$f_n = 8.88 \times 10^{-9} \frac{q^{1.73}}{\omega_w} . \tag{8.7}$$

Combining Equations (8.6) and (8.7), the footprint growth rate (the growth rate of the zones affected by bubble nucleation) might be estimated with the correlation

$$f_n D_f = 4.03 \times 10^{-10} \frac{q^{1.54}}{\omega_w} . \tag{8.8}$$

Correlations (8.6) to (8.8) are valid for the range of the investigated water mass fractions $0.60 \leq \omega_w \leq 1.00$ and for the heat flux range $100 \leq q \leq 200\,\mathrm{kW\,m^{-2}}$. To use correlations (8.6) to (8.8), the heat flux q needs to be in $(\mathrm{W\,m^{-2}})$, ω_w is dimensionless, D_f is given in (m), f_n is in $(\mathrm{s^{-1}})$ and $f_n D_f$ in $(\mathrm{m\,s^{-1}})$. Although all three correlations are rather informative since the confidence intervals of their coefficients are relatively wide due to the limited number of experimental points and fluctuations of the measured parameters, they might still be used for a rough estimate of the investigated boiling parameters.

Although it might seem that more or less constant values of boiling parameters presented in Tables 8.1 to 8.3, which were calculated with the correlations published in the literature, indicate that these parameters are not influenced by the variations of thermophysical properties caused by additions of glycerin, one should bear in mind that all employed correlations were developed for pool boiling of pure fluids and that these correlations do not consider the impact of the *mixture effects* on the boiling parameters. Measured values might, therefore, significantly differ from the results of these correlations. Nevertheless, the measured footprint diameter D_f corresponds very well to the results of the Fritz correlation (1.26). The bubble growth rates $f_n D_b$ predicted by the correlation of Malenkov (1.50) roughly correspond to the growth rates of the footprint area $f_n D_f$ measured for the highest investigated heat flux of $200\,\mathrm{kW\,m^{-2}}$. The same holds true for the measured and correlated nucleation frequencies f_n.

According to Table 8.1 and correlation (8.6), the bubble departure diameter is independent of the composition of the liquid phase, which agrees with the findings published by Tolubinsky and Ostrovsky [188]. They explain that D_b is independent of ω_w due to the fact that the equilibrium vapor composition and the *bubble-point* temperature both remain more or less constant for the mixtures with $\omega_w > 0.30$.

As reported by Dhir [23], the nucleation frequency f_n should increase with the superheat which agrees with Table 8.2. On the other hand, Zuber [57] reported that for pure fluids boiling at low heat fluxes (although for some liquids, it might be as much as 80 % of the critical heat flux), both D_b as well as f_n should be rather independent of the heat flux, and that the enhancement of HTC at higher heat fluxes is primarily caused by the increased number of active nucleation sites. The different trends observed in this work might be caused either by the impact of the *mixture effects* on the nucleation cycles of bubbles or by the fact that the number of active nucleation sites was rather small on the investigated foil and the activation of new sites was limited. In other words, the findings stated by Zuber might be valid only for those surfaces which are able to provide a wider distribution of the sizes and shapes of cavities, gradual activation of nucleation spots, and higher number of departing bubbles.

Tolubinsky and Ostrovsky [58] observed that for aqueous sugar solutions and aqueous solutions of NaCl and Na_2CO_3, the bubble growth rates were more or less the same as for the pure solvent (water) without any noticeable effect of the viscosity and Prandtl number of the boiling liquid. On the other hand, they also observed that for ethanol–water mixtures, the bubble departure diameter D_b and the bubble growth rate $f_n D_b$ decrease when the equilibrium molar fraction difference $|y_i - x_i|$ increases, which contradicts the trends in Tables 8.1 and 8.3. However, by looking at their data, a strong decrease was measured only at smaller concentrations of ethanol (which is the more volatile component) in water (the less volatile component). For higher concentrations of the less volatile component (which is more relevant with respect to the investigated water–glycerin mixtures), both parameters were rather constant, see Figure 8 in the

work of Tolubinsky and Ostrovsky [58]. Moreover, they investigated mixtures with very different nature relative to water–glycerin mixtures (studied fluids significantly differ in the vapor–liquid equilibrium, boiling range, viscosity ratio of both pure components, etc.) which might also be the reason why the trends presented in this section do not correspond to their observations.

Thermal Energy Consumed by Bubbles

Since the footprint diameter D_f (which represents the bubble departure diameter D_b) was found to be a weak function of q independent of the concentration of the boiling mixture and since the nucleation frequency f_n seems to increase for a lower ω_w, the deterioration of HTC with the decrease of ω_w cannot be explained by the trends observed for the investigated parameters related to bubble nucleation. Another possible cause of the HTC deterioration might be lower intensity of heat transfer even despite the increased nucleation frequencies and bubble growth rates. This was further analyzed by the evaluation of the average thermal energy Q_b consumed during individual nucleation cycles. The thermal energy Q_b was calculated from the three-dimensional matrices $[T_s]$ and $[q]$ of the surface temperature and the heat flux, respectively, according to the equation

$$Q_b = \int_{t_g} \left(\iint_{S_{affected}} q \, dS \right) dt \approx \sum_{n=n_0}^{n_1} \left(\sum_{i=i_0}^{i_1} \sum_{j=j_0}^{j_1} q_{i,j}^n \right) \Delta L_{px}^2 \, \tau_{film} \,, \tag{8.9}$$

where the individual nodal values of the heat flux $q_{i,j}^n$ were calculated with Equations (8.2), (8.3) and (8.4), $\Delta L_{px} = 0.11$ mm is the spatial resolution of the IR camera, and $\tau_{film} = 625$ µs is the time period of the video recording. In Equation (8.9), the differences between the summation bounds $(n_1 - n_0)$, $(i_1 - i_0)$ and $(j_1 - j_0)$ are equal to the number of time layers corresponding to the growth period t_g, the number of vertical pixels affected by nucleation and the number of horizontal pixels affected by nucleation, respectively.

Table 8.4 lists the calculated values of the thermal energy Q_b consumed by bubble nucleation calculated as the average of the values obtained from the analysis of bubbles which originated from Zone 44. The

Table 8.4: The values of the thermal energy Q_b (mJ) consumed by individual nucleating bubbles. Each value represents the average thermal energy obtained from the analysis of the bubbles emerging from Zone 44.

q	ω_w (−)							
(kW m^{-2})	1.00	0.98	0.95	0.90	0.85	0.80	0.70	0.60
100	–	42	43	37	42	49	41	58
125	47	41	33	41	42	60	51	43
150	48	39	38	44	54	59	53	38
175	41	45	44	49	45	72	–	34
200	49	46	44	47	49	–	–	–

analysis did not result in a clear trend of the thermal energy Q_b, as was also confirmed by a series of *F-tests* according to which, the thermal energy Q_b is likely a constant which has a value of about 46 mJ and a standard deviation of 8 mJ. This result suggests that the transport of heat enhanced by individual nucleating bubbles was not significantly affected by the heat flux q or by the concentration of glycerin in the boiling mixture. Most of the thermal energy is consumed by bubbles in the early stages of nucleation, as noticeable from the recorded IR videos which showed very rapid drops of surface temperature and significant enhancement of heat transfer just moments after a new bubble was formed on the heating surface.

Suggested Explanation of HTC Deterioration

The measured values of the nucleation parameters and of the thermal energy, which were presented in Tables 8.1 to 8.4, suggest that the measured decrease of HTC with ω_w is probably not directly related to the transport of latent heat during bubble nucleation. The deterioration of HTC for higher concentration of glycerin in the boiling mixture is likely caused by reduced heat transfer to the liquid phase due to lower intensity of enhanced convection, transient conduction, and natural convection. The deterioration of heat transfer might be explained as a consequence of retardation of convective mechanisms in the liquid phase caused by the increased viscosity, increased density, or decreased specific heat capacity of the boiling mixtures with lower ω_w, see Table 3.1. This would also explain the measured decrease of HTC, despite the contradictory enhancive trends observed for the nucleation frequency f_n and footprint growth rate $f_n D_f$. Higher superheats were generally measured for mixtures with a lower ω_w during bubble growth periods as well as during waiting periods, which also supports the suggested explanation.

8.7 Summary of Experimental Results

The analysis of IR footage presented in this section revealed that HTC deteriorates for higher concentration of glycerin in the boiling mixture and that the deterioration is pronounced for mixtures with a higher water content. Similar behavior was already observed during experiments performed with the copper and nickel-plated surfaces in Sections 6 and 7, respectively.

Besides that, the following conclusions were drawn for boiling of water–glycerin mixtures on titanium foils:

- The bubble footprint diameter was found to be independent of the concentration of glycerin in the investigated mixtures. On the other hand, increased nucleation frequencies and bubble growth rates were measured for higher concentrations of glycerin in the boiling mixture. The values of the investigated nucleation parameters were found to be comparable with the results of the correlations developed for pure fluids.
- The thermal energy consumed by bubbles during nucleation was found to be independent of the heat flux and composition of the boiling mixture. The initial stages of bubble nucleation were found to be characterized by intense heat transfer.
- The trends of the evaluated boiling parameters and the independent value of thermal energy $Q_b = 46 \pm 8$ mJ obtained at different concentrations of glycerin in the boiling mixture indicate that heat transfer into the liquid phase is more significant than the transport of latent heat related to bubble nucleation for the investigated water–glycerin mixtures.
- Random activation of nucleation sites was observed during the repeated runs performed under the same experimental conditions with the same heating surface.
- Boiling on the investigated titanium foil was characterized by lower HTC values relative to the values measured for the copper and nickel-plated surfaces presented in Sections 6 and 7, respectively. The HTCs measured on the titanium foil was of about 45 % compared with those measured for the copper surface and about 70 % compared with the HTCs measured for the nickel-plated surfaces. The lower HTCs were most likely caused by a limited number of active nucleation sites.

9. Generalization of Experimental Findings

In Sections 6, 7, and 8, HTCs were measured during boiling of water–glycerin mixtures on three different materials of the heating surface. Although it is always a difficult task to draw general conclusions from a limited set of experiments, the following empirical findings valid for all three investigated materials indicate that at least some of our observations might be considered universal for mixtures of water and glycerin. The following general trends were valid for all of the surfaces and conditions investigated:

- The measured HTCs were found to deteriorate with increasing concentration of glycerin in the mixture. The deterioration was stronger at higher heat fluxes and for mixtures with a lower concentration of glycerin.
- For the investigated thick nickel-plated samples, the decrease of HTC due to the addition of the less volatile component (glycerin) followed an asymptotic trend, see Figure 7.8, which means that although the decrease is quite significant for mixtures with a lower glycerin content, it becomes much weaker when the amount of glycerin in the mixture is higher. The asymptotic decrease of HTC was confirmed for the nickel-plated surfaces using a three-parametric exponential function, see Equation (7.4), which provided a reasonable agreement with the experiments. Although for the investigated copper surface, a simpler three-parametric function was proposed, see Equation (6.4), the three-parametric exponential correlation
$$\alpha = q^{0.70}\left[6.67\,\mathrm{e}^{-0.58(1-\omega_\mathrm{w})} - 3.43\right] \tag{9.1}$$
is also very well applicable for the copper surface and produces SEE and MRE between the calculated and measured HTCs of about 0.7 kW m^{-2} K^{-1} and 7 %, respectively. Likewise, the equation
$$\alpha = q^{0.70}\left[0.58\,\mathrm{e}^{-3.15(1-\omega_\mathrm{w})} + 0.71\right] \tag{9.2}$$
is applicable instead of correlation (8.5) for the calculation of HTC during boiling on the titanium foil and produces SEE and MRE around 0.2 kW m^{-2} K^{-1} and 6.3 %, respectively. The reason why correlations (9.1) and (9.2) were omitted from Sections 6 and 8, respectively, is that the confidence intervals of their coefficients are considerably wider relative to those calculated for the coefficients of the original correlations. Nevertheless, the relatively low errors achieved with both correlations suggest that the data obtained for the tested copper and titanium surfaces also follow the asymptotic trend of HTC deterioration.
- From the measurement of HTCs on all investigated surfaces, it is evident that the *mixture effects* have a substantial impact on HTC and have to be considered even for the water–glycerin mixtures with the lowest investigated glycerin content of 2 % by weight.
- No significant enhancement of HTC was observed during the experiments performed for any of the investigated glycerin concentrations, heat flux levels, and heating surfaces.

10. Recapitulation of Experimental Results and Findings

10.1 Boiling of Water–Glycerin Mixtures on the Copper Surface

Performed Experiments

- The commonly-used steady-state method of measurement and the own dynamic measurement method were applied.
- A single copper block with a smooth planar heating surface (R_a of 0.4 µm) was investigated.
- The water mass fractions $0.40 \leq \omega_w \leq 1.00$ and heat fluxes $25 \leq q \leq 270\ \mathrm{kW\,m^{-2}}$ were studied.
- In total, 9 experimental runs were performed and 109 data points obtained.

Outputs

- The empirical correlation for HTC (SEE = $0.5\ \mathrm{kW\,m^{-2}\,K^{-1}}$, MRE = 6 %)

$$\alpha = 0.59\, q^{0.714+0.130\omega_w}\ .$$

- The proposed and verified dynamic method.

Findings

- HTC decreased with increasing ω_w, the trend was accented for higher q and ω_w.
- The *mixture effects* were significant for all investigated conditions.
- No HTC enhancement was observed under the investigated conditions.
- HTC might be correlated with the combination of the Schlünder correlation and the correlation of Stephan and Abdelsalam (SEE = $1.0\ \mathrm{kW\,m^{-2}\,K^{-1}}$, MRE = 14 %).
- A systematically lower HTCs were measured for the $\omega_w = 0.90$ mixture during the performed repeated run.

Published in

[200] Vajc V., Šulc R., Dostál M., Pool Boiling Heat Transfer Coefficients in Mixtures of Water and Glycerin, *Processes*, vol. 9, no. 5, article no. 830, May 2021, pp. 1–19. doi:10.3390/pr9050830.

10.2 Boiling of Water–Glycerin Mixtures on the Nickel-Plated Surfaces

Performed Experiments

- HTCs during saturated and subcooled boiling were measured.
- Five nickel-plated surfaces with a smooth planar heating surface (R_a of about 0.4 µm) were investigated.
- The water mass fractions $0.60 \leq \omega_w \leq 1.00$ and heat fluxes $0 \leq q \leq 650\ \mathrm{kW\,m^{-2}}$ were studied.
- Subcooled experiments were done for $q = 250, 450$, and $650\ \mathrm{kW\,m^{-2}}$ at the subcooling $0 \leq \Delta T_{sub} \leq 30\ \mathrm{K}$.
- Long-term measurements of the boiling performance stability were conducted.
- In total, 110 saturated and 82 subcooled runs were performed.

Outputs

- The empirical correlation for the HTC during saturated boiling (SEE = $1.7\ \mathrm{kW\,m^{-2}\,K^{-1}}$, MRE = 11 %)
$$\alpha = q^{0.70}\left[1.30\,\mathrm{e}^{-10.6(1-\omega_w)} + 1.18\right].$$
- The empirical correlation for the *total* HTC during subcooled boiling (SEE = $1.1\ \mathrm{kW\,m^{-2}\,K^{-1}}$, MRE = 7 %)
$$\frac{1}{\alpha_{tot}} = \frac{1}{q^{0.70}\left[1.30\,\mathrm{e}^{-10.6(1-\omega_w)} + 1.18\right]} + \frac{\Delta T_{sub}}{q}.$$

Findings

- HTC decreased with increasing ω_w, the trend is accented for higher q and ω_w.
- The *mixture effects* were significant for all investigated conditions.
- No HTC enhancement was observed under the investigated conditions.
- HTCs reached about 65 % relative to those measured for the copper surface.
- The investigated nickel-plated surfaces were found to provide a very stable boiling performance.
- HTC might be correlated with the combination of the Inoue and Monde correlation and the correlation of Yagov (SEE = $1.9\ \mathrm{kW\,m^{-2}\,K^{-1}}$, MRE = 12 %).
- The developed subcooled boiling regime was reached for all investigated mixtures.
- The effects of subcooling and composition on HTC were stronger for less subcooled mixtures with a lower content of glycerin.

Published in

[214] Vajc V., Može M., Hadžić A., Zupančič M., Golobič I., Saturated and Subcooled Pool Boiling Heat Transfer in Mixtures of Water and Glycerin, *Experimental Heat Transfer*, Jan. 2022, pp. 1–29. doi:10.1080/08916152.2022.2027574.

10.3 Boiling of Water–Glycerin Mixtures on the Titanium Foil

Performed Experiments

- Infrared thermometry was applied to measure the temperature distribution of the heating surface in space and time.
- A single titanium foil ($R_a = 0.07$ µm, $\delta_{foil} = 25$ µm) was investigated.
- The water mass fractions $0.60 \leq \omega_w \leq 1.00$ and heat fluxes $0 \leq q \leq 200$ kW m^{-2} were studied.
- In total, 155 IR videos were captured. Two runs were performed for each of the eight investigated concentrations. Each run contained from 8 to 11 measurements at discrete heat flux levels.

Outputs

- The empirical correlation for the HTC during saturated boiling (SEE = 1.7 kW m^{-2} K^{-1}, MRE = 11 %)
$$\alpha = 1.08\, q^{0.625+0.089\omega_w} .$$
- The empirical correlation for the measured diameter of the temperature footprint of bubbles
$$D_f = 4.54 \times 10^{-2}\, q^{-0.19} .$$
- The empirical correlation for the measured nucleation frequency
$$f_n = 8.88 \times 10^{-9}\, \frac{q^{1.73}}{\omega_w} .$$
- The empirical correlation for the measured growth rate of temperature footprints
$$f_n = 4.03 \times 10^{-10}\, \frac{q^{1.54}}{\omega_w} .$$

Findings

- HTC decreased with increasing ω_w, the trend is accented for higher q and ω_w.
- The values of the investigated nucleation parameters were comparable with some of the correlations developed for pure fluids.
- Despite the HTC deterioration, more bubbles were produced for mixtures with a higher ω_w.
- The thermal energy transferred during bubble nucleation was independent of ω_w and q.
- The transport of latent heat by nucleating bubbles was found not to be the governing heat transfer mechanism.
- Random activation of nucleation sites was recorded despite the same measurement procedure and experimental conditions.
- HTCs reached about 45 % and 70 % relative to those measured for the copper and nickel-plated surfaces, respectively.

Published in

[222] Vajc V., Može M., Zupančič M., Šulc R., Golobič I., IR Measurements of Heat Transfer Coefficients and Nucleation Parameters during Saturated Nucleate Boiling of Water–Glycerin Mixtures, *Case Studies in Thermal Engineering*, vol. 32, Apr. 2022, pp. 1–13. doi:10.1016/j.csite.2022.101917.

PART III
Conclusions

Boiling is a commonly utilized process characterized by intense heat transfer, but also a complicated and complex phenomenon which, to date, is still not fully understood and satisfactorily explained. Nevertheless, much effort has been and is being made, and important findings are being published despite the lack of an underlying theory of boiling. In any case, waiting for a universal correlation or for a groundbreaking theory which would enable one to estimate boiling performance for a variety of different heating surfaces, boiling fluids, and conditions, seems to be a utopia. In Part I of this thesis, I tried to emphasize that neither the mechanisms nor the correlations for calculation of the most important boiling parameters are generally valid and that there always exist specific cases for which these models eventually fail. This might be viewed as a consequence of the complexity of boiling.

Despite the fact that boiling of mixtures almost always leads to significant deterioration of HTC and is often unavoidable in industrial processes (for example, it is necessary and inevitable to treat mixtures during distillation or thickening), some mixtures might also bring several advantages over pure fluids, such as environmental friendliness or improved thermodynamic efficiency. The heat transfer correlations formulated for boiling of mixtures aim to cover the impact of various influential mechanisms which are present during mixture boiling and are together called the *mixture effects*.

Various aspects, characteristic parameters, and boiling behavior of water–glycerin mixtures were introduced and discussed in Section 3. The employment of glycerin and research of new suitable techniques for its utilization are required due to the overproduction of glycerin on the global market. However, detailed knowledge and study of the thermophysical, technological, and transport properties of glycerin and its mixtures are required. From the perspective of boiling, the binary mixtures of water and glycerin evince a rather extraordinary boiling behavior, mostly because of the significant values of their boiling range and due to the fact that the vapor phase consists solely of water for a wide range of mixture composition.

The following conclusions based on the experimental results presented in Part II of this thesis might be drawn for the investigated water–glycerin mixtures:

- HTC deteriorates with an increasing amount of the less volatile component (glycerin) in water–glycerin mixtures, which is in agreement with the trends reported in the literature for tubular surfaces. The HTC deterioration was observed for all of the investigated surfaces (copper, nickel-plated, and titanium), heat fluxes, and concentrations of the boiling mixture. The decrease of HTC with increasing concentration of glycerin follows an asymptotic trend (it is substantial for mixtures with a lower content of glycerin, but becomes weaker as the amount of glycerin increases). All of these trends might be considered universal for all investigated water–glycerin mixtures.
- The *mixture effects* were found to affect the HTC during boiling of water–glycerin mixtures on all surfaces and compositions investigated.
- HTC enhancement was not detected for any of the concentrations and heating surfaces investigated.
- The heating surfaces made of copper were found to be less stable compared with the nickel-plated and titanium surfaces, most likely due to interaction of copper with glycerin. The nickel-plated and titanium samples maintained a stable boiling performance during multiple repeated runs. The stability of nickel-plated samples was also confirmed by long-term boiling experiments.
- Bubble departure diameters (represented by the maximum footprint diameters of zones on the titanium foil whose temperatures were clearly affected by bubble nucleation) were found to be weakly dependent on the heat flux, independent of the concentration, and well predictable by the often used correlation of Fritz.
- The nucleation frequencies increased significantly with the heat flux and gradually with the concentration of glycerin in the boiling mixture. The increase of the bubble growth rate, measured for lower water mass fractions and higher heat fluxes, was caused by the increase of the nucleation frequency.

- The thermal energy transferred into nucleating bubbles of about 46 ± 8 mJ was found to be independent of the heat flux and concentration. Most of the energy was observed to be transferred in the early stages of nucleation cycles.
- Trends of the investigated boiling parameters measured for the titanium heating surface indicate that heat transfer to the liquid phase by convection and transient conduction is more important than the mechanisms related to the transport of latent heat.
- The subcooled boiling experiments performed on the nickel-plated surfaces proved that when the developed regime of subcooled boiling is established, the correlations suitable for saturated boiling might be employed to predict HTCs during subcooled boiling of pure fluids as well as mixtures. The regime of developed subcooled boiling manifests itself by more or less constant temperature of the heating surface, which is independent of subcooling of the liquid bulk.
- The effects of subcooling and composition on the *total* HTC were observed to be more important for the less subcooled mixtures with lower glycerin content.
- The investigated titanium foil was characterized by relatively low measured HTCs which reached about 45 % and 70 % of those measured for the copper and nickel-plated surfaces, respectively. The HTCs measured for the nickel-plated surfaces reached approximately 65 % relative to those measured for the copper surface. This was caused by the different materials and structures of the investigated surfaces which resulted in variations of active nucleation site density.
- Suitable correlations adopted from the literature and own empirical correlations developed for the investigated water–glycerin mixtures were proposed. Different correlations have to be used with respect to the heating surface.

The results and conclusions of the experimental measurements presented in this thesis might be used to estimate the HTC or important boiling parameters during boiling of water–glycerin mixtures. Suitable correlations for boiling of water–glycerin mixtures were identified, and new empirical correlations were proposed for fast and straightforward calculation of HTC.

The data and information presented in and related to this thesis were previously published in the author's works [199,200,203,214,222].

References

[1] Kandlikar S.G., Shoji M., Dhir V.K., *Handbook of Phase Change: Boiling and Condensation*. Ann Arbor, MI, USA: Taylor & Francis, ISBN 1-56032-634-4, 1999.

[2] Hsu C.C., Lee M.R., Wu C.H., Chen P.H., Effect of Interlaced Wettability on Horizontal Copper Cylinders in Nucleate Pool Boiling, *Applied Thermal Engineering*, vol. 112, Feb. 2017, pp. 1187–1194. doi:10.1016/j.applthermaleng.2016.10.176.

[3] Mo D.C., Yang S., Luo J.L., Wang Y.Q., Lyu S.S., Enhanced Pool Boiling Performance of a Porous Honeycomb Copper Surface with Radial Diameter Gradient, *International Journal of Heat and Mass Transfer*, vol. 157, Aug. 2020, p. 119867. doi:10.1016/j.ijheatmasstransfer.2020.119867.

[4] Nukiyama S., The Maximum and Minimum Values of the Heat Q Transmitted from Metal to Boiling Water Under Atmospheric Pressure, *International Journal of Heat and Mass Transfer*, vol. 9, no. 12, Dec. 1966, pp. 1419–1433. doi:10.1016/0017-9310(66)90138-4.

[5] Honda H., Wei J.J., Enhanced Boiling Heat Transfer from Electronic Components by Use of Surface Microstructures, *Experimental Thermal and Fluid Science*, vol. 28, no. 2, Jan. 2004, pp. 159–169. doi:10.1016/S0894-1777(03)00035-9.

[6] Fujita Y., Tsutsui M., Heat Transfer in Nucleate Pool Boiling of Binary Mixtures, *International Journal of Heat and Mass Transfer*, vol. 37, Mar. 1994, pp. 291–302. doi:10.1016/0017-9310(94)90030-2.

[7] Adib T.A., Heyd B., Vasseur J., Experimental Results and Modeling of Boiling Heat Transfer Coefficients in Falling Film Evaporator Usable for Evaporator Design, *Chemical Engineering and Processing: Process Intensification*, vol. 48, no. 4, Apr. 2009, pp. 961–968. doi:10.1016/j.cep.2009.01.004.

[8] Allred T.P., Weibel J.A., Garimella S.V., Enabling Highly Effective Boiling from Superhydrophobic Surfaces, *Physical Review Letters*, vol. 120, no. 17, Apr. 2018, p. 174501. doi:10.1103/PhysRevLett.120.174501.

[9] Fujita Y., Bai Q., Critical Heat Flux of Binary Mixtures in Pool Boiling and Its Correlation in Terms of Marangoni Number, *International Journal of Refrigeration*, vol. 20, no. 8, Dec. 1997, pp. 616–622. doi:10.1016/S0140-7007(97)00026-1.

[10] Lu D., Yu Z., Zhong Y., Wang H., Zhang Y., Cao Q., Gao S., Experimental Investigation on Boiling Heat Transfer Characteristics of the Spent Fuel Bundle Under Flooded Condition, *Nuclear Engineering and Design*, vol. 344, Apr. 2019, pp. 168–173. doi:10.1016/j.nucengdes.2019.01.002.

[11] Liang G., Mudawar I., Review of Pool Boiling Enhancement by Surface Modification, *International Journal of Heat and Mass Transfer*, vol. 128, Jan. 2019, pp. 892–933. doi:10.1016/j.ijheatmasstransfer.2018.09.026.

[12] Golobič I., Zupančič M., Wall-Temperature Distributions of Nucleate Pool Boiling Surfaces Vs. Boiling Curves: A New Approach, *International Journal of Heat and Mass Transfer*, vol. 99, Aug. 2016, pp. 541–547. doi:10.1016/j.ijheatmasstransfer.2016.04.033.

[13] Kim J., Review of Nucleate Pool Boiling Bubble Heat Transfer Mechanisms, *International Journal of Multiphase Flow*, vol. 35, no. 12, Dec. 2009, pp. 1067–1076. doi:10.1016/j.ijmultiphaseflow.2009.07.008.

[14] Forster H.K., Greif R., Heat Transfer to a Boiling Liquid—Mechanisms and Correlations, *ASME Journal of Heat Transfer*, vol. 81, no. 1, Feb. 1959, pp. 43–53. doi:10.1115/1.4008129.

[15] Hewitt G.F., Boiling, in *Handbook of Heat Transfer* (Rohsenow W.M., Hartnett J.P., Cho Y.I., eds.), pp. 989–1156, New York, NY, USA: McGraw-Hill, third ed., ISBN 0-07-053555-8, 1998.

[16] Nishikawa K., Fujita Y., Uchida S., Ohta S., Effect of Heating Surface Orientation on Nucleate Boiling Heat Transfer, in *Proceedings of ASME-JSME Thermal Engineering Joint Conference*, vol. 1, (Honolulu, Hawai, USA), American Society of Mechanical Engineers, 1983, pp. 129–136.

[17] Yagov V.V., The Scientific Legacy of D.A. Labuntsov and Modern Ideas on the Nucleate Boiling Process, *Thermal Engineering*, vol. 42, no. 3, 1995, pp. 181–189.

[18] Borishanski V.M., Correlation of the Effect of Pressure on the Critical Heat Flux and Heat Transfer Rates Using the Theory of Thermodynamic Similarity, in *Problems of Heat Transfer and Hydraulics of Two-Phase Media* (Kutateladze S., ed.), pp. 16–37, Oxford, UK: Pergamon Press, first ed., ISBN 978-0-08-012077-5, 1969.

[19] Hahne E., Müller J., Boiling on a Finned Tube and a Finned Tube Bundle, *International Journal of Heat and Mass Transfer*, vol. 26, no. 6, June 1983, pp. 849–859. doi:10.1016/s0017-9310(83)80109-4.

[20] Rohsenow W.M., A Method of Correlating Heat Transfer Data for Surface Boiling of Liquids, Tech. Rep., Division of Industrial Cooperation, Heat Transfer Laboratory, Cambridge, MA, USA, 1952. Available at: http://hdl.handle.net/1721.1/61431.

[21] Zuber N., Nucleate Boiling. The Region of Isolated Bubbles and the Similarity with Natural Convection, *International Journal of Heat and Mass Transfer*, vol. 6, no. 1, Jan. 1963, pp. 53–78. doi:10.1016/0017-9310(63)90029-2.

[22] Moissis R., Berenson P.J., On the Hydrodynamic Transitions in Nucleate Boiling, *Journal of Heat Transfer*, vol. 85, no. 3, Aug. 1963, p. 221. doi:10.1115/1.3686075.

[23] Dhir V.K., Numerical Simulations of Pool-Boiling Heat Transfer, *AIChE Journal*, vol. 47, no. 4, 2001, pp. 813–834. doi:10.1002/aic.690470407.

[24] Monde M., Pool Boiling, in *Boiling: Research and Advances* (Koizumi Y., Shoji M., Monde M., Takata Y., Nagai N., eds.), pp. 2–4, Amsterdam, Netherlands: Elsevier, first ed., ISBN 978-0-08-101010-5, 2017. Available at: https://www.sciencedirect.com/book/9780081010105/boiling#book-description.

[25] Wu J., Dhir V.K., Numerical Simulations of the Dynamics and Heat Transfer Associated With a Single Bubble in Subcooled Pool Boiling, *Journal of Heat Transfer*, vol. 132, no. 111501, Aug. 2010. doi:10.1115/1.4002093.

[26] Sathyamurthi V., Ahn H.S., Banerjee D., Lau S.C., Subcooled Pool Boiling Experiments on Horizontal Heaters Coated With Carbon Nanotubes, *Journal of Heat Transfer*, vol. 131, no. 071501, Apr. 2009. doi:10.1115/1.3000595.

[27] Ono A., Sakashita H., Liquid–Vapor Structure Near Heating Surface at High Heat Flux in Subcooled Pool Boiling, *International Journal of Heat and Mass Transfer*, vol. 50, no. 17, Aug. 2007, pp. 3481–3489. doi:10.1016/j.ijheatmasstransfer.2007.01.026.

[28] Zhang S., Tang Y., Zeng J., Yuan W., Chen J., Chen C., Pool Boiling Heat Transfer Enhancement by Porous Interconnected Microchannel Nets at Different Liquid Subcooling, *Applied Thermal Engineering*, vol. 93, Jan. 2016, pp. 1135–1144. doi:10.1016/j.applthermaleng.2015.10.044.

[29] Yabuki T., Nakabeppu O., Microscale Wall Heat Transfer and Bubble Growth in Single Bubble Subcooled Boiling of Water, *International Journal of Heat and Mass Transfer*, vol. 100, Sept. 2016, pp. 851–860. doi:10.1016/j.ijheatmasstransfer.2016.04.112.

[30] El-Genk M.S., Parker J.L., Nucleate Boiling of FC-72 and HFE-7100 on Porous Graphite at Different Orientations and Liquid Subcooling, *Energy Conversion and Management*, vol. 49, no. 4, Apr. 2008, pp. 733–750. doi:10.1016/j.enconman.2007.07.028.

[31] Dhir V.K., Mechanistic Prediction of Nucleate Boiling Heat Transfer–Achievable or a Hopeless Task?, *Journal of Heat Transfer*, vol. 128, no. 1, Jan. 2006, pp. 1–12. doi:10.1115/1.2136366.

[32] Gorenflo D., Knabe V., Bieling V., Bubble Density on Surfaces with Nucleate Boiling – Its Influence on Heat Transfer and Burnout Heat Flux at Elevated Saturation Pressures, in *Proceedings of 8th International Heat Transfer Conference*, (San Francisco, CA, USA), Begel House Inc., 1986 17-22 August, pp. 1995–2000. doi:10.1615/ihtc8.3920.

[33] Stephan K., *Heat Transfer in Condensation and Boiling*. Berlin, Germany: Springer Berlin Heidelberg, 1992. doi:10.1007/978-3-642-52457-8.

[34] Mikic B.B., Rohsenow W.M., A New Correlation of Pool-Boiling Data Including the Effect of Heating Surface Characteristics, *Journal of Heat Transfer*, vol. 91, no. 2, May 1968, pp. 245–250. doi:10.1115/1.3580136.

[35] Tong L.S., Tang Y.S., *Boiling Heat Transfer And Two-Phase Flow*. Washington, D.C: CRC Press, first ed., ISBN 978-1-56032-485-0, Feb. 1997.

[36] Bergles A.E., What Is the Real Mechanism of CHF in Pool Boiling, in *Pool and External Flow Boiling* (Dhir V.K., Bergles A.E., eds.), New York, NY, USA: ASME, ISBN 978-0-7918-0667-8, 1992.

[37] Hsu Y.Y., Graham R.W., *Transport Processes in Boiling and Two-Phase Systems*. Series in Thermal and Fluids Engineering, La Grange Park, IL, USA: American Nuclear Society, Inc., ISBN 0-89448-030-8, 1986.

[38] Forster H.K., Zuber N., Dynamics of Vapor Bubbles and Boiling Heat Transfer, *AIChE Journal*, vol. 1, no. 4, 1955, pp. 531–535. doi:10.1002/aic.690010425.

[39] Jakob M., Linke W., Der Wärmeübergang von einer waagerechten Platte an siedendes Wasser, *Forschung auf dem Gebiete des Ingenieurwesens*, vol. 4, no. 2, Apr. 1933, pp. 75–81. doi:10.1007/bf02717048.

[40] Kurihara H.M., Myers J.E., The Effects of Superheat and Surface Roughness on Boiling Coefficients, *AIChE Journal*, vol. 6, no. 1, 1960, pp. 83–91. doi:10.1002/aic.690060117.

[41] Tien C.L., A Hydrodynamic Model for Nucleate Pool Boiling, *International Journal of Heat and Mass Transfer*, vol. 5, no. 6, June 1962, pp. 533–540. doi:10.1016/0017-9310(62)90164-3.

[42] Lienhard J.H., A Semi-Rational Nucleate Boiling Heat Flux Correlation, *International Journal of Heat and Mass Transfer*, vol. 6, no. 3, Mar. 1963, pp. 215–219. doi:10.1016/0017-9310(63)90108-X.

[43] Levy S., Generalized Correlation of Boiling Heat Transfer, *ASME Journal of Heat Transfer, Series C*, vol. 81, no. 1, Feb. 1959, pp. 37–42. doi:10.1115/1.4008126.

[44] Stephan P., Sielaff A., Fischer S., Dietl J., Herbert S., A Contribution to the Basic Understanding of Nucleate Boiling Phenomena: Generic Experiments and Numerical Simulations, *Thermal Science & Engineering*, vol. 21, no. 2, 2013, pp. 39–57. doi:10.11368/tse.21.39.

[45] Cooper M.G., Lloyd A.J.P., The Microlayer in Nucleate Pool Boiling, *International Journal of Heat and Mass Transfer*, vol. 12, no. 8, Aug. 1969, pp. 895–913. doi:10.1016/0017-9310(69)90154-9.

[46] Yabuki T., Nakabeppu O., MEMS Sensor Technology and the Mechanism of Isolated Bubble Nucleate Boiling, in *Boiling: Research and Advances* (Koizumi Y., Shoji M., Monde M., Takata Y., Nagai N., eds.), pp. 2–4, Amsterdam, Netherlands: Elsevier, first ed., ISBN 978-0-08-101010-5, 2017. Available at: https://www.sciencedirect.com/book/9780081010105/boiling#book-description.

[47] Utaka Y., Chen Z., Measurement of the Microlayer During Nucleate Boiling and Its Heat Transfer Mechanism, in *Boiling: Research and Advances* (Koizumi Y., Shoji M., Monde M., Takata Y., Nagai N., eds.), pp. 2–4, Amsterdam, Netherlands: Elsevier, first ed., ISBN 978-0-08-101010-5, 2017. Available at: https://www.sciencedirect.com/book/9780081010105/boiling#book-description.

[48] Ghiaasiaan S.M., *Two-Phase Flow, Boiling, and Condensation in Conventional and Miniature Systems*. Cambridge, UK: Cambridge University Press, second ed., ISBN 978-1-139-46890-9, 2017.

[49] Stephan P., Hammer J., A New Model for Nucleate Boiling Heat Transfer, *Wärme- und Stoffübertragung*, vol. 30, no. 2, Nov. 1994, pp. 119–125. doi:10.1007/BF00715018.

[50] Golobič I., Pavlovič E., Von Hardenberg J., Berry M., Nelson R.A., Kenning D.B.R., Smith L.A., Comparison of a Mechanistic Model for Nucleate Boiling with Experimental Spatio-Temporal

Data, *Chemical Engineering Research and Design*, vol. 82, no. 4, Apr. 2004, pp. 435–444. doi:10.1205/026387604323050146.

[51] Kenning D., Golobič I., Xing H., Bašelj M., Lojk V., von Hardenberg J., Mechanistic Models for Pool Nucleate Boiling Heat Transfer: Input and Validation, *Heat and Mass Transfer*, vol. 42, no. 6, Apr. 2006, pp. 511–527. doi:10.1007/s00231-005-0648-3.

[52] Yagov V.V., Generic features and puzzles of nucleate boiling, *International Journal of Heat and Mass Transfer*, vol. 52, no. 21, Oct. 2009, pp. 5241–5249. doi:10.1016/j.ijheatmasstransfer.2009.03.071.

[53] Kern J., Stephan P., Theoretical Model for Nucleate Boiling Heat and Mass Transfer of Binary Mixtures, *Journal of Heat Transfer*, vol. 125, no. 6, Dec. 2003, pp. 1106–1115. doi:10.1115/1.1622717.

[54] Kangude P., Srivastava A., Understanding the Growth Mechanism of Single Vapor Bubble on a Hydrophobic Surface: Experiments Under Nucleate Pool Boiling Regime, *International Journal of Heat and Mass Transfer*, vol. 154, June 2020, p. 119775. doi:10.1016/j.ijheatmasstransfer.2020.119775.

[55] Zupančič M., Može M., Gregorčič P., Golobič I., Nanosecond Laser Texturing of Uniformly and Non-Uniformly Wettable Micro Structured Metal Surfaces for Enhanced Boiling Heat Transfer, *Applied Surface Science*, vol. 399, Mar. 2017, pp. 480–490. doi:10.1016/j.apsusc.2016.12.120.

[56] Judd R.L., Hwang K.S., A Comprehensive Model for Nucleate Pool Boiling Heat Transfer Including Microlayer Evaporation, *Journal of Heat Transfer*, vol. 98, no. 4, Nov. 1976, pp. 623–629. doi:10.1115/1.3450610.

[57] Zuber N., *Hydrodynamic Aspects of Boiling Heat Transfer*. PhD thesis, California University and Ramo-Wooldridge Corporation, Los Angeles, CA, USA, 1959. doi:10.2172/4175511.

[58] Tolubinsky V.I., Ostrovsky Y.N., On the Mechanism of Boiling Heat Transfer (vapour Bubbles Growth Rate in the Process of Boiling of Liquids, Solutions, and Binary Mixtures), *International Journal of Heat and Mass Transfer*, vol. 9, no. 12, Dec. 1966, pp. 1463–1470. doi:10.1016/0017-9310(66)90142-6.

[59] Fritz W., Berechnung des Maximulvolumens von Dampfblasen, *Physikalische Zeitschrift*, vol. 36, no. 11, 1935, pp. 379–384.

[60] Dhir V.K., Kandlikar S.G., Fujita Y., Iida Y., Heist R., Chapter 4. Nucleate Boiling, in *Handbook of Phase Change: Boiling and Condensation* (Kandlikar S.G., Shoji M., Dhir V.K., eds.), pp. 113–162, Ann Arbor, MI, USA: Edwards Brothers, Taylor & Francis, ISBN 1-56032-634-4, 1999.

[61] Godinez J.C., Fadda D., Lee J., You S.M., Development of a Stable Boehmite Layer on Aluminum Surfaces for Improved Pool Boiling Heat Transfer in Water, *Applied Thermal Engineering*, vol. 156, June 2019, pp. 541–549. doi:10.1016/j.applthermaleng.2019.04.065.

[62] Lu Y.W., Kandlikar S.G., Nanoscale Surface Modification Techniques for Pool Boiling Enhancement—A Critical Review and Future Directions, *Heat Transfer Engineering*, vol. 32, no. 10, Sept. 2011, pp. 827–842. doi:10.1080/01457632.2011.548267.

[63] Takata Y., Effect of Surface Wettability on Boiling and Evaporation, in *Boiling: Research and Advances* (Koizumi Y., Shoji M., Monde M., Takata Y., Nagai N., eds.), pp. 2–4, Amsterdam, Netherlands: Elsevier, first ed., ISBN 978-0-08-101010-5, 2017. Available at: https://www.sciencedirect.com/book/9780081010105/boiling#book-description.

[64] Zupančič M., Steinbücher M., Gregorčič P., Golobič I., Enhanced Pool-Boiling Heat Transfer on Laser-Made Hydrophobic/Superhydrophilic Polydimethylsiloxane-Silica Patterned Surfaces, *Applied Thermal Engineering*, vol. 91, Dec. 2015, pp. 288–297. doi:10.1016/j.applthermaleng.2015.08.026.

[65] Roy Chowdhury S.K., Winterton R.H.S., Surface Effects in Pool Boiling, *International Journal of Heat and Mass Transfer*, vol. 28, no. 10, Oct. 1985, pp. 1881–1889. doi:10.1016/0017-9310(85)90210-8.

[66] Šesták J., Žitný R., *Tepelné Pochody II. Výměníky Tepla, Odpařování, Sušení, Průmyslové Pece a Elektrický Ohřev*. Praha: Vydavatelství ČVUT, first ed., ISBN 80-01-01630-7, 1997.

[67] Vejražka J., Tihon J., Bubbles, Drops and Particles (Ph.D. lectures at the Institute of Chemical Process Fundamentals of the Czech Academy of Sciences), 2018.

[68] Raben I.A., Beaubouef R.T., Commerford G.E., A Study of Heat Tranfer in Nucleate Pool Boiling of Water at Low Pressure, in *Chemical Engineering Progresses Symposium Series*, vol. 61, 1965, pp. 249–257.

[69] Stephan K., Abdelsalam M., Heat-Transfer Correlations for Natural Convection Boiling, *International Journal of Heat and Mass Transfer*, vol. 23, no. 1, Jan. 1980, pp. 73–87. doi:10.1016/0017-9310(80)90140-4.

[70] Lienhard IV J., Lienhard V J., *A Heat Transfer Textbook*. Cambridge, MA, USA: J. H. Lienhard V, third ed., 2000.

[71] Mohanty R.L., Das M.K., Development of Non-Dimensional Two Phase Heat Transfer Correlation Based on Physics of Boiling, *International Journal of Thermal Sciences*, vol. 156, Oct. 2020, p. 106433. doi:10.1016/j.ijthermalsci.2020.106433.

[72] Cole R., Rohsenow W.M., Correlation of Bubble Departure Diameters for Boiling of Saturated Liquids, *Chemical Engineering Progress Symposium Series*, vol. 65, no. 92, 1969, pp. 211–213.

[73] Bier K., Schmidt J., Bubble Formation with Pool Boiling of Pure Fluids and Binary Fluid Mixtures, in *Proceedings of 2nd European Thermal Sciences*, vol. 3, (Rome, Italy), ETS, 1996, pp. 1661–1668. Available at: https://ci.nii.ac.jp/naid/10018602386/#cit.

[74] McGillis W.R., van Carey P., Fitch J.S., Hamburgen W.R., Pool Boiling Enhancement Techniques for Water at Low Pressure, in *SEMI-THERM VII. Proceedings*, Semiconductor Thermal Measurement and Management Symposium, IEEE, 1991, pp. 64–72. doi:10.1109/STHERM.1991.152914.

[75] Hsu Y.Y., On the Size Range of Active Nucleation Cavities on a Heating Surface, *Journal of Heat Transfer*, vol. 84, no. 3, Aug. 1962, pp. 207–213. doi:10.1115/1.3684339.

[76] Thome J.R., Shock R.A.W., Boiling of Multicomponent Liquid Mixtures, in *Advances in Heat Transfer* (Hartnett J.P., Irvine T.F., eds.), vol. 16, pp. 59–156, Elsevier, Jan. 1984. doi:10.1016/S0065-2717(08)70204-1.

[77] Bourdon B., Bertrand E., Di Marco P., Marengo M., Rioboo R., De Coninck J., Wettability Influence on the Onset Temperature of Pool Boiling: Experimental Evidence Onto Ultra-Smooth Surfaces, *Advances in Colloid and Interface Science*, vol. 221, July 2015, pp. 34–40. doi:10.1016/j.cis.2015.04.004.

[78] Li C., Wang Z., Wang P.I., Peles Y., Koratkar N., Peterson G.P., Nanostructured Copper Interfaces for Enhanced Boiling, *Small*, vol. 4, no. 8, 2008, pp. 1084–1088. doi:10.1002/smll.200700991.

[79] Narayan S., Singh T., Singh S., Srivastava A., Experiments on the Effects of Varying Subcooled Conditions on the Dynamics of Single Vapor Bubble and Heat Transfer Rates in Nucleate Pool Boiling Regime, *International Journal of Heat and Mass Transfer*, vol. 134, May 2019, pp. 85–100. doi:10.1016/j.ijheatmasstransfer.2018.12.139.

[80] Fazel S.A.A., Hosseyni G., Experimental Investigation on Partial Pool Boiling Heat Transfer in Pure Liquids, *Chemical Industry and Chemical Engineering Quarterly*, vol. 22, no. 1, 2016, pp. 17–26. Available at: http://www.doiserbia.nb.rs/Article.aspx?ID=1451-93721500014F.

[81] Webb R.L., The Evolution of Enhanced Surface Geometries for Nucleate Boiling, *Heat Transfer Engineering*, vol. 2, no. 3-4, Jan. 1981, pp. 46–69. doi:10.1080/01457638108962760.

[82] Scriven L.E., On the Dynamics of Phase Growth, *Chemical Engineering Science*, vol. 10, no. 1, Apr. 1959, pp. 1–13. doi:10.1016/0009-2509(59)80019-1.

[83] Calus W., Rice P., Pool Boiling—Binary Liquid Mixtures, *Chemical Engineering Science*, vol. 27, no. 9, Sept. 1972, pp. 1687–1697. doi:10.1016/0009-2509(72)80083-6.

[84] Thome J.R., Boiling Heat Transfer in Binary Liquid Mixtures, in *Advances in Two-Phase Flow and Heat Transfer: Fundamentals and Applications Volume 1* (Kakaç S., Ishii M., eds.), NATO ASI Series, pp. 275–319, Dordrecht: Springer Netherlands, ISBN 978-94-009-6845-5, 1983. doi:10.1007/978-94-009-6845-5_14.

[85] Benjamin R.J., Balakrishnan A.R., Nucleate Pool Boiling Heat Transfer of Pure Liquids at Low to Moderate Heat Fluxes, *International Journal of Heat and Mass Transfer*, vol. 39, no. 12, Aug. 1996, pp. 2495–2504. doi:10.1016/0017-9310(95)00320-7.

[86] Van Stralen S.J.D., The Mechanism of Nucleate Boiling in Pure Liquids and in Binary Mixtures—Part I, *International Journal of Heat and Mass Transfer*, vol. 9, no. 10, Oct. 1966, pp. 995–1020. doi:10.1016/0017-9310(66)90025-1.

[87] Levitskiy S.P., Khusid B.M., Shulman Z.P., Growth of Vapour Bubbles in Boiling Polymer Solutions—II. Nucleate Boiling Heat Transfer, *International Journal of Heat and Mass Transfer*, vol. 39, no. 3, Feb. 1996, pp. 639–644. doi:10.1016/0017-9310(95)00086-O.

[88] Ohta H., Nucleate Boiling of Mixtures, in *Boiling: Research and Advances* (Koizumi Y., Shoji M., Monde M., Takata Y., Nagai N., eds.), pp. 2–4, Amsterdam, Netherlands: Elsevier, first ed., ISBN 978-0-08-101010-5, 2017. Available at: https://www.sciencedirect.com/book/9780081010105/boiling#book-description.

[89] McHale J.P., Garimella S.V., Bubble Nucleation Characteristics in Pool Boiling of a Wetting Liquid on Smooth and Rough Surfaces, *International Journal of Multiphase Flow*, vol. 36, no. 4, Apr. 2010, pp. 249–260. doi:10.1016/j.ijmultiphaseflow.2009.12.004.

[90] Nishikawa K., Fujita Y., Nawata Y., Hirahaya K., Effect of Pressure on Nucleate Boiling Heat Transfer of Water, *Memoirs of the Faculty of Engineering, Kyushu University*, vol. 30, no. 2, 1970, pp. 27–49.

[91] Peebles F.N., Garber H.J., Studies on the Motion of Gas Bubbles in Liquid, *Chemical Engineering Progress*, vol. 49, no. 2, 1953, pp. 88–97. Available at: https://ci.nii.ac.jp/naid/10006284049/.

[92] Cole R., Bubble Frequencies and Departure Volumes at Subatmospheric Pressures, *AIChE Journal*, vol. 13, no. 4, July 1967, pp. 779–783. doi:10.1002/aic.690130434.

[93] ANSYS Inc., *ANSYS Fluent Theory Guide, Release 15.0*, vol. 15.0. Canonsburg, PA, USA: SAS IP, Inc., Nov. 2013.

[94] von Hoffmann T., Untersuchungen des Blasensiedens einiger verflüssigter Gase und ihrer binären Mischungen, *Wärme- und Stoffübertragung*, vol. 11, no. 3, Sept. 1978, pp. 189–193. doi:10.1007/BF01805658.

[95] Nishikawa K., Fujita Y., Nawata Y., Nishijima T., Studies on Nucleate Pool Boiling at Low Pressures, *Heat Transfer—Japanese Research*, vol. 5, no. 2, 1976, pp. 66–89.

[96] Cooper M.G., Saturation Nucleate Pool Boiling—a Simple Correlation, in *The Institution of Chemical Engineers Symposium Series*, vol. 86, 1984, pp. 785–793. doi:10.1016/B978-0-85295-175-0.50013-8.

[97] Vajc V., *Pool Boiling (master's thesis)*. Prague, Czech Republic: Czech Technical University in Prague, 2017. Available at: https://dspace.cvut.cz/handle/10467/73374.

[98] Thome J.R., Shakir S., A New Correlation for Nucleate Pool Boiling of Aqueous Mixtures, in *Proceedings of the Eighth International Heat Transfer Conference*, vol. 18 (9), (USA), INIS, 1987.

[99] Gorenflo D., Kenning D., Chapter H2 Pool Boiling, in *VDI Heat Atlas* (Stephan P., Kabelac S., Kind M., Holger M., Mewes D., Schaber K., eds.), pp. 757–792, Berlin, Germany: Springer, VDI, second ed., 2010.

[100] Nishikawa K., Fujita Y., Ohta H., Hidaka S., Effect of the Surface Roughness on the Nucleate Boiling Heat Transfer Over the Wide Range of Pressure, in *Proceedings of the Seventh International Heat Transfer Conference*, vol. 4, 1982, pp. 61–66.

[101] Cooper M.G., Correlations for Nucleate Boiling—Formulation Using Reduced Properties, *Physico Chemical hydrodynamics*, vol. 3, no. 2, 1982, pp. 89–111.

[102] Mostinski I.L., Calculation of Heat Transfer and Critical Heat Flux in Boiling Liquids Based on the Law of Corresponding States, *Teploenergetika*, vol. 10, no. 4, 1963, pp. 66–71.

[103] Palen J.W., Shell and tube reboilers: Thermal design, in *Heat Exchanger Design Handbook*, vol. 3, New York, USA: Hemisphere Publishing Corp., 1988.

[104] Vinayak Rao G., Balakrishnan A.R., Nucleate Pool Boiling Heat Transfer of Multicomponent Mixtures, *Chemical Engineering Research and Design*, vol. 82, no. 1, Jan. 2004, pp. 43–52. doi:10.1205/026387604772803061.

[105] Park K.J., Jung D., Nucleate Boiling Heat Transfer Coefficients of Mixtures Containing Propane, Isobutane and HFC134a, *Journal of Mechanical Science and Technology*, vol. 20, no. 3, 2006, pp. 399–408. doi:10.1007/BF02917523.

[106] Dang C., Jia L., Peng Q., Huang Q., Zhang X., Experimental and Analytical Study on Nucleate Pool Boiling Heat Transfer of R134a/R245fa Zeotropic Mixtures, *International Journal of Heat and Mass Transfer*, vol. 119, Apr. 2018, pp. 508–522. doi:10.1016/j.ijheatmasstransfer.2017.11.143.

[107] Gorenflo D., Pool Boiling Heat Transfer from Horizontal Tubes to Mixtures, in *Proceedings of Engineering Foundation*, (Irsee, Germany), May 1997. Available at: https://ci.nii.ac.jp/naid/10018602390/.

[108] Inoue T., Kawae N., Monde M., Characteristics of Heat Transfer Coefficient During Nucleate Pool Boiling of Binary Mixtures, *Heat and Mass Transfer*, vol. 33, no. 4, Feb. 1998, pp. 337–344. doi:10.1007/s002310050199.

[109] Afgan N.H., Boiling Heat Transfer and Burnout Heat Flux of Ethyl Alcohol - Benzene Mixtures, in *International Heat Transfer Conference*, vol. 3, (Chicago, IL, USA), Begel House Inc., 1966, pp. 175–185. doi:10.1615/IHTC3.1030.

[110] McGillis W., Carey V., Fitch J., Hamburgen W., Boiling Binary Mixtures at Subatmospheric Pressures, in *Intersociety Conference on Thermal Phenomena in Electronic Systems*, (Texas, USA), IEEE, Feb. 1992. doi:10.1109/itherm.1992.187750.

[111] Spindler K., Hahne E., The Influence of Oil on Nucleate Pool Boiling Heat Transfer, *Heat and Mass Transfer*, vol. 45, no. 7, July 2007, pp. 979–990. doi:10.1007/s00231-007-0321-0.

[112] Stephan K., Boiling in Multicomponent Mixtures, *Thermopedia, A-to-Z Guide to Thermodynamics, Heat & Mass Transfer, and Fluids Engineering*, 2011. Available at: http://www.thermopedia.com/content/968/.

[113] Sathyabhama A., Ashok Babu T., Experimental Investigation in Pool Boiling Heat Transfer of Ammonia/Water Mixture and Heat Transfer Correlations, *International Journal of Heat and Fluid Flow*, vol. 32, no. 3, June 2011, pp. 719–729. doi:10.1016/j.ijheatfluidflow.2011.02.007.

[114] Arima H., Monde M., Mitsutake Y., Heat Transfer in Pool Boiling of Ammonia/Water Mixture, *Heat and Mass Transfer*, vol. 39, no. 7, 2003, pp. 535–543. doi:10.1007/s00231-002-0302-2.

[115] Inoue T., Monde M., Teruya Y., Pool Boiling Heat Transfer in Binary Mixtures of Ammonia/Water, *International Journal of Heat and Mass Transfer*, vol. 45, no. 22, Oct. 2002, pp. 4409–4415. doi:10.1016/s0017-9310(02)00153-9.

[116] Jungnickel H., Wassilew P., Kraus W.E., Investigations on the Heat Transfer of Boiling Binary Refrigerant Mixtures, *International Journal of Refrigeration*, vol. 3, no. 3, May 1980, pp. 129–133. doi:10.1016/0140-7007(80)90092-4.

[117] Schlünder E.U., Heat Transfer in Nucleate Boiling of Mixtures, *International Chemical Engineering*, vol. 23, no. 4, 1983, pp. 589–599.

[118] Fujita Y., Tsutsui M., Heat Transfer in Nucleate Boiling of Binary Mixtures. (Development of a Heat Transfer Correlation)., *JSME International Journal Series B*, vol. 40, no. 1, 1997, pp. 134–141. doi:10.1299/jsmeb.40.134.

[119] Jung D., Song K., Ahn K., Kim J., Nucleate Boiling Heat Transfer Coefficients of Mixtures Containing HFC32, HFC125, and HFC134a, *International Journal of Refrigeration*, vol. 26, no. 7, Nov. 2003, pp. 764–771. doi:10.1016/S0140-7007(03)00066-5.

[120] Calus W., Leonidopoulos D., Pool Boiling—Binary Liquid Mixtures, *International Journal of Heat and Mass Transfer*, vol. 17, no. 2, Feb. 1974, pp. 249–256. doi:10.1016/0017-9310(74)90086-6.

[121] Thome J.R., Prediction of Binary Mixture Boiling Heat Transfer Coefficients Using Only Phase Equilibrium Data, *International Journal of Heat and Mass Transfer*, vol. 26, no. 7, 1983, pp. 965–974. doi:10.1016/s0017-9310(83)80121-5.

[122] Nishiguchi S., Shoji M., Boiling Heat Transfer of Butanol Aqueous Solution-Augmentation of Critical Heat Flux, *Journal of ASTM International*, vol. 8, no. 6, July 2011, pp. 1–8. doi:10.1520/JAI103452.

[123] Cheng K.K., Park C., Surface tension of dilute alcohol-aqueous binary fluids: N-Butanol/water, n-Pentanol/water, and n-Hexanol/water solutions, *Heat and Mass Transfer*, vol. 53, no. 7, July 2017, pp. 2255–2263. doi:10.1007/s00231-017-1976-9.

[124] Fujita Y., Tsutsui M., Experimental Investigation in Pool Boiling Heat Transfer of Ternary Mixture and Heat Transfer Correlation, *Experimental Thermal and Fluid Science*, vol. 26, no. 2-4, June 2002, pp. 237–244. doi:10.1016/s0894-1777(02)00132-2.

[125] Kandlikar S.G., Boiling Heat Transfer with Binary Mixtures: Part I—A Theoretical Model for Pool Boiling, *Journal of Heat Transfer*, vol. 120, no. 2, May 1998, pp. 380–387. doi:10.1115/1.2824260.

[126] Sarafraz M.M., Peyghambarzadeh S.M., Influence of Thermodynamic Models on the Prediction of Pool Boiling Heat Transfer Coefficient of Dilute Binary Mixtures, *International Communications in Heat and Mass Transfer*, vol. 39, no. 8, Oct. 2012, pp. 1303–1310. doi:10.1016/j.icheatmasstransfer.2012.06.020.

[127] Nahra Z., Næss E., Heat Transfer in Pool Boiling of Binary and Ternary Non-Azeotropic Mixtures, *Heat and Mass Transfer*, vol. 45, no. 7, June 2009, pp. 951–958. doi:10.1007/s00231-007-0294-z.

[128] McNeil D.A., Burnside B.M., Elsaye E.A., Salem S.M., Baker S., Shell-Side Boiling of a Glycerol-Water Mixture at Low Sub-Atmospheric Pressures, *Applied Thermal Engineering*, vol. 115, Mar. 2017, pp. 1438–1450. doi:10.1016/j.applthermaleng.2016.11.169.

[129] Das S., Bhaumik S., Nucleate Pool Boiling Heat Transfer in Multicomponent Mixtures on Surfaces: An Review, *International Journal of Mechanical and Industrial Engineering*, vol. 2, no. 4, 2012. doi:10.47893/IJMIE.2014.1154.

[130] Peyghambarzadeh S.M., Jamialahmadi M., Alavi Fazel S.A., Azizi S., Experimental and Theoretical Study of Pool Boiling Heat Transfer to Amine Solutions, *Brazilian Journal of Chemical Engineering*, vol. 26, no. 1, Mar. 2009, pp. 33–43. doi:10.1590/s0104-66322009000100004.

[131] Wang S.P., Chato J.C., Review of Recent Research on Boiling and Condensation Heat Transfer with Mixtures, Tech. Rep. TR-23, Air Conditioning and Refrigeration Center / University of Illinois, USA, Illinois, USA, 1992.

[132] Fujita Y., Tsutsui M., Nucleate Boiling of Two and Three-Component Mixtures, *International Journal of Heat and Mass Transfer*, vol. 47, no. 21, Oct. 2004, pp. 4637–4648. doi:10.1016/j.ijheatmasstransfer.2003.09.039.

[133] Gorenflo D., Blein P., Herres G., Rott W., Schömann H., Sokol P., Heat Transfer at Pool Boiling of Mixtures with R22 and R114, *International Journal of Refrigeration*, vol. 11, no. 4, July 1988, pp. 257–263. doi:10.1016/0140-7007(88)90084-9.

[134] Inoue T., Monde M., Yamagawa E., Bubble Behavior and Heat Transfer During Pool Boiling of Binary Mixtures, *Heat Transfer—Asian Research*, vol. 34, no. 7, 2005, pp. 449–459. doi:10.1002/htj.20087.

[135] Inoue T., Monde M., Teruya Y., Nucleate Pool Boiling Heat Transfer in Binary Mixtures, *Heat and Mass Transfer*, vol. 29, no. 3, 1994, pp. 171–180. doi:10.1007/BF01548601.

[136] Sun Z., Gong M., Qi Y., Li Z., Wu J., Nucleate Pool Boiling Heat Transfer of Pure Refrigerants and Binary Mixtures, *Journal of Thermal Science*, vol. 13, no. 3, Aug. 2004, pp. 259–263. doi:10.1007/s11630-004-0040-5.

[137] Stephan K., Preusser P., Heat Transfer and Critical Heat Flux in Pool Boiling of Binary and Ternary Mixtures, *German Chemical Engineering*, vol. 2, 1979, pp. 161–169.

[138] Inoue T., Monde M., Prediction of Pool Boiling Heat Transfer Coefficient in Ammonia/Water Mixtures, *Heat Transfer—Asian Research*, vol. 38, no. 2, 2009, pp. 65–72. doi:10.1002/htj.20234.

[139] Popov D.M., Heat Transfer in Boiling Solutions of Liquids, *Theoretical Foundations of Chemical Engineering*, vol. 36, no. 5, 2002, pp. 419–426. doi:10.1023/a:1020661425665.

[140] Tolubinsky V.I., Ostrovsky Y.N., Mechanism of Heat Transfer in Boiling of Binary Mixtures, *Heat Transfer-Soviet Research*, vol. 1, no. 6, 1969, pp. 6–11.

[141] Jung D., Lee H., Bae D., Oho S., Nucleate Boiling Heat Transfer Coefficients of Flammable Refrigerants, *International Journal of Refrigeration*, vol. 27, no. 4, June 2004, pp. 409–414. doi:10.1016/j.ijrefrig.2003.11.007.

[142] Sitar A., Golobič I., Heat Transfer Enhancement of Self-Rewetting Aqueous n-Butanol Solutions Boiling in Microchannels, *International Journal of Heat and Mass Transfer*, vol. 81, Feb. 2015, pp. 198–206. doi:10.1016/j.ijheatmasstransfer.2014.10.034.

[143] Alavi Fazel S.A., Sarafraz M., Arabi Shamsabadi A., Peyghambarzadeh S.M., Pool Boiling Heat Transfer in Diluted Water/Glycerol Binary Solutions, *Heat Transfer Engineering*, vol. 34, no. 10, Aug. 2013, pp. 828–837. doi:10.1080/01457632.2012.746157.

[144] Manglik R., Pool Boiling, in *Heat Transfer and Fluid Flow Data Books*, pp. 1–9, New York, USA: Genium Publishing Corporation, ISBN 978-1-68015-598-3, Jan. 1992.

[145] Alavi Fazel S.A., Mahboobpour M., Pool Boiling Heat Transfer in Monoethyleneglycol Aqueous Solutions, *Experimental Thermal and Fluid Science*, vol. 48, July 2013, pp. 177–183. doi:10.1016/j.expthermflusci.2013.02.021.

[146] Hui T.O., Thome J.R., A Study of Binary Mixture Boiling: Boiling Site Density and Subcooled Heat Transfer, *International Journal of Heat and Mass Transfer*, vol. 28, no. 5, May 1985, pp. 919–928. doi:10.1016/0017-9310(85)90273-X.

[147] Sathyanarayana A., Warrier P., Joshi Y., Teja A., Saturated and Subcooled Pool Boiling of HFE-7200 Mixtures on a Copper Nanowire Surface, *Frontiers in Heat and Mass Transfer*, vol. 2, Jan. 2012. doi:10.5098/hmt.v2.4.3007.

[148] Arik M., Bar-Cohen A., Pool Boiling of Perfluorocarbon Mixtures on Silicon Surfaces, *International Journal of Heat and Mass Transfer*, vol. 53, no. 23, Nov. 2010, pp. 5596–5604. doi:10.1016/j.ijheatmasstransfer.2010.06.034.

[149] Lee T.Y.T., Application of Dielectric Binary Mixtures in Electronic Cooling — Nucleate Pool Boiling Regime, *Journal of Electronics Manufacturing*, vol. 07, no. 02, June 1997, pp. 93–103. doi:10.1142/S0960313197000117.

[150] Ma T., Yuki K., Furusho T., Kibushi R., Unno N., Suzuki K., Immersion Cooling Technology of SiC-Based on-Vehicle Inverter by Anti-Freezing Liquid with Subcooled Boiling, in

2017 International Conference on Electronics Packaging (ICEP), Apr. 2017, pp. 199–201. doi:10.23919/ICEP.2017.7939356.

[151] Furusho T., Yuki K., Suzuki K., Fundamental Study on Subcooled Boiling of Binary Mixture of Anti-Freezing Liquid Toward Advanced Cooling Technology for a SiC-Based on-Vehicle Inverter, in *2016 15th IEEE Intersociety Conference on Thermal and Thermomechanical Phenomena in Electronic Systems (ITherm)*, May 2016, pp. 193–198. doi:10.1109/ITHERM.2016.7517549.

[152] Hu Y., Zhang S., Li X., Wang S., Heat Transfer Enhancement of Subcooled Pool Boiling with Self-Rewetting Fluid, *International Journal of Heat and Mass Transfer*, vol. 83, Apr. 2015, pp. 64–68. doi:10.1016/j.ijheatmasstransfer.2014.11.081.

[153] Abe Y., Savino R., Self-Rewetting Fluids, in *Boiling: Research and Advances* (Koizumi Y., Shoji M., Monde M., Takata Y., Nagai N., eds.), pp. 2–4, Amsterdam, Netherlands: Elsevier, first ed., ISBN 978-0-08-101010-5, 2017. Available at: https://www.sciencedirect.com/book/9780081010105/boiling#book-description.

[154] Hu Y., Chen S., Huang J., Song M., Marangoni Effect on Pool Boiling Heat Transfer Enhancement of Self-Rewetting Fluid, *International Journal of Heat and Mass Transfer*, vol. 127, Dec. 2018, pp. 1263–1270. doi:10.1016/j.ijheatmasstransfer.2018.08.003.

[155] Celata G.P., Cumo M., Setaro T., A Review of Pool and Forced Convective Boiling of Binary Mixtures, *Experimental Thermal and Fluid Science*, vol. 9, no. 4, Nov. 1994, pp. 367–381. doi:10.1016/0894-1777(94)90015-9.

[156] Thome J.R., Nucleate Pool Boiling of Binary Liquids-an Analytical Equation, in *AIChE Symp. Ser.*, vol. 77, 1981, p. 238.

[157] Inoue T., Monde M., Pool Boiling Heat Transfer in Binary Mixtures, *Trans JSME*, vol. 57, 1991, pp. 4197–4202. doi:10.1299/kikaib.57.4197.

[158] Stephan K., Körner M., Berechnung des Wärmeübergangs verdampfender binärer Flüssigkeitsgemische, *Chemie Ingenieur Technik*, vol. 41, no. 7, 1969, pp. 409–417. doi:10.1002/cite.330410702.

[159] Ünal H., Prediction of Nucleate Pool Boiling Heat Transfer Coefficients for Binary Mixtures, *International Journal of Heat and Mass Transfer*, vol. 29, no. 4, Apr. 1986, pp. 637–640. doi:10.1016/0017-9310(86)90096-7.

[160] Happel O., Stephan K., Heat Transfer from Nucleate to the Beginning of Film Boiling in Binary Mixtures, in *Proceedings of the Fifth International Conference*, vol. 4, (Tokyo, Japan), Sept. 1974, pp. 340–344.

[161] Schlünder E.U., Über den Wärmeübergang bei der Blasenverdampfung von Gemischen, *Verfahrenstechnik*, vol. 16, 1982, p. 692.

[162] Gorenflo D., Behaltersieden (Pool Boiling), in *VDI-Wärmeatlas (Heat Atlas)*, Berlin Heidelberg, Germany: VDI-Verlag, seventh ed., ISBN 978-3-540-62358-8, 1994.

[163] The Soap and Detergent Association, *Glycerine: An Overview*. New York, NY, USA: Glycerine & Oleochemical Division, 1990.

[164] Yeong S.K., Idris Z., Hassan H.A., Palm Oleochemicals in Non-food Applications, in *Palm Oil* (Lai O.M., Tan C.P., Akoh C.C., eds.), pp. 587–624, USA: AOCS Press, first ed., ISBN 978-0-9818936-9-3, Jan. 2012. doi:10.1016/B978-0-9818936-9-3.50023-X.

[165] Wiley-VCH, *Ullmann's Encyclopedia of Industrial Chemistry*. 40 Volume Set, Wiley-VCH Verlag GmbH & Co. KGaA, ISBN 978-3-527-32943-4, Aug. 2011.

[166] Vignesh G., Barik D., Toxic Waste From Biodiesel Production Industries and Its Utilization, in *Energy from Toxic Organic Waste for Heat and Power Generation* (Barik D., ed.), Woodhead Publishing Series in Energy, pp. 69–82, Duxford, United Kingdom: Woodhead Publishing, first ed., ISBN 978-0-08-102528-4, Jan. 2019. doi:10.1016/B978-0-08-102528-4.00006-7.

[167] Ganesan D., Rajendran A., Thangavelu V., An Overview on the Recent Advances in the Transesterification of Vegetable Oils for Biodiesel Production Using Chemical and Biocatalysts, *Reviews in Environmental Science and Bio/Technology*, vol. 8, no. 4, Oct. 2009, p. 367. doi:10.1007/s11157-009-9176-9.

[168] Souza W.L.R., Silva C.S., Meleiro L.A.C., Mendes M.F., Ethanol Dehydration in Packed Distillation Column Using Glycerol as Entrainer: Experiments and HETP Evaluation, *Brazilian Journal of Chemical Engineering*, vol. 33, no. 2, June 2016, pp. 415–426. doi:10.1590/0104-6632.20160332s20150341.

[169] Banu I., Guta G., Bildea C.S., Bozga G., Design and Performance Evaluation of a Plant for Glycerol Conversion to Acrolein, *Environmental Engineering and Management Journal*, vol. 14, no. 3, 2015, pp. 509–517. doi:10.30638/eemj.2015.054.

[170] OECD, OECD-FAO Agricultural Outlook (Edition 2021), Tech. Rep., Organisation for Economic Co-operation and Development, Paris, 2021. Available at: https://www.oecd-ilibrary.org/agriculture-and-food/data/oecd-agriculture-statistics/oecd-fao-agricultural-outlook-edition-2021_4bde2d83-en.

[171] Zhang L., Yang B., Zhang W., Vapor-Liquid Equilibrium of Water + Ethanol + Glycerol: Experimental Measurement and Modeling for Ethanol Dehydration by Extractive Distillation, *Journal of Chemical and Engineering Data*, vol. 60, no. 6, 2015, pp. 1892–1899. doi:10.1021/acs.jced.5b00116.

[172] Gu Y., Jérôme F., Glycerol as a Sustainable Solvent for Green Chemistry, *Green Chemistry*, vol. 12, no. 7, July 2010, pp. 1127–1138. doi:10.1039/C001628D.

[173] Navarrete-Contreras S., Sánchez-Ibarra M., Barroso-Muñoz F.O., Hernández S., Castro-Montoya A.J., Use of Glycerol as Entrainer in the Dehydration of Bioethanol Using Extractive Batch Distillation: Simulation and Experimental Studies, *Chemical Engineering and Processing: Process Intensification*, vol. 77, Mar. 2014, pp. 38–41. doi:10.1016/j.cep.2014.01.003.

[174] Cardoso V., Bernardo A., Giulietti M., Ethanol Absorption from CO2 Using Solutions of Glycerol and Glycols, *Chemical Engineering Communications*, vol. 205, no. 10, 2018, pp. 1507–1519. doi:10.1080/00986445.2018.1458027.

[175] Isahak W.N.R.W., Ramli Z.A.C., Ismail M., Jahim J.M., Yarmo M.A., Recovery and Purification of Crude Glycerol from Vegetable Oil Transesterification, *Separation & Purification Reviews*, vol. 44, no. 3, July 2015, pp. 250–267. doi:10.1080/15422119.2013.851696.

[176] Kuo W.C., Avedisian C.T., Tsang W., Conversion of Glycerine to Synthesis Gas and Methane by Film Boiling, in *ASME 2011 International Mechanical Engineering Congress and Exposition*, American Society of Mechanical Engineers Digital Collection, Aug. 2012, pp. 1445–1449. doi:10.1115/IMECE2011-64449.

[177] Wang S., Qiu L., Dai H., Zeng X., Fang B., Highly Pure 1,3-Propanediol: Separation and Purification from Crude Glycerol-Based Fermentation, *Engineering in Life Sciences*, vol. 15, no. 8, 2015, pp. 788–796. doi:10.1002/elsc.201500004.

[178] Gil I.D., Gómez J.M., Rodríguez G., Control of an Extractive Distillation Process to Dehydrate Ethanol Using Glycerol as Entrainer, *Computers & Chemical Engineering*, vol. 39, Apr. 2012, pp. 129–142. doi:10.1016/j.compchemeng.2012.01.006.

[179] Pla-Franco J., Lladosa E., Loras S., Montón J.B., Phase Equilibria for the Ternary Systems Ethanol, Water + Ethylene Glycol or + Glycerol at 101.3 kPa, *Fluid Phase Equilibria*, vol. 341, Mar. 2013, pp. 54–60. doi:10.1016/j.fluid.2012.12.022.

[180] Zhang Y.H., Lu D.G., Wang Z.Y., Wu G.H., Fu X.L., Yang Y.H., Experimental Investigation on Heat Transfer Model for Secondary Side of Scaled C-Shape Bundle used in PRHR HX of AP1000, *Yuanzineng Kexue Jishu/Atomic Energy Science and Technology*, vol. 50, no. 10, 2016, pp. 1763–1770. doi:10.7538/yzk.2016.50.10.1763.

[181] Zhang L., Zhang W., Yang B., Experimental Measurement and Modeling of Ternary Vapor-Liquid Equilibrium for Water + 2-Propanol + Glycerol, *Journal of Chemical and Engineering Data*, vol. 59, no. 11, 2014, pp. 3825–3830. doi:10.1021/je500724p.

[182] Zhang K., Qin Y., He F., Liu J., Zhang Y., Liu L., Concentration of Aqueous Glycerol Solution by Using Continuous-Effect Membrane Distillation, *Separation and Purification Technology*, vol. 144, Apr. 2015, pp. 186–196. doi:10.1016/j.seppur.2015.02.034.

[183] Mokbel I., Sawaya T., Zanota M.L., Naccoul R.A., Jose J., de Bellefon C., Vapor–Liquid Equilibria of Glycerol, 1,3-Propanediol, Glycerol + Water, and Glycerol + 1,3-Propanediol, *Journal of Chemical & Engineering Data*, vol. 57, no. 2, Feb. 2012, pp. 284–289. doi:10.1021/je200766t.

[184] Glycerine Producers' Association, *Physical Properties of Glycerine and Its Solutions*. 1963.

[185] Watkins C.H., *Vapor-Liquid Equilibrium Data and Other Physical Properties of the Ternary System Ethanol, Glycerine, and Water*. PhD thesis, University of Louisville, Louisville, KY, USA, 1936. Available at: https://ir.library.louisville.edu/etd/1940/.

[186] Rausch M.H., Heller A., Fröba A.P., Binary Diffusion Coefficients of Glycerol–Water Mixtures for Temperatures from 323 to 448 K by Dynamic Light Scattering, *Journal of Chemical & Engineering Data*, vol. 62, no. 12, Dec. 2017, pp. 4364–4370. doi:10.1021/acs.jced.7b00717.

[187] Chenlo F., Moreira R., Pereira G., Bello B., Kinematic Viscosity and Water Activity of Aqueous Solutions of Glycerol and Sodium Chloride, *European Food Research and Technology*, vol. 219, no. 4, Sept. 2004, pp. 403–408. doi:10.1007/s00217-004-0974-6.

[188] Tolubinsky V.I., Ostrovsky Y.N., Kriveshko A.A., Heat Transfer to Boiling Water-Glycerine Mixtures, *Heat Transfer–Soviet Research*, vol. 2, no. 1, 1970, pp. 22–24.

[189] Soujanya J., Satyavathi B., Vittal Prasad T.E., Experimental (Vapour+Liquid) Equilibrium Data of (Methanol+Water), (Water+Glycerol) and (Methanol+Glycerol) Systems at Atmospheric and Sub-Atmospheric Pressures, *The Journal of Chemical Thermodynamics*, vol. 42, no. 5, May 2010, pp. 621–624. doi:10.1016/j.jct.2009.11.020.

[190] Green D., Southard M.Z., *Perry's Chemical Engineers' Handbook, 9th Edition*. New York, NY: McGraw-Hill Education, ninth ed., ISBN 978-0-07-183408-7, Aug. 2018.

[191] Carr A.R., Townsend R.E., Badger W.L., Vapor Pressures of Glycerol-Water and Glycerol-Water-Sodium Chloride Systems, *Industrial and Engineering Chemistry*, vol. 17, no. 6, 1925, pp. 643–645. doi:10.1021/ie50186a043.

[192] Sternling C.V., Tichacek L.J., Heat Transfer Coefficients for Boiling Mixtures: Experimental Data for Binary Mixtures of Large Relative Volatility, *Chemical Engineering Science*, vol. 16, no. 3, Dec. 1961, pp. 297–337. doi:10.1016/0009-2509(61)80040-7.

[193] Sarafraz M.M., Peyghambarzadeh S.M., Alavi Fazel S.A., Enhancement of Nucleate Pool Boiling Heat Transfer to Dilute Binary Mixtures Using Endothermic Chemical Reactions Around the Smoothed Horizontal Cylinder, *Heat and Mass Transfer*, vol. 48, no. 10, Oct. 2012, pp. 1755–1765. doi:10.1007/s00231-012-1019-5.

[194] Kuo W.C., *Thermal Decomposition Of Aqueous Glycerine Mixtures, Ethyl Acetate, Diethyl Carbonate, And Ethanol At High Temperatures In A Film Boiling Reactor*. PhD thesis, Cornell University, Ithaka, NY, USA, Aug. 2014. Available at: https://ecommons.cornell.edu/handle/1813/38943.

[195] Yang B., Sarafraz M.M., Arjomandi M., Marangoni Effect on the Thermal Performance of Glycerol/Water Mixture in Microchannel, *Applied Thermal Engineering*, vol. 161, Oct. 2019, p. 114142. doi:10.1016/j.applthermaleng.2019.114142.

[196] Može M., Zupančič M., Hočevar M., Golobič I., Gregorčič P., Surface Chemistry and Morphology Transition Induced by Critical Heat Flux Incipience on Laser-Textured Copper Surfaces, *Applied Surface Science*, vol. 490, Oct. 2019, pp. 220–230. doi:10.1016/j.apsusc.2019.06.068.

[197] Rishi A.M., Kandlikar S.G., Rozati S.A., Gupta A., Effect of Ball Milled and Sintered Graphene Nanoplatelets–Copper Composite Coatings on Bubble Dynamics and Pool Boiling Heat Transfer, *Advanced Engineering Materials*, vol. 22, no. 7, 2020, p. 1901562. doi:10.1002/adem.201901562.

[198] Rahman M.M., Ölçeroğlu E., McCarthy M., Role of Wickability on the Critical Heat Flux of Structured Superhydrophilic Surfaces, *Langmuir*, vol. 30, no. 37, Sept. 2014, pp. 11225–11234. doi:10.1021/la5030923.

[199] Može M., Vajc V., Zupančič M., Golobič I., Hydrophilic and Hydrophobic Nanostructured Copper Surfaces for Efficient Pool Boiling Heat Transfer with Water, Water/Butanol Mixtures and Novec 649, *Nanomaterials*, vol. 11, no. 12, Dec. 2021, pp. 1–24. doi:10.3390/nano11123216.

[200] Vajc V., Šulc R., Dostál M., Pool Boiling Heat Transfer Coefficients in Mixtures of Water and Glycerin, *Processes*, vol. 9, no. 5, article no. 830, May 2021, pp. 1–19. doi:10.3390/pr9050830.

[201] Cengel Y.A., Ghajar A.J., *Heat and Mass Transfer: Fundamentals & Applications*. New York, NY, USA: McGraw-Hill Education, fifth ed., ISBN 978-0-07-339818-1, 2015.

[202] Može M., Zupančič M., Golobič I., Pattern Geometry Optimization on Superbiphilic Aluminum Surfaces for Enhanced Pool Boiling Heat Transfer, *International Journal of Heat and Mass Transfer*, vol. 161, Nov. 2020, p. 120265. doi:10.1016/j.ijheatmasstransfer.2020.120265.

[203] Može M., Vajc V., Zupančič M., Šulc R., Golobič I., Pool Boiling Performance of Water and Self-Rewetting Fluids on Hybrid Functionalized Aluminum Surfaces, *Processes*, vol. 9, no. 6, June 2021, pp. 1–27. doi:10.3390/pr9061058.

[204] Attinger D., Frankiewicz C., Betz A.R., Schutzius T.M., Ganguly R., Das A., Kim C.J., Megaridis C.M., Surface Engineering for Phase Change Heat Transfer: A Review, *MRS Energy & Sustainability*, vol. 1, 2014/ed. doi:10.1557/mre.2014.9.

[205] Mallozzi R., Judd R.L., Balakrishnan N., Investigation of Randomness, Overlap and the Interaction of Bubbles Forming at Adjacent Nucleation Sites in Pool Boiling, *International Journal of Heat and Mass Transfer*, vol. 43, no. 18, Sept. 2000, pp. 3317–3330. doi:10.1016/S0017-9310(99)00377-4.

[206] Judd R.L., Chopra A., Interaction of the Nucleation Processes Occurring at Adjacent Nucleation Sites, *Journal of Heat Transfer*, vol. 115, no. 4, Nov. 1993, pp. 955–962. doi:10.1115/1.2911392.

[207] Cornwell K., Houston S.D., Nucleate Pool Boiling on Horizontal Tubes: A Convection-Based Correlation, *International Journal of Heat and Mass Transfer*, vol. 37, Mar. 1994, pp. 303–309. doi:10.1016/0017-9310(94)90031-0.

[208] Može M., Zupančič M., Golobič I., Investigation of the Scatter in Reported Pool Boiling CHF Measurements Including Analysis of Heat Flux and Measurement Uncertainty Evaluation Methodology, *Applied Thermal Engineering*, vol. 169, Mar. 2020, p. 114938. doi:10.1016/j.applthermaleng.2020.114938.

[209] Nam Y., Ju Y.S., A Comparative Study of the Morphology and Wetting Characteristics of Micro/Nanostructured Cu Surfaces for Phase Change Heat Transfer Applications, *Journal of Adhesion Science and Technology*, vol. 27, no. 20, Oct. 2013, pp. 2163–2176. doi:10.1080/01694243.2012.697783.

[210] Može M., Effect of Boiling-Induced Aging on Pool Boiling Heat Transfer Performance of Untreated and Laser-Textured Copper Surfaces, *Applied Thermal Engineering*, vol. 181, Nov. 2020, p. 116025. doi:10.1016/j.applthermaleng.2020.116025.

[211] Xu C.H., Woo C.H., Shi S.Q., Formation of CuO nanowires on Cu foil, *Chemical Physics Letters*, vol. 399, no. 1, Nov. 2004, pp. 62–66. doi:10.1016/j.cplett.2004.10.005.

[212] Jiang X., Herricks T., Xia Y., CuO Nanowires Can Be Synthesized by Heating Copper Substrates in Air, *Nano Letters*, vol. 2, no. 12, Dec. 2002, pp. 1333–1338. doi:10.1021/nl0257519.

[213] Može M., Senegačnik M., Gregorčič P., Hočevar M., Zupančič M., Golobič I., Laser-Engineered Microcavity Surfaces with a Nanoscale Superhydrophobic Coating for Extreme Boiling Per-

formance, *ACS Applied Materials & Interfaces*, vol. 12, no. 21, May 2020, pp. 24419–24431. doi:10.1021/acsami.0c01594.

[214] Vajc V., Može M., Hadžić A., Šulc R., Golobič I., Saturated and Subcooled Pool Boiling Heat Transfer in Mixtures of Water and Glycerin, *Experimental Heat Transfer*, vol. 0, no. 0, Jan. 2022, pp. 1–29. doi:10.1080/08916152.2022.2027574.

[215] National Institute of Standards and Technology (NIST), ITS-90 Table for Thermocouples, 2008. Available at: https://srdata.nist.gov/its90/type_k/kcoefficients_inverse.html.

[216] Lee L., Singh B.N., The Influence of Subcooling on Nucleate Pool Boiling Heat Transfer, *Letters in Heat and Mass Transfer*, vol. 2, no. 4, July 1975, pp. 315–323. doi:10.1016/0094-4548(75)90015-6.

[217] Henry C.D., Kim J., A Study of the Effects of Heater Size, Subcooling, and Gravity Level on Pool Boiling Heat Transfer, *International Journal of Heat and Fluid Flow*, vol. 25, no. 2, Apr. 2004, pp. 262–273. doi:10.1016/j.ijheatfluidflow.2003.11.019.

[218] Rainey K.N., You S.M., Lee S., Effect of Pressure, Subcooling, and Dissolved Gas on Pool Boiling Heat Transfer From Microporous Surfaces in FC-72, *Journal of Heat Transfer*, vol. 125, no. 1, Jan. 2003, pp. 75–83. doi:10.1115/1.1527890.

[219] Yaghoubi M., Hirbodi K., Nematollahi M.R., Bashiri S., Experimental Study of Subcooled Pool Boiling around a Circular Rough Cylinder, *AUT Journal of Mechanical Engineering*, vol. 1, no. 1, 2017, pp. 21–28. doi:10.22060/mej.2016.793.

[220] Judd R.L., Merte H., Jr., Ulucakli M.E., Variation of Superheat With Subcooling in Nucleate Pool Boiling, *Journal of Heat Transfer*, vol. 113, no. 1, Feb. 1991, pp. 201–208. doi:10.1115/1.2910525.

[221] Ulucakli M.E., Merte H., Jr., Nucleate Boiling With High Gravity and Large Subcooling, *Journal of Heat Transfer*, vol. 112, no. 2, May 1990, pp. 451–457. doi:10.1115/1.2910399.

[222] Vajc V., Može M., Zupančič M., Šulc R., Golobič I., IR Measurements of Heat Transfer Coefficients and Nucleation Parameters During Saturated Nucleate Boiling of Water–Glycerin Mixtures, *Case Studies in Thermal Engineering*, vol. 32, article no. 101917, Apr. 2022, pp. 1–13. doi:10.1016/j.csite.2022.101917.

[223] Voglar J., Zupančič M., Peperko A., Birbarah P., Miljkovic N., Golobič I., Analysis of Heater-Wall Temperature Distributions During the Saturated Pool Boiling of Water, *Experimental Thermal and Fluid Science*, vol. 102, Apr. 2019, pp. 205–214. doi:10.1016/j.expthermflusci.2018.11.012.

[224] Zupančič M., Zakšek P., Golobič I., Experimental Investigation of Single-Bubble Growth During the Saturated Pool Boiling of Water and Self-Rewetting Aqueous N-Butanol Mixtures, *Case Studies in Thermal Engineering*, vol. 28, Dec. 2021, p. 101513. doi:10.1016/j.csite.2021.101513.

[225] Milošević N.D., Maglić K.D., Thermophysical Properties of Solid Phase Titanium in a Wide Temperature Range, *High Temperatures – High Pressures*, vol. 37, no. 3, June 2008, pp. 187–204. Available at: http://search.ebscohost.com/login.aspx?direct=true&db=a9h&AN=35766590&site=ehost-live&scope=site.

[226] Petkovsek J., Heng Y., Zupančič M., Gjerkes H., Cimerman F., Golobič I., IR Thermographic Investigation of Nucleate Pool Boiling at High Heat Flux, *International Journal of Refrigeration*, vol. 61, Jan. 2016, pp. 127–139. doi:10.1016/j.ijrefrig.2015.10.018.

[227] Zupančič M., Gregorčič P., Bucci M., Wang C., Matana Aguiar G., Bucci M., The Wall Heat Flux Partitioning During the Pool Boiling of Water on Thin Metallic Foils, *Applied Thermal Engineering*, vol. 200, Jan. 2022, p. 117638. doi:10.1016/j.applthermaleng.2021.117638.

Author's Publications

Publications Cited in This Thesis

[97] Vajc V., *Pool boiling (master's thesis).* Prague, Czech Republic: Czech Technical University in Prague, 2017. Available at: https://dspace.cvut.cz/handle/10467/73374.

[199] Može M., Vajc V., Zupančič M., Golobič I., Hydrophilic and Hydrophobic Nanostructured Copper Surfaces for Efficient Pool Boiling Heat Transfer with Water, Water/Butanol Mixtures and Novec 649, *Nanomaterials*, vol. 11, no. 12, article no. 3216, Dec. 2021, pp. 1–24. doi:10.3390/nano11123216.

[200] Vajc V., Šulc R., Dostál M., Pool Boiling Heat Transfer Coefficients in Mixtures of Water and Glycerin, *Processes*, vol. 9, no. 5, article no. 830, May 2021, pp. 1–19. doi:10.3390/pr9050830.

[203] Može M., Vajc V., Zupančič M., Šulc R., Golobič I., Pool Boiling Performance of Water and Self-Rewetting Fluids on Hybrid Functionalized Aluminum Surfaces, *Processes*, vol. 9, no. 6, article no. 1058, June 2021, pp. 1–27. doi:10.3390/pr9061058.

[214] Vajc V., Može M., Hadžić A., Zupančič M., Golobič I., Saturated and Subcooled Pool Boiling Heat Transfer in Mixtures of Water and Glycerin, *Experimental Heat Transfer*, Jan. 2022, pp. 1–29. doi:10.1080/08916152.2022.2027574.

[222] Vajc V., Može M., Zupančič M., Šulc R., Golobič I., IR Measurements of Heat Transfer Coefficients and Nucleation Parameters during Saturated Nucleate Boiling of Water–Glycerin Mixtures, *Case Studies in Thermal Engineering*, vol. 32, Apr. 2022, pp. 1–13. doi:10.1016/j.csite.2022.101917.

Other Publications

- Vajc V., Dostál M., First Testing Experiments with Measurement of Pool Boiling Heat Transfer Coefficient on a New Apparatus, in *Proceedings of Experimental Fluid Mechanics 2018 Conference (EFM 2018)*, Les Ulis Cedex, France: EDP Sciences, EPJ Web of Conferences. vol. 213., 2019, pp. 1–5, ISSN 2100-014X. Available at: https://www.epj-conferences.org/articles/epjconf/pdf/2019/18/epjconf_efm18_02090.pdf.
- Vajc V., Dostál M., Fixation of Thermocouples and Insulation for Heated Block, in *Advances in Heat Transfer and Thermal Engineering, Proceedings of 16th UK Heat Transfer Conference (UKHTC2019)*, Springer Nature Singapore Pte Ltd., vol. 1, 2021. pp. 71–77. ISBN 978-981-334-764-9, doi:10.1007/978-981-33-4765-6_13.
- Vajc V., Dostál M., How Does Uncertainty of Thermal Conductivity Impact Measurements of Pool Boiling Heat Transfer Coefficient?, in: *Proceedings of the 8th International Conference on Chemical Technology*. Prague, Czech Republic: Czech Society of Industrial Chemistry, 2021, pp. 316–320. ISBN 978-80-88307-08-2. Available at: https://www.icct.cz/cs/Amca-ICCT/media/content/2021/proceedings/ICCT2021-Proceedings.pdf.
- Vajc V., Dostál M., How to Improve a Temperature Distribution inside a Heated Block in a Typical Pool-Boiling Apparatus, in *Proceedings of the 14th International Conference on Heat Transfer, Fluid Mechanics and Thermodynamics (HEFAT2019)*. Caps Town, South Africa: HEFAT, 2019, pp. 808–813. ISBN 978-1-77592-191-2. Available at: https://bit.ly/3oZXixp.
- Vajc V., Dostál M., Pool Boiling, in *Book of Abstracts, Full Papers of 6th International Conference on Chemical Technology*, Prague, Czech Republic: Czech Society of Industrial Chemistry, Apr. 2018. Available at: https://dev8-admin.morbo.puxdesign.cz/Amca-ICCT/media/content/2018/ICCT-2018-Proceedings.pdf.

- Vajc V., Multicomponent Boiling and Tube-Bundle Boiling with Focus on Heat Transfer, unpublished lecture from the conference *Energie z Biomasy*, Brno University of Technology, Faculty of Mechanical Engineering, Energy Institute, Sep. 2018.
- Vajc V., Heat Transfer in Pool Boiling, in *Proceedings of CHISA 2017 Conference*, Prague, Czech Republic: Czech Society of Chemical Engineering, Oct. 2017, pp. 157.
- Vajc V., Dostál M., Laboratory Apparatus for Measurement of Heat Transfer Coefficient during Pool Boiling, 2020, identification label U12118-FVZ-2020-1, identification no. VV-2020-Var-01.

PART IV
Appendices

Appendix A: Treatment of IR Videos

The files recorded with the IR camera during measurements presented in Section 8 were processed in the following four consecutive steps:

1. *Conversion.* Data were converted from *.ats* files to *.mat* files using script *FlirMovieReader.m* provided by the camera manufacturer. Three-dimensional matrices of digital counts were thus obtained for each heat flux and concentration investigated.

2. *Recalculation of counts to temperatures* which was done in two steps. Each element of individual converted matrices of digital counts was first recalculated to radiance using a third degree polynomial. The radiance value was then recalculated to temperature with a fourth-degree polynomial. Both polynomials were obtained from the calibration procedure. After the recalculation, three-dimensional matrices $[T_{\mathrm{raw}}](x,y,t)$ of raw temperatures were obtained for each of the heat fluxes and concentrations investigated.

3. *Correction of temperatures*. The matrices of raw temperatures $[T_{\mathrm{raw}}]$ were corrected based on the assumption that for a very low heat flux of 10 kW m^{-2} (which is too low to trigger nucleate boiling), the time averages of local temperatures should be homogeneous across the foil. For each experimental run, the temperature matrix $[T_{\mathrm{raw}}]$ obtained at 10 kW m^{-2}, denoted $[T_{\mathrm{raw}}]_{q10}$, was used to calculate the correction matrix

$$[C] = \frac{\left[\bar{T}_{\mathrm{raw}}\right]_{q10}(x,y)}{\bar{T}_{\mathrm{raw},q10}} \,, \tag{A1}$$

   where $[\bar{T}_{\mathrm{raw}}]_{q10}(x,y)$ is the two-dimensional matrix of raw temperatures, which was obtained by averaging the matrix $[T_{\mathrm{raw}}]_{q10}$ in time. The scalar value of average raw temperature $\bar{T}_{\mathrm{raw},q10}$ was obtained by averaging the matrix $[T_{\mathrm{raw}}]_{q10}$ in space and time. The correction matrix $[C]$ was then used to calculate the matrices of corrected temperatures $[T_{\mathrm{cor}}]$ for all investigated heat fluxes. The elements of $[T_{\mathrm{cor}}]$ in a time layer t' were calculated as

$$[T_{\mathrm{cor}}](x,y,t=t') = \frac{[T_{\mathrm{raw}}](x,y,t=t')}{[C]} \,. \tag{A2}$$

   Equation (A2) was applied for all time layers.

4. *Offset of temperatures*. For each investigated heat flux and concentration, the matrix of corrected temperatures $[T_{\mathrm{cor}}]$ was offset so that the temperature of the coldest pixel in the entire $[x,y,t]$ domain of the matrix $[T_{\mathrm{cor}}]$ obtained at the heat flux of 1 kW m^{-2}, denoted $[T_{\mathrm{cor}}]_{q1}$, corresponded to the *bubble-point* temperature of the boiling liquid. Three-dimensional matrices of surface temperatures, denoted $[T_{\mathrm{s}}]$, were thus obtained. The relation between the individual elements of matrices $[T_{\mathrm{s}}]$ and $[T_{\mathrm{cor}}]$ is

$$T_{\mathrm{s}} = T_{\mathrm{cor}} + \left\{ T_{\mathrm{b}} - \min\left([T_{\mathrm{cor}}]_{q1} \right) \right\} \,, \tag{A3}$$

   where the term in curly brackets is the offset. The *bubble-point* temperature T_{b} is the temperature of the boiling fluid measured with the immersed TCs.

The surface temperature matrices $[T_{\mathrm{s}}]$ were used for the calculation of the heat flux matrices $[q]$, see Equations (8.2) to (8.4), and for all of the analyzes presented and discussed in Section 8. Each individual matrix $[T_{\mathrm{s}}]$ corresponds to a certain experimental run, heat flux, and mixture concentration. Each single matrix $[T_{\mathrm{s}}]$ contains $94 \times 126 \times 4800 \approx 5.69 \times 10^7$ measured temperatures.

Appendix B: Distibutions of Superheat on the Titanium Foil

Table A1 presents the arithmetic means and standard deviations of the normal Gaussian distributions of the surface superheat ΔT_{sat} recorded during the experiments on the titanium foil, which were evaluated for all investigated heat fluxes q and water mass fractions ω_w. Two of these distributions were shown in Section 8.6, see Figure 8.3. The listed mean values and standard deviations increase with the heat flux and amount of glycerin in the boiling mixture.

Table A1: The mean values and standard deviations of the normal distributions of superheat for all investigated concentrations and heat fluxes. Published in [222].

q	ω_w (−)							
(kW m^{-2})	1.00	0.98	0.95	0.90	0.85	0.80	0.70	0.60
25 (run 1)	14.3 ± 2.5	12.7 ± 2.5	14.1 ± 2.5	13.3 ± 2.6	14.1 ± 2.5	17.1 ± 2.4	16.7 ± 2.9	19.1 ± 3.3
25 (run 2)	13.6 ± 2.4	12.7 ± 2.2	12.8 ± 2.5	14.4 ± 2.6	16.7 ± 2.6	16.3 ± 3.0	17.6 ± 3.1	19.3 ± 2.9
50 (run 1)	22.7 ± 4.2	20.4 ± 3.8	21.6 ± 4.1	22.0 ± 4.4	22.8 ± 4.4	25.0 ± 4.9	25.2 ± 4.5	28.1 ± 4.9
50 (run 2)	22.6 ± 3.9	19.3 ± 3.6	21.9 ± 3.9	22.0 ± 4.0	25.1 ± 4.4	26.0 ± 4.6	26.6 ± 4.7	29.5 ± 5.3
75 (run 1)	25.6 ± 5.1	23.5 ± 5.1	24.7 ± 4.9	23.7 ± 5.3	29.5 ± 5.9	30.2 ± 6.3	32.1 ± 6.9	32.9 ± 7.1
75 (run 2)	23.1 ± 4.7	25.7 ± 5.1	24.8 ± 5.5	26.8 ± 5.5	28.1 ± 6.0	30.1 ± 6.3	30.2 ± 6.2	34.4 ± 7.3
100 (run 1)	24.9 ± 5.1	27.3 ± 6.0	27.4 ± 6.0	27.8 ± 6.4	30.1 ± 6.4	31.9 ± 7.3	35.5 ± 7.4	36.8 ± 8.7
100 (run 2)	25.9 ± 5.6	28.1 ± 6.4	27.8 ± 6.1	28.8 ± 6.3	32.6 ± 6.9	30.6 ± 6.0	35.7 ± 7.3	38.9 ± 8.5
125 (run 1)	26.8 ± 5.6	29.3 ± 6.6	30.1 ± 7.6	30.4 ± 6.9	32.4 ± 7.5	33.3 ± 7.2	35.9 ± 7.9	39.9 ± 8.9
125 (run 2)	28.8 ± 7.1	28.8 ± 6.5	28.3 ± 6.3	30.8 ± 6.9	32.5 ± 6.9	35.1 ± 7.9	37.7 ± 8.5	39.2 ± 8.1
150 (run 1)	27.9 ± 7.0	29.6 ± 7.7	30.8 ± 7.9	30.9 ± 7.6	33.8 ± 8.3	34.8 ± 7.6	38.0 ± 9.2	41.3 ± 8.8
150 (run 2)	27.8 ± 7.1	31.0 ± 6.9	29.7 ± 7.8	31.2 ± 7.4	35.9 ± 8.5	36.2 ± 8.5	37.4 ± 8.7	38.8 ± 9.0
175 (run 1)	27.4 ± 7.0	29.8 ± 7.6	32.6 ± 8.5	31.7 ± 8.2	33.7 ± 8.4	35.7 ± 8.8	–	–
175 (run 2)	27.0 ± 6.9	30.0 ± 7.5	30.0 ± 7.9	32.2 ± 8.1	35.8 ± 8.9	35.7 ± 9.4	–	43.2 ± 10.5
200 (run 1)	26.9 ± 7.7	30.9 ± 8.1	31.7 ± 9.0	32.4 ± 8.6	35.8 ± 9.7	–	–	–
200 (run 2)	28.1 ± 7.8	30.6 ± 8.1	31.3 ± 8.5	31.9 ± 8.7	36.4 ± 9.5	–	–	–

Appendix C: Boiling Curves Obtained from the IR Footage

Figure A1 shows the boiling curves measured during both experimental runs with the titanium foil. The boiling curves were calculated from the captured IR videos after the integration of the matrix of surface temperatures $[T_s]$ and matrix of heat flux $[q]$ in space and time. The HTCs plotted in Figure 8.4 correspond to the boiling curves in Figure A1, but they were averaged across both runs.

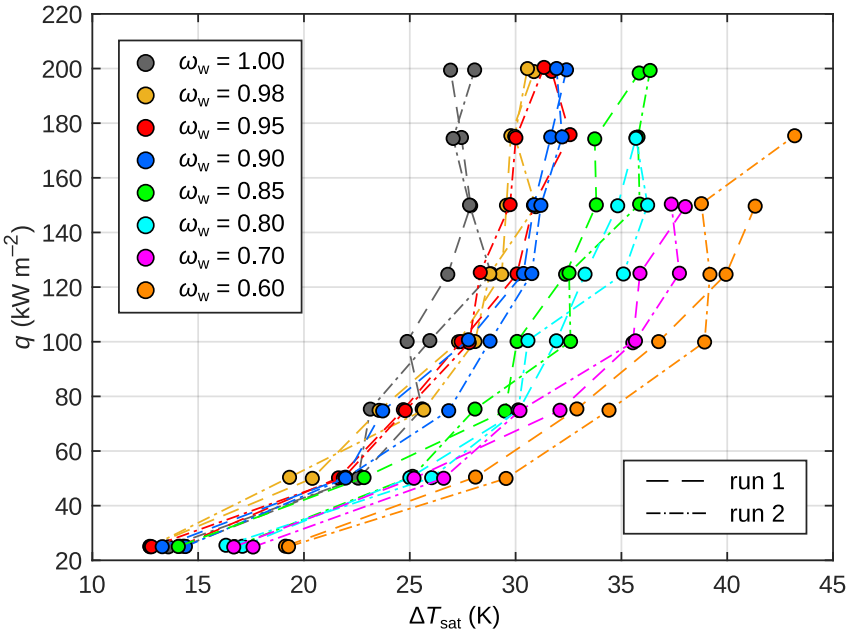

Figure A1: The boiling curves obtained from the IR footage after the integration in space and time.

Appendix D: The Total Number of Bubbles Detected on the Titanium Foil

Table A2 shows the number of the bubbles detected for all active nucleation sites of the titanium foil using custom-made scripts. The number of bubbles increases significantly with the heat flux q, but there is no clear trend with respect to ω_w. The significant differences between the certain pairs of runs corresponding to a given q and ω_w (compare, for instance, the numbers obtained during the first and second run for pure water at $q = 200$ kW m^{-2}, or the numbers for the $\omega_w = 0.85$ mixture at $q = 175$ kW m^{-2}) are caused by random activation of different nucleation sites, as was documented in Figure 8.6.

Table A2: The number of the bubbles detected for all the active nucleation sites of the filmed area.

q	ω_w (−)							
(kW m^{-2})	1.00	0.98	0.95	0.90	0.85	0.80	0.70	0.60
50 (run 1)	3	19	14	13	6	10	13	8
50 (run 2)	4	30	8	36	7	10	1	11
75 (run 1)	9	13	13	19	13	11	14	15
75 (run 2)	10	16	25	12	13	10	14	24
100 (run 1)	29	29	22	38	28	27	30	36
100 (run 2)	21	23	21	26	20	21	27	41
125 (run 1)	55	49	44	49	45	43	54	71
125 (run 2)	46	30	40	44	39	47	46	75
150 (run 1)	78	71	64	75	64	65	77	99
150 (run 2)	80	54	78	64	48	58	69	118
175 (run 1)	154	75	83	105	110	84	–	–
175 (run 2)	141	80	126	99	65	78	–	113
200 (run 1)	230	95	123	145	117	–	–	–
200 (run 2)	137	109	130	108	99	–	–	–

Table A3 gives the number of the bubbles detected for the cavity located in Zone 44 of the titanium foil, see Figure 8.5. The number of the detected bubbles increases with the heat flux q and also with the water mass fraction ω_w. The bubbles emerging from Zone 44 were analyzed in Section 8.6 to evaluate the investigated nucleation parameters and thermal energy consumed during the nucleation of individual bubbles.

Table A3: The number of the bubbles originating from the cavity in Zone 44.

q	ω_w (−)							
(kW m^{-2})	1.00	0.98	0.95	0.90	0.85	0.80	0.70	0.60
50 (run 1)	0	0	0	0	0	0	2	4
50 (run 2)	0	0	0	0	3	2	0	3
75 (run 1)	0	0	3	0	4	7	4	9
75 (run 2)	0	3	5	4	3	2	4	11
100 (run 1)	5	12	6	12	9	13	9	15
100 (run 2)	1	6	9	8	8	13	12	18
125 (run 1)	9	15	18	14	15	21	20	28
125 (run 2)	9	8	14	18	19	19	20	28
150 (run 1)	22	15	26	26	28	26	33	36
150 (run 2)	16	15	23	25	27	31	27	33
175 (run 1)	19	27	28	33	40	35	–	–
175 (run 2)	22	28	39	35	32	34	–	42
200 (run 1)	32	31	37	47	40	–	–	–
200 (run 2)	28	37	38	42	43	–	–	–